MECHANISM OF THE OUTER-SPHERE OXIDATION OF AQUEOUS *L*-CYSTEINE

AND OF IODIDE IN ACETONITRILE BY A SERIES OF IRON(III) COMPLEXES

Except where reference is made to the work of others, the work described in this dissertation is my own or was done in collaboration with my advisory committee. This dissertation does not include proprietary or classified information.

_____

Xiaoguang Wang

Certificate of Approval:

_____	_____
Michael L. McKee Professor Chemistry and Biochemistry	David M. Stanbury, Chair Professor Chemistry and Biochemistry
_____	_____
Peter D. Livant Associate Professor Chemistry and Biochemistry	Holly R. Ellis Assistant Professor Chemistry and Biochemistry

_____

George T. Flowers
Interim Dean
Graduate School

MECHANISM OF THE OUTER-SPHERE OXIDATION OF AQUEOUS *L*-CYSTEINE AND OF IODIDE IN ACETONITRILE BY A SERIES OF IRON(III) COMPLEXES

Xiaoguang Wang

A Dissertation

Submitted to

the Graduate Faculty of

Auburn University

in Partial Fulfillment of the

Requirements for the

Degree of

Doctor of Philosophy

Auburn, Alabama
May 10, 2007

MECHANISM OF THE OUTER-SPHERE OXIDATION OF AQUEOUS *L*-CYSTEINE AND OF IODIDE IN ACETONITRILE BY A SERIES OF IRON(III) COMPLEXES

Xiaoguang Wang

_____
Signature of Author

_____
Date of Graduation

VITA

Xiaoguang Wang, son of Jiucheng Wang and Guirong Liu, was born on July 1, 1973, in Tonghua, Jilin Province, the People's Republic of China. He graduated with a Bachelor's degree in Chemical Engineering in 1994 from Jilin Institute of Technology. He received his M.E. degree in Chemical Engineering in 1997 from Jilin Institute of Technology. From 1997 to 2001, he worked as a research assistant in National Synchrotron Radiation Laboratory, P. R. China. In Fall 2001, he entered the Graduate School at Auburn University in the Department of Chemistry and Biochemistry and is currently pursuing the Ph.D degree.

DISSERTATION ABSTRACT

MECHANISM OF THE OUTER-SPHERE OXIDATION OF AQUEOUS *L*-CYSTEINE AND OF IODIDE IN ACETONITRILE BY A SERIES OF IRON(III) COMPLEXES

Xiaoguang Wang

Doctor of Philosophy, May 10, 2007
(M.E., Jilin Institute of Technology, 1997)
(B.E., Jilin Institute of Technology, 1994)

238 Typed Pages

Directed by David M. Stanbury

Trace copper catalysis was observed in the oxidation of *L*-cysteine by $[Fe(bpy)_2(CN)_2]^+$ and $[Fe(bpy)(CN)_4]^-$ in anaerobic aqueous solution. The copper catalysis was effectively inhibited with the addition of dipicolinate (abbreviated asdipic^{2-}) for the reduction of $[Fe(bpy)_2(CN)_2]^+$, and completely suppressed with the addition of EDTA (pH ≤ 10.0) or 1,4,8,11-tetraazacyclotetradecane (abbreviated as cyclam) (pH > 10.0) for that of $[Fe(bpy)(CN)_4]^-$. ^{1}H-NMR and UV-vis spectra show that the products of the reaction are *L*-cystine and the corresponding Fe(II) complexes, with the stoichiometric ratio 1:2 for Δ[*L*-cystine]/Δ[Fe(II)]. The kinetics for the direct oxidation of *L*-cysteine by $[Fe(bpy)(CN)_4]^-$ were studied over the pH range 5.98 ~ 11.9, at μ = 0.10 M and 25.0 ˚C. The kinetics for the direct oxidation of *L*-cysteine by $[Fe(bpy)_2(CN)_2]^+$ were

studied over the pH range 3.48 ~ 7.89, at μ = 0.10 M and 25.0 ˚C, with the addition of 0.20 mM N-tert-butyl-α-phenylnitrone (PBN). The mechanism of the reactions was proposed. The rate-limiting step is electron transfer to form cysteine radicals and Fe(II). Only the thiolate forms of cysteine are reactive. Applying Marcus theory, the self-exchange rate constants (k_{11}) of $^{\bullet}SCH_2CH(NH_3^+)CO_2^-/^-SCH_2CH(NH_3^+)CO_2^-$ and $^{\bullet}SCH_2CH(NH_2)CO_2^-/^-SCH_2CH(NH_2)CO_2^-$, were obtained. The relatively smaller k_{11} value of $^{\bullet}SCH_2CH(NH_2)CO_2^-/^-SCH_2CH(NH_2)CO_2^-$ is ascribed to negative-negative charge repulsion. The redox reactions may occur through one-electron outer-sphere transfer reactions.

The oxidations of iodide by $[Fe^{III}(bpy)_2(CN)_2]^+$, $[Fe^{III}(dmbpy)_2(CN)_2]^+$, $[Fe^{III}(CH_3Cp)_2]^+$ and $[Fe^{III}(5\text{-Cl-phen})_2(CN)_2]^+$ at 25.0 ^oC and μ = 0.10 M in acetonitrile were studied. Trace copper catalysis was observed for the above four redox reactions. The kinetics of the direct oxidation of iodide were studied with the addition of 2,2'-bipyridine (bpy). According to ^{1}H-NMR and UV-vis spectra, the products of the reaction are I_3^- and the corresponding Fe(II) complexes, with the stoichiometric ratio of 3:2 between I^- and Fe(III). Linear Free-Energy Relationships (LFER) were obtained for both log k_1 and log k_2 vs $E_{1/2}$, implying that the reaction follows a one-electron outer-sphere mechanism. The standard-potential ($E_{1/2}$) of $I^{\bullet}/I^-$ was derived from the kinetic inhibition by $Fe^{II}(bpy)_2(CN)_2$, with the value of (0.60 ± 0.01) V (vs $[Fe(Cp)_2]^{+/0}$). However, the exchange rate constant of $I^{\bullet}/I^-$ could not be obtained due to the diffusion-control rate constant of k_{-1}.

ACKNOWLEDGMENTS

Firstly, I would like to express my deepest appreciation to my advisor, Dr. David M. Stanbury, for his academically careful instruction and financial support. I am also grateful for his extensive patience and understanding during my Ph.D study.

I want to thank my committee members for their kind help and good advice in my research. I thank their careful correction of my manuscript and instructive guidance in my preparation of final defense.

I also would like to express my gratitude to Dr. German Mills for his generous help, especially in my first two years at Auburn University. I want to thank Thomas Carrington for his kind help in running Atomic Absorption Spectroscopy. I also appreciate that Dr. Leonard N. Bell allowing us to use his AF7 Coulometric Titrator for water content analysis. I thank my previous and current lab colleagues, Meiling Hung, Anastasia V, Makarycheva-Mikhailova, Thanasekaran Pounraj, and Na Song, for their generous help during my study at Auburn. I also appreciate that the Department of Chemistry and Biochemistry, Auburn University, and National Science Foundation provided funding support for my research.

Last but not least, I am extremely grateful for my uncle, grandfather, and parents. Without their consistent and selfless support, I could not finish my Ph.D study at Auburn University.

Style manual used: Journal of the American Chemical Society

Computer software used: Microsoft Office 2001 Microsoft Word, ChemDraw Ultra 7.0.1, Datafit version 8.1, Prism 4 version 4.0a, SPECFIT/32 3.0.20.

TABLE OF CONTENTS

LIST OF TABLES AND FIGURES

CHAPTER ONE

LITERATURE REVIEW

GENERAL INTRODUCTION

Sulfur, one of the chalcogen elements, is the source for the biosynthesis of sulfur-containing amino acids that play a wide range of roles in essential biological processes.[1-6] Homocysteine, glutathione, and cysteine, the most important α-aminothiols in biological chemistry, will not easily break their C-S bonds, and they can be regenerated for further use after oxidation to the disulfide.[7,8] Under physiological conditions, α-aminothiols can undergo a range of reactions, such as nucleophilic substitution, electron transfer, proton transfer, hydrogen atom transfer, hydride transfer, and oxygen atom transfer, etc.[2,9]

Glutathione (GSH; a tripeptide formed by the amino acids glycine, cysteine, and glutamic acid), an abundant nonprotein extracellular and intracellular thiol present in animals, plants, and many bacteria, plays an important role in physiologically relevant antitoxic function; it participates in the maintenance of cellular redox potentials and protein thiol-disulfide ratios. The conversion of glutathione into its disulfide (GSSG) is readily reversible. There is suggestive evidence that the glutathione/glutathione disulfide redox couple modulates the regulation of DNA repair, gene expression and signal transduction in the immune system.[1,10] Generally, the in vivo thiol/disulfide balance is tightly controlled, and the variations of its redox state represent proliferation,

differentiation, or apoptosis of the cells. The GSH/GSSG redox couple has the lowest intracellular reduction potential during the cells' proliferation, at -260 ~ -230 mV; while it has the highest value during apoptosis, with values ranging between -170 and -150 mV.[1] The reductive capability of GSH/GSSR may be related to the concentration of GSH in the cell: there is the highest concentration of GSH during cell proliferation, while there is the lowest concentration of GSH during apoptosis.[1,11] In differentiation and apoptosis of cells, the regeneration of GSH by cysteine may be suppressed, or the oxidation of GSH facilitated by free radicals. Studying the oxidation of GSH may help understand the role of enzymes in biological processes, or may help retard the apoptosis of cells.

Cysteine, one of the simplest biological thiols, exists widely inside and outside of cells. The sulfur in cysteine is fully reduced (the oxidation state of -2 is assigned), and its thiol group can undergo a range of reactions to form a variety of redox-active sulfur-containing compounds: thiyl radicals, sulfenic, sulfinic and sulfonic acids, sulfenyl-amides, thiosulfinates and polysulfides.[5] All reactions related to the formation of the above redox-active sulfur-containing compounds are shown in Scheme 1-1. Although its concentration is much less than that of glutathione,[4,12,13] cysteine also fulfills various functions in proteins, including maintenance of the intracellular redox equilibrium, disulfide formation, metal-binding, electron donation, hydrolysis, biologic redox signaling, and redox-catalysis. All of the above functions are directly or indirectly related to the reductive capability of intracellular cysteine. The oxidation of cysteine can be reversible or irreversible, depending on the sulfur oxidation states involved. In many cases, oxidation is a reversible process resulting in disulfide formation, which is considered to be a common mechanism of protein stabilization and folding.

Scheme 1-1. Redox reactions of *L*-cysteine. (RSH: *L*-cysteine; GSSG: oxidized dimeric form of glutathione)

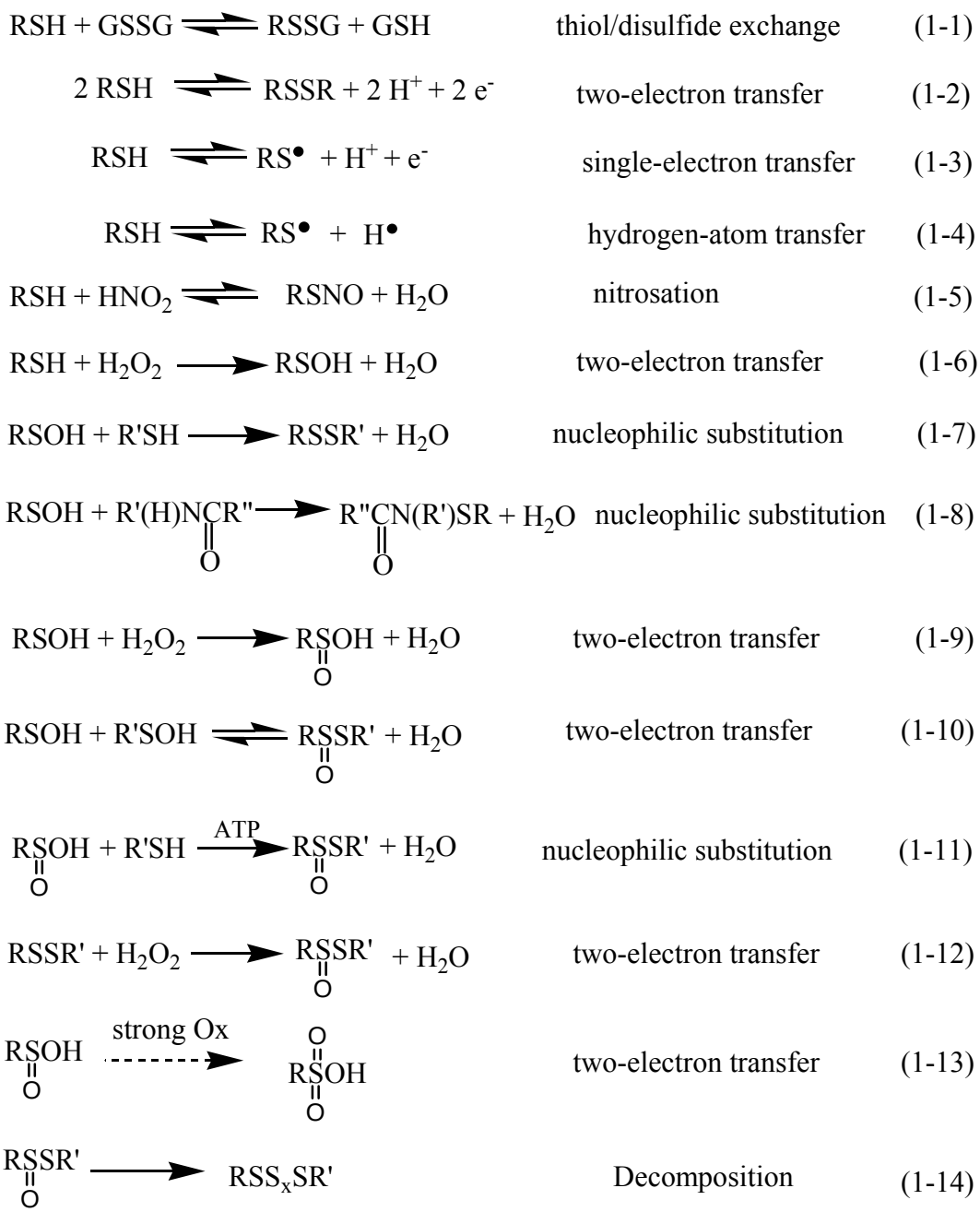

Cysteine also participates in the maintenance of the intracellular redox balance.[12,14] Generally, thiol/disulfide exchange reactions of cysteine/cystine involve balancing the intracellular redox potential. Thiol/disulfide exchange reactions, nucleophilic substitutions of a thiol or thiolate on a disulfide bond, lead to the formal oxidation of the nucleophile and reduction of the leaving group, as shown in Equation 1-1, in which there is no implication of involvement of electron transfer. However, thiol/disulfide exchange reactions can be accompanied by two-electron or two sequential one-electron transfers. For example, regeneration of GSH from GSSG is catalyzed by human glutathione reductase, which involves direct two-electron transfer from $FADH_2$ to Cys 58-S-S-Cys 63;[15] the reduction of oxidized thioredoxins in plants and bacteria that is catalyzed by ferredoxin-thioredoxin reductase (FTR) occurs by two sequential one-electron transfers.[16] Many human diseases related to oxidative stress, such as rheumatoid arthritis, autoinflammatory and neurodegenerative disease and cancer, are associated with the imbalance of the intracellular redox equilibrium. It is assumed that disturbances in the intracellular redox equilibrium are due to a significant increase in the concentration of oxidizing species, which may oxidize cysteine to form a wide range of chemically distinct reactive sulfur species. Understanding the mechanism of the oxidation of cysteine may help provide a clue in the prevention and cure of potentially fatal diseases, such as leukemia and hepatocirrhosis.

Cysteine-based radicals play important roles in biological systems as well.[17] They are formed either by a long-range one-electron transfer from the thiol (Equation 1-3) or by short-range hydrogen atom abstraction from the thiol (Equation 1-4). Cysteine-based radicals are involved in protecting biological systems from ionizing radiation and

participating directly in enzyme-catalyzed reactions. For instance, it was found that sulfur-centered radicals take part in cycles catalyzed by pyuvate formate lyase (PFL).[18]

Recent results have shown that redox-active sulfur, including sulfenic acids (RSOH), sulfinic acids [RS(O)OH], sulfonic acids [$RS(O)_2OH$], sulfenyl-amides [RC(O)N(R')SR"], thiosulfinates [RS(O)SR'] and polysulfides (RS_xR', $x \geq 3$), play significant biological roles.[19-21] Apart from glutathionylation, the formation of the cyclic sulfenyl-amide from sulfenic acid effectively prevents overoxidation of cysteine to sulfinic and sulfonic acid, as demonstrated by van Montfort[20] and Salmeen.[21] Sulfiredoxin (Srx), a 13kDa yeast protein, was also shown to reduce the sulfinic acid in peroxiredoxin (Prx) back to sulfenic acid.[19] So the reversible reaction between sulfinic and sulfenic acid in the presence of certain Prx enzymes contributes to redox-related cell signaling. As shown in Scheme 1-1, the formation of all of the sulfur-related compounds originates from the oxidation of cysteine.

Increasingly, experimental studies have demonstrated that cysteine participates in electron-transfer process of proteins that modulate essential biological functions, such as photosynthesis and aerobic respiration.[22] Cytochrome P 450, a class of mono-heme enzymes with cysteine as the proximal axial ligand, activates the conversion of O_2 to water and catalyzes the oxidation of a wide range of organic substrates. Results from Sono et al.[22] and Auclair et al.[23] confirm that the thiolate ligand in P 450 enzymes facilitates the O–O bond cleavage, and electron transfer may participate in the process. More recently, Hirota, et al.[24] proposed that the heme of myoglobin (Mb) is reduced by cysteine thiolate in cysteine-introduced Mbs, and the cysteine radical produced reacts with another cysteinyl radical of a different Mb molecule to form a Mb dimer, which

implies that intramolecular electron transfer from cysteine to Fe(III) is involved in the process.

Erv2p, a yeast endoplasmic reticulum (ER) thiol oxidase, catalyzes the activation of O_2 by the following two reactions (Equation 1-15 and 1-16). Firstly, the enzyme accepts electrons from reducing substrates, resulting in a reduction of the bound flavin cofactor. Secondly, the enzyme transfers the electrons to molecular oxygen to restore the bound cofactor to its initial state.[25] Unfortunately, the mechanism of electron transfer from the reducing substrates to the enzyme remains unclear.

$$E\bullet FAD + 2\ R\text{-}SH \rightarrow E\bullet FADH_2 + R\text{-}S\text{-}S\text{-}R \qquad (1\text{-}15)$$

$$E\bullet FADH_2 + O_2 \rightarrow E\bullet FAD + H_2O_2 \qquad (1\text{-}16)$$

Azurin, a single blue copper protein (type 1) present in several bacteria, mediates electron transport between cytochrome C_{551} and nitrite reductase. Generally, copper ion is bound at one end of the β-sandwich-shaped molecule, and the disulfide bridge is located at the opposite end from the copper ion with a distance of 2.6 nm in azurin molecule.[26] The cysteine disulfide radical could be the intermediate state of the disulfide, although no supportive evidence was provided. The disulfide radical that was generated from pulse radiolysis can transfer one electron to Cu(II) in azurin. Farver et al.[27] reported that the rate constant increases by one order of magnitude upon decreasing pH from 8.0 to 4.0 in all azurins, and they proposed that this pH-dependent behavior is either due to changes in the electron-transfer distance or due to changes in the electronic coupling.

All of these biological roles of cysteine are directly or indirectly related to its reductive property, so it is of high importance to understand the mechanisms of the oxidation of cysteine. Many groups have focused on this interesting subject --- the oxidation of cysteine, and over 400 research papers have been published. A wide range of oxidants have been selected, from nonmetallic to metallic compounds.

Of all nonmetallic oxidants involved in the reaction with cysteine, hydrogen peroxide, chlorine dioxide, and chlorite are particularly important. A significant increase in the concentration of intracellular oxidizing species, such as hydrogen peroxide and superoxide, is indicative of oxidative stress. It has triggered intensive research into understanding the reaction of cysteine with hydrogen peroxide and superoxide. For the reaction of hydrogen peroxide with excess cysteine, hydrogen peroxide reacts with cysteine to produce the corresponding sulfenic acid, and then the sulfenic acid reacts with excess cysteine to give cystine and water.[28-33] At least two groups determined the rate constant of the reaction at pH 7.4, and both obtained similar results. The rate constant determined by Barton et al. [32] was around 1.4 M^{-1} s^{-1}; while Winterbourn et al. [33] reported that the rate constant was 2.9 M^{-1} s^{-1}. The difference in rate constants may be due to copper-catalysis effect.[28,32] Unfortunately, no copper catalyst was tested in the above two experiments. Chlorine dioxide, an effective disinfectant of bacteria, may oxidize the –SH group of glucose oxidase to an –S-S- group. The oxidation of cysteine (CSH) by chlorine dioxide (ClO_2) and chlorite (ClO_2^-) was stimulated by such an assumption. Firstly, Lynch et al.[34] reported that cystine is formed in the oxidation of cysteine by the mixture of ClO_2 and ClO_2^- at pH 7.0. Recently, Darkwa et al.[8] reported that cysteic acid (CSO_3H) is the product of the oxidation of cysteine by ClO_2 and ClO_2^- in acidic solution ($pH \leq 1.0$). For

the oxidation of cysteine by excess ClO_2^-, a 28-step mechanism was proposed to fit the experimental data. More recently, the oxidation of cysteine by ClO_2 was investigated in a rather wide pH range (pH: 2.7–9.5) by Margerum's group.[35] The reaction rate is first order in both CSH and ClO_2, and increases rapidly with the increase of pH. The following mechanism was proposed: an electron transfers from CS^- to ClO_2, with a subsequent rapid reaction between the $CS^\bullet$ radical and a second ClO_2 to form a cysteinyl-ClO_2 adduct. In acidic solutions, the product of the reaction is cysteic acid; as the pH increases, the adduct reacts with CS^- by a second pathway to form cystine (CSSC) and chlorite ion (ClO_2^-). Thus, the results from Margerum's paper explain the above two seemingly contradictory reports. However, no copper catalytic effect was tested in that paper.

Metallic cations also serve as good oxidants of cysteine, and this type of redox reaction has attracted much attention. The transition-metal cations of chromium(VI) and vanadium(V) are well known to be of high toxicity, while chromium(III) and vanadium(IV) are not detrimental to human health.[36] It has been disclosed that exposure of cells to Cr(VI) and V(V) results in various forms of DNA damage.[36,37] The reduction of Cr(VI) and V(V) by biothiols in the cells may contribute to the DNA damage. For the oxidation of cysteine by Cr(VI), a long lived cysteine-Cr ion (RS-Cr) was observed by McCann et al.[38] and Kwong et al.,[39] although different mechanisms were proposed by them. For the reaction of V(V) with cysteine, two different methods were employed by two groups. The UV-vis spectra of a bisulfate-vanadium complex was observed by Payasi et al.,[40] while cysteinyl radical was detected by Shi et al.[37] using EPR technique. The oxidations of cysteine by other metal ions, such as Tc(V),[41] Fe^{3+},[42-44] Mn^{3+},[45] and

Ce(IV)[46], also were reported. Cysteinyl radicals were found in the reduction of Mn^{3+} and Ce(IV), while only long lived cysteine-metal ions were observed with Tc(V) and Fe^{3+}.

Relative to metal ions, substitution-inert transition-metal complexes are considered as good model compounds in understanding the electron transfer (ET) process of metalloproteins. Several such metal complexes were selected for the reaction with cysteine, including $[Co^{III}(ox)_3]^{3-}$ (ox: oxalate ligand),[47] $[Ir^{IV}Cl_6]^{2-}$,[48] $[Co^{III}W_{12}O_{40}]^{5-}$,[49] $[Fe^{III}(CN)_6]^{3-}$,[50,51] $[Mo^{V}(CN)_8]^{3-}$,[52] $[Co_2(CN)_{10}(O)_2]^{5-}$,[53] and $[(bpy)_2(H_2O)Ru^{III}ORu^{III}(H_2O)(bpy)_2]^{4+}$.[54] The products of the oxidation of cysteine by $[Co^{III}(ox)_3]^{3-}$, $[Fe(CN)_6]^{3-}$, and $[Co^{III}W_{12}O_{40}]^{5-}$ are cystine and their corresponding reduced metal complexes; for the reactions of cysteine with $[Co_2(CN)_{10}(O)_2]^{5-}$ and $[(bpy)_2(H_2O)Ru^{III}ORu^{III}(H_2O)(bpy)_2]^{4+}$, the products are cystine and their reduced mononuclear complexes; in the cases of $[Mo^{V}(CN)_8]^{3-}$ and $[Ir^{IV}Cl_6]^{2-}$, except for their reduced metal complexes, mixtures of cystine and cysteinesulfinate are formed for $[Mo^{V}(CN)_8]^{3-}$, and only cysteic acid is produced for $[Ir^{IV}Cl_6]^{2-}$. The above results seem to demonstrate that the products of sulfur-containing compounds are correlated with the oxidative capability of the metal complex: with weak oxidants, only cystine is formed; with strong oxidants, sulfur-containing compounds with higher oxidation states are obtained, such as cysteinesulfinate and cysteic acid. Moreover, the ubiquitous copper catalytic effect was tested only in the reactions of $[Fe^{III}(CN)_6]^{3-}$, $[Mo^{V}(CN)_8]^{3-}$, and $[Co_2(CN)_{10}(O)_2]^{5-}$. For the oxidations of *L*-cysteine by the other outer-sphere transition metal complexes, the copper-catalysis effect may be overlooked. So it seems reasonable to correlate the sulfur-containing products of the redox reaction to the oxidative capability of the transition metal complex.

Both $[Fe^{III}(bpy)_2(CN)_2]^+$ and $[Fe^{III}(bpy)(CN)_4]^-$ are substitution-inert metal complexes with mild oxidative capabilities. In Chapter Two, we report the results of studies of these two complexes as oxidants of cysteine. Copper catalysis is observed in the above reactions. The direct oxidations of cysteine by the Fe(III) complexes are achieved by the addition of chelating reagents: $dipic^{2-}$ (dipicolinate) for reaction of $[Fe(bpy)_2(CN)_2]^+$; EDTA ($pH \leq 10.0$) or 1,4,8,11-tetraazacyclotetradecane (abbreviated as cyclam) ($pH > 10.0$) for the reduction of $[Fe(bpy)(CN)_4]^-$. The mechanism for the direct oxidation of cysteine is proposed.

Moreover, the energy crisis is another concern of mankind. In Chapter Three, the oxidation of iodide by a series of Fe(III) complexes in acetonitrile is studied. Understanding the mechanism of the redox reaction may help improve the efficiency of dye-sensitized solar cells (DSSC) in the near future.

Oil, gas, and coal are three major energy resources on which humans rely. In 1998, the mean global energy consumption rate was about 12.8 Trillion watts (TW) per year, from which the three major sources account for 80%.[55] The global energy consumption rate is expected to reach 28-35 TW per year by 2050. So there would be an estimated 15-22 TW shortage of energy supply in the planet if the same amount of fuel were consumed. Renewable energy is a good candidate to fill the 15-22 TW gap, although it currently constitutes less than 1%. Furthermore, the earth's oil reserves will last for 50 years; natural gas is adequate for 70 years; coal reserves are available for 200 years.[55] In the long run, the substitution of fossil energy resources by renewable energy is inevitable. The five most common renewable sources of primary power in the world are hydroelectric, geothermal, wind, biomass, and solar. Of all of them, solar energy is one of

the best choices for noncarbon primary power.[56] The supply of energy from the sun to the Earth is about 10^4 times more than what mankind consumes today. It indicates that solar cells with an efficiency of 10 % that cover only 0.1 % of the Earth would suffice to meet our current needs. In 1991, Grätzel and coworkers initially made a nanoncrystalline dye-sensitized solar cell (DSSC), a low-cost alternative to traditional inorganic photovoltaic devices.[57]

The DSSCs consist of five major components: (1) conductive mechanical support, (2) nanocrystalline semiconductor film, (3) dye sensitizer, (4) redox couple, and (5) Pt counter-electrode.[58,59] Among them, the nanocrystalline semiconductor film is at the heart of the DSSCs system. Figure 1-1 shows the principle of operation and energy level scheme of the DSSC. The operating principles of the DSSC are as follows: generally, a monolayer of the dye sensitizer is attached to the surface of the nanocrystalline film. The injection of an electron into the conduction band of the oxide (generally, TiO_2 is selected) follows photoexcitation of the sensitizer. The dye is regenerated by electron transfer from the electrolyte, such as the I^-/ I_3^- couple. Then iodide is regenerated by the reduction of triiodide at the counter electrode. The circuit is completed via electron migration through the external load.[58,59] All in all, with the employment of DSSCs, electric power is generated from light without suffering any permanent chemical transformation. Further extensive investigations of this type of cell are stimulated by its increasing academic and industrial importance. Most studies are focusing on modifications of the nanocrystalline semiconductor, the redox electrolyte and the dye.[58-63]

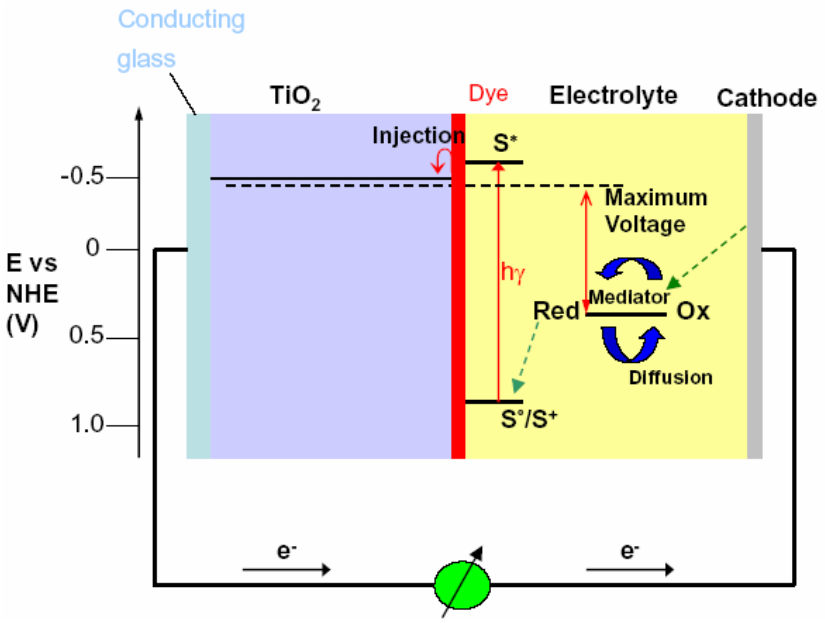

Figure 1-1. Principle of operation and energy level scheme of the dye-sensitized nanocrystalline solar cell. Photoexcitation of the sensitizer (S) is followed by electron injection into the conduction band of an oxide semiconductor film. The dye molecule is regenerated by the redox system, which itself is regenerated at the counter-electrode by electrons passed through the load. Potentials are referred to the normal hydrogen electrode (NHE). The open circuit voltage of the solar cell corresponds to the difference between the redox potential of the mediator and the Fermi level of the nanocrystalline film indicated with a dashed line.

Wide-band gap semiconductor oxides, such as ZnO, SnO_2, Nb_2O_5 or TiO_2, have been employed in DSSCs. TiO_2 is the most widely used oxide material among them.[58,60] The morphology of the nanocrystalline film plays a key role in photovoltaic conversion. A bipyramidal TiO_2 nanoparticle film, with average particle size of 20 nm and (101) orientation on the exposed facets, is successfully prepared by a hydrothermal method.[58] The high surface roughness of the mesoporous film slows down charge carrier loss by recombination, the efficiency of DSSCs therefore being improved. In case of the redox electrolyte, it has been demonstrated that DSSCs with I^-/I_3^- redox electrolyte solution display the highest efficiency, although several drawbacks impede its wide application.[64,65] A number of alternative redox mediators and electrolyte systems have been explored to redress these limitations, including I^-/I_3^- in either solid polymer, gel, ionic liquid, plastic crystal system, solid inorganic materials, Co^{II}/Co^{III}, or $SeCN^-/(SeCN)_3^-$ redox couples.[66-70] Unfortunately, all of them have a decreased efficiency relative to that of I^-/I_3^- in volatile solvent. The inefficient performance of the cells prepared with all other redox electrolytes is ascribed to their poorer electron-transfer kinetics, and poor contact at the dye-HTM (hole-transport material) interface. The Br^-/Br_3^- redox couple is an exception. Very recently, Sugihara and his coworkers demonstrated that DSSCs with Br^-/Br_3^- redox couple have higher overall energy conversion efficiency and higher open-circuit photovotage (V_{oc}) production than I^-/I_3^- if the dye sensitizer has a more positive potential than that of Br^-/Br_3^-.[71] However, their allegation awaits further verification. Currently, I^-/I_3^-/volatile solvent cells are still the first option.

Selection of dyes is also of high importance in improving the efficiency of DSSCs. Basically, the dye must bind strongly to TiO_2 by means of an anchoring group to guarantee efficient electron injection into the TiO_2 conduction band. The dye must absorb solar energy in the visible or near-IR range. Electron injection from the dye to the TiO_2 must be much faster than decay to ground state of the dye. Following these essential requirements, a variety of mononuclear and polynuclear metal complexes have been tested, such as Ru^{II}, Os^{II}, Pt^{II}, Re^{I}, Cu^{I}, and Fe^{II}.[64,72-76] Progress has been made in the optimization of the dye component of the cell by systematically varying the ligands, metal and other substituent groups in candidate transition-metal complexes. The family of complexes $[\{(4,4'\text{-}CO_2H)_2\ (bpy)_2\}RuX_2]$ (bpy = 2,2'-bipyridyl; X = Cl, Br, I, CN, NCS) have shown good performance. DSSCs with the highest solar-to-electrical energy conversion efficiency of 11 % are achieved by applying the dye $[\{(4,4'\text{-}CO_2H)_2(bpy)\}_2Ru(NCS)_2]$ (*cis*-$RuL_2(NCS)_2$ is known as N3 dye) now.[64]

Furthermore, the kinetics of electron transfer at the semiconductor/dye/electrolyte interface is critical to the efficiency of the device. Electron-transfer processes and the associated rate constants at the sensitized nanocrystalline titanium dioxide –electrolyte interface are shown in Scheme 1-2.[72] To generate electric power efficiently and permanently, injection of an electron from the dye excited state into the semiconductor conduction band must be much faster than decay of the excited state to the ground state, and faster than the reverse charge recombination between the injected electrons in the

Scheme 1-2: Electron-Transfer Processes and the Associated Rate Constants k_i at DSSCs interface[a]

$$S \mid TiO_2 + h\nu \rightarrow S^* \mid TiO_2 \qquad k_1 \qquad (1\text{-}17)$$

$$S^* \mid TiO_2 + Q \rightarrow S \mid TiO_2 + Q^* \qquad k_{-1} \qquad (1\text{-}18)$$

$$S^* \mid TiO_2 \rightarrow S^+ \mid TiO_2 + e^-_{cb}(TiO_2) \qquad k_2 \qquad (1\text{-}19)$$

$$S^+ \mid TiO_2 + e^-_{cb}(TiO_2) \rightarrow S \mid TiO_2 \qquad k_3 \qquad (1\text{-}20)$$

$$S^+ \mid TiO_2 + 3/2\ I^- \rightarrow S \mid TiO_2 + 1/2\ I_3^- \qquad k_4 \qquad (1\text{-}21)$$

conduction band and the oxidized form of the dye, *i.e.* $k_2 >> k_{-1}, k_3$; the rate of reduction of the dye cation by a redox couple in liquid electrolyte must be greater than the rate of recombination of this dye cation with electrons injected into the semiconductor, *i.e.* $k_4 > k_3$ (see Scheme 1-2). This general rule arouses great interest in the kinetics of both the photoinduced electron injection and recombination reactions. Increasing evidence has shown that, with favorable energetics and strong dye binding to the film surface, the electron injection in the N3-sensitized TiO_2 and similar system proceeds largely on ultrafast time scales ($10^{12} - 10^{13}$ s^{-1}).[77-79] For instance, Tachibana et al.[77] used subpicosecond transient absorption spectroscopy to study the rate of electron injection from an excited state of N3 to conduction band of TiO_2, with a rate constant close to 10^{12} s^{-1}. Ellingson et al.[78] measured the near- and mid-IR transient absorption for N3 adsorbed to films of nanocrystalline TiO_2, and an electron injection time with an upper limit of about 50 fs was obtained; Hannappel et al.[79] measured a transient absorption signal of the

injected hot electrons with a rise time of less than 25 fs. More importantly, Durrant and his coworkers[77] found that the electron injection kinetics are insensitive to the solvent environment, applied electrical potential, and the redox potential of the excited-state dye, which is consistent with the activationless electron injection into the TiO_2 conduction band acceptor state.[77] However, the recombination kinetics between the N3 dye cation and electron injected into the TiO_2 film are strongly dependent on the excitation intensity, solvent/electrolyte composition, and the applied electrical bias, with recombination time constants from tens of picoseconds to milliseconds.[80] A rapid acceleration of the charge recombination kinetics is observed provided that the excitation intensity is above a certain level or the applied potential is more negative than a threshold potential V_{kin}; the recombination rate constant in CH_3CH_2OH/0.1 M TBAT (tetrabutylammonium triflate) is about 10^6 faster than that in dry acetonitrile/0.1 M TBAP (tetrabutylammonium perchlorate)/0.1 M $LiClO_4$/0.5 M 4-tert-butypyridine if the applied potential is -400 mV vs Ag/AgCl, while it is weakly dependent upon electrolyte composition if no or positive applied potentials are applied, with the recombination time constants of milliseconds.[80] A very interesting result was also obtained by Tachibana et al. in their comparison of ruthenium bipyridyl with porphyrin sensitizer dyes.[77] They found that the three different dyes have similar electron injection and recombination rate constants, while only Ru(2,2′-bipyridyl-4,4′-dicarboxylate)$_2$-*cis*-$(NCS)_2$ ($Ru(dcbpy)_2(SCN)_2$) dye shows high photoelectrochemical conversion. They ascribed the lower efficiency of porphyrin sensitizers to an increasing probability of their excitation annihilation, which may slow down the electron transfer from the iodide to the dye cation.

The important role of the interfacial oxidation of iodide by the dye cation in DSSC cells prompted several groups to study its kinetics. The complexity of the interfacial interaction impedes our understanding of its kinetic behavior. So far only a few inconsistent results have been given. Meyer and his coworkers found that *cis*-$Ru(dcb)_2(CN)_2/TiO_2$ (dcb: 4,4′-$(COOH)_2$-2,2′-bipyridine) converts absorbed photons to electrons nearly quantitatively while *cis*-$Os(dcb)_2(CN)_2/TiO_2$ does not.[81] Then they measured the rate constants of the oxidation of iodide by these two dye cations using in-situ time-resolved diffuse reflectance, with 2×10^7 M^{-1} s^{-1} (with an assumed 1st-order iodide dependence) for *cis*-$Ru(dcb)_2(CN)_2/TiO_2$ and less than 9.0×10^6 M^{-1} s^{-1} for *cis*-$Os(dcb)_2(CN)_2/TiO_2$; they ascribed this poor photon conversion of *cis*-$Os(dcb)_2(CN)_2/TiO_2$ to the sluggish oxidation of iodide by Os(III), the rate-limiting step in the sensitization of the *cis*-$Os(dcb)_2(CN)_2/TiO_2$ photoelectrochemical cell. However, for *cis*-$Ru(dcb)_2(CN)_2/TiO_2$, the rate-limiting step is the recombination of injected electron with dye cation. Iodide can efficiently regenerate the sensitizer ground state within about 200 ns. So the efficient photocurrents are realized in *cis*-$Ru(dcb)_2(CN)_2/TiO_2$ solar cells. Kuciauskas et al.[72] also determined the rate constants (k_4 in Scheme 1-2) for the oxidation of 0.50 M iodide by Ru/Os dye cations by transient absorption spectroscopy, with 8.0×10^5 s^{-1} for $Ru(dcb)_2(CN)_2/TiO_2$ and 6.5×10^5 s^{-1} for $Os(dcb)_2(CN)_2/TiO_2$. Unfortunately, no iodide-dependent kinetic results were provided by these two reports, so the rate constants obtained are incomparable. The regeneration of the Ru(II) dye by iodide in $[Ru(bpy)_2(dcb)]^{2+}/SnO_2$ photoelectrochemical solar cells was studied by Nasr, et al.,[60] from which an intermediate state of $I_2^{\bullet-}$ was observed. The reaction is first order in iodide and Ru(III) with the rate constant of 1.2×10^{10} M^{-1} s^{-1}, and

the mechanism of the reaction was proposed. The higher oxidation potential of $[Ru(bpy)_2(dcb)]^{2+}$ and the interfacial interaction between $[Ru(bpy)_2(dcb)]^{2+}$ and SnO_2 may contribute to the higher rate constant of the reduction of $[Ru^{III}(bpy)_2(dcb)]^{3+}$.

The kinetics and the mechanism of the oxidation of iodide by substitution-inert transition metal coordination complexes in aqueous solution are well understood. [82-85] The stoichiometry of the reaction is:

$$2\ M_{ox} + 2I^- \rightleftharpoons 2\ M_{red} + I_2 \qquad (1\text{-}22)$$

with the rate law being

$$-\frac{d[M_{ox}]}{dt} = 2(k_1[I^-] + k_2[I^-]^2)[M_{ox}] \qquad (1\text{-}23)$$

The reversibility of Equation 1-22 is dependent on the oxidative capability of the transition metal complexes. With a strong oxidants, the reverse reaction is negligible; otherwise, the forward and reverse reactions are included. The oxidation of iodide by outer-sphere transition metal complexes in aqueous solution proceeds by two parallel paths, with the formation of $I^\bullet$ and $I_2^{\bullet-}$ intermediate states, as shown in Equations 1-24 and 1-25. Both reactions are first order in transition metal complex, but are first order and second order in iodide, respectively.

$$M_{ox} + I^- \rightarrow M_{red} + I^\bullet \qquad k_1 \qquad (1\text{-}24)$$

$$M_{ox} + 2\ I^- \rightarrow M_{red} + I_2^{\bullet-} \qquad k_2 \qquad (1\text{-}25)$$

The standard potentials of $I^{\bullet}/I^-$ and $I_2^{\bullet-}/2I^-$ in aqueous solution have been determined, with E^o ($I^{\bullet}/I^-$) = 1.33 V, and E^o ($I_2^{\bullet-}/2I^-$) = 0.94 V vs NHE.[86] Moreover, no trace metal-ion catalysis has been reported in the oxidation of iodide in aqueous solution, with one exception for the reduction of $[Fe(CN)_6]^{3-}$.[87] Unfortunately, the oxidation of iodide by outer-sphere transition metal complexes in a genuine nonaqueous solvent has not been reported. Our research is stimulated by this paradox — the important role of the interfacial oxidation of iodide by dye cation in acetonitrile, and the lack of understanding of the kinetics and mechanism of such redox reactions.

In Chapter Three, the oxidation of iodide by $[Fe^{III}(bpy)_2(CN)_2]NO_3$, $[Fe^{III}(CH_3Cp)_2]PF_6$, $[Fe^{III}(dmbpy)_2(CN)_2]NO_3$, and $[Fe^{III}(5\text{-Cl-phen})_2(CN)_2]NO_3$ in acetonitrile is described. The general copper catalysis is inhibited with the addition of 2,2'-bipyridine. The kinetics of the direct oxidation of iodide was studied with the addition of 2,2'-bipyridine. Linear Free-Energy Relationships (LFER) were obtained for both log k_1 and log k_2 vs $E_{1/2}$. The reaction of $[Fe^{III}(bpy)_2(CN)_2]^+$ is mildly inhibited by Fe(II), and a quantitative study of this effect leads to a value of 0.60 ± 0.01 V (vs $[Fe(Cp)_2]^{+/0}$) for the reduction potential ($E°$) of $I^{\bullet}/I^-$. Deriving from this work, two papers have been published: *J. Phys. Chem. A*, **2004**, 108, 7637-7638; *Inorg. Chem.* **2006**, 45, 3415-3423.

Next, in this chapter, we briefly introduce some of the basic concepts, theories and techniques that are related to this dissertation.

BASIC CONCEPTS IN KINETICS

Chemical kinetics is the study of the rates of reactions. The overall goal is to understand reactions in terms of simple steps involving atomic, molecular, or ionic interactions and collisions. The reaction rate is the increase in molar concentration of the product of a reaction per unit time, or the decrease in molar concentration of the reactant per unit time. For general reaction

$$aA + bB\cdots \rightarrow mM + nN\cdots \tag{1-26}$$

the reaction rate, the rate of disappearance of reactants and rate of formation of products are related by

$$\text{Rate} = -\frac{1}{a}\frac{d[A]}{dt} = -\frac{1}{b}\frac{d[B]}{dt} = \frac{1}{m}\frac{d[M]}{dt} = \frac{1}{n}\frac{d[N]}{dt} \tag{1-27}$$

Another important concept is the rate law. The rate law is the experimentally determined dependence of the reaction rate on reagent concentrations. In simple cases it has the following general form:

$$\text{Rate} = k[A]^{\alpha}[B]^{\beta} \tag{1-28}$$

where k is a proportionality constant called the rate constant. The rate of a reaction is dependent on the concentrations of reactants and products, while the rate constant is not.

The rate constant is affected by temperature, pressure, catalyst, and properties of solvent. The exponents m and n are determined experimentally from kinetic studies. The sum of the exponents is the overall order of the rate law. However, the order of the reaction is usually represented with respect to individual reagents. The exponents in the rate law have no necessary relationship to the stoichiometric coefficients in the balanced chemical reaction.

Combining Equation 1-27 with 1-28, the following equation is obtained:

$$-\frac{1}{a}\frac{d[A]}{dt} = -\frac{1}{b}\frac{d[B]}{dt} = \frac{1}{m}\frac{d[M]}{dt} = \frac{1}{n}\frac{d[N]}{dt} = k[A]^{\alpha}[B]^{\beta} \qquad (1\text{-}29)$$

If the reaction were monitored by the disappearance of A, then the experimental rate constant would be *ak*, and it must be divided by *a* to get the numerical value of *k* as defined by Equation 1-28.

The half-life is one more important concept in kinetics. The half-life, $t_{1/2}$, is the time required for a reactant concentration to reach half of its initial value. This term has a quantitative relationship to the rate constant in simple cases, for example, $t_{1/2} = 1n2/k$ for first-order reactions. When the kinetic traces are not well fit by mathematical models, the half-life is a good way to represent the rate of the reactions.

Reactions can be of zero-order, first-order or second-order. Here we are interested in first-order and pseudo-first-order reactions. For the irreversible elementary reaction:

$$A \xrightarrow{k_1} B \qquad (1\text{-}30)$$

the rate of disappearance of A and appearance of B are given by:

$$\text{Rate} = -\frac{\text{d[A]}}{\text{dt}} = \frac{\text{d[B]}}{\text{dt}} = k_1[\text{A}] \tag{1-31}$$

Suppose the concentrations of A at time of zero and t are $[A]_0$ and $[A]_t$, integration of Equation 1-31 gives the following equations.

$$[\text{A}]_t = [\text{A}]_0 e^{-k_1 t} \tag{1-32}$$

$$\ln[\text{A}]_t - \ln[\text{A}]_0 = -k_1 t \tag{1-33}$$

Generally, some physical properties (*P*) proportional to the concentration of reactants/products are followed in kinetics. In the simplest situation of first-order reactions, if only the reactant A contributes to this property *P*, it is easy to see that the fractional change in *P* is proportional to [A], and may be substituted for it in Equation 1-32 and 1-33. It has been demonstrated by Espenson[88] that the same result also holds when the product contributes to the value of *P* for first-order reactions. Therefore, in our kinetic studies, the reaction could be monitored by the absorbance at any wavelength provided it follows first order kinetic behavior.

Pseudo-first-order reaction conditions are widely used in kinetic studies. The pseudo-first-order condition is that the concentration of the limiting reactant is much less

than that of any of other reactants, from which the reaction is first-order in the limiting reactant. For example:

$$5\ Br^- + BrO_3^- + 6\ H^+ = 3\ Br_2 + 3\ H_2O \qquad (1\text{-}34)$$

The rate law is:[88]

$$-\frac{d[BrO_3^-]}{dt} = k[BrO_3^-][Br^-][H^+]^2 \qquad (1\text{-}35)$$

When the concentrations of H^+ and Br^- are at least ten times that of BrO_3^-, the rate of the reaction would become:

$$-\frac{d[BrO_3^-]}{dt} = k[BrO_3^-][Br^-][H^+]^2 = k'[BrO_3^-] \qquad (1\text{-}36)$$

where k' is:

$$k' = k[Br^-][H^+]^2 \qquad (1\text{-}37)$$

In our research, the concentration of cysteine (in Chapter Two) or iodide (in Chapter Three) is at least ten times greater than that of transition metal complexes. The

reactions are monitored by the loss of Fe(III) or the increase of Fe(II). Applying pseudo-first-order conditions simplifies our kinetic studies, and good results are obtained.

ELECTRON-TRANSFER REACTION MECHANISM AND MARCUS THEORY

Generally, inorganic reactions can be divided into either substitution reactions or oxidation-reduction (redox) reactions. Redox reactions, in which one or more electrons transfer from the reducing reagent to the oxidant, are involved in many biological and environmental processes. According to the mechanism, Taube classified the electron-transfer processes into inner-sphere or outer-sphere reactions.[89,90]

In inner-sphere redox reactions, there exists a bridged transition state such that a chemical bond is formed between one of the reactants and a ligand that is still bonded to the other reactant. Any inner-sphere reaction must include three steps: 1. formation of the bridged complex; 2. the redox process; and 3. decomposition of the successor complex to final products. The first thoroughly investigated inner-sphere reaction, the oxidation of Cr^{2+} by $[CoCl(NH_3)_5]^{2+}$, is a good example, as shown in Scheme 1-3.[91]

From their central electronic structures, the complexes of cobalt(III) (low spin d^6) are inert, of chromium (II)(high-spin d^4) are labile, of cobalt (II)(high-spin d^7) are labile, and of chromium(III) (d^3) are inert.[91] This combination of conditions allowed the reaction products to establish definitively an inner-sphere mechanism for the reaction in Scheme 1-3. The metal ions keep their original oxidation states in the precursor complex. The relative labilities of Co(II) and Cr(III) result in the successor complex decomposing to the Cr(III) product in which the Cl^- ligand originally on cobalt(III) has been transferred to chromium(III).[91] The inner-sphere mechanism of the above reaction was also

experimentally proven in the radioactive $^{36}Cl^-$ tracer studies,[90] from which it was revealed that over 99% of the chloride incorporated into the product arises from the $[CoCl(NH_3)_5]^{2+}$ oxidant.

Scheme 1-3

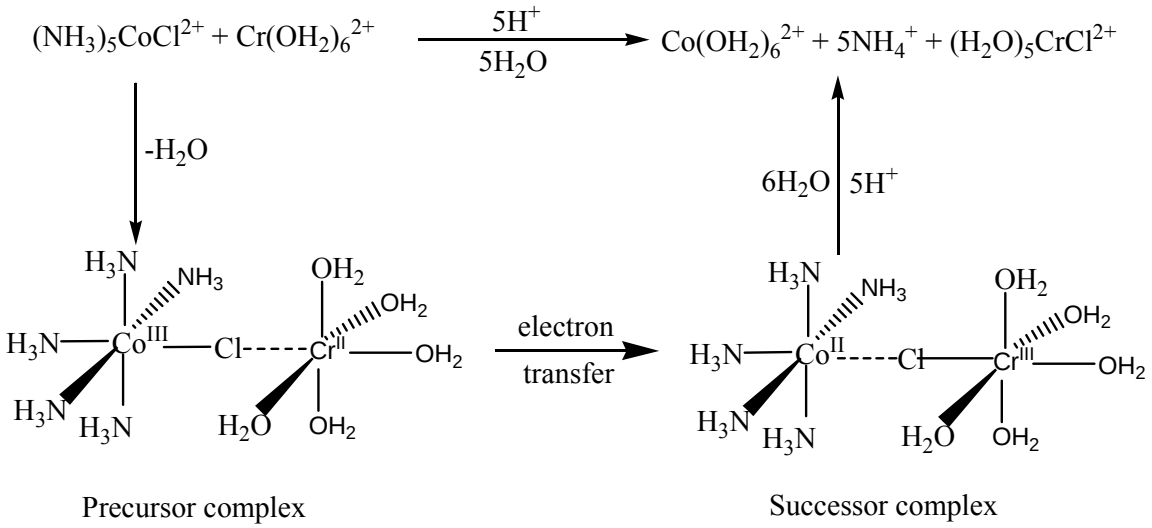

For outer-sphere electron transfer reactions, the coordination spheres of the oxidant and reductant remain intact during the electron transfer. Generally, both reductant and oxidant have nonlabile coordination spheres, and no ligand substitution occurs during the reaction. There are three steps in outer-sphere reactions. The first step is the formation of precursor. The second step is the electron transfer itself. The third step is dissociation of the successor complex, which is generally fast. In most cases, the electron-transfer step is rate limiting.

In 1954, Marcus theory was developed to better describe the behavior of outer-sphere reactions. The Franck-Condon principle is fundamental to the theory. The Franck-

Condon principle states that electron movement is much faster than nuclear motion. According to the Franck-Condon principle and Marcus theory, the time required for electron transfer between donor and acceptor nuclei is markedly less than the time needed for those nuclei to change their positions. Before the electron can be transferred, however, the free energies of the donor and acceptor species must become identical. This can only be achieved if the inner-sphere coordination shells and their solvent environments both simultaneously come into new and appropriate configurations. The reaction rate constant will depend largely on the reorganization energy ($\Delta G_{IS}^{\ddagger}$ and $\Delta G_{OS}^{\ddagger}$). Moreover, the Coulombic work ($\Delta G_{CO}^{\ddagger}$) between the donor and acceptor contributes to the free energy of activation as well. The self-exchange rate constants of outer-sphere reaction are obtained by applying the following equation:[91]

$$k_{calc} = \kappa_{el} \Gamma_n K_{os} \exp\left(\frac{-\Delta G^{\ddagger}}{RT}\right) \qquad (1\text{-}38)$$

$$\Delta G^{\ddagger} = \Delta G_{IS}^{\ddagger} + \Delta G_{OS}^{\ddagger} + \Delta G_{CO}^{\ddagger} \qquad (1\text{-}39)$$

where κ_{el} is the transmission coefficient, Γ_n represents the tunneling constant (unit: s^{-1}), K_{os} is the pre-exponential factor (unit: M^{-1}), $\Delta G^{\ddagger}$ represents the overall activation free energy.

However, the unavailability of $\Delta G_{IS}^{\ddagger}$, $\Delta G_{OS}^{\ddagger}$, and $\Delta G_{co}^{\ddagger}$ impedes the wide application of Equation 1-38. To overcome this limitation, the following simplified equation was developed by Marcus to calculate the self-exchange rate constant.[92]

$$k_{12} = (k_{11}k_{22}K_{12}f_{12})^{1/2}W_{12} \quad (1\text{-}40)$$

where k_{12} is the observed cross electron-transfer rate constant, k_{11} and k_{22} are the self-exchange rate constants of redox couple **1** and **2**, K_{12} is the cross electron-transfer equilibrium constant, W_{12} is work term, f_{12} is a factor, usually close to one.

In this research, the Marcus cross relationship was used to calculate the self-exchange rate constants for $^{\bullet}SCH_2CH(NH_3^+)CO_2^-/^-SCH_2CH(NH_3^+)CO_2^-$,and $^{\bullet}SCH_2CH(NH_2)CO_2^-/^-SCH_2CH(NH_2)CO_2^-$.

TECHNIQUES

Several techniques were used in this research, including NMR, UV-vis spectroscopy, cyclic voltammetry, atomic absorption spectroscopy, and stopped-flow spectrophotometry. NMR spectroscopy was used to determine the purity of synthesized ligands, identify the products of the reaction, and determine stoichiometric reaction ratios; cyclic voltammetry was employed to determine the standard potential of the outer-sphere Fe(III) complexes; atomic absorption spectroscopy was used to determine the copper concentration in the reactants and products; UV-vis spectroscopy was used to identify the reaction products, determine the stoichiometric ratio, and perform kinetic studies with slow rate constants. Most of the kinetic studies were carried out on a stopped-flow instrument. Here, we will present the basic principle of the stopped-flow technique.

The basic principle of the stopped-flow technique is to mix equal volumes of two reactant solutions in the flow cell simultaneously. Solutions are transferred into the

driving syringes and stored in a thermostated tank to keep the temperature of the solutions constant. Solutions are then injected into the optical flow cell by applying 5 bar of compressed air on the driving plate to push the plungers of the driving syringes. The solution mixture in the cell is then expelled to the stopping syringe and the plunger is pushed against the stopping block. The trigger on the stopping block then initiates the computing system to collect the signal from the detector at the same time.[93,94]

CHAPTER TWO

Direct Oxidation of *L*-Cysteine by $[Fe^{III}(bpy)_2(CN)_2]^+$ and $[Fe^{III}(bpy)(CN)_4]^-$

Introduction

Thiol-containing compounds play important roles in biochemical process, including maintaining cellular redox potentials, protecting cells against oxidative stress, and regulating metabolism and gene expression.[1-3,10,12] All of these processes involve thiol/disulfide exchange, hydrogen-atom transfer, or electron transfer.[2] The most important thiols in biological chemistry are cysteine, homocysteine, and glutathione. Cysteine, one of the essential α-amino acids and one of the simplest biological thiols with the oxidation state of -2 on element of sulfur, will not easily cleave at the C-S bond, and can undergo oxidation either by metal ions or nonmetallic oxidants to form sulfinic acid or disulfide, depending on the oxidative capability of the oxidant. The electron-transfer reaction of cysteine may be the mechanistic basis for the anti-oxidation of DNA, lipids and proteins.[95,8] Furthermore, the concentration of cysteine in living cells is very much indicative of a human being's physical condition: depletion of cysteine can accompany leukemia and several types of cancer; abnormally high levels of cysteine can be associated with brain disorders, chromosome aberrations, etc. Understanding the mechanism of the oxidation of cysteine by metal complexes will be beneficial to

developing rapid and reliable sensing techniques for detection of cysteine and other biological thiols, and therefore it will contribute to the prevention of some fatal disease.[3,96-98]

The oxidation of cysteine by metal cations or metal complexes has been widely investigated, and a variety of mechanisms have been proposed.[38,40,44,48-53,99-101] For metal-ion oxidants, such as V(V),[40] Cr(VI),[38] Fe(III),[44] a long lived cysteine-metal ion (RS-M) complex was observed in the reactions. To simplify their kinetic behavior, metal ions were replaced by some typical outer-sphere transition metal complexes, including $[Ir^{IV}Cl_6]^{2-}$,[48] $[Co^{III}W_{12}O_{40}]^{5-}$,[49] $[Fe^{III}(CN)_6]^{3-}$,[50] $[Co_2(CN)_{10}(O)_2]^{5-}$,[53] $[Mo^{V}(CN)_8]^{3-}$,[52] and $[\{(bpy)_2H_2ORu^{III}\}_2O]^{4+}$.[54] The reductions of $[Fe(^{III}CN)_6]^{3-}$, $[Co_2(CN)_{10}(O)_2]^{5-}$ and $[Mo^{V}(CN)_8]^{3-}$ are trace copper catalyzed, while no catalysis was reported for the reactions of $[Co^{III}W_{12}O_{40}]^{5-}$, $[Ir^{IV}Cl_6]^{2-}$, and $[\{(bpy)_2H_2ORu^{III}\}_2O]^{4+}$. It is possible that the copper catalysis was overlooked by the investigators of these reactions.

The ubiquitous copper catalysis was also observed in our group for the oxidation of thioglycolate (TGA) by $[Ir^{IV}Cl_6]^{2-}$,[102] $[Mo^{V}(CN)_8]^{3-}$,[103] and $[Os^{III}(phen)_3]^{3+}$,[104] and for the oxidation of *L*-cysteine by $[Mo^{V}(CN)_8]^{3-}$.[52] The kinetic complication due to copper catalysis was overcome with the addition of 2,6-pyridinedicarboxylic acid (dipicolinic acid, abbreviated as dipic hereafter). For the oxidation of TGA by $[Ir^{IV}Cl_6]^{2-}$, $[Mo^{V}(CN)_8]^{3-}$ and $[Os^{III}(phen)_3]^{3+}$, the weakest oxidant, $[Mo^{V}(CN)_8]^{3-}$, gives only disulfide as product; the strongest oxidant, $[Ir^{IV}Cl_6]^{2-}$, yields a mixture of the disulfide and the sulfonic acid; and the reduction of $[Os^{III}(phen)_3]^{3+}$, with intermediate standard potential between $[Mo^{V}(CN)_8]^{3-}$ and $[Ir^{IV}Cl_6]^{2-}$, shows dramatically different products: disulfide, $[Os^{III}(phen)_3]^{2+}$, and $[Os(phen)_2(phen\text{-}TGA)]^{2+}$. The different products of the

above direct outer-sphere redox reactions may be closely related to the oxidative capability of substitution inert transition-metal complexes. In the case of oxidation of *L*-cysteine by $[Mo^{V}(CN)_8]^{3-}$, the reaction also follows a similar mechanism—electron transfer from thiolate to form cysteinyl radical. The products of the reaction of $[Mo^{V}(CN)_8]^{3-}$ are a mixture of cystine and cysteinesulfinate.

To extend our understanding of the mechanism of oxidation of cysteine, two relatively weaker oxidants, $[Fe^{III}(bpy)_2(CN)_2]^{+}$ and $[Fe^{III}(bpy)(CN)_4]^{-}$, were selected in this study. The direct reduction of $[Fe^{III}(bpy)_2(CN)_2]^{+}$ is achieved with the addition of 1.0 mM $dipic^{2-}$, while that of $[Fe^{III}(bpy)(CN)_4]^{-}$ is achieved by the addition of EDTA (pH ≤ 10.0) or cyclam (pH > 10.0). No cysteinesulfinate was detected in the above two reactions. The rate of the reaction is pH-dependent. The mechanism for the direct oxidation of cysteine is proposed, revealing the rate limiting step of the reaction—electron transfer from the thiolate of cysteine to Fe(III). The self-exchange rate constants of $\bullet SCH_2CH(NH_3^{+})CO_2^{-}/^{-}SCH_2CH(NH_3^{+})CO_2^{-}$ and $^{\bullet}SCH_2CH(NH_2)CO_2^{-}$ $/^{-}SCH_2CH(NH_2)CO_2^{-}$ are obtained by applying Marcus' equations.

Experimental section

Reagents and solutions. Ferrous ammonium sulfate hexahydrate (Fisher), potassium cyanide (Fisher), 2,2'-bipyridyl (Aldrich), *L*-cysteine (Fluka), *L*-cystine (Aldrich), N-tert-butyl-α-phenylnitrone (PBN, Aldrich), cacodylic acid (Sigma), sodium phosphate monobasic monohydrate (J. T. Baker), sodium phosphate dibasic (MCB), sodium hydroxide (Fisher), D_2O (Aldrich), 3-(trimethylsilyl)-1-propanesulfonic acid, sodium salt (DSS, Aldrich), 5,5'-dithiobis (2-nitrobenzoic acid) (DTNB, Aldrich),

ammonium chloride (Fisher), sodium bicarbonate (J. T. Baker), sodium carbonate (Fisher), cupric sulfate (Fisher), nickel sulfate hexahydrate (Fisher), ferric nitrate nonahydrate (Fisher), ferrous sulfate heptahydrate (J. T. Baker), cobalt sulfate heptahydrate (Fisher), manganese sulfate monohydrate (Fisher), zinc sulfate heptahydrate (J. T. Baker), ammonium molybdate (Aldrich), ethylenediaminetetraacetic acid disodium salt dihydrate (abbreciated as EDTA hereafter, MCB), 2,6-pyridinedicarboxylic acid (abbreviated as dipic hereafter, Aldrich), 1,4,8,11-tetraazacyclotetradecane (cyclam, Aldrich), tetraphenylphosphonium chloride (Aldrich), chlorine gas (Matheson Gas Products, Inc), acetic acid (Fisher), sulfuric acid (Fisher), nitric acid (Fisher), hydrochloric acid (Fisher), chloroform (Fisher), dimethyl sulfoxide (DMSO, Fisher), and Dowex 50W-X8 resin (J. T. Baker) were used without further purification. The structure of several compounds is shown in Scheme 2-1.

Scheme 2-1

Thioglycolic acid

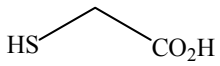

***L*-cysteine**

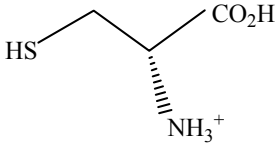

Dipicolinic acid

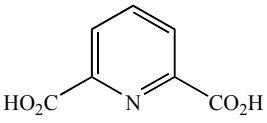

PBN

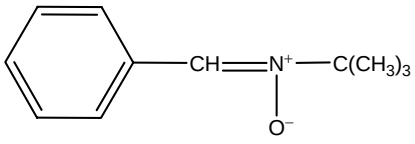

Cyclam

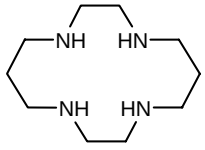

Sodium perchlorate (Fisher), lithium perchlorate (GFS chemical Co.), and sodium triflate (Aldrich) were recrystallized from hot water; their stock solutions were standardized by running an aliquot through a cation-exchange column packed with Dowex 50W-X8 resin, then titrating by standardized NaOH aqueous solution. Sodium acetate trihydrate (Fisher) was recrystallized from hot water and dried in a vacuum desiccator. Chloroacetic acid (Fisher) was recrystallized from hot water, and dried in a vacuum desiccator; stock solutions were titrated with standardized NaOH aqueous solution.

Distilled deionized water was obtained from a Barnstead NANO pure infinity ultrapure water system. All Fe(III) and *L*-cysteine solutions were prepared in de-ionized water just prior to use, and purged with Ar or N_2 for at least 15 minutes prior to the reaction to prevent possible complications caused by O_2. Fe(III) solutions were kept in the dark to prevent any photochemical changes. The concentration of *L*-cysteine was determined spectrophotometrically with Ellman's reagent at pH 7.46.[105,106]

Preparation of $[Fe^{II}(bpy)_2(CN)_2]\cdot 3H_2O$. $[Fe^{II}(bpy)_2(CN)_2]\cdot 3H_2O$ was prepared following a standard procedure.[107] 0.47 g of 2,2'-bipyridyl (3.0 mmol) and 0.39 g of ferrous ammonium sulfate hexahydrate (1.0 mmol) were added to 40.0 mL of water. The solution became dark red. Then it was heated to just below the boiling point. A freshly prepared solution of 1.00 g of KCN (15.4 mmol) in 2.0 mL of water was immediately added to the heated solution. After brief stirring, the solution was left to cool at room temperature for 4 hours. The dark violet product was obtained by vacuum filtration, rinsed with cool water, and dried in vacuum at room temperature. Yield of crude $[Fe^{II}(bpy)_2(CN)_2]\cdot 3H_2O$: 0.36 g (76%). For purpose of electronic spectra and

electrochemical measurements, a portion of the initial products was recrystallized from concentrated sulfuric acid (96.4%). The yield of recrystallized $[Fe^{II}(bpy)_2(CN)_2]\bullet 3H_2O$: 70%. Anal. Calcd for $C_{22}FeH_{22}N_6O_3$: C, 55.71; H, 4.68; N, 17.72. Found: C, 55.66; H, 4.41; N, 17.67. ^{1}H-NMR (400 MHz/D_2O): 9.40 (d, J = 6.5, 2H); 8.36 (d, J = 7.7, 2H); 8.32 (d, J = 8.0, 2H); 8.09 (t, J = 7.8, 2H); 7.92 (t, J = 7.8, 2H); 7.60 (t, J = 5.8, 2H); 7.32 (d, J = 6.0, 2H); 7.21 (t, J = 7.0, 2H).

Preparation of $[Fe^{III}(bpy)_2(CN)_2]NO_3\bullet 2H_2O$. $[Fe^{III}(bpy)_2(CN)_2]NO_3\bullet 2H_2O$ was synthesized by oxidation of $[Fe^{II}(bpy)_2(CN)_2]\bullet 3H_2O$ with nitric acid.[107] 1.60 mL of concentrated nitric acid (70%) was added to 0.40 g of the crude $[Fe^{II}(bpy)_2(CN)_2]\bullet 3H_2O$. A deep purple solution was formed, with the evolution of nitrogen dioxide. The mixture was slightly warmed to make the reaction complete. It was then diluted with 40.0 mL of distilled deionized water to give a purple precipitate. A purple solution was obtained by heating the mixture. Then the filtrate was obtained by filtering the hot clear solution. A purple precipitate was recovered after putting the filtrate in a refrigerator overnight. The product was obtained by vacuum filtration, rinsed with cool water, and dried in vacuum at room temperature. Yield of recrystallized $[Fe^{III}(bpy)_2(CN)_2]NO_3\bullet 2H_2O$: 0.28 g (65%). Anal. Calcd for $C_{22}FeH_{20}N_7O_5$: C, 50.98; H, 3.89; N, 18.92. Found: C, 51.02; H, 3.58; N, 19.11.

Preparation of $K_2[Fe^{II}(bpy)(CN)_4]\bullet 3H_2O$. Schilt's method[107] was used to prepare $K_2[Fe^{II}(bpy)(CN)_4]\bullet 3H_2O$. 0.474 g of $[Fe^{II}(bpy)_2(CN)_2]\bullet 3H_2O$ (1.00 mmol) and 19.5 g of KCN (0.299 mol) were mixed in 150.0 mL of water, and the solution was refluxed for 24 hrs. It was extracted with 50.0 mL of chloroform to remove the remaining $[Fe^{II}(bpy)_2(CN)_2]\bullet 3H_2O$. 90.0 mL of water was removed by heating the solution on a hot

plate at 70 °C. The remaining heated solution was placed in a refrigerator overnight. The dark brown precipitate was obtained by vacuum filtration. Yield of $K_2[Fe^{II}(bpy)(CN)_4]\cdot 3H_2O$: 0.425 g (95%). For purpose of electronic spectra and electrochemical measurements, a portion of the initial products was recrystallized from hot water. The yield of recrystallized $K_2[Fe^{II}(bpy)(CN)_4]\cdot 3H_2O$: 23%. ^{1}H-NMR (400 MHz/D_2O): 9.32 (d, J = 4.9, 2H), 8.20 (d, J = 7.6, 2H), 7.94 (t, J = 7.8, 2H), 7.47 (t, J = 6.7, 2H)

Preparation of $Li[Fe^{III}(bpy)(CN)_4]\cdot 2.5H_2O$. $Li[Fe^{III}(bpy)(CN)_4]\cdot 2.5H_2O$ was prepared according to published procedures.[108] Chlorine gas was bubbled through a warm (T ≈ 50 °C) dark red aqueous solution (40.0 mL) of $K_2[Fe^{II}(bpy)(CN)_4]\cdot 3H_2O$ (1.10 mmol) for 30.0 minutes under continuous stirring, leading to a color change from red to orange. A concentrated warm aqueous solution of tetraphenylphosphonium chloride (0.449 g/6.0 mL H_2O, 1.20 mmol) was added to the above solution, and the solution was kept heating and stirring for 10 minutes. An orange solid ($PPh_4[Fe^{III}(bpy)(CN)_4]\cdot H_2O$) was obtained by vacuum filtration. To prepare $Li[Fe^{III}(bpy)(CN)_4]\cdot 2.5H_2O$, 0.251 g of lithium perchlorate (1.50 mmol) was slowly added to an acetonitrile solution (0.805 g/13.0 mL) of $PPh_4[Fe^{III}(bpy)(CN)_4]\cdot H_2O$ (1.20 mmol). An orange precipitate was collected by vacuum filtration and dried in a vacuum desiccator for 12 hrs. Yield of $Li[Fe^{III}(bpy)(CN)_4]\cdot 2.5H_2O$: 0.292 g (66%). Anal. Calcd for $C_{14}FeH_{12.4}LiN_6O_{2.2}$: C, 46.32; H, 3.39; N, 23.17. Found: C, 46.37; H, 3.54; N, 22.90.

Methods. All single UV-vis spectra were recorded on a HP-8453 or HP-8452 diode-array spectrophotometer equipped with 1 cm cells and a Brinkman Lauda RM6 thermostated water bath to maintain the temperature at 25.0 ± 0.1 °C. Cyclic

voltammograms and Osteryoung Square Wave Voltammograms (OSWV) were recorded at room temperature on a BAS 100 B electrochemical analyzer equipped with BAS cell stand C3 with purging and stirring system, using a glassy carbon working electrode (d = 3.1 mm), Ag/AgCl (3.0 M NaCl) reference electrode, and a Pt wire auxiliary electrode. The scan rate was 100 mV/s. A 450 Corning pH/ion meter with a Mettler Toledo InLab 421 pH electrode was used for pH measurement. ^{1}H NMR spectra were obtained on a multi-pulse Bruker AV 400 spectrometer. Kinetic studies were performed by mixing equal volumes of the two reactants on a Hi-Tech Scientific model SF-51 stopped-flow apparatus that was equipped with a SU-40 spectrophotometer unit and a 2095 circulatory water bath. Temperature was maintained at 25.0 ± 0.1^{o}C. An Olis 4300S system was used for data acquisition and analysis. All apparent rate constants were the average of at least five runs with ± 5% error or less. Reactions were monitored at 522 nm ($Fe^{II}(bpy)_2(CN)_2$, ε_{522} = 5115 M^{-1} cm^{-1}) and 482 nm ($[Fe^{II}(bpy)(CN)_4]^{2-}$, ε_{482} = 2825 M^{-1} cm^{-1}), and the rate constants were obtained by fitting the data with OLIS-supplied first-order functions. A nonlinear-least squares computer program with relative weighting (weighting by $1/Y^2$) was used to fit the overall rate law to the values of k_{obs}. SPECFIT/32 version 3.0.15 global analysis system was applied to simulate the reaction traces. For all kinetics studies, the concentration of *L*-cysteine was at least ten times greater than that of Fe(III) complexes.

Results

Characterization of the iron complexes. The UV-vis absorbance characteristics of the iron complexes are shown in Table 2-1, in which the extinction coefficients are very

close to previous reports.[107,109] The cyclic voltammograms (CV) of $[Fe^{III}(bpy)_2(CN)_2]^+$ and $[Fe^{III}(bpy)(CN)_4]^-$ are quasi-reversible. The CV of 1.0 mM $[Fe^{III}(bpy)_2(CN)_2]^+$ in 0.10 M $NaCF_3SO_3$ is shown in Figure 2-1, with $\Delta E_{p/p} = 67$ mV, and $E_{1/2} = 554$ mV ($E_{1/2} = (E_{pc} + E_{pa})/2$) versus $Ag/AgCl_{(s)}$ ($E^o_{Ag/AgCl(s)} = 0.205$ V vs NHE[110]) that is, 0.759 V versus a normal hydrogen electrode, the same as Terrettaz's report.[111] The CV of 0.70 mM $[Fe^{III}(bpy)(CN)_4]^-$ in 0.10 M $NaCF_3SO_3$ is shown in Figure 2-2, with $\Delta E_{p/p} = 64$ mV, and $E_{1/2} = 332$ mV versus $Ag/AgCl_{(s)}$ ($E^o_{Ag/AgCl(s)} = 0.205$ V vs NHE[110]), that is, 0.537 V versus a normal hydrogen electrode, the same as previous reports.[111,112] The OSWVs of 1.0 mM $[Fe^{III}(bpy)_2(CN)_2]^+$ and 0.70 mM $[Fe^{III}(bipy)(CN)_4]^-$ in 0.10 M $NaCF_3SO_3$ are shown in Figure 2-3 and Figure 2-4, both of them consistent with their CV results. Figure 2-5 shows the ^{1}H-NMR spectrum of 0.20 mM $Fe^{II}(bpy)_2(CN)_2$ with 1.0 mM DSS as reference in D_2O, the same as Agrawala's NMR report.[113] The ^{1}H-NMR spectrum of 1.0 mM $[Fe^{II}(bipy)(CN)_4]^{2-}$ in D_2O is shown in Figure 2-6, which is consistent with its structure, except that one very small singlet at 8.43 ppm is unexplainable.

Table 2-1. UV-visible absorbance and electrochemical characteristics of the iron complexes in aqueous solution

Compounds	Band	λ_{max}, nm	ε, M^{-1} cm^{-1}		$E_{1/2}$, mV [a]
			our work	references	
$Fe^{II}(bpy)_2(CN)_2$	I	352	5258		
	II	522	5522	5800	
$[Fe^{III}(bpy)_2(CN)_2]NO_3$	I	394	1224	1200	759 ± 2
	II	544	241	200	
$K_2[Fe^{II}(bpy)(CN)_4]$	I	346	3437	3470	
	II	482	2825	2880	
$Li[Fe^{III}(bpy)(CN)_4]$	I	375	1474	1450	
	II	416	938	920	537 ± 2

[a] $E_{1/2}$ vs NHE, at 22.0 °C and μ = 0.10 M. $E_{1/2} = E_f$

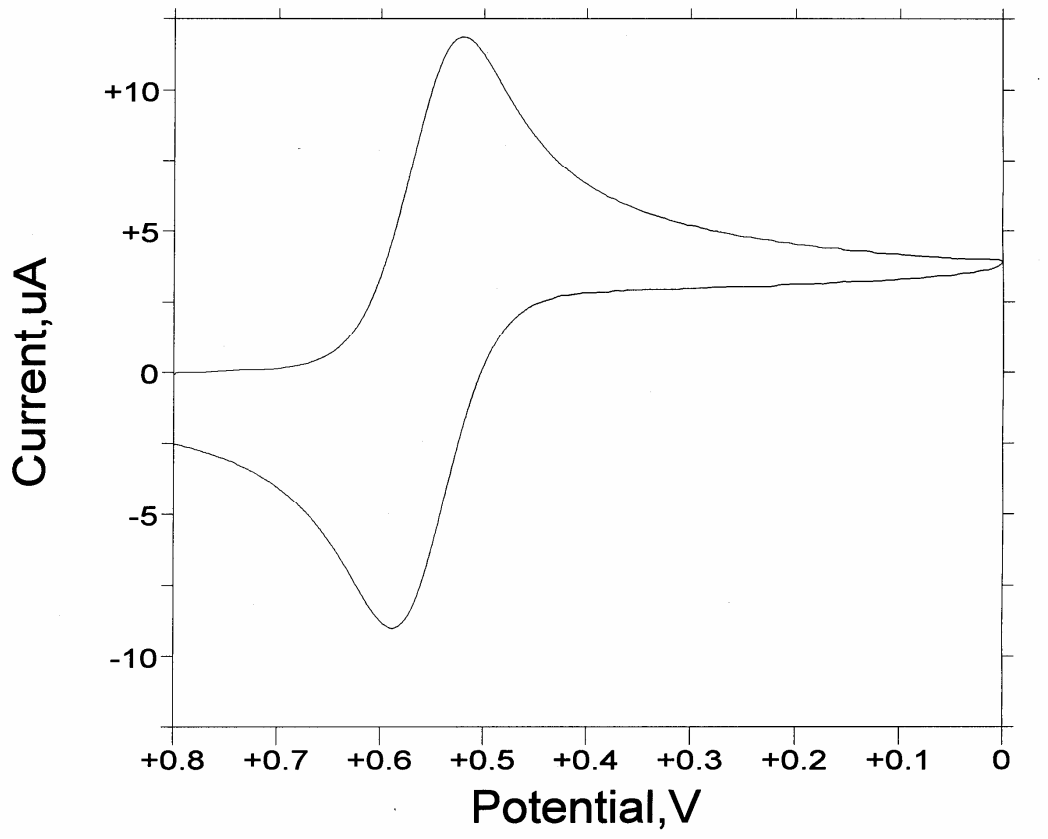

Figure 2-1. The CV of 1.0 mM $[Fe^{III}(bpy)_2(CN)_2]^+$ in 0.10 M $NaCF_3SO_3$. With a glassy carbon disc as working electrode, an Ag/AgCl(s) reference electrode, and a Pt wire as a counter electrode.

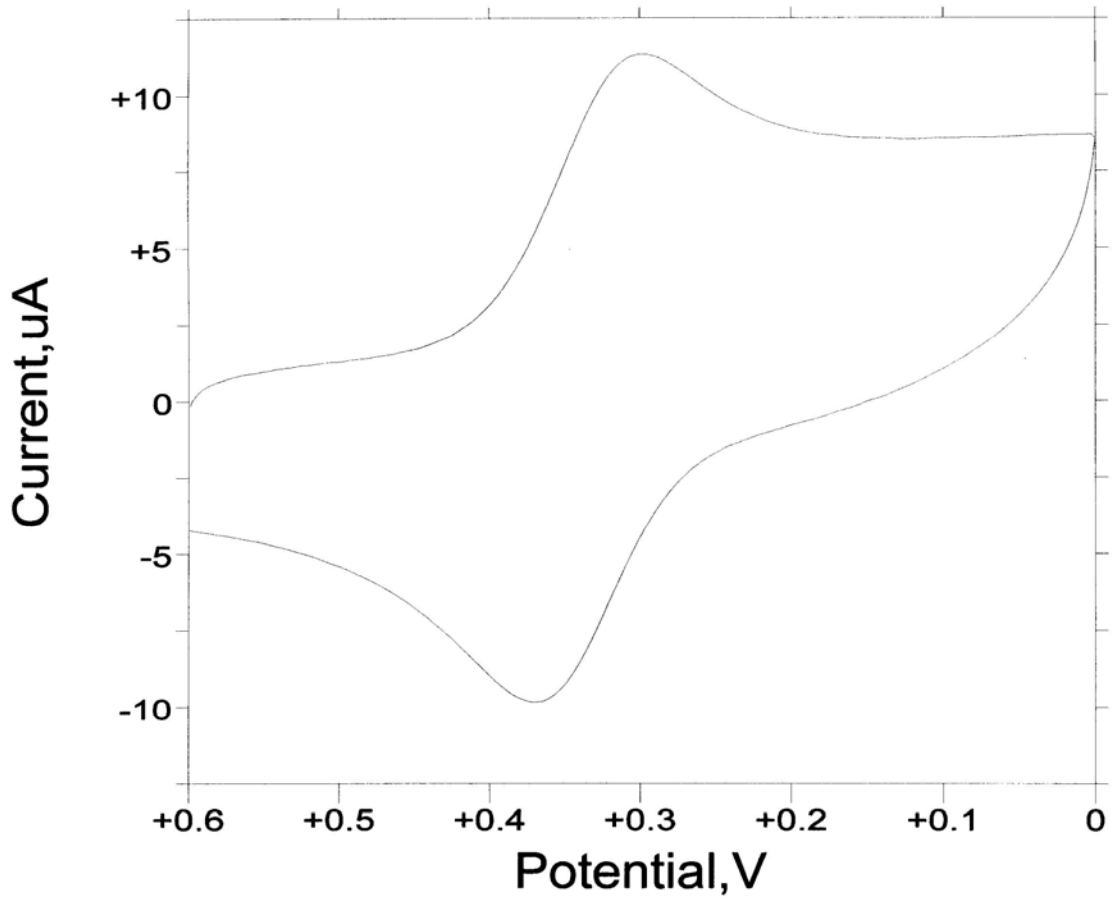

Figure 2-2. The CV of 0.70 mM $[Fe^{III}(bpy)(CN)_4]^-$ in 0.10 M $NaCF_3SO_3$. With a glassy carbon disc as working electrode, an Ag/AgCl(s) reference electrode, and a Pt wire as a counter electrode.

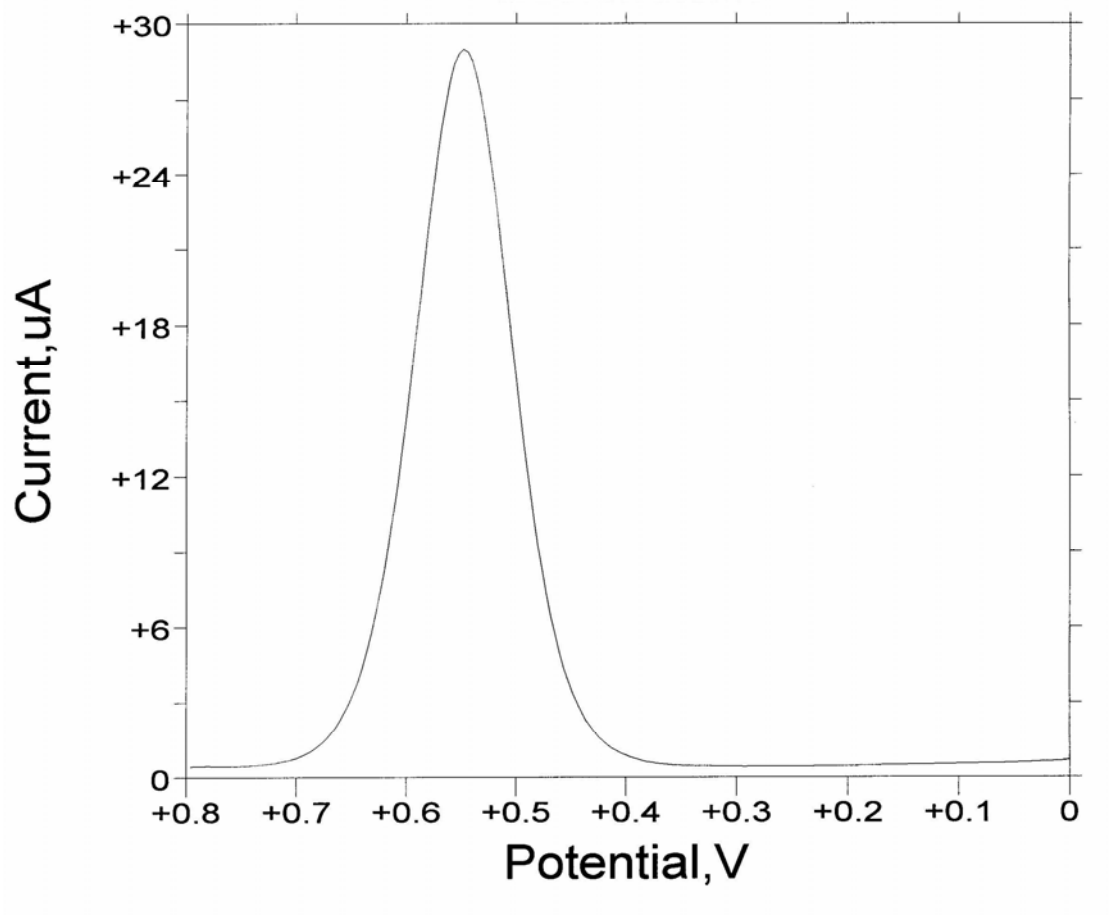

Figure 2-3. The OSWV of 1.0 mM $[Fe^{III}(bpy)_2(CN)_2]^+$ in 0.10 M $NaCF_3SO_3$. With a glassy carbon disc as working electrode, an Ag/AgCl(s) reference electrode, and a Pt wire as a counter electrode, with E_p = 556 mV.

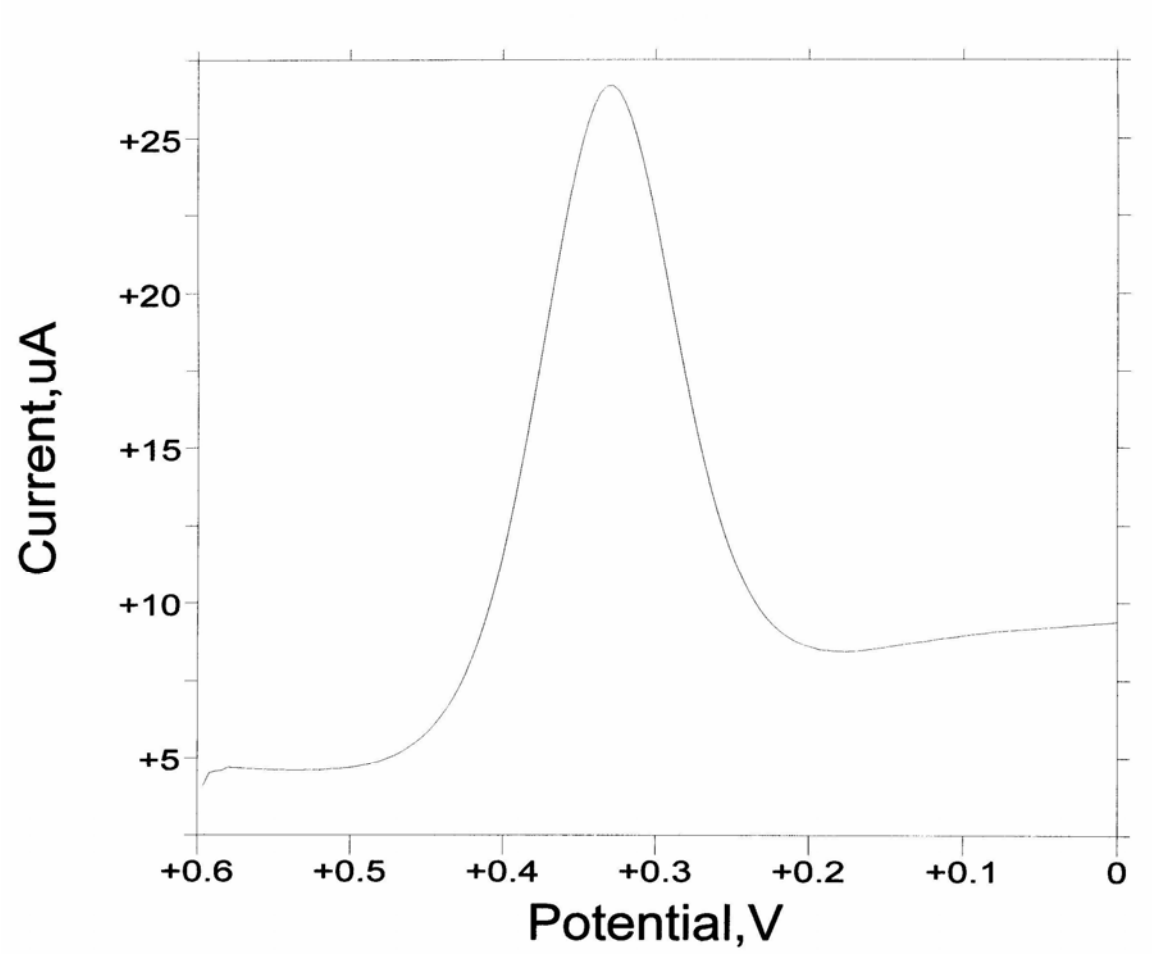

Figure 2-4. The OSWV of 0.70 mM $[Fe^{III}(bpy)(CN)_4]^-$ in 0.10 M $NaCF_3SO_3$. With a glassy carbon disc as working electrode, an Ag/AgCl(s) reference electrode, and a Pt wire as a counter electrode, with E_p = 335 mV.

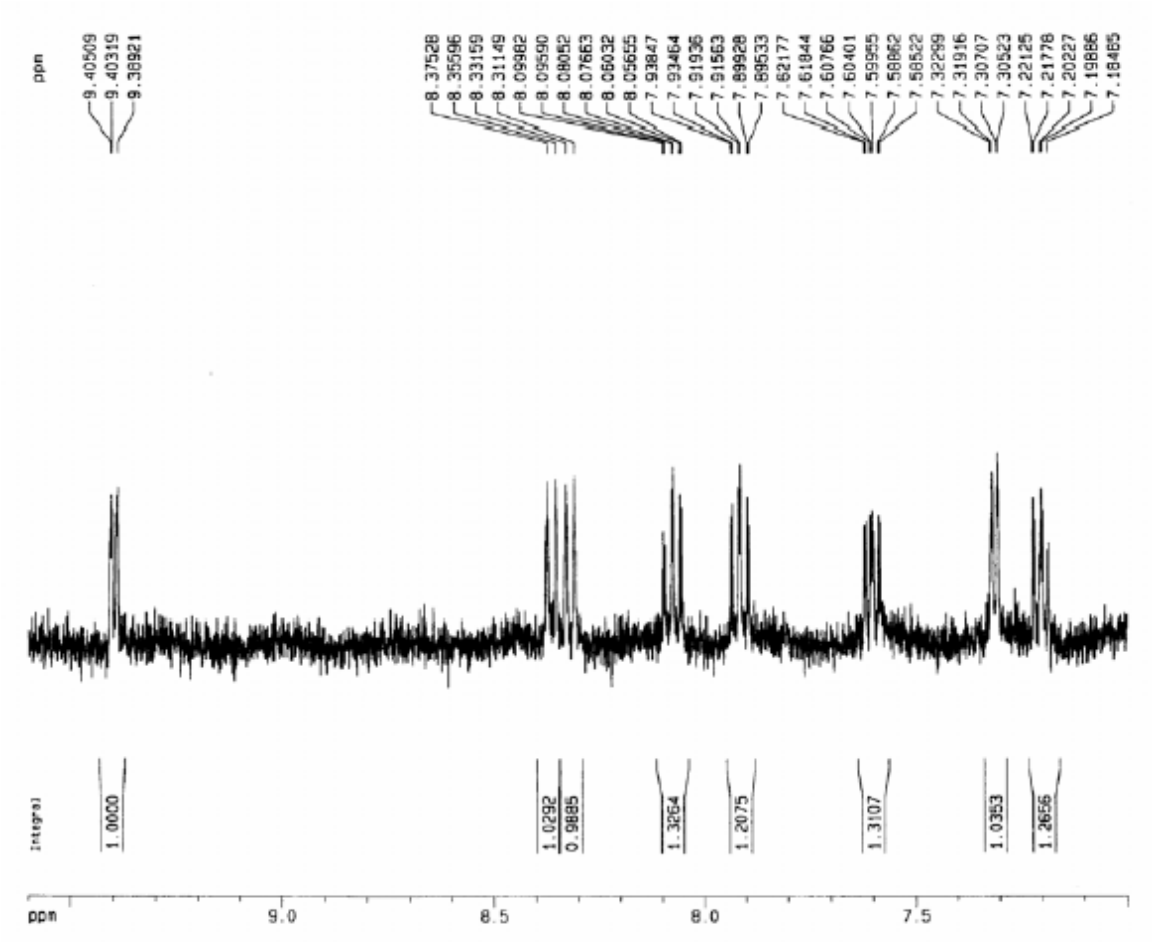

Figure 2-5. ^{1}H-NMR spectrum of 0.20 mM $Fe^{II}(bpy)_2(CN)_2$ in D_2O, with 1.0 mM DSS as reference.

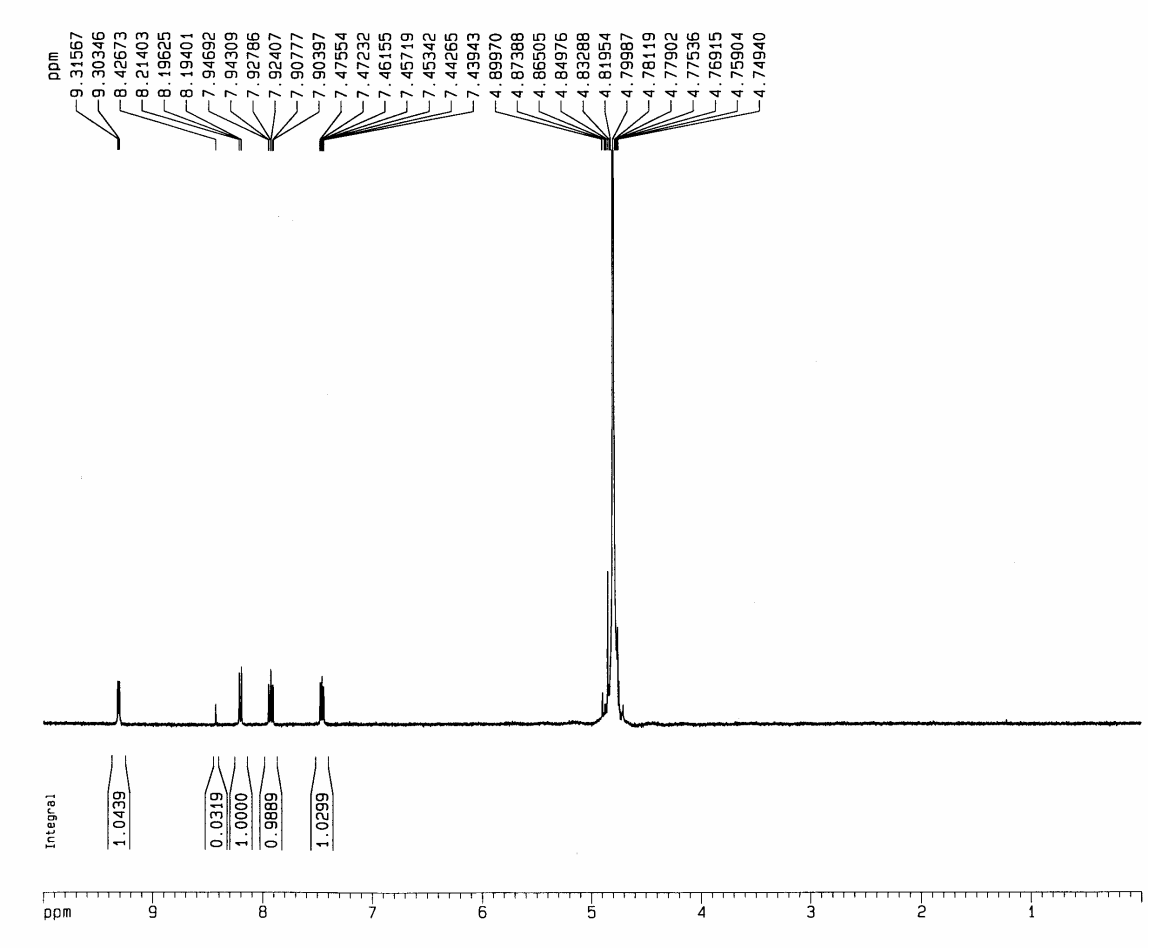

Figure 2-6. ^{1}H-NMR spectrum of 1.0 mM $[Fe^{II}(bpy)(CN)_4]^{2-}$ in D_2O.

Stability of $[Fe^{III}(bpy)_2(CN)_2]^+$ in aqueous solution. Although cyanide ligands stabilize the +3 oxidation state of iron in $[Fe^{III}(bpy)_2(CN)_2]^+$ and $[Fe^{III}(bpy)(CN)_4]^-$, Papula et al. have found that $[Fe^{III}(bpy)_2(CN)_2]^+$ is photo-reduced to $Fe^{II}(bpy)_2(CN)_2$ with a slow rate under a mercury arc lamp at pH 7.0.[109] In our kinetic studies, the pH ranges from 2.95 to 7.89 for the reduction of $[Fe^{III}(bpy)_2(CN)_2]^+$. So it is of importance to know the stability of the Fe(III) complex in the dark under the pH studied. The UV-vis spectra of 0.50 mM $[Fe^{III}(bpy)_2(CN)_2]^+$ in 10.0 mM chloroacetate buffer (pH = 3.05) and 10.0 mM phosphate buffer (pH = 7.98) were recorded on a HP 8453 diode-array spectrophotometer with a cycle time of 30 s in the range of 3600 s, respectively. The absorbance at 394 nm for the above solutions was constant over 3600 s. Therefore, it is safe to run kinetic experiments in the dark.

Metal-ion catalysis and scavenger effect. The copper catalysis is ubiquitous in the oxidation of thiols by inert transition metal complexes.[50,52,53,102-104,114] For the oxidation of *L*-cysteine by $[Fe^{III}(bpy)_2(CN)_2]^+$ and $[Fe^{III}(bpy)(CN)_4]^-$, some preliminary experiments were performed on the SF-51 stopped-flow apparatus. For the oxidation of 1.20×10^{-3} M *L*-cysteine by 5.0×10^{-5} M $[Fe^{III}(bpy)_2(CN)_2]^+$ at pH 4.76 (10.0 mM acetate buffer) and 25.0 ^oC, in the presence of 0.092 M $NaCF_3SO_3$ (μ = 0.10 M), the half-life is 0.36 s. With the addition of 5.0 μM $CuSO_4$, the rate of the reaction is so fast that it occurs within the deadtime of the instrument (~ 2 ms). Then 5.0 μM Zn^{2+}, Ni^{2+}, Fe^{2+}, Co^{2+}, Mn^{2+} and Mo(VI) were deliberately added to the above reactants (no Cu^{2+}), respectively, the half-life is about 0.22 s for each reaction (Table 2-2). For the oxidation of 2.60×10^{-3} M *L*-cysteine by 5.0×10^{-5} M $[Fe^{III}(bpy)(CN)_4]^-$ at pH 5.96 (10.0 mM cacodylate buffer) and 25.0 ^oC, in the presence of 0.093 M $NaClO_4$, the half-life is 0.373 s; With the addition of

1.0 μM $CuSO_4$, the half-life of the reaction is only 0.0250 s, as shown in Table 2-3. The above results clearly demonstrate that traces of copper ions are good catalysts for the oxidation of *L*-cysteine by $[Fe^{III}(bpy)_2(CN)_2]^+$ and $[Fe^{III}(bpy)(CN)_4]^-$ in aqueous solution.

Table 2-2. Effect of metal cations on the oxidation of *L*-cysteine by $[Fe^{III}(bpy)_2(CN)_2]^+$. With the addition of 0.092 M $NaCF_3SO_3$ and 10.0 mM acetate buffer, at 25.0 °C.[a]

$[M^{n+}]$, μM	$t_{1/2}$, s	pH of product
0	0.36	4.76
$[Cu^{2+}] = 5.0$	< 0.002[b]	4.76
$[Ni^{2+}] = 5.0$	0.25	4.75
$[Fe^{2+}] = 5.0$	0.20	4.78
$[Co^{2+}] = 5.0$	0.21	4.74
$[Mn^{2+}] = 5.0$	0.22	4.78
$[Mo^{VI}] = 5.0$	0.24	4.76
$[Zn^{2+}] = 5.0$	0.24	4.77

[a] $[L\text{-cysteine}]_0 = 1.20 \times 10^{-3}$ M, $[Fe^{III}(bpy)_2(CN)_2^+]_0 = 5.0 \times 10^{-5}$ M. [b] the dead time for SF-51 apparatus is 2 ms.

Table 2-3. Effect of EDTA on the reaction of $[Fe^{III}(bpy)(CN)_4]^-$ with *L*-cysteine. In the presence of 0.093 M $NaClO_4$ and 10.0 mM cacodylate buffer (pH = 5.96), at 25.0 °C.

	$[Cu^{2+}]$, μM	[EDTA], mM	$t_{1/2}$, s
#1	0.0	0.0	0.373
#2	1.0	0.0	0.0250
#3	0.0	2.0	20.3
#4	0.0	5.0	20.3
#5	1.0	2.0	19.7
#6	1.0	5.0	19.5

[a] $[L\text{-cysteine}]_0 = 2.60 \times 10^{-3}$ M, $[Fe^{III}(bpy)(CN)_4^-]_0 = 5.0 \times 10^{-5}$ M.

The copper-catalysis effect was successfully inhibited with the addition of 2,6-pyridinedicarboxylic acid (dipic) in the oxidation of TGA and *L*-cysteine by $[Mo(CN)_8]^{3-}$.[52,103] For the oxidation of *L*-cysteine by $[Fe^{III}(bpy)_2(CN)_2]^+$, the copper-catalysis effect was completely suppressed by adding sodium dipicolinate dihydrate ($Na_2(C_7H_3NO_4)\bullet 2H_2O$), which was synthesized by mixing dipic with 2 equivalent NaOH, then drying by rotary evaporation. The ^{1}H-NMR spectrum of sodium dipicolinate is shown in Figure 2-7, in which the doublet and triplet are overlapped. The Differential Scanning Calorimetry (DSC) of sodium dipicolinate is shown in Figure 2-8. Thermodynamic calculation based on the enthalpy value at 100 ^oC confirms that it has two molecules of water. For the oxidation of 6.0×10^{-4} M *L*-cysteine by 5.0×10^{-5} M $[Fe^{III}(bpy)_2(CN)_2]^+$ at pH 3.60 (10.0 mM chloroacetate buffer) and 25.0 ^oC, in the presence of 0.092 M $NaCF_3SO_3$ (μ = 0.10 M), 1.0 mM $dipic^{2-}$/dipic(1:1) is sufficient to control the pH and inhibit the copper ion catalysis, as shown in Table 2-4. For the later kinetic studies, 1.0 mM $dipic^{2-}$/dipic (1:1, for pH < 4.0), and 1.0 mM $dipic^{2-}$ (for pH > 4.0) were added to inhibit the copper-catalysis effect.

Table 2-4. Effect of $dipic^{2-}$ on the reaction of $[Fe^{III}(bpy)_2(CN)_2]^+$ with *L*-cysteine. In the presence of 10.0 mM chloroacetate buffer (pH = 3.60), at μ = 0.10 M (0.092 M $NaCF_3SO_3$) and 25 ^oC.[a]

	$[Cu^{2+}]$, μM	$[dipic^{2-}/dipic]$, mM	$t_{1/2}$, s
#1	0.0	0.0	0.770
#2	0.0	1.0	20.0
#3	5.0	0.0	0.006
#4	5.0	1.0	20.0
#5	5.0	2.0	20.0

[a] $[L\text{-cysteine}]_0 = 6.0 \times 10^{-4}$ M, $[Fe^{III}(bpy)_2(CN)_2^+]_0 = 5.0 \times 10^{-5}$ M.

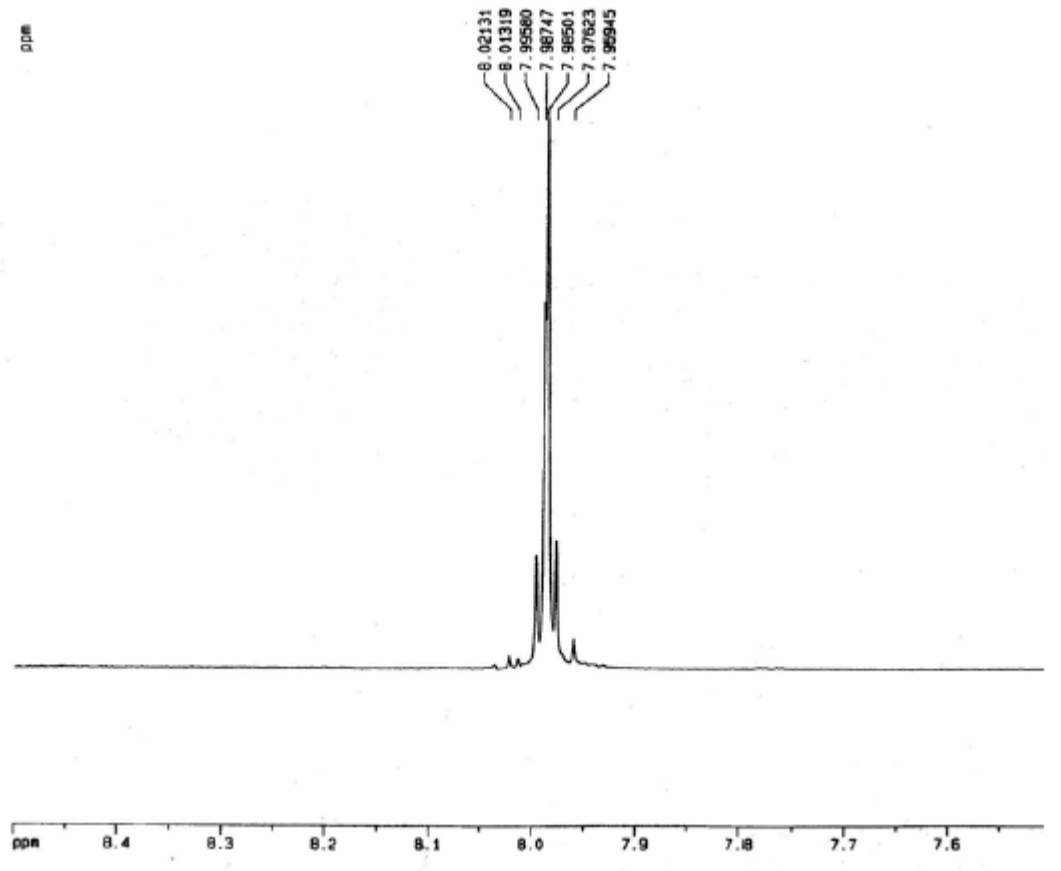

Figure 2-7. ^{1}H-NMR spectrum of 12.0 mM sodium dipicolinate in D_2O.

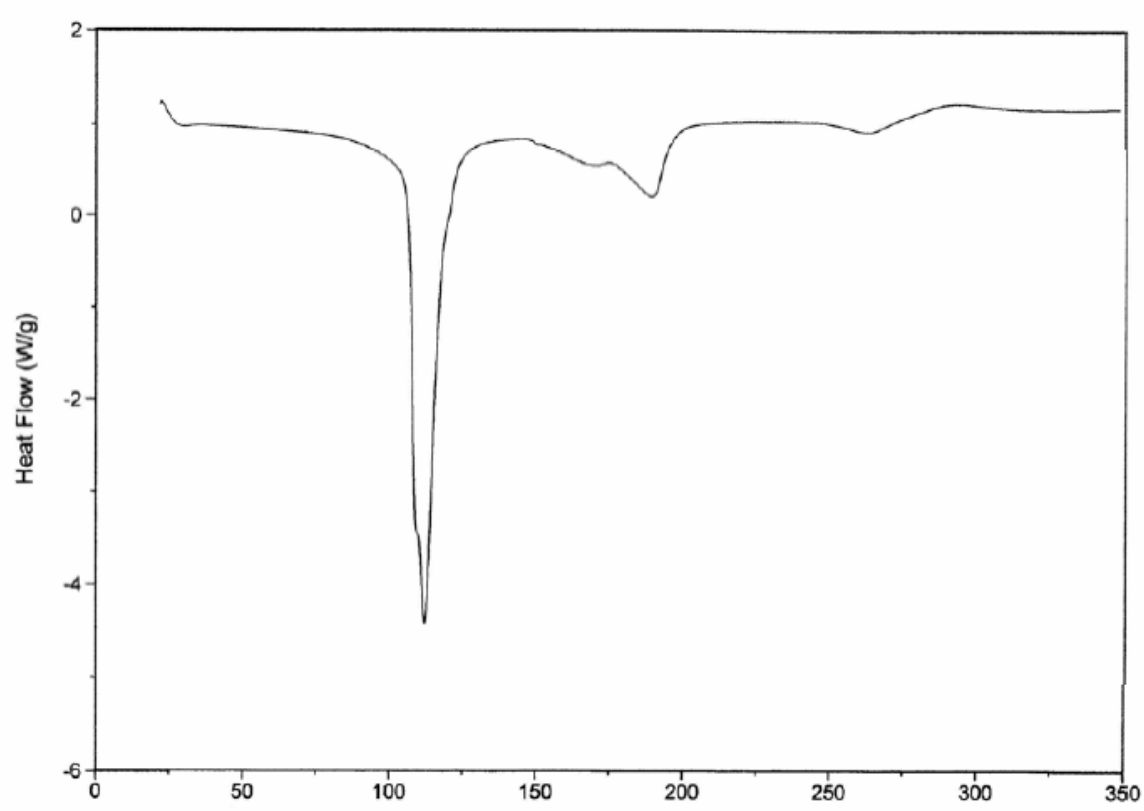

Figure 2-8. DSC (Differential Scanning Calorimetry) of sodium dipicolinate dihydrate

However, for the oxidation of *L*-cysteine by $[Fe^{III}(bpy)(CN)_4]^-$, the copper-catalysis is still dominant with the addition of 1.0 mM $dipic^{2-}$. At pH 6.0, when the concentration of dipic is 2.0 mM or higher is the copper-catalysis well masked. When the pH of the solution is 7.80 or greater, copper-catalysis can't be inhibited even with the addition of 5.0 mM $dipic^{2-}$, as shown in Table 2-5 and the highly non-first-order kinetics shown in Figure 2-9. Compared with $[Mo^V(CN)_8]^{3-}$($E_{1/2}$ = 0.771 V[103] vs NHE) and $[Fe^{III}(bpy)_2(CN)_2]^+$ ($E_{1/2}$ = 0.759 V[111] vs NHE), $[Fe^{III}(bpy)(CN)_4]^-$ is a much weaker oxidant. To completely inhibit strong copper catalysis, EDTA (pH ≤ 10.0), and cyclam (pH > 10.0) were used in our kinetic studies.

Table 2-5. Effect of $dipic^{2-}$ on the reaction of 5.0×10^{-5} M $[Fe^{III}(bpy)(CN)_4]^-$ with *L*-cysteine at various pHs. In the presence of $dipic^{2-}$ and 10.0 mM buffer solution, at 25.0 °C.

$[L\text{-cysteine}]_0$, mM	$[dipic^{2-}]$, mM	$[Cu^{2+}]_{added}$, μM	$[NaCF_3SO_3]$, M	pH	$t_{1/2}$, s	k_{obs}, s^{-1}
2.54	1.0	0.0	0.093	5.99	14.9	×[a]
2.54	2.0	0.0	0.093	6.00	17.0	0.0384
2.51	2.0	1.0	0.093	6.01	16.3	×[a]
2.54	5.0	0.0	0.093	6.02	17.0	0.0419
2.50	5.0	1.0	0.093	6.03	18.0	0.0393
2.50	7.5	0.0	0.093	6.04	16.0	0.0420
2.50	10.0	0.0	0.093	6.05	18.0	0.0421
0.470	5.0	0.0	0.056	7.80	1.63[b]	×[a]
1.02	2.0	0.0	0.075	9.89	0.017	40.2
1.02	5.0	0.0	0.075	9.87	0.021	32.2
1.02	5.0	0.25	0.075	9.88	0.0085	78.2
1.02	5.0	1.0	0.075	9.88	0.0031	207

[a] Non-first order; [b] irreproducible.

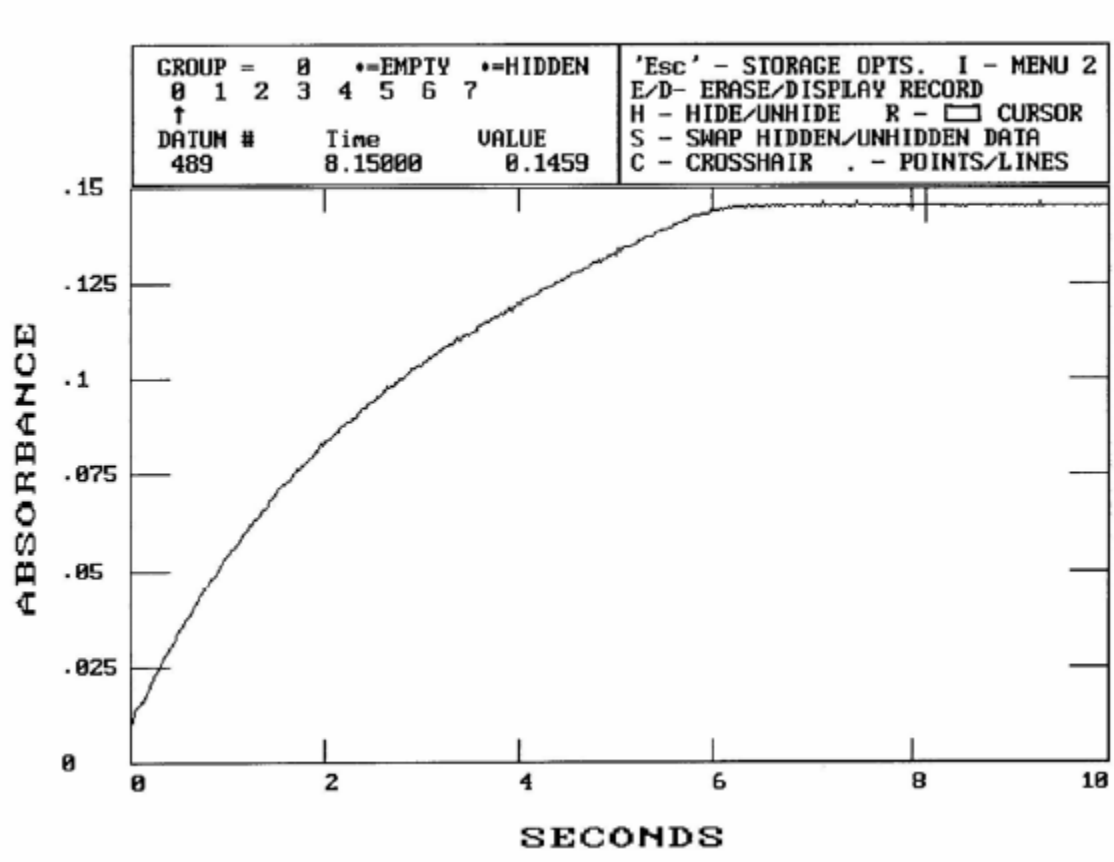

Figure 2-9. A reaction trace of oxidation of 4.7×10^{-4} M *L*-cysteine by 5.0×10^{-5} M $[Fe^{III}(bpy)(CN)_4]^-$ at pH 7.80 (10.0 mM phosphate buffer), with the addition of 5.0 mM $dipic^{2-}$. At $\mu = 0.10$ M (0.056 M $NaClO_4$) and 25.0 ^oC.

For the oxidation of 2.60×10^{-3} M *L*-cysteine by 5.0×10^{-5} M $[Fe^{III}(bpy)(CN)_4]^-$ at pH 5.96 (10.0 mM cacodylate buffer) and 25.0 ^oC, in the presence of 0.093 M $NaClO_4$, 2.0 mM EDTA is able to inhibit the copper ion catalysis, as shown in Table 2-3. Furthermore, iron cation is an omnipresent impurity in the chemical reagents, and it was reported that Fe-EDTA complex is a good catalyst for the oxidation of hydroxylamine by hexacyanoferrate(III).[115] The above catalytic feature prompted us to test whether the Fe-EDTA complex acts as a catalyst in the oxidation of *L*-cysteine by $[Fe^{III}(bpy)(CN)_4]^-$. For the oxidation of 2.50×10^{-3} M *L*-cysteine by 5.0×10^{-5} M $[Fe^{III}(bpy)(CN)_4]^-$ at pH 5.90 (10.0 mM cacodylate buffer) and 25.0 ^oC, in the presence of 0.093 M $NaCF_3SO_3$, a series of experiments was performed on SF-51 apparatus. First, 1.0 mM EDTA was added; second, 1.0 mM EDTA and 1.0 μM $CuSO_4$ were added; third, 1.0 mM EDTA and 1.0 μM $Fe(NO_3)_3$ were added. The rate constants for these three reactions shown in Table 2-6 are about 0.030 s^{-1}, ruling out catalysis by Fe-EDTA. To completely inhibit copper catalysis, 5.0 mM EDTA was employed in later kinetic studies at pH values no higher than 9.0. For the oxidation of 5.0×10^{-4} M *L*-cysteine by 5.0×10^{-5} M $[Fe^{III}(bpy)(CN)_4]^-$, the data in Table 2-7 indicate that copper ion catalysis is fully masked with the addition of 10.0 mM EDTA (pH = 10.0). However, our preliminary kinetic results demonstrate that EDTA fails to suppress copper catalysis at pH values higher than 10.0. The higher stability constant of 1,4,8,11-tetra-azacyclotetradecane (cyclam) with copper (II) than that of EDTA makes it a possible alternative chelating reagent in the above reaction.[116,117] It is assumed that, at very high pH, the fully deprotonated cyclam are coordinated to copper(II) cation. The relativly high pK_a values of cyclam and its poor solubility at low pH limits its chelating efficiency at lower pH.[118,119] Our preliminary kinetic studies (see Table 2-7)

confirm that copper-catalysis is inhibited with the addition of 1.0 mM cyclam at pH higher than 10.0. In our later kinetic studies, 5.0 mM EDTA (pH ≤ 9.00), 10.0 mM EDTA (9.00 < pH ≤ 10.0) and 1.0 mM cyclam (pH > 10.0) were added to inhibit the copper-catalysis.

Table 2-6. Effects of Fe^{3+} and Cu^{2+} on reaction of $[Fe^{III}(bpy)(CN)_4]^-$ with *L*-cysteine. In the presence of 0.093 M $NaCF_3SO_3$ and 10.0 mM cacodylate buffer, at 25.0 °C

	$[Fe^{3+}]$, μM	[EDTA], mM	pH	$t_{1/2}$, s	k_{obs}, s^{-1}
#1	0.0	1.0	5.89	26.0	0.0278
#2	1.0	1.0	5.91	24.5	0.0299
#3	0.0[b]	1.0	5.91	24.0	0.0301

[a] $[L\text{-cysteine}]_0 = 2.50 \times 10^{-3}$ M, $[Fe^{III}(bpy)(CN)_4^-]_0 = 5.0 \times 10^{-5}$ M, [b] $[Cu^{2+}] = 1.0$ μM

Table 2-7. Effect of EDTA/cyclam on reaction of $[Fe^{III}(bpy)(CN)_4]^-$ with *L*-cysteine. In the presence 10.0 mM EDTA or 1.0 mM cyclam, at 25.0 °C

[EDTA], mM	$[Cu^{2+}]_{added}$, μM	$[NaClO_4]$, M	[buffer], mM	pH	$t_{1/2}$, s	k_{obs}, s^{-1}
10.0	0.0	0.0	0.0	10.21	0.28	2.21
10.0	0.25	0.0	0.0	10.22	0.25	×[b]
0.0[c]	0.0	0.099	0.0[d]	10.98	0.16	4.30
0.0[c]	0.50	0.099	0.0[d]	10.91	0.15	4.35
0.0[c]	0.0	0.090	0.0[e]	11.90	0.28	5.19
0.0[c]	0.50	0.090	0.0[e]	11.85	0.24	5.19

[a] $[L\text{-cysteine}]_0 = 5.0 \times 10^{-4}$ M, $[Fe^{III}(bpy)(CN)_4^-]_0 = 5.0 \times 10^{-5}$ M, [b] Non pseudo-first order; [c] [cyclam] = 1.0 mM; [d] [NaOH] = 1.0 mM; [e] [NaOH] = 10.0 mM.

Note the concentration of copper cation in products' solution was determined by AA 240 Atomic Absorption Spectrometer. For the oxidation of 2.0×10^{-3} M *L*-cysteine by 5.0×10^{-5} M $[Fe^{III}(bpy)_2(CN)_2]^+$ at $\mu = 0.10$ M and pH = 6.94, the concentration of copper cation in the product solution is 0.25 μM; for the oxidation of 2.0×10^{-3} M *L*-cysteine by 5.0×10^{-5} M $[Fe^{III}(bpy)(CN)_4]^-$ at $\mu = 0.10$ M and pH = 9.94, the concentration of copper cation in the product solution is 0.22 μM, of which most of the copper is from sodium perchlorate and sodium carbonate buffer. According to the above preliminary kinetic studies, the copper cation can be completely scavenged even with the deliberate addition of 1.0 μM $CuSO_4$ (for reduction of $[Fe^{III}(bpy)_2(CN)_2]^+$) and 0.50 μM $CuSO_4$ (for reduction of $[Fe^{III}(bpy)(CN)_4]^-$). However, the concentration of copper cation from AA measurements is much less than 1.0 μM. So the copper catalysis is definitely inhibited with the addition of 1.0 mM $dipic^{2-}$ for the oxidation of *L*-cysteine by $[Fe^{III}(bpy)_2(CN)_2]^+$, 5.0 mM EDTA (pH ≤ 9.00), 10.0 mM EDTA (9.00 < pH ≤ 10.0) and 1.0 mM cyclam (pH > 10.0) for the oxidation of *L*-cysteine by $[Fe^{III}(bpy)(CN)_4]^-$.

The oxidation of EDTA and cyclam by $[Fe^{III}(bpy)(CN)_4]^-$. According to the above preliminary studies, the addition of EDTA and cyclam slows down the copper-catalyzed reaction dramatically. Does $[Fe^{III}(bpy)(CN)_4]^-$ react with EDTA or cyclam? How fast is it? To investigate these questions, 1.0 mL of 1.0×10^{-4} M $[Fe^{III}(bpy)(CN)_4]^-$ was mixed with 1.0 mL of 2.0×10^{-3} M EDTA in one cuvette, in the presence of 10.0 mM cacodylate (pH = 6.04), and the absorbance at 482 nm was recorded over time on HP-8453 diode-array spectrophotometer (optical cutoff filter: 455 nm). There is no reaction between $[Fe^{III}(bpy)(CN)_4]^-$ and EDTA at pH 6.04 within 6000 s. Then the above

reaction was retested at higher pH. For the reaction between 1.0×10^{-3} M EDTA and 5.0×10^{-5} $[Fe^{III}(bpy)(CN)_4]^-$, in the presence of 10.0 mM sodium carbonate buffer (pH = 10.20), the rate of the reaction is fairly slow, with a rate constant of 3.0×10^{-3} s^{-1}. Finally, the reaction between 5.0×10^{-5} M $[Fe^{III}(bpy)(CN)_4]^-$ and 1.0×10^{-3} M cyclam was tested at pH 10.1. The reaction is very slow, with the half-life longer than 2400 s. So it is safe to add 5.0 mM EDTA (pH < 9.00), 10.0 mM EDTA (9.0 < pH ≤ 10.0) and 1.0 mM cyclam (pH > 10.0) to the flask containing cysteine for the oxidation of *L*-cysteine by $[Fe^{III}(bpy)(CN)_4]^-$.

Effect of Fe(II) and *L*-cystine on the rate of the reaction.

(1). The oxidation of *L*-cysteine by $[Fe^{III}(bpy)_2(CN)_2]^+$. According to our study (in the product identification section), the products of the copper-catalysis inhibited reaction are $Fe^{II}(bpy)_2(CN)_2$ and *L*-cystine. Figure 2-10 shows a typical kinetic trace for the oxidation of 1.25×10^{-3} M *L*-cysteine by 2.5×10^{-5} M $[Fe^{III}(bpy)_2(CN)_2]^+$, with 10.0 mM chloroacetate buffer (pH 3.20), μ = 0.10 M (0.093 M $NaCF_3SO_3$) and 1.0 mM $dipic^{2-}$/dipic(1:1) at 25.0 ^oC. In Figure 2-10, it shows that the rate constant of the reaction is $(1.391 \pm 0.012) \times 10^{-2}$ s^{-1}, with final absorbance of 0.1277, standard deviation (SD) of 2.17×10^{-3}, and Durbin-Watson (DW) factor of 0.03/1.6. Numerically, a good fit is characterized by a low standard deviation and a relatively high value for the Durbin-Watson (DW) factor. Therefore, the above fitting result demonstrates a significant deviation from pseudo-first-order kinetics, suggesting that product inhibition exists in the above reaction. Possible inhibition by Fe(II) was tested by adding different concentrations of $Fe^{II}(bpy)_2(CN)_2$ to the reactants. For the oxidation of 1.25×10^{-3} M *L*-

cysteine by 2.5×10^{-5} M $[Fe^{III}(bpy)_2(CN)_2]^+$, with 10.0 mM chloroacetate buffer (pH = 3.20), 1.0 mM $dipic^{2-}$/dipic (1:1) and at $\mu = 0.10$ M ($NaCF_3SO_3$), 1.0×10^{-4} M and 2.5×10^{-5} M $Fe^{II}(bpy)_2(CN)_2$ were deliberately added to the above reactants, separately. The half-lives were 90.0 and 52.2 s, respectively, much longer than that without the addition of $Fe^{II}(bpy)_2(CN)_2$, as shown in Table 2-8. The above results indicate that a step in the reaction is reversible, and not favorable in the forward direction at such a pH. In order to obtain perfect pseudo-first-order fitting, PBN was added to the reactants for all kinetic studies, which will be discussed in detail. Most importantly, the addition of 0.20 mM PBN counteracts the inhibition by $Fe^{II}(bpy)_2(CN)_2$, as shown in Table 2-8. The reaction between *L*-cystine and $[Fe^{III}(bpy)_2(CN)_2]^+$ was tested. 2.5×10^{-4} M *L*-cystine and 2.5×10^{-5} M $[Fe^{III}(bpy)_2(CN)_2]^+$, in the presence of 10.0 mM phosphate buffer (pH = 7.94), were mixed with equal volume in the cuvette. The rate of the reaction is very slow, with the half-life at least 900 s. So the reaction between $[Fe^{III}(bpy)_2(CN)_2]^+$ and *L*-cystine is neglectable.

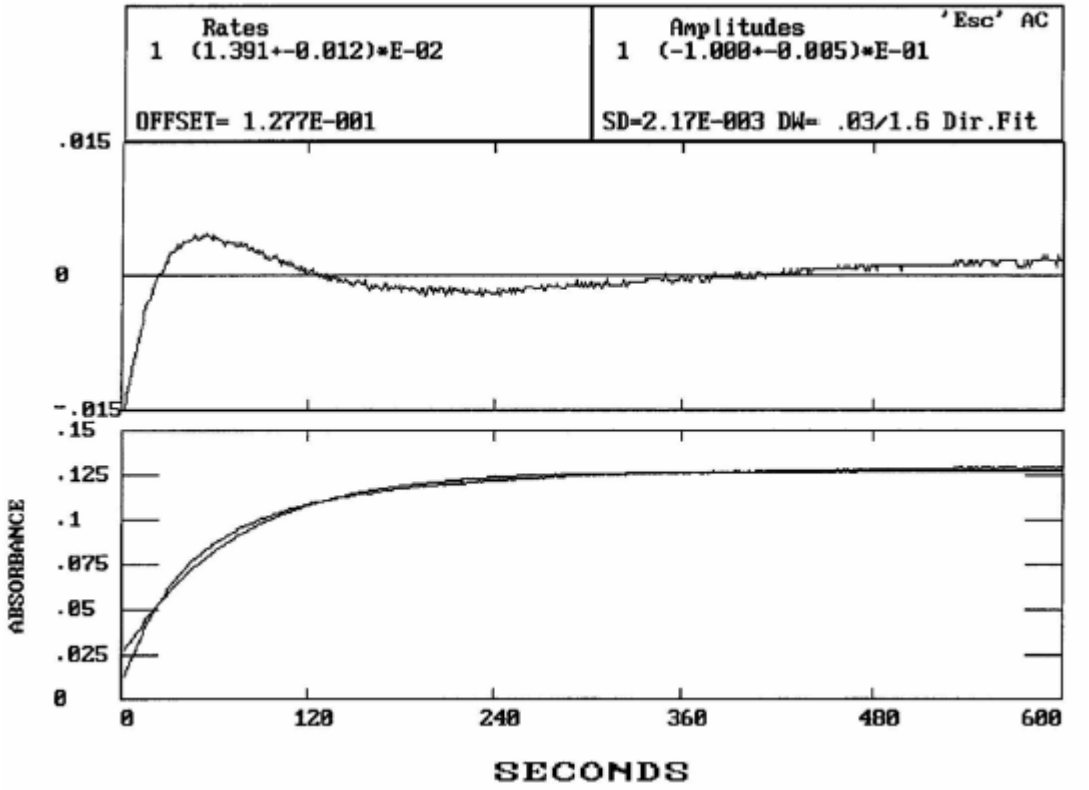

Figure 2-10. A reaction trace of oxidation of 1.25×10^{-3} M *L*-cysteine by 2.5×10^{-5} M $[Fe^{III}(bpy)_2(CN)_2]^+$ at pH 3.20 (10.0 mM chloroacetate buffer), with the addition of 1.0 mM $dipic^{2-}$/dipic(1:1). At μ = 0.10 M (0.093 M $NaCF_3SO_3$) and 25.0 ^oC.

Table 2-8. The effect of $Fe^{II}(bpy)_2(CN)_2$ and PBN on the oxidation of *L*-cysteine by $[Fe^{III}(bpy)_2(CN)_2]^+$ in anaerobic aqueous solution.[a]

$[Fe^{II}(bpy)_2(CN)_2]_0$, M	[PBN], mM	$t_{1/2}$, s	k_{obs}, s^{-1}
0.0	0.00	36.8	×[c]
2.5×10^{-5}	0.00	52.2	×[c]
1.0×10^{-4}	0.00	90.0	×[c]
0.0	0.10	36.1[b]	1.92×10^{-2}
2.5×10^{-5}	0.10	39.8[b]	1.74×10^{-2}
1.0×10^{-4}	0.10	52.5[b]	1.32×10^{-2}
0.0	0.20	35.2[b]	1.97×10^{-2}
2.5×10^{-5}	0.20	38.1[b]	1.82×10^{-2}
1.0×10^{-4}	0.20	46.8[b]	1.48×10^{-2}

[a] $[L\text{-cysteine}]_0 = 1.25 \times 10^{-3}$ M, $[Fe^{III}(bpy)_2(CN)_2^+]_0 = 2.5 \times 10^{-5}$ M, pH = 3.20, μ = 0.10 M ($NaCF_3SO_3$), $[dipic^{2-}/dipic]$ = 1.0 mM; μ = 0.10 M ($NaCF_3SO_3$); [b] $t_{1/2}$ is calculated from k_{obs}, $t_{1/2} = \ln 2/k_{obs}$. [c] non-first-order.

(2). The oxidation of *L*-cysteine by $[Fe^{III}(bpy)(CN)_4]^-$. According to our study (in the product identification section), the products of the direct oxidation of *L*-cysteine by $[Fe^{III}(bpy)(CN)_4]^-$ are $[Fe^{II}(bpy)(CN)_4]^{2-}$ and *L*-cystine. It is known that $[Fe^{III}(bpy)(CN)_4]^-$ has weaker oxidative capabilities than $[Fe^{III}(bpy)_2(CN)_2]^+$. Therefore, it is of importance to test the effect of $[Fe^{II}(bpy)(CN)_4]^{2-}$ on the oxidation of *L*-cysteine by $[Fe^{III}(bpy)(CN)_4]^-$. For the oxidation of 2.60×10^{-3} M *L*-cysteine by 5.0×10^{-5} M $[Fe^{III}(bpy)(CN)_4]^-$, with 10.0 mM cacodylate buffer (pH = 5.98), 5.0 mM EDTA and 0.093 M $NaClO_4$, 1.0×10^{-4} M and 5.0×10^{-5} M $[Fe^{II}(bpy)(CN)_4]^{2-}$ were deliberately added to the above reactants. The half-lives were 28.0 and 25.4 s, very close to that without the addition of $[Fe^{II}(bpy)(CN)_4]^{2-}$, as shown in Table 2-9. The inhibition by $[Fe^{II}(bpy)(CN)_4]^{2-}$ at pH 5.98

will be discussed in detail (see discussion section). Then can *L*-cystine, one of the products of the reaction, react with $[Fe^{III}(bpy)(CN)_4]^-$? Due to the poor solubility of *L*-cystine [120] from pH values between 3.0 and 7.0, the following experiment was carried out at pH 8.00. 1.0×10^{-3} M *L*-cystine and 1.0×10^{-4} M $[Fe^{III}(bpy)(CN)_4]^-$, in the presence of 10.0 mM phosphate buffer (pH = 8.00), were mixed in equal volume, and the kinetic experiment was monitored on HP-8452 diode-array spectrophotometer. There is no reaction between *L*-cystine and $[Fe^{III}(bpy)(CN)_4]^-$over 4800 seconds.

Table 2-9. The effect of $[Fe^{II}(bpy)(CN)_4]^{2-}$ on the oxidation of *L*-cysteine by $[Fe^{III}(bpy)(CN)_4]^-$ at pH 5.98. With 5.0 mM EDTA, and μ = 0.10 M (0.093 M $NaClO_4$)

$[Fe(II)]_0$, μM	$t_{1/2}$, s
0.0	20.3
50	25.4
100	28.0

[a] $[L\text{-cysteine}]_0 = 2.60 \times 10^{-3}$ M, $[Fe^{III}(bpy)(CN)_4^-]_0 = 5.0 \times 10^{-5}$ M

N-tert-butyl-α-phenylnitrone (PBN) effect on kinetics.

(1). The oxidation of *L*-cysteine by $[Fe^{III}(bpy)_2(CN)_2]^+$. Our preliminary results have demonstrated that, at pH values less than 4.76, the rate of the reaction between *L*-cysteine and $[Fe^{III}(bpy)_2(CN)_2]^+$ is non-first order even when 1.0 mM dipic was added to the reactants. The non-first-order kinetics was also observed by Hung and Stanbury in their studying the kinetics of the oxidation of thioglycolate by $[Os(phen)_3]^{3+}$. Perfect pseudo-first-order kinetics was obtained by adding 1.0 mM PBN to the reactants to scavenge the TGA radicals.[104] The efficient scavenging of cysteine thiyl radical by PBN

was also observed by Graceffa.[121] Here, a series of kinetic experiments was carried out with the addition of various concentrations of PBN at different pHs. For the oxidation of 1.25×10^{-3} M *L*-cysteine by 2.5×10^{-5} M $[Fe^{III}(bpy)_2(CN)_2]^+$, with 10.0 mM chloroacetate buffer (pH 3.20), μ = 0.10 M (0.093 M $NaCF_3SO_3$) and 1.0 mM $dipic^{2-}$/dipic(1:1) at 25.0 ^oC, the rate of the reaction is non-pseudo-first-order, as shown in Figure 2-10; with the addition of 0.10 mM PBN, the rate of reaction follows pseudo-first-order kinetic behavior, as shown in Figure 2-11, and the rate constant increases by a factor of 1.4. Then 0.20, 0.50 and 1.0 mM PBN was added to the above reactants separately. The rate constants were the same as that for the addition of 0.10 mM PBN. The reaction has the same behavior at pH 4.62. For the oxidation of 1.00×10^{-3} M *L*-cysteine by 2.5×10^{-5} M $[Fe^{III}(bpy)_2(CN)_2]^+$, with 10.0 mM acetate buffer (pH 4.62), μ = 0.10 M (0.092 M $NaCF_3SO_3$) and 1.0 mM $dipic^{2-}$/dipic(1:1) at 25 ^oC, the rate of the reaction is non-pseudo-first-order, and the rate constant increases from 0.310 to 0.360 s^{-1} after the addition of 1.0 mM PBN. However, the rate of the reaction decreases with the addition of PBN at pH 7.62. For the oxidation of 2.50×10^{-4} M *L*-cysteine by 2.5×10^{-5} M $[Fe^{III}(bpy)_2(CN)_2]^+$, with 10.0 mM phosphate buffer (pH = 7.62), μ = 0.10 M (0.075 M $NaCF_3SO_3$) and 1.0 mM $dipic^{2-}$ at 25.0 ^oC, the rate of the reaction is pseudo-first-order; the rate constant decreases from 75.0 to 71.0 s^{-1}after the addition of 0.10 mM PBN. Unexpectedly, the rate constant decreases with the increase of PBN. When 7.5 mM PBN was added to the above reaction system, the rate constant decreased by 32.5 %. All of the results are shown in Table 2-10.

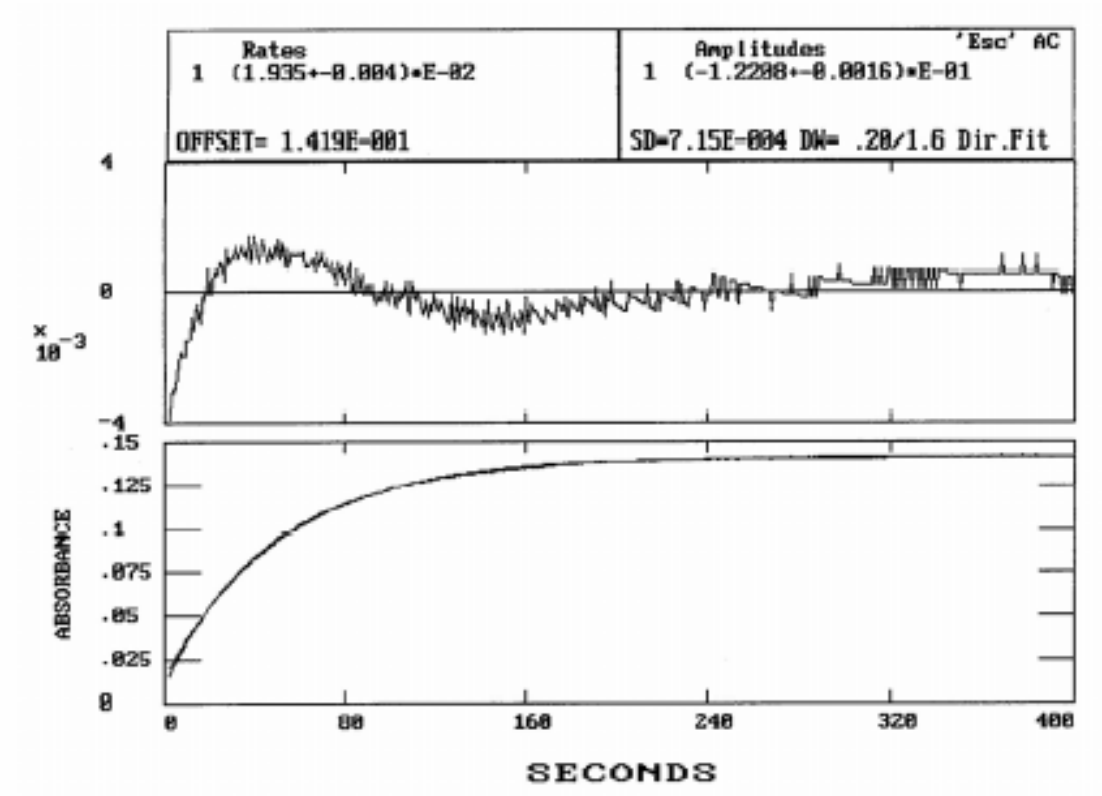

Figure 2-11. A reaction trace of oxidation of 1.25×10^{-3} M *L*-cysteine by 2.5×10^{-5} M $[Fe^{III}(bpy)_2(CN)_2]^+$ at pH 3.20 (10.0 mM chloroacetate buffer), with 1.0 mM $dipic^{2-}$ /dipic(1:1) and 0.10 mM PBN. At μ = 0.10 M (0.093 M $NaCF_3SO_3$) and 25.0 ^oC.

Table 2-10. The effect of PBN on the oxidation of *L*-cysteine by $[Fe^{III}(bpy)_2(CN)_2]^+$.[a]

$[L\text{-cysteine}]_0$, mM	[PBN], mM	Buffer solution	pH of products	k_{obs}, s^{-1}	$t_{1/2}$, s
1.25	0.0	chloroacetate	3.20	0.0139[b]	36.8
1.25	0.10	chloroacetate	3.22	0.0194	35.7[c]
1.25	0.20	chloroacetate	3.21	0.0196	35.7[c]
1.25	0.50	chloroacetate	3.21	0.0199	35.4[c]
1.25	1.0	chloroacetate	3.24	0.0205	33.8[c]
1.00	0.0	acetate	4.61	0.310[b]	2.00
1.00	1.0	acetate	4.61	0.360	1.92[c]
1.00	2.0	acetate	4.62	0.367	1.89[c]
0.25	0.0	phosphate	7.62	75.0	0.0092 [c]
0.25	0.10	phosphate	7.62	71.0	0.0098 [c]
0.25	0.50	phosphate	7.62	63.0	0.011 [c]
0.25	1.0	phosphate	7.62	56.0	0.012 [c]
0.25	2.0	phosphate	7.61	51.3	0.014 [c]
0.25	5.0	phosphate	7.62	51.5	0.013 [c]
0.25	7.5	phosphate	7.61	50.6	0.014 [c]

[a] $[Fe(III)]_0$ = 25.0 μM; $[dipic^{2-}]$ = 1.0 mM; μ = 0.10 M ($NaCF_3SO_3$); [buffer] = 10.0 mM.
[b] Fitting is not perfect. [c] $t_{1/2}$ is calculated from k_{obs}, $t_{1/2} = \ln 2/k_{obs}$.

In the absence of PBN, it has been found that the rate constant decreases with the addition of $Fe^{II}(bpy)_2(CN)_2$ at lower pH vlaues. With the addition of PBN, the inhibition by $Fe^{II}(bpy)_2(CN)_2$ becomes insignificant. Here, for the oxidation of *L*-cysteine by $[Fe^{III}(bpy)_2(CN)_2]^+$ at pH 3.20, in the presence of various concentrations of Fe(II), 0.10 and 0.20 mM PBN was added to the reaction systems ($[L\text{-cysteine}]_0 = 1.25 \times 10^{-3}$ M; $[Fe(III)]_0 = 2.5 \times 10^{-5}$ M; [chloroacetate] = 10.0 mM; $[dipic^{2-}/dipic]$ = 1.0 mM; μ = 0.10

M ($NaCF_3SO_3$); $[Fe(II)]_0 = 2.5 \times 10^{-5}$ or 1.0×10^{-4} M), respectively. The results shown in Table 2-8 indicate that 0.20 mM PBN is high enough to counteract the inhibition by $Fe^{II}(bpy)_2(CN)_2$. (In the presence of 0.20 mM PBN, for $[Fe(II)]_0/[Fe(III)]_0 = 0$, the rate constant is 1.97×10^{-2} s^{-1}; for $[Fe(II)]_0/[Fe(III)]_0 = 1$, the rate constant is 1.82×10^{-2} s^{-1}.)

Can PBN react with $[Fe^{III}(bpy)_2(CN)_2]^+$ or *L*-cysteine? The kinetic experiments were run by mixing equal volume of 5.0×10^{-5} M $[Fe^{III}(bpy)_2(CN)_2]^+$ with 1.0×10^{-2} M PBN, in the presence of 1.0 mM $dipic^{2-}$ and 10.0 mM phosphate buffer (pH = 7.56). The rate of the reaction between $[Fe^{III}(bpy)_2(CN)_2]^+$ and PBN is rather slow, with the half-life over 900 s. Recently, Potapenko et al. reported that 5-diethoxyphosphoryl-5-methyl-1-pyrroline *N*-oxide (DEPMPO) is nucleophilically attacked by *L*-cysteine to form DEPMPO hydroxylamine derivatives with equilibrium constant of 0.03 M^{-1}.[122] Then 1.50 mL 0.050 mM PBN was spectrophotometrically titrated by 10.0 mM *L*-cysteine at pH 7.60. The absorbance of PBN at 287 nm decreases with the dilution of PBN by *L*-cysteine. Therefore, it is safe to add small amounts of PBN to the reaction to scavenge the cysteine radicals that are produced in the reaction.

Based on the above experimental results, 0.20 mM PBN was added to the reactants for all kinetic studies.

(2). The oxidation of *L*-cysteine by $[Fe^{III}(bpy)(CN)_4]^-$. For the oxidation *L*-cysteine by $[Fe^{III}(bpy)(CN)_4]^-$, the pH for the kinetic experiments was selected from 6.00 to 12.0. Figure 2-12 shows that it follows perfect pseudo-first-order behavior for the reaction between 2.60×10^{-2} M *L*-cysteine and 5.0×10^{-5} M $[Fe^{III}(bpy)(CN)_4]^-$ (5.0 mM EDTA and 0.066 M $NaClO_4$), at $\mu = 0.10$ M and pH 6.09, which demonstrates that no PBN need be added to the reactants.

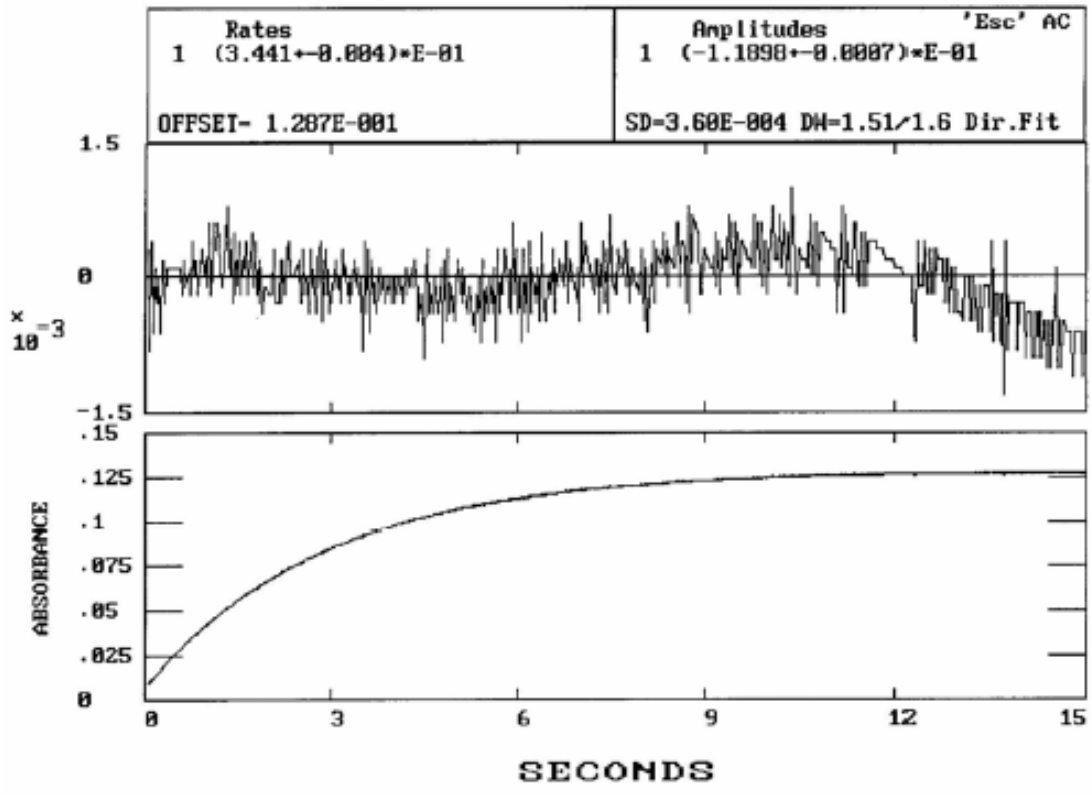

Figure 2-12. A reaction trace of oxidation of 2.60×10^{-2} M *L*-cysteine by 5.0×10^{-5} M $[Fe^{III}(bpy)(CN)_4]^-$ at pH 6.09 (10.0 mM cacodylate buffer), with 5.0 mM EDTA. At μ = 0.10 M (0.066 M $NaClO_4$) and 25.0 ^oC.

Product identification and stoichiometry.

(1). The oxidation of *L*-cysteine by $[Fe^{III}(bpy)_2(CN)_2]^+$. Without the addition of PBN. The products of the non-copper-catalyzed reaction were identified by UV-vis and ^{1}H-NMR spectra. Figure 2-13 shows UV-vis spectra for the oxidation of 2.5×10^{-4} M *L*-cysteine by 2.5×10^{-5} M $[Fe^{III}(bpy)_2(CN)_2]^+$ with 10.0 mM cacodylate buffer (pH = 6.02), μ = 0.10 M (0.093 M $NaCF_3SO_3$) and 1.0 mM $dipic^{2-}$ at room temperature. At the beginning of the reaction, there are two peaks at 394 and 544 nm, which correspond to the UV-vis absorbance of $[Fe^{III}(bpy)_2(CN)_2]^+$. Within the time of the reaction, these two peaks disappeared, and two new peaks appeared. After 2.5 s of reaction, the shape of the curve did not change. Comparing it with the UV-vis spectrum of pure $Fe^{II}(bpy)_2(CN)_2$ (Figure 2-14), it very strongly suggests that $Fe^{II}(bpy)_2(CN)_2$ is one of the products of the reaction. Furthermore, the well-defined isosbestic point at 339 nm in Figure 2-13 suggests that there is no accumulation of any long-lived intermediate during the reaction. The identity of the sulfur-containing product was determined by ^{1}H-NMR spectroscopy, from which the formation of $Fe^{II}(bpy)_2(CN)_2$ was also observed. A sample for ^{1}H-NMR spectra was prepared as follows: 0.36 mM $[Fe^{III}(bpy)_2(CN)_2]^+$ and 2.0 mM *L*-cysteine were equally mixed in anaerobic D_2O, in the presence of 1.0 mM $dipic^{2-}$ and 1.0 mM DSS at pH 8.78 (adjusted by 1.0 M NaOD). The ^{1}H-NMR spectra shown in Figure 2-15 clearly reveals that *L*-cystine (3.91 (dd, J = 7.9, 4.1; 2H), 3.28, (dd, J = 14.6, 4.1; 2H), 3.07, (dd, J = 14.5, 8.0; 2H)) and $Fe^{II}(bpy)_2(CN)_2$ (four triplets and four doublets, chemical shift from 7.20 to 9.40 ppm) are the products of the reaction. Unlike the reaction of *L*-cysteine with octacyanomolybdate(V),[52] the ^{1}H-NMR spectra for the oxidation of *L*-cysteine by $[Fe^{III}(bpy)_2(CN)_2]^+$ provided no evidence for the formation of

L-cysteine-sulfinate. The stoichiometry of the reaction was determined by the quantitative analysis of the ^{1}H-NMR spectra of the product, with Δ[Fe(II)]/Δ[*L*-cystine], is 1.5 ± 0.1.

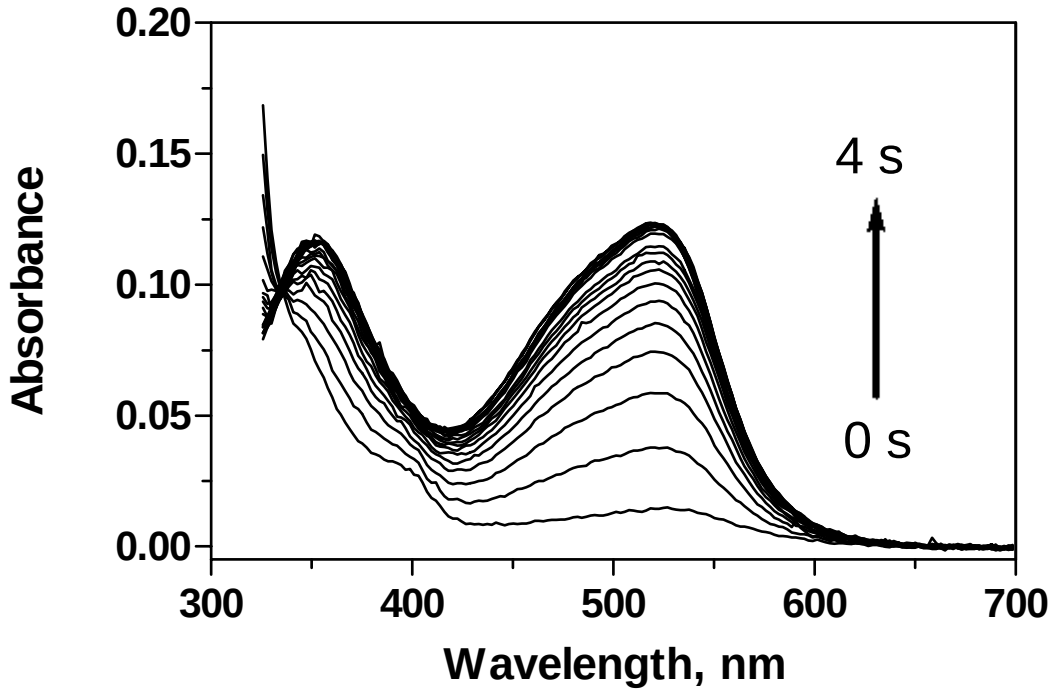

Figure 2-13. The UV-vis spectra for the oxidation of 2.5×10^{-4} M *L*-cysteine by 2.5×10^{-5} M $[Fe^{III}(bpy)_2(CN)_2]^+$ at pH 6.02 (10.0 mM cacodylate buffer), with 1.0 mM $dipic^{2-}$. At μ = 0.10 M (0.093 M $NaCF_3SO_3$) and room temperature. (time interval: 0.10 s)

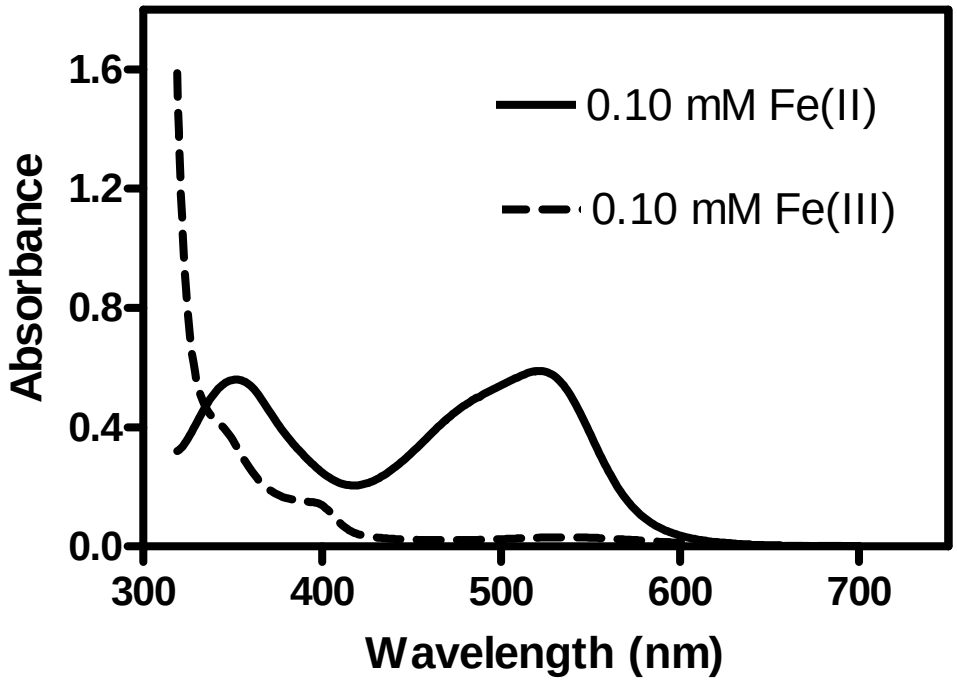

Figure 2-14. UV-vis spectra of 1.0×10^{-4} M $[Fe^{III}(bpy)_2(CN)_2]^+$ (---) and $Fe^{II}(bpy)_2(CN)_2$ (—) in aqueous solution.

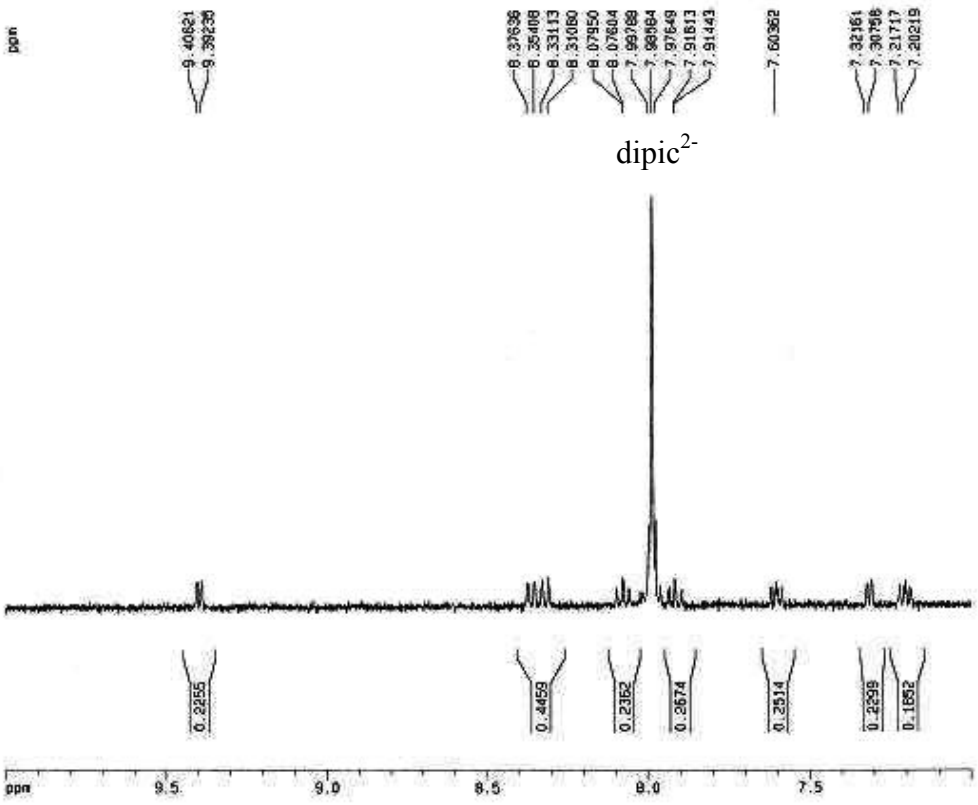

Figure 2-15a. ^{1}H-NMR spectrum of the product for the reaction of $[Fe^{III}(bpy)_2(CN)_2]^+$ with *L*-cysteine in D_2O, with 1.0 mM $dipic^{2-}$ and 1.0 mM DSS, at pH 8.78 (adjusted by 1.0 M NaOD). $[Fe^{III}(bpy)_2(CN)_2^+]_0$ = 0.18 mM, [*L*-cysteine]$_0$ = 1.0 mM.

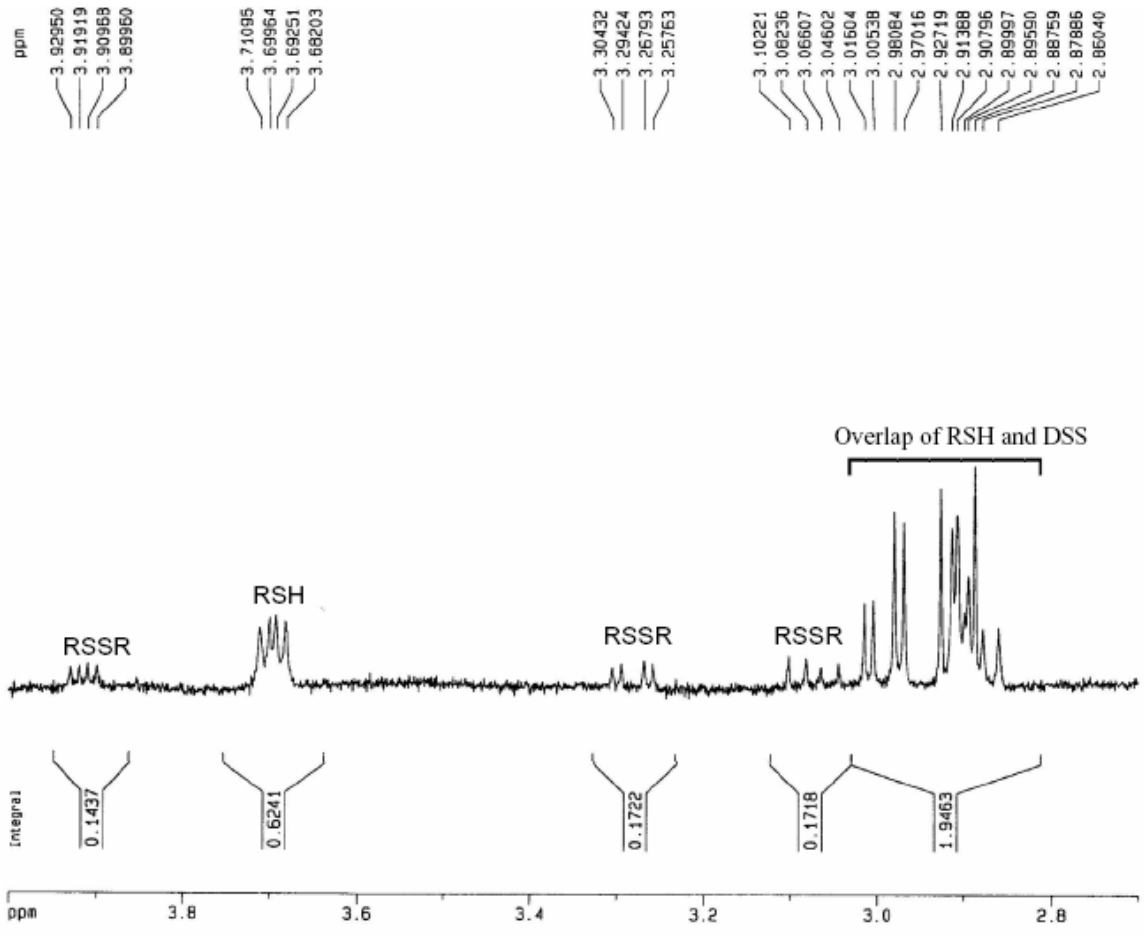

Figure 2-15b. ^{1}H-NMR spectrum of the product for the reaction of $[Fe^{III}(bpy)_2(CN)_2]^{+}$ with *L*-cysteine in D_2O, with 1.0 mM $dipic^{2-}$ and 1.0 mM DSS, at pH 8.78 (adjusted by 1.0 M NaOD). $[Fe^{III}(bpy)_2(CN)_2^{+}]_0$ = 0.18 mM, [*L*-cysteine]$_0$ = 1.0 mM.

The stoichiometry of the reaction between $[Fe^{III}(bpy)_2(CN)_2]^+$ and *L*-cysteine in the presence of $dipic^{2-}$ was also determined by spectrophotometric titration. Titration of 2.0 mL of 1.04×10^{-4} M *L*-cysteine by 5.09×10^{-3} M $[Fe^{III}(bpy)_2(CN)_2]^+$ at pH 7.61 was monitored at 522 nm, with 1.0 mM $dipic^{2-}$ and 10.0 mM phosphate buffer. The consumption ratio of Δ[Fe(II)]/Δ[*L*-cysteine] was calculated from the titration curve that is shown in Figure 2-16, with 1.12 ± 0.02 for Δ[Fe(II)]/Δ[*L*-cysteine].

The stoichiometry of the reaction between $[Fe^{III}(bpy)_2(CN)_2]^+$ and *L*-cysteine in the presence of $dipic^{2-}$ was determined by spectrophotometric analysis as well. Equal volumes of 0.40 mM deaerated *L*-cysteine and 0.20 mM $[Fe^{III}(bpy)_2(CN)_2]^+$, with 1.0 mM $dipic^{2-}$ and 10.0 mM phosphate buffer (pH = 6.94), were mixed together in a bubbling flask for 10.0 minutes, then the product solution was transferred to a stopcocked cuvette. The concentration of $Fe^{II}(bpy)_2(CN)_2$ was determined from its characteristic absorbance at 522 nm, and the concentration of *L*-cysteine before and after the reaction was determined by Ellman's reagent.[105,106] The stoichiometric ratio, Δ[Fe(II)]/Δ[*L*-cysteine], was calculated as 1.002 ± 0.002, similar to results obtained from spectrophotometric titrations. The above results imply that the overall reaction is:

$$2\,[Fe^{III}(bpy)_2(CN)_2]^+ + 2\,HSCH_2CH(NH_3^+)CO_2^- \rightarrow$$

$$2\,Fe^{II}(bpy)_2(CN)_2 + {}^-O_2CCH(NH_3^+)CH_2SSCH_2CH(NH_3^+)CO_2^- + 2H^+ \quad (2\text{-}1\text{-}a)$$

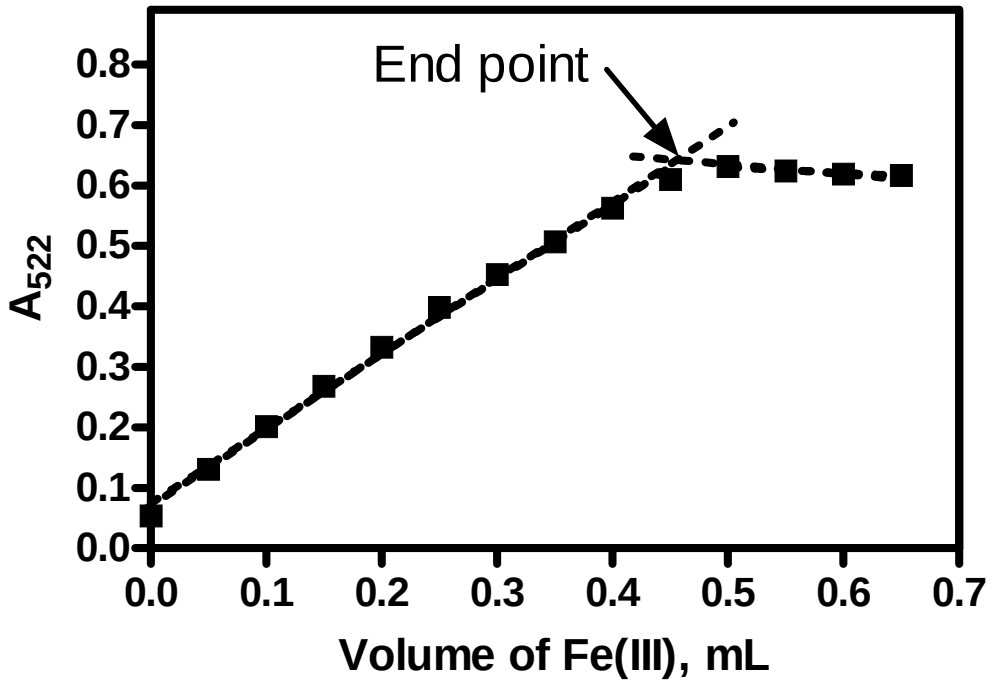

Figure 2-16. Spectrophotometric titration of *L*-cysteine with $[Fe^{III}(bpy)_2(CN)_2]^+$, in the absence of PBN. Absorbance at 522 nm is shown as a function of the volume of Fe(III) added. pH =7.61, $[L\text{-cysteine}]_0 = 1.04 \times 10^{-4}$ M, $n_0(L\text{-cysteine}) = 0.00208$ mmol, [Fe(III)] $= 5.09 \times 10^{-4}$ M, and the initial volume of *L*-cysteine is 2.0 mL.

In the presence of PBN. The products for the oxidation of *L*-cysteine by $[Fe^{III}(bpy)_2(CN)_2]^+$ in anaerobic aqueous solution, in the presence of PBN, are identified by their ^{1}H-NMR spectra in D_2O. Figure 2-17 shows the ^{1}H-NMR spectrum of the product of 0.20 mM $[Fe^{III}(bpy)_2(CN)_2]^+$ and 1.0 mM *L*-cysteine in D_2O, in the presence of 1.0 mM dipic and 0.10 mM PBN at pH 3.10. From 7.19 to 9.40 ppm, there are eight peaks with the same intensity, confirming the formation of $Fe^{II}(bpy)_2(CN)_2$. The chemical shifts at 4.00 and 3.09 ppm are ascribed to *L*-cysteine. Comparing Figure 2-17 with Figure 2-18, the chemical shifts at 8.61 and 8.41 ppm in Figure 2-17 are assigned as PBN and overlap of PBN with dipic^{2-}. The ratio of the integrated intensity of the chemical shift at 7.20 (2H in $Fe^{II}(bpy)_2(CN)_2$) and 1.56 ppm (9H in tert-butyl in PBN) in the above ^{1}H-NMR spectrum demonstrates that around 40 % of PBN was consumed in the reaction. The consumption of PBN was thought to scavenge the cysteine thiyl radical, and it is found that the PBN adduct of cysteine thiyl radical is not very stable.[121] So the two singlets (1.33 and 2.05 ppm) are ascribed to the decomposition of the PBN-cysteine radical adduct. Moreover, no *L*-cystine was detected in the ^{1}H-NMR spectrum. The stoichiometric ratio for the reaction was obtained from the integrated intensities of the ^{1}H-NMR spectrum, from which Δ[*L*-cysteine]/Δ[Fe(III)] = 1.0 ± 0.2.

According to PBN effect on kinetics, the rate for the oxidation of *L*-cysteine by $[Fe^{III}(bpy)_2(CN)_2]^+$ at pH 7.61 (see Table 2-10) decreases with the addition of PBN. Furthermore, *L*-cystine is more soluble in alkaline solution,[120] so it is significant to identify the products and determine the stoichiometric ratio in alkaline media. The ^{1}H-NMR spectrum for the oxidation of 1.0 mM *L*-cysteine by 0.20 mM $[Fe^{III}(bpy)_2(CN)_2]^+$ in D_2O, in the presence of 1.0 mM dipic^{2-}, 0.50 mM PBN and 1.0 mM DSS at pH 8.70, is

shown in Figure 2-19, which indicates that the products of the reaction are $Fe^{II}(bpy)_2(CN)_2$ and *L*-cystine. The concentration of PBN decreases by 16 % during the reaction, much less than that of PBN in acidic solution. Combined with the above kinetic results, it implies that PBN scavenges more cysteine thiyl radical at lower pH values. The stoichiometric ratio was obtained from the integrated intensities of the ^{1}H-NMR spectrum, from which Δ[Fe(II)]/Δ[*L*-cystine] = 1.82 ± 0.07.

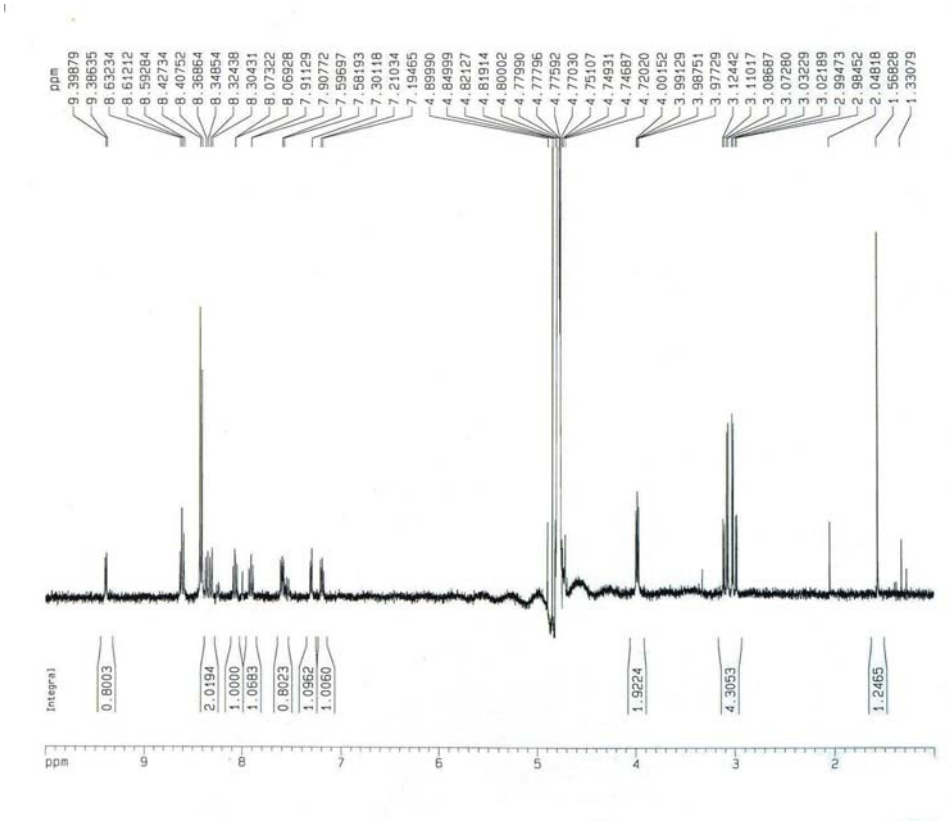

Figure 2-17. ^{1}H-NMR spectrum of the product of $[Fe^{III}(bpy)_2(CN)_2]^+$ and *L*-cysteine in D_2O, with 1.0 mM $dipic^{2-}$ and 0.10 mM PBN, at pH 3.10 (adjusted by 1.0 M NaOD). $[Fe^{III}(bpy)_2(CN)_2^+]_0$ = 0.20 mM, [*L*-cysteine]$_0$ = 1.0 mM.

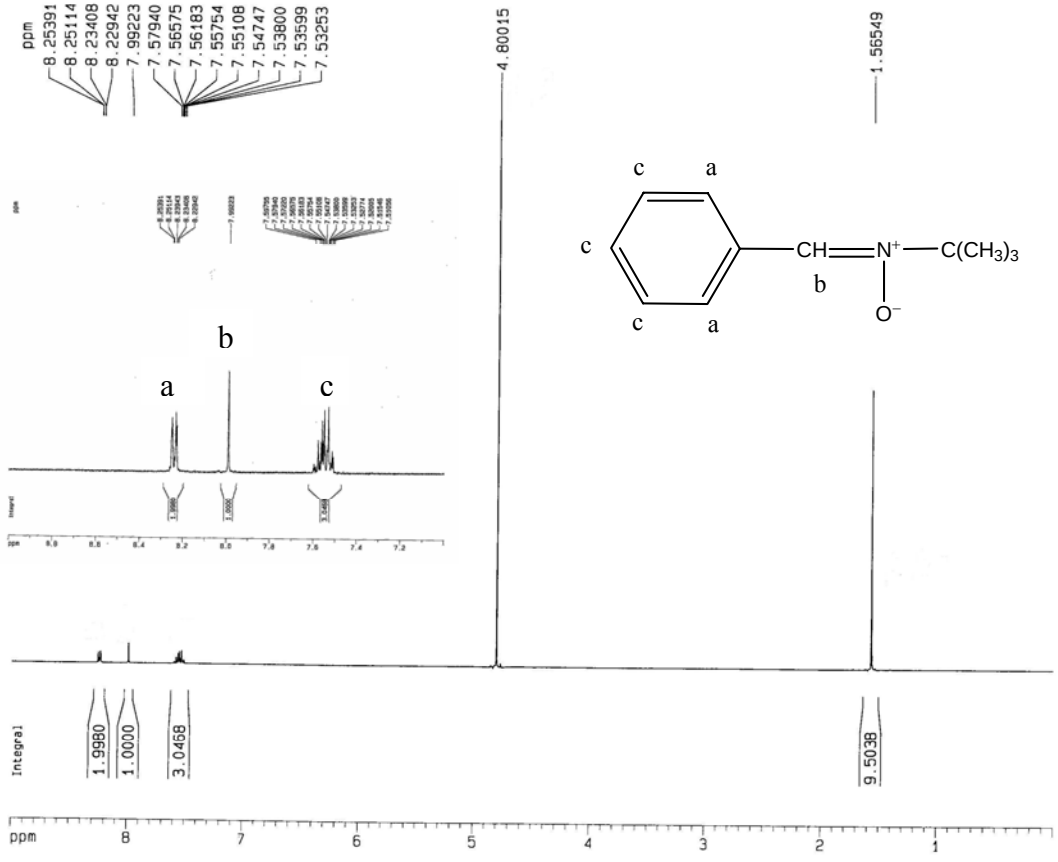

Figure 2-18. ^{1}H-NMR spectrum of 10.0 mM PBN in D_2O

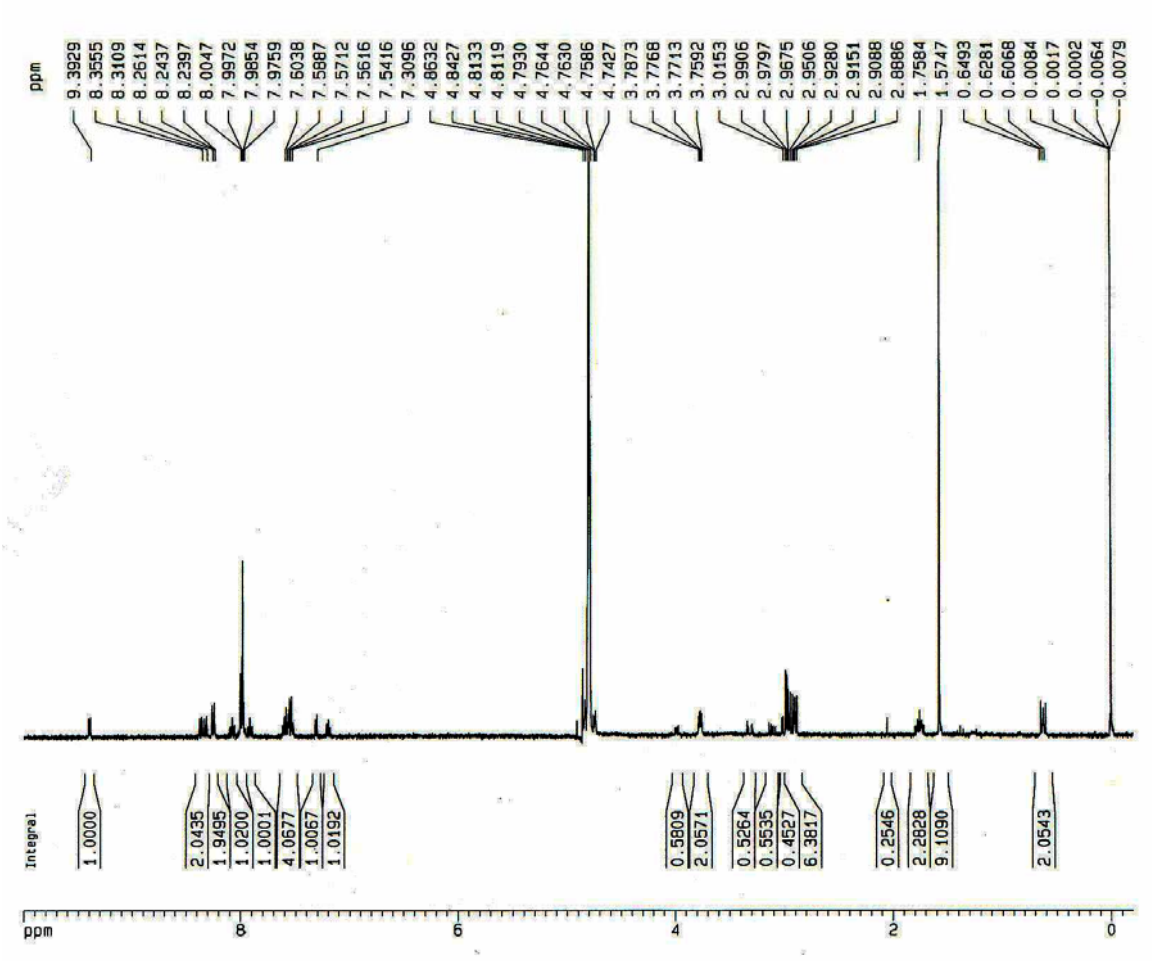

Figure 2-19a. ^{1}H-NMR spectrum of the product of $[Fe^{III}(bpy)_2(CN)_2]^+$ and *L*-cysteine in D_2O, with 1.0 mM $dipic^{2-}$, 0.50 mM PBN and 1.0 mM DSS, at pH 8.70 (adjusted by 1.0 M NaOD). $[Fe^{III}(bpy)_2(CN)_2^+]_0$ = 0.20 mM, [*L*-cysteine]$_0$ = 1.0 mM.

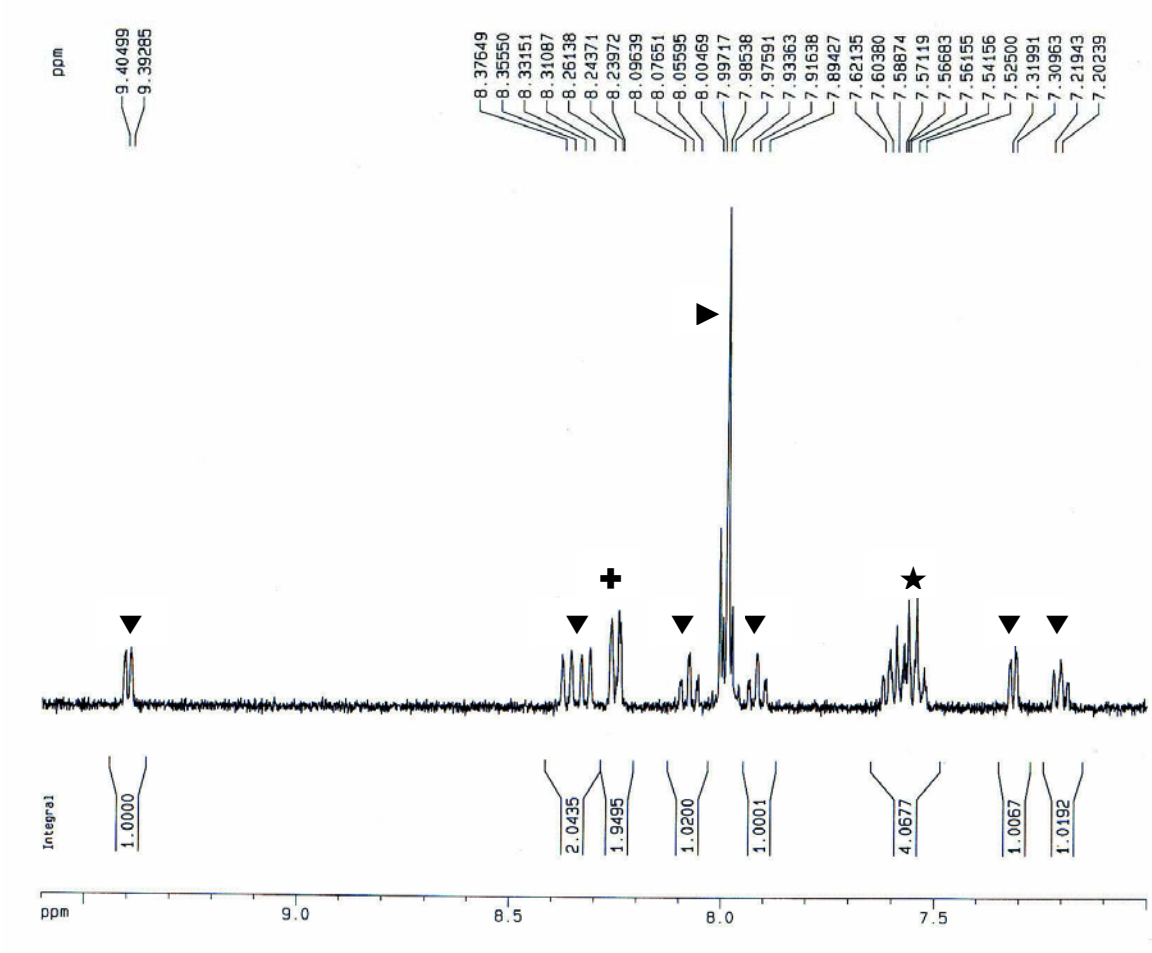

Figure 2-19b. ^{1}H-NMR spectrum of the product of $[Fe^{III}(bpy)_2(CN)_2]^+$ and *L*-cysteine in D_2O, with 1.0 mM dipic^{2-}, 0.50 mM PBN and 1.0 mM DSS, at pH 8.70 (adjusted by 1.0 M NaOD). $[Fe^{III}(bpy)_2(CN)_2^+]_0$ = 0.20 mM, [*L*-cysteine]$_0$ = 1.0 mM.

▼: $Fe(bpy)_2(CN)_2$; ✚: PBN; ►: overlap of dipic^{2-} and PBN;
★: overlap of PBN and $Fe(bpy)_2(CN)_2$.

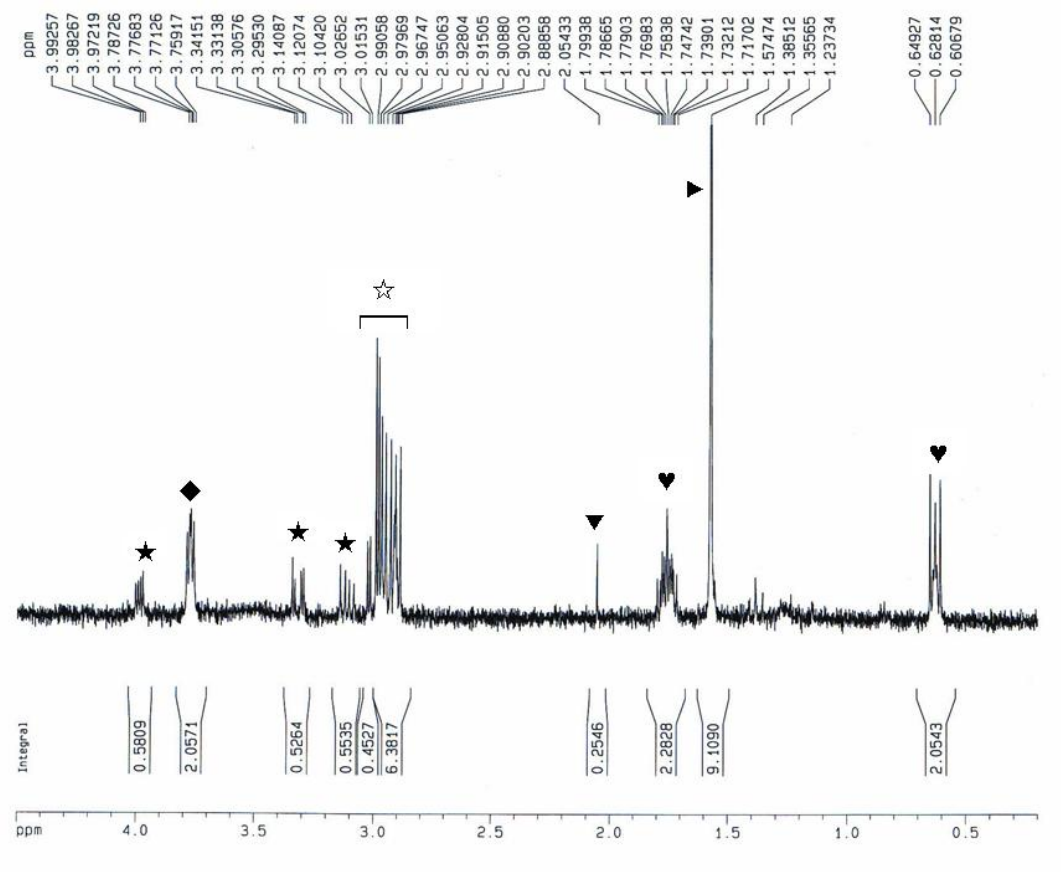

Figure 2-19c. ^{1}H-NMR spectrum of the product of $[Fe^{III}(bpy)_2(CN)_2]^+$ and *L*-cysteine in D_2O, with 1.0 mM $dipic^{2-}$, 0.50 mM PBN and 1.0 mM DSS, at pH 8.70 (adjusted by 1.0 M NaOD). $[Fe^{III}(bpy)_2(CN)_2^+]_0$ = 0.20 mM, [*L*-cysteine]$_0$ = 1.0 mM.

★: RSSR; ◆: RSH; ♥: DSS; ▸: PBN; ▼: RSH/PBN adduct; ☆: overlap of RSH and DSS.

The stoichiometry of the reaction between $[Fe^{III}(bpy)_2(CN)_2]^+$ and *L*-cysteine in the presence of 1.0 mM $dipic^{2-}$ and 1.0 mM PBN was also determined by spectrophotometric titration. Titration of 2.0 mL of 1.04×10^{-4} M *L*-cysteine by 4.92×10^{-3} M $[Fe^{III}(bpy)_2(CN)_2]^+$ at pH 7.61 was monitored at 522 nm, with 1.0 mM $dipic^{2-}$, 1.0 mM PBN and 10.0 mM phosphate buffer. The stoichiometric ratio was determined from the titration curve (Figure 2-20), with 1.13 ± 0.09 for Δ[Fe(II)]/Δ[*L*-cysteine], consistent with the results from ^{1}H-NMR. Therefore, the products and stoichiometric ratio of the reaction are the same even when PBN is added.

(2). The oxidation of *L*-cysteine by $[Fe^{III}(bpy)(CN)_4]^-$. The products of the non-copper-catalyzed reaction were identified by ^{1}H-NMR spectra. A sample for running ^{1}H-NMR spectra was prepared as follows: equal volume of 0.80 mM $[Fe^{III}(bpy)(CN)_4]^-$ and 4.0 mM *L*-cysteine were mixed in anaerobic D_2O, in the presence of 1.0 mM cyclam and 2.0 mM DSS at pH 11.1 (adjusted by 0.10 M NaOD). The ^{1}H-NMR spectrum shown in Figure 2-21 clearly shows that *L*-cystine (two doublets of doublets, (3.62, dd, J = 7.6, 4.4; 2H), (3.12, dd, J = 16, 4.4; 2H), and $[Fe^{II}(bpy)(CN)_4]^-$ (two triplets and two doublets,[113] chemical shift from 7.47 to 9.34 ppm) are the products of the reaction, consistent with that of the oxidation *L*-cysteine by $[Fe^{III}(bpy)_2(CN)_2]^+$. Furthermore, the third doublet of doublets of ^{1}H-NMR spectra of *L*-cystine overlap with that of cyclam. Unlike the oxidation of *L*-cysteine by octacyanomolybdate(V)[52], the ^{1}H-NMR spectra for the oxidation of *L*-cysteine by $[Fe^{III}(bpy)(CN)_4]^-$ provided no evidence for the formation of *L*-cysteine-sulfinate. The stoichiometry of the reaction was determined by the quantitative analysis of the ^{1}H-NMR spectra of the product, with Δ[Fe(II)]/Δ[*L*-cystine] = 1.97 ± 0.03.

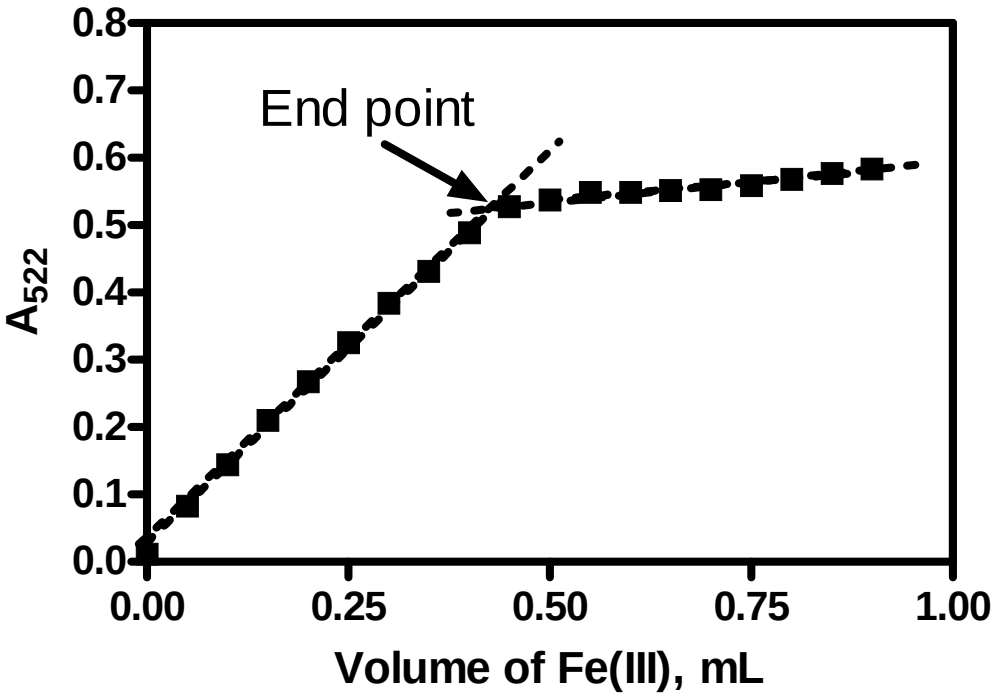

Figure 2-20. Spectrophotometric titration of *L*-cysteine with $[Fe^{III}(bpy)_2(CN)_2]^+$, in the presence of 1.0 mM PBN. Absorbance at 522 nm is shown as a function of the volume of Fe(III) solution added. pH = 7.57, $[L\text{-cysteine}]_0 = 1.04 \times 10^{-4}$ M, $n_0(L\text{-cysteine}) = 2.09 \times 10^{-4}$ mmol, [Fe(III)] = 0.492 mM, and the initial volume of *L*-cysteine was 2.0 mL.

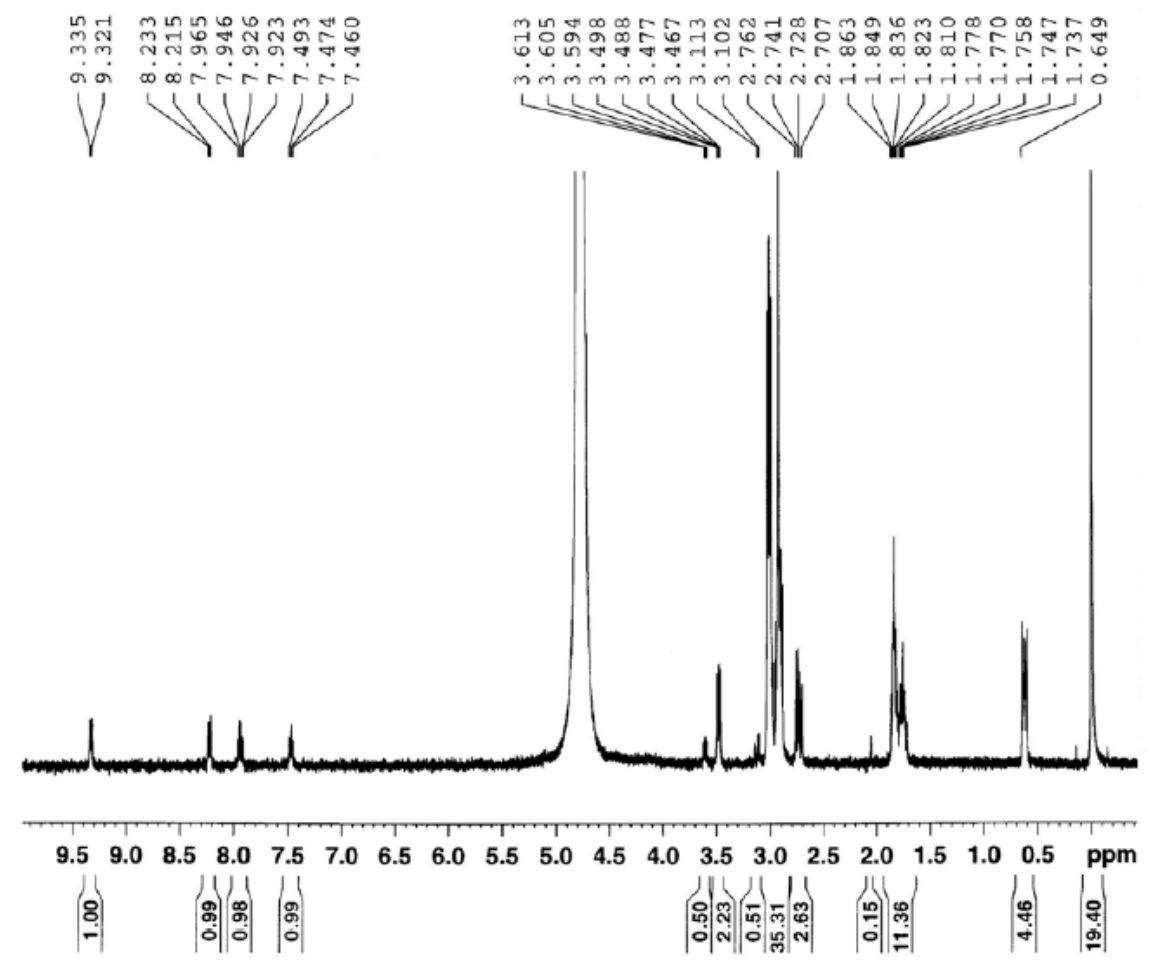

Figure 2-21a. ^{1}H-NMR spectrum of the product of $[Fe^{III}(bpy)(CN)_4]^-$ and *L*-cysteine in D_2O, in the presence of 1.0 mM cyclam and 2.0 mM DSS, at pH 11.1 (adjusted by 0.10 M NaOD). $[Fe^{III}(bpy)(CN)_4^-]_0$ = 0.40 mM, [*L*-cysteine]$_0$ = 2.0 mM.

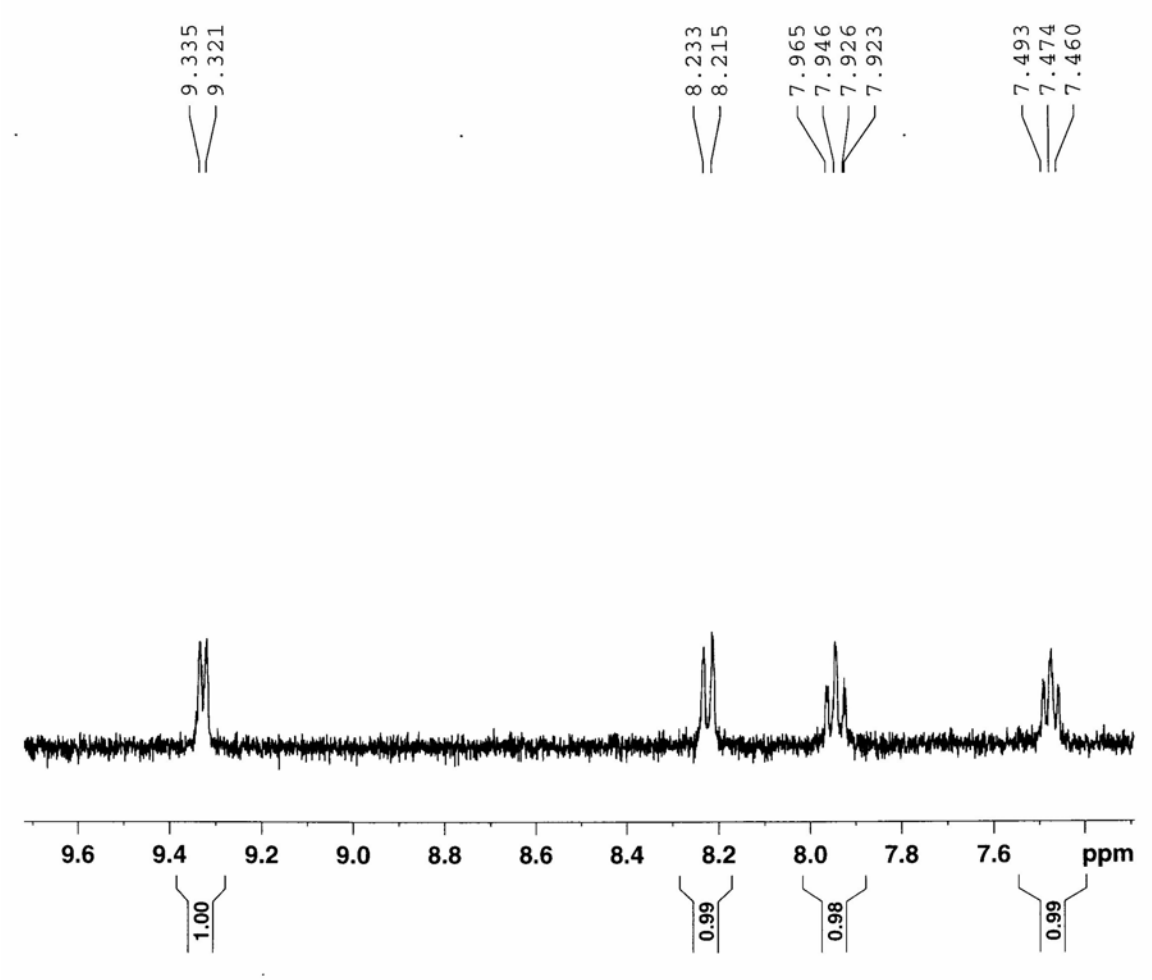

Figure 2-21b. ^{1}H-NMR spectrum of the product of $[Fe^{III}(bpy)(CN)_4]^-$ and *L*-cysteine in D_2O, in the presence of 1.0 mM cyclam and 2.0 mM DSS, at pH 11.1 (adjusted by 0.10 M NaOD). $[Fe^{III}(bpy)(CN)_4^-]_0$ = 0.40 mM, [*L*-cysteine]$_0$ = 2.0 mM.

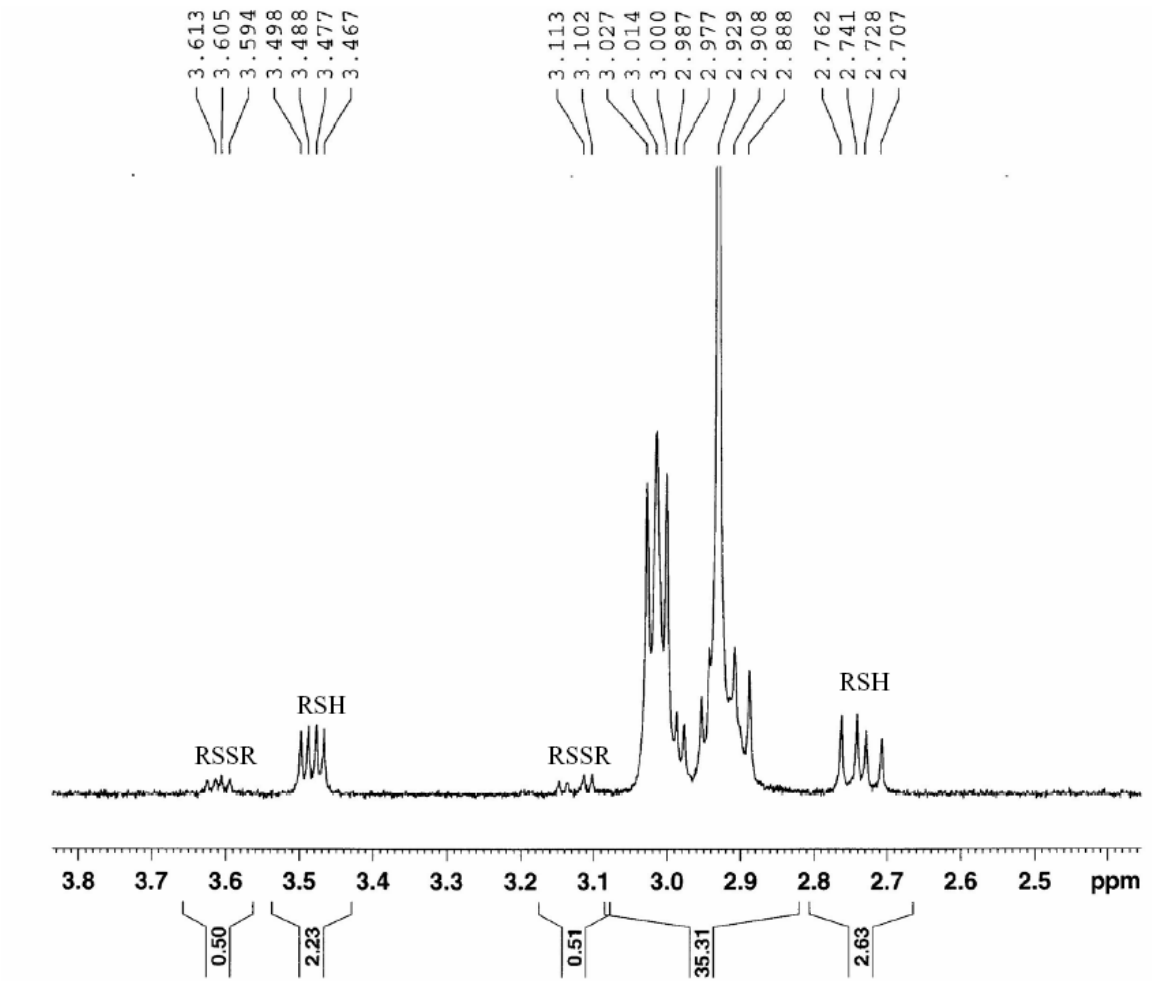

Figure 2-21c. ^{1}H-NMR spectrum of the product of $[Fe^{III}(bpy)(CN)_4]^-$ and *L*-cysteine in D_2O, in the presence of 1.0 mM cyclam and 2.0 mM DSS, at pH 11.1 (adjusted by 0.10 M NaOD). $[Fe^{III}(bpy)(CN)_4^-]_0$ = 0.40 mM, [*L*-cysteine]$_0$ = 2.0 mM.

The stoichiometry of the reaction between $[Fe^{III}(bpy)(CN)_4]^-$ and *L*-cysteine in the presence of EDTA was determined by spectrophotometric analysis as well. Two experiments were performed. Equal volume of 0.50 mM deaerated *L*-cysteine and 0.30 mM $[Fe^{III}(bpy)(CN)_4]^-$, with 5.0 mM EDTA and 10.0 mM ammonia buffer (pH = 8.78), was mixed together in a bubbling flask for 10.0 minutes, then the product solution was transferred to a stopcocked cuvette. The concentration of $[Fe^{II}(bpy)(CN)_4]^{2-}$ was determined from its characteristic absorbance at 482 nm, and the concentration of *L*-cysteine before and after reaction was determined by Ellman's reagent.[105,106] The stoichiometric ratio, Δ[Fe(II)]/Δ[*L*-cysteine], was calculated as 1.28 ± 0.02. The above result implies that *L*-cysteine-sulfinate could be formed when the concentration of *L*-cysteine is slightly higher than that of $[Fe^{III}(bpy)(CN)_4]^-$. But in later kinetic experiments, the concentration of *L*-cysteine is at least ten times that of $[Fe^{III}(bpy)(CN)_4]^-$. Equal volumes of 1.0 mM deaerated *L*-cysteine and 0.30 mM $[Fe^{III}(bpy)(CN)_4]^-$, with 5.0 mM EDTA and 10.0 mM ammonia buffer (pH = 8.78), were mixed together in a bubbling flask for 10.0 minutes, and the product solution was transferred to a stopcocked cuvette. The concentration of $[Fe^{II}(bpy)(CN)_4]^{2-}$ was determined from its characteristic absorbance at 482 nm, and the concentration of *L*-cysteine before and after the reaction was determined by Ellman's reagent.[105,106] The stoichiometric ratio was calculated as 1.05 ± 0.04 for Δ[Fe(II)]/Δ[*L*-cysteine], the same as the results from ^{1}H-NMR spectra.

Based on the above results, the overall reaction is as follows:

$$2\,[Fe^{III}(bpy)(CN)_4]^- + 2\,HSCH_2CH(NH_3^+)CO_2^- \rightarrow$$
$$2\,[Fe^{II}(bpy)(CN)_4]^{2-} + {}^-O_2CCH(NH_3^+)CH_2SSCH_2CH(NH_3^+)CO_2^- + 2H^+ \qquad (2\text{-}1\text{-}b)$$

Kinetics.

(1). The oxidation of *L*-cysteine by $[Fe^{III}(bpy)_2(CN)_2]^+$. The reduction of 2.5×10^{-5} M $[Fe^{III}(bpy)_2(CN)_2]^+$ by various concentrations of *L*-cysteine, in the presence of 1.0 mM $dipic^{2-}$, 0.20 mM PBN, and pH from 3.0 to 7.87, was investigated at 25.0 ^oC and at constant ionic strength (μ = 0.10 M, $NaCF_3SO_3$). The pseudo-first-order rate constants (k_{obs}, s^{-1}) were evaluated by exponential fits of the kinetic curves, and replicate runs agreed to better than ± 5%. Figure 2-22 shows a kinetic trace of oxidation of 4.7×10^{-4} M *L*-cysteine by 2.5×10^{-5} M $[Fe^{III}(bpy)_2(CN)_2]^+$ at pH 5.99 (10.0 mM cacodylate buffer), with 1.0 mM $dipic^{2-}$, 0.20 mM PBN, μ = 0.10 M (0.092 M $NaCF_3SO_3$), and at 25.0 ^oC. The rate of the reaction follows pseudo-first-order behavior, with a rate constant (k_{obs}) of 3.84 s^{-1}. A series of kinetic experiments was run by changing $[L\text{-cysteine}]_{tot}$ (the total concentration of *L*-cysteine), with 2.5×10^{-5} M $[Fe^{III}(bpy)_2(CN)_2]^+$, 1.0 mM $dipic^{2-}$, 10.0 mM cacodylate buffer (pH = 6.01), 0.20 mM PBN, and μ = 0.10 M at 25.0 ^oC. The rate of the reaction follows pseudo-first-order behavior over 3 half-lives. The rate constant dependence on $[L\text{-cysteine}]_{tot}$ is summarized in Table 2-11, and a plot of k_{obs} versus $[L\text{-cysteine}]_{tot}$ is shown in Figure 2-23. It is linear with slope of $(7.25 \pm 0.09) \times 10^3$ $M^{-1}s^{-1}$ and an intercept of (0.30 ± 0.05) s^{-1}. The intercept value is statistically significant. To determine if it is chemically important, lower concentrations of *L*-cysteine should be added in the kinetic experiments. The small non-zero intercept value will be omitted in our kinetic studies. So the rate of the reaction has a first-order dependence on $[L\text{-cysteine}]_{tot}$.

$$k_{obs} = k[L\text{-cysteine}]_{tot} \qquad (2\text{-}2)$$

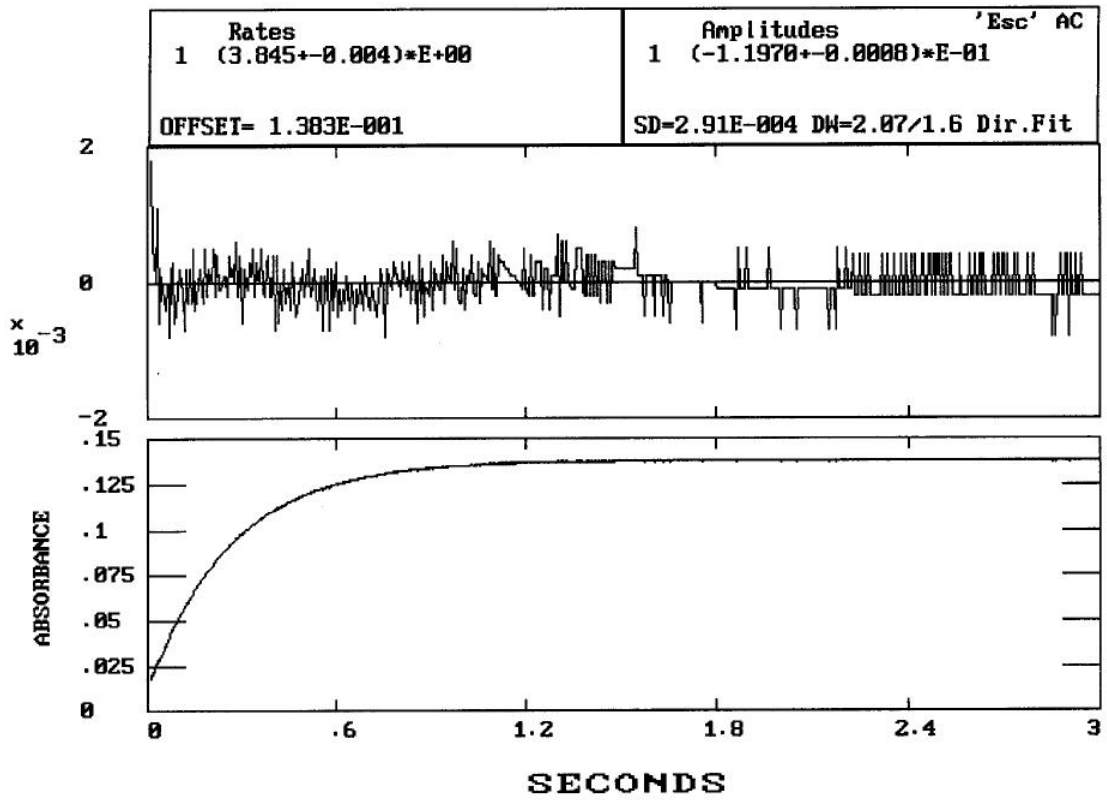

Figure 2-22. Reaction trace of the oxidation of *L*-cysteine by $[Fe^{III}(bpy)_2(CN)_2]^+$ at pH 5.99 (10.0 mM cacodylate buffer), in the presence of 0.20 mM PBN and 1.0 mM $dipic^{2-}$. At μ = 0.10 M (0.093 M $NaCF_3SO_3$) and 25.0 ^oC, using first-order fitting. $[Fe^{III}(bpy)_2(CN)_2^+]_0 = 2.5 \times 10^{-5}$ M, [*L*-cysteine]$_0 = 4.7 \times 10^{-4}$ M.

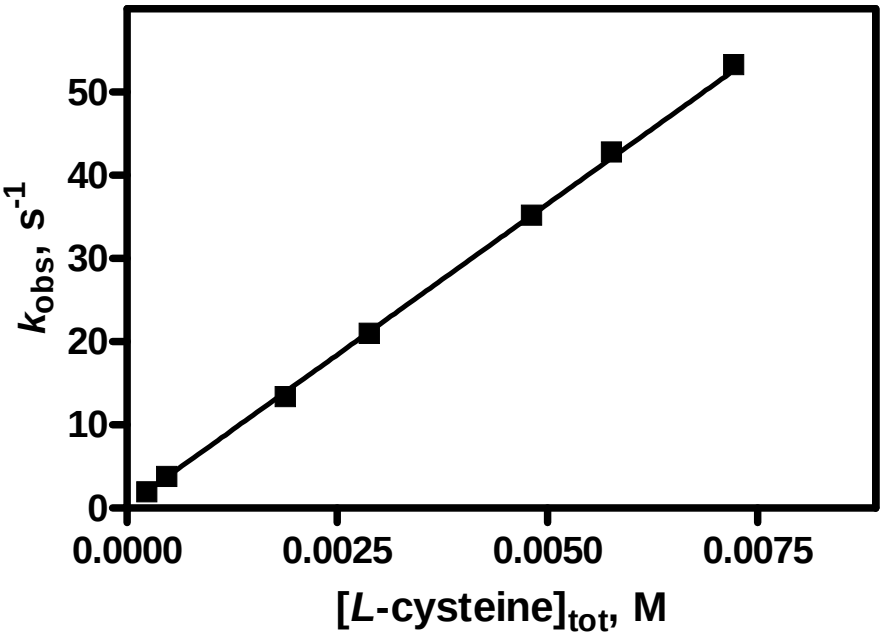

Figure 2-23. k_{obs} vs $[RSH]_{tot}$ for the oxidation of *L*-cysteine by $[Fe^{III}(bpy)_2(CN)_2]^+$ at pH 6.00 (10.0 mM cacodylate buffer), with 1.0 mM $dipic^{2-}$ and 0.20 mM PBN. At $\mu = 0.10$ M (0.093 M $NaCF_3SO_3$), and 25.0 ^oC, $[Fe^{III}(bpy)_2(CN)_2^+]_0 = 2.5 \times 10^{-5}$ M. (Weight by $1/Y^2$, $1/Y^2 = \Sigma(Y_{data} - Y_{curve})^2/Y_{data}^2$).

Table 2-11. [*L*-cysteine] dependence for the oxidation of *L*-cysteine by 2.5×10^{-5} M $[Fe^{III}(bpy)_2(CN)_2]^+$ at pH 6.00 (10.0 mM cacodylate buffer). In the presence of 1.0 mM $dipic^{2-}$, at μ= 0.10 M ($NaCF_3SO_3$) and 25.0 °C.

$[L\text{-cysteine}]_0$, M	k_{obs}, s^{-1}
0.000236	1.99
0.000471	3.82
0.00188	13.4
0.00288	21.0
0.00481	35.2
0.00576	42.8
0.00721	53.3

The kinetic pH dependence was revealed in a series of kinetic runs with the pH varied from 2.95 to 7.89 (the rate of the reaction is too fast when pH is higher than 7.89, and out of limit of the SF-51 instrument), the values of k_{obs} are summarized in Table 2-12. A plot of (log k_{obs}/ $[L\text{-cysteine}]_{tot}$) versus pH shown in Figure 2-24 indicates that the rates increase with the increase of pH. The rate pH dependence is clearly related to the three proton dissociation equilibrium constants of *L*-cysteine as follows,[117] and it implies that sulfur is the reactive center in the oxidation of *L*-cysteine.

$$HSCH_2CH(NH_3^+)CO_2H \rightleftharpoons HSCH_2CH(NH_3^+)CO_2^- + H^+ \qquad pK_{a1} = 1.90 \qquad (2\text{-}3)$$

$$HSCH_2CH(NH_3^+)CO_2^- \rightleftharpoons {}^-SCH_2CH(NH_3^+)CO_2^- + H^+ \qquad pK_{a2} = 8.18 \qquad (2\text{-}4)$$

$${}^-SCH_2CH(NH_3^+)CO_2^- \rightleftharpoons {}^-SCH_2CH(NH_2)CO_2^- + H^+ \qquad pK_{a3} = 10.30 \qquad (2\text{-}5)$$

Table 2-12. pH-dependent kinetic data for the oxidation of *L*-cysteine by $[Fe^{III}(bpy)_2(CN)_2]^+$. At μ= 0.10 M ($NaCF_3SO_3$) and 25.0 °C.[a]

[*L*-cysteine]$_0$, mM	[Buffer], mM	[CF_3SO_3Na], M	pH	k_{obs}, s^{-1}	k_{obs}/[*L*-cysteine]$_0$, M^{-1} s^{-1}
10.3	[chloroacetate]=10	0.095	2.95	0.0953	9.23
1.25	[chloroacetate]=10	0.092	3.21	0.0197	15.8
10.3	[chloroacetate]=10	0.090	3.62	0.366	35.5
2.06	[acetate]=10.0	0.096	4.06	0.203	98.5
2.06	[acetate]=10.0	0.092	4.44	0.467	2.26×10^2
2.48	[acetate]=10.0	0.092	4.85	1.42	5.73×10^2
2.48	[acetate]=10.0	0.089	5.23	3.26	1.31×10^3
2.48	[cacodylate]=10.0	0.094	5.69	8.74	3.52×10^3
0.470	[cacodylate]=10.0	0.093	5.99	3.82	8.11×10^3
0.990	[cacodylate]=10.0	0.093	6.46	19.1	1.93×10^4
0.488	[phosphate]=10.0	0.075	6.98	34.7	7.11×10^4
0.244	[phosphate]=10.0	0.075	7.40	41.6	1.70×10^5
0.244	[phosphate]=10.0	0.075	7.57	57.3	2.35×10^5
0.244	[phosphate]=10.0	0.075	7.89	106	4.33×10^5

[a] $[Fe^{III}(bpy)_2(CN)_2^+]_0$ = 25.0 μM; [PBN] = 0.20 mM; $[dipic^{2-}]$ = 1.0 mM.

In principle, the four different forms of *L*-cysteine can react with $[Fe^{III}(bpy)_2(CN)_2]^+$ through kinetically distinguishable terms, as shown in Equation 2-6-a:

$$k_{obs} = \left\{ \frac{k_1[H^+]^3 + k_2K_{a1}[H^+]^2 + k_3K_{a1}K_{a2}[H^+] + k_4K_{a1}K_{a2}K_{a3}}{[H^+]^3 + K_{a1}[H^+]^2 + K_{a1}K_{a2}[H^+] + K_{a1}K_{a2}K_{a3}} \right\} [RSH]_{tot} \qquad (2\text{-}6\text{-a})$$

where k_1-k_4 represent the reactivity of protonated, neutral, monoanionic, and dianionic *L*-cysteine species, respectively. A nonlinear least-squares fit of the data in Table 2-12 to

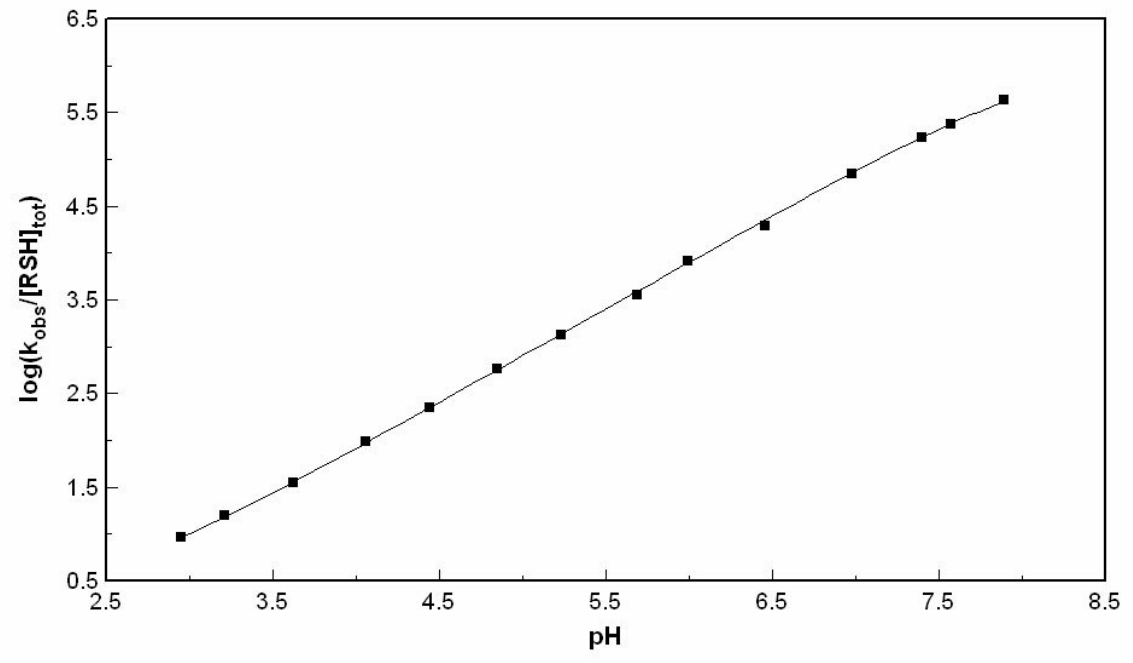

Figure 2-24. Plot of $\log(k_{obs}/[\text{L-cysteine}]_{tot})$ vs pH for the oxidation of *L*-cysteine by $[Fe^{III}(bpy)_2(CN)_2]^+$, in the presence of 0.20 mM PBN and 1.0 mM $dipic^{2-}$. At μ = 0.10 M and 25.0 ^oC. Solid line shows the fit to eq 2-8. (Weight by $1/Y^2$, $1/Y^2 = \Sigma(Y_{data}-Y_{curve})^2/Y_{data}^2$)

Equation 2-6-a yields (-21.3 ± 9.2) M^{-1} s^{-1} for k_1. In the oxidation of *L*-cysteine by octacyanomolybdate, Hung et al.[52] reported the rate constants, k_1 to k_4, with such order: 0 ≈ $k_1 < k_2 < k_3 > k_4$, and the smaller k_4 is thought due to the greater repulsion between dianionic *L*-cysteine and $[Mo(CN)_8]^{3-}$. Since $[Fe^{III}(bpy)_2(CN)_2]^+$, with + 1 charge, has very close standard potential as $[Mo(CN)_8]^{3-}$, the rate constants may be in such order: 0 ≈ $k_1 < k_2 < k_3 < k_4$. Then Equation 2-6-a can be converted to:

$$k_{obs} = \left\{ \frac{k_2 K_{a1}[H^+]^2 + k_3 K_{a1} K_{a2}[H^+] + k_4 K_{a1} K_{a2} K_{a3}}{[H^+]^3 + K_{a1}[H^+]^2 + K_{a1} K_{a2}[H^+] + K_{a1} K_{a2} K_{a3}} \right\} [RSH]_{tot} \qquad (2\text{-}7\text{-a})$$

The data in Table 2-12 were fit to Equation 2-7-a by using nonlinear least-squares model, with pK_{a1}, pK_{a2} and pK_{a3} held at the literature values of 1.90, 8.18 and 10.30.[117] The rate constants k_2, k_3 and k_4 that were obtained from the above fitting are (2.94 ± 0.24) M^{-1} s^{-1}, (1.22 ± 0.02) × 10^6 M^{-1} s^{-1}, and (6.30 ± 32.3) × 10^6 M^{-1} s^{-1}, respectively. The large statistical error in the value of k_4 implies that the contribution of dianionic *L*-cysteine is kinetically insignificant in such pH range. Then Equation 2-7-a can be simplified as:

$$k_{obs} = \left\{ \frac{k_2 K_{a1}[H^+]^2 + k_3 K_{a1} K_{a2}[H^+]}{[H^+]^3 + K_{a1}[H^+]^2 + K_{a1} K_{a2}[H^+] + K_{a1} K_{a2} K_{a3}} \right\} [RSH]_{tot} \qquad (2\text{-}8)$$

Applying a nonlinear least-squares model, the data in Table 2-12 were refit by Equation 2-8, as shown in Figure 2-24. The obtained rate constants k_2 and k_3 are (2.93 ± 0.23) and

$(1.22 \pm 0.02) \times 10^{6}$ M^{-1} s^{-1}. These results demonstrate that Equation 2-8 accurately represents the data.

(2). The oxidation of *L*-cysteine by $[Fe^{III}(bpy)(CN)_4]^-$. The reduction of 5.0×10^{-5} M $[Fe^{III}(bpy)(CN)_4]^-$ by various concentrations of *L*-cysteine, in the presence of 5.0 mM EDTA (pH ≤ 9.00), 10.0 mM EDTA (9.00 < pH ≤ 10.0) and 1.0 mM cyclam (pH > 10.0), was investigated at 25.0 ^{o}C and at constant ionic strength (μ = 0.10 M, $NaClO_4$). The rate of the reaction follows pseudo-first-order behavior over 3 half-lives. The pseudo-first-order rate constants (k_{obs}, s^{-1}) were evaluated by exponential fits of the kinetic curves, and replicate runs agreed to better than ± 5%. Figure 2-25 shows a reaction trace of oxidation of 5.05×10^{-3} M *L*-cysteine by 5.0×10^{-5} M $[Fe^{III}(bpy)(CN)_4]^-$ at pH 6.94 (10.0 mM cacodylate buffer), with 5.0 mM EDTA, at ionic strength of 0.10 M (0.061 M $NaClO_4$) and 25.0 ^{o}C. The rate of the reaction follows pseudo-first-order behavior, with a rate constant (k_{obs}) of 0.556 s^{-1}. A series of kinetic experiments was run by changing $[L\text{-cysteine}]_{tot}$ (the total concentration of *L*-cysteine), with 5.0×10^{-5} M Fe(III), 5.0 mM EDTA, and 10.0 mM cacodylate buffer (pH = 7.04), at μ = 0.10 M and 25.0 ^{o}C. The rate constant dependence on $[L\text{-cysteine}]_{tot}$ is summarized in Table 2-13, and plot of k_{obs} versus $[L\text{-cysteine}]_{tot}$ is shown in Figure 2-26. It is linear with slope of $(1.11 \pm 0.02) \times 10^{2}$ $M^{-1}s^{-1}$ and intercept of $(8.44 \pm 26.1) \times 10^{-4}$ s^{-1}. The intercept value is statistically zero. So the rate of the reaction has a first-order dependence on $[L\text{-cysteine}]_{tot.}$

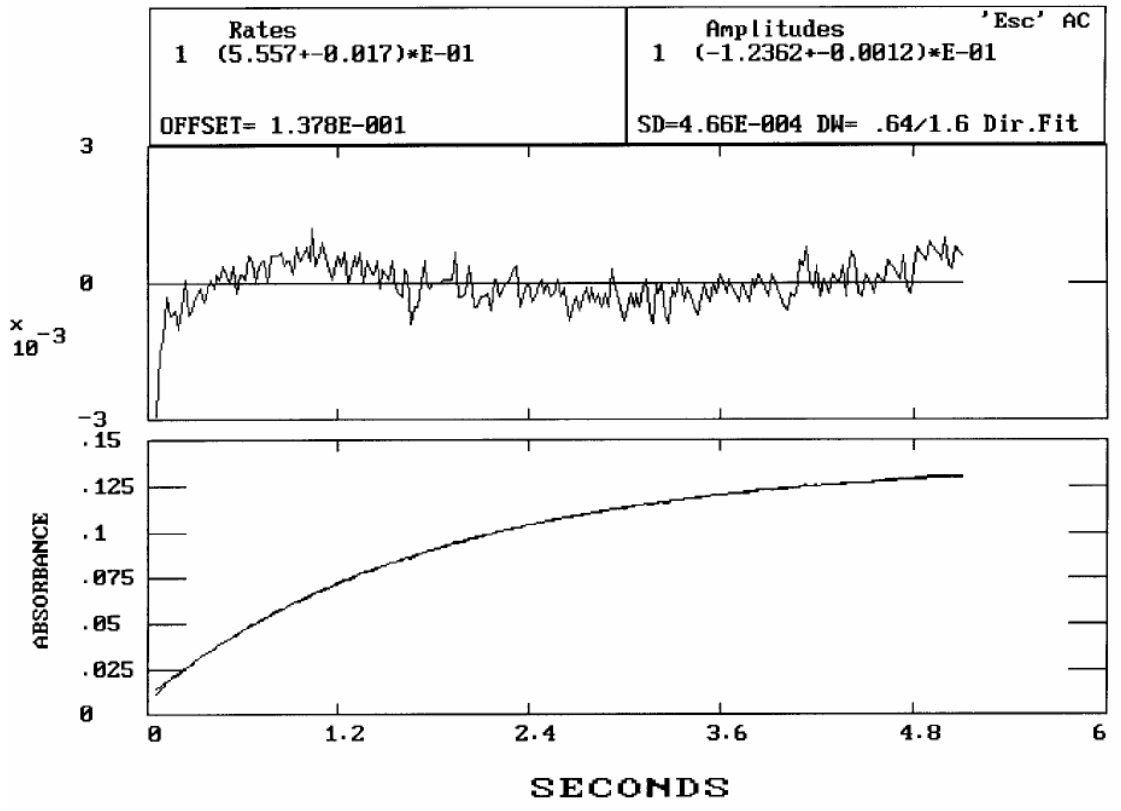

Figure 2-25. A reaction trace of oxidation of *L*-cysteine by $[Fe^{III}(bpy)(CN)_4]^-$ at pH 7.04 (10.0 mM cacodylate buffer), with 5.0 mM EDTA. At μ = 0.10M (0.061 M $NaClO_4$) and 25.0 ^oC. $[Fe^{III}(bpy)(CN)_4^-]_0 = 5.0 \times 10^{-5}$ M, $[L\text{-cysteine}]_0 = 5.05 \times 10^{-3}$ M

Table 2-13. [*L*-cysteine] dependence for the oxidation of *L*-cysteine by 5.0×10^{-5} M $[Fe^{III}(bpy)(CN)_4]^-$ at pH 6.92 (10.0 mM cacodylate). In the presence of 5.0 mM EDTA, at $\mu = 0.10$ M (0.061 M $NaClO_4$) and 25.0 ^oC.

$[L\text{-cysteine}]_0$, mM	pH	k_{obs}, s^{-1}
0.50	6.91	0.058
0.98	6.87	0.102
2.02	6.91	0.230
3.64	6.90	0.428
5.05	6.90	0.555
7.35	6.92	0.819
9.80	6.94	1.07
12.3	6.95	1.36

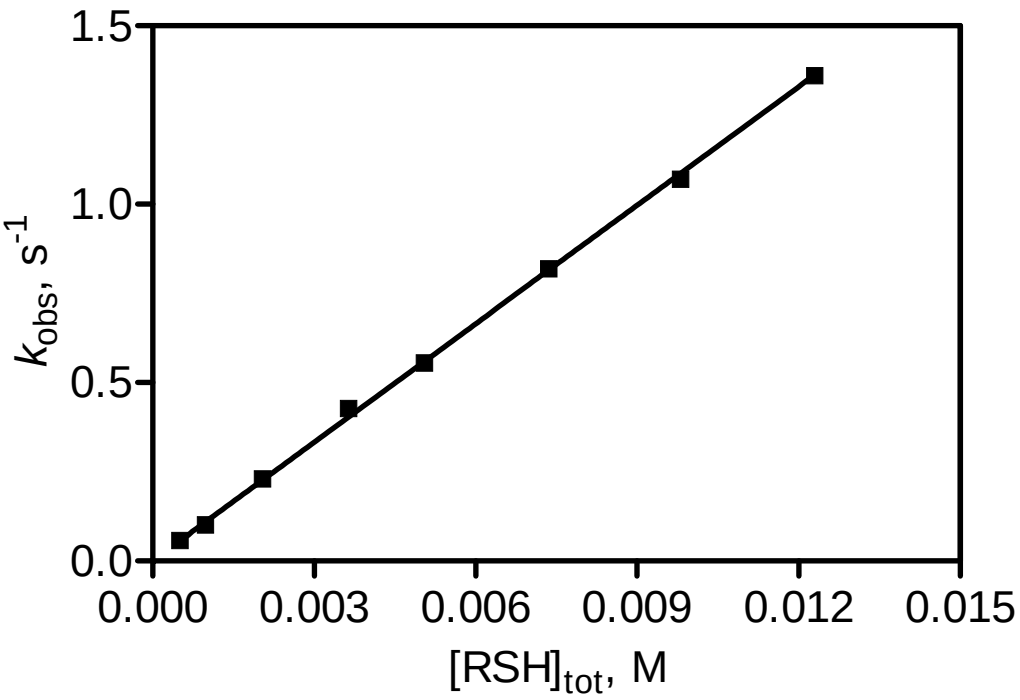

Figure 2-26. k_{obs} vs $[RSH]_{tot}$ for the oxidation of *L*-cysteine by $[Fe^{III}(bpy)(CN)_4]^-$ at pH 6.92 (10.0 mM cacodylate buffer), in the presence of 5.0 mM EDTA. At μ = 0.10 M (0.061 M $NaClO_4$), and 25.0 ^oC, $[Fe^{III}(bpy)(CN)_4^-]_0 = 5.0 \times 10^{-5}$ M.
(Weight by $1/Y^2$, $1/Y^2 = \Sigma(Y_{data} - Y_{curve})^2/Y_{data}^2$).

The kinetic pH dependence was revealed in a series of kinetic runs with pH values from 6.09 to 11.9, the values of k_{obs} being summarized in Table 2-14. A plot of (log k_{obs}/ [*L*-cysteine]$_{tot}$) versus pH is shown in Figure 2-27. The rate of the reaction increases with the increase of pH. The rate pH-dependence is clearly related to the three proton dissociation equilibrium constants of *L*-cysteine.[117]

Table 2-14. pH-dependent kinetic data for the oxidation of *L*-cysteine by 5.0×10^{-5} M $[Fe^{III}(bpy)(CN)_4]^-$ in aqueous solution.[a]

[*L*-cysteine]$_0$, mM	[EDTA], mM	[$NaClO_4$], M	[buffer], mM	pH	k_{obs}, s^{-1}	k_{obs}/[*L*-cysteine]$_0$, s^{-1} M^{-1}
24.6	5.0	0.075	10.0	6.09	0.371	15.1
9.70	5.0	0.063	10.0	6.44	0.406	41.8
10.4	5.0	0.063	10.0	6.61	0.469	45.1
5.05	5.0	0.061	10.0	6.90	0.555	110
1.04	5.0	0.046	10.0	7.37	0.305	293
0.47	5.0	0.041	10.0	7.72	0.300	638
0.50	5.0	0.041	10.0	8.06	0.521	1.04×10^3
0.52	5.0	0.060	10.0	8.59	0.939	1.80×10^3
0.51	5.0	0.050	10.0	9.04	1.21	2.37×10^3
0.49	10.0	0.034	0.0	9.56	1.75	3.57×10^3
0.49	10.0	0.026	0.0	9.86	2.01	4.10×10^3
0.52	0.0[b]	0.076	10.0	10.6	3.83	7.36×10^3
0.52	0.0[b]	0.099	0.0[c]	11.0	4.30	8.26×10^3
0.52	0.0[b]	0.090	0.0[d]	11.9	5.19	9.98×10^3

[a] at 25.0 °C, μ = 0.10 M; [b] [cyclam] = 1.0 mM; [c] [NaOH] = 1.0 mM; [d] [NaOH] = 10.0 mM.

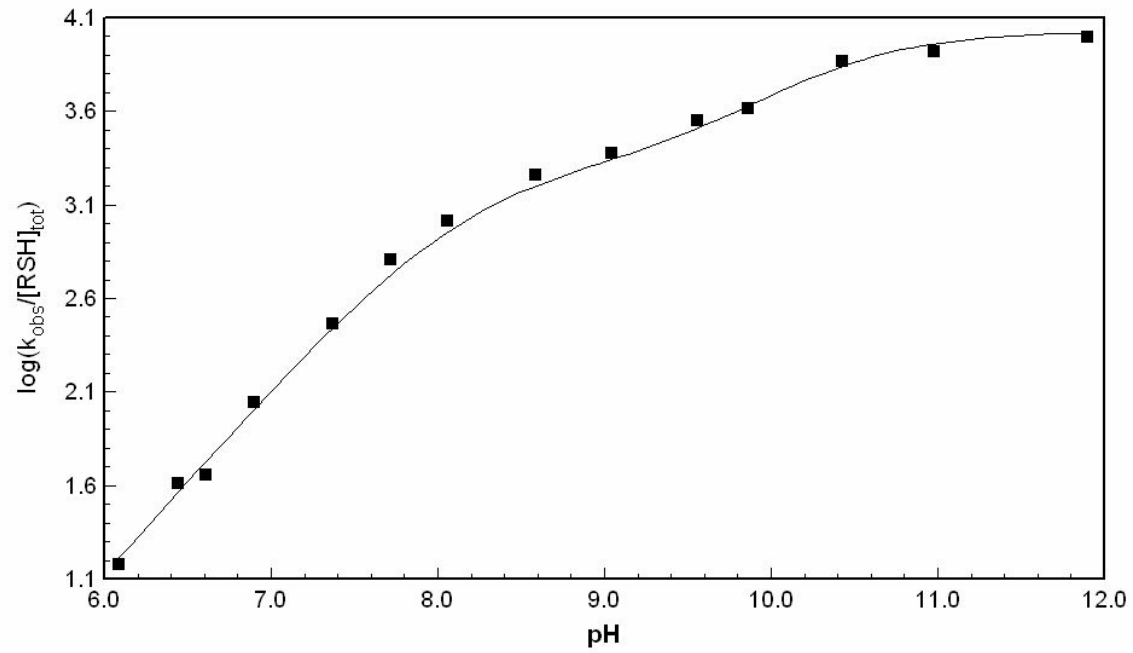

Figure 2-27. Plot of $\log(k_{obs}/[\text{L-cysteine}]_{tot})$ vs pH for the oxidation of *L*-cysteine by $[Fe^{III}(bpy)(CN)_4]^-$. With 5.0 mM EDTA (pH from 6.0 to 9.0), 10.0 mM EDTA (pH from 9.0 to 10.0) or 1.0 mM cyclam (pH > 10.0), at ionic strength of 0.10 M and 25.0 ^oC. Solid line shows the fit to eq 2-9. (Weight by $1/Y^2$, $1/Y^2 = \Sigma(Y_{data} - Y_{curve})^2/Y_{data}^2$)

$$k_{obs} = \left\{ \frac{k_{1'}[H^+]^3 + k_{2'}K_{a1}[H^+]^2 + k_{3'}K_{a1}K_{a2}[H^+] + k_{4'}K_{a1}K_{a2}K_{a3}}{[H^+]^3 + K_{a1}[H^+]^2 + K_{a1}K_{a2}[H^+] + K_{a1}K_{a2}K_{a3}} \right\} [RSH]_{tot} \qquad (2\text{-}6\text{-}b)$$

$$k_{obs} = \left\{ \frac{k_{2'}K_{a1}[H^+]^2 + k_{3'}K_{a1}K_{a2}[H^+] + k_{4'}K_{a1}K_{a2}K_{a3}}{[H^+]^3 + K_{a1}[H^+]^2 + K_{a1}K_{a2}[H^+] + K_{a1}K_{a2}K_{a3}} \right\} [RSH]_{tot} \qquad (2\text{-}7\text{-}b)$$

In principle, the four different forms of *L*-cysteine can react with $[Fe^{III}(bpy)(CN)_4]^-$ through kinetically distinguishable terms, as shown in Equation 2-6-a, where k_1-k_4 represent the reactivity of protonated, neutral, monoanionic, and dianionic *L*-cysteine species, respectively. In the oxidation of *L*-cysteine by octacyanomolybdate, Hung et al. reported the rate constants, k_1 to k_4, with such order: $0 \approx k_1 < k_2 < k_3 > k_4$, the smaller k_4 value is thought due to the greater repulsion between dianionic *L*-cysteine and $[Mo(CN)_8]^{3-}$.[52] In our case, $[Fe^{III}(bpy)(CN)_4]^-$ is a much weaker oxidant than $[Mo(CN)_8]^{3-}$, so $k_{1'}$ probably be close to zero and this term is omitted in the fitting. Then Equation 2-6-b is simplified into Equation 2-7-b. The data in Table 2-14 were fit to Equation 2-7-b by using nonlinear least-squares model, with pK_{a1}, pK_{a2} and pK_{a3} held at the literature values of 1.90, 8.18 and 10.30.[117] The rate constants $k_{2'}$, $k_{3'}$ and $k_{4'}$ were obtained from the above fitting are (-2.83 ± 2.74) M^{-1} s^{-1}, $(2.21 \pm 0.22) \times 10^3$ M^{-1} s^{-1}, and $(1.04 \pm 0.22) \times 10^4$ M^{-1} s^{-1} respectively. Excluding both $k_{1'}$ and $k_{2'}$ terms still yields good fitting results, as shown in Figure 2-27, with $k_{3'}$, $k_{4'}$ being $(2.04 \pm 0.16) \times 10^3$ M^{-1} s^{-1}, and $(1.07 \pm 0.25) \times 10^4$ M^{-1} s^{-1}. Therefore, Equation 2-9 represents the experimental data best.

$$k_{obs} = \left\{ \frac{k_{3'} K_{a1} K_{a2} [H^+] + k_{4'} K_{a1} K_{a2} K_{a3}}{[H^+]^3 + K_{a1}[H^+]^2 + K_{a1} K_{a2} [H^+] + K_{a1} K_{a2} K_{a3}} \right\} [RSH]_{tot} \qquad (2\text{-}9)$$

Alkaline cation effect. The alkaline cation catalysis was recently observed for the oxidation of *L*-cysteine by $[Mo^{V}(CN)_8]^{3-}$ in alkaline condition.[52] In that reaction, there is strong electrostatic repulsion between the –3 charge in $[Mo^{V}(CN)_8]^{3-}$ and the negative charge in the dianion form of *L*-cysteine. Since $[Fe^{III}(bpy)(CN)_4]^-$ has –1 charge, does it have alkaline cation effect in the oxidation of *L*-cysteine? For the oxidation of 5.1×10^{-4} M *L*-cysteine by 5.01×10^{-5} M $[Fe^{III}(bpy)(CN)_4]^-$ at pH 11.0, in the presence of 1.0 mM cyclam and 1.0 mM NaOH, 0.099 M $LiClO_4$ and $NaClO_4$ were added separately. The pseudo-first-order constants are 4.45 and 4.30 s^{-1}. It implies that no alkaline cation catalysis exists for the oxidation of *L*-cysteine by $[Fe^{III}(bpy)(CN)_4]^-$ at pH 11.0.

Discussion

In anaerobic aqueous solution, the oxidation of *L*-cysteine by the typical outer-sphere oxidants, $[Fe^{III}(bpy)_2(CN)_2]^+$ and $[Fe^{III}(bpy)(CN)_4]^-$, are strongly catalyzed by trace amount of Cu^{2+}. The copper-catalysis is well inhibited with the addition of 1.0 mM $dipic^{2-}$ for oxidation of *L*-cysteine by $[Fe^{III}(bpy)_2(CN)_2]^+$. The direct oxidation of *L*-cysteine by $[Fe^{III}(bpy)_2(CN)_2]^+$ was studied with the addition of 1.0 mM $dipic^{2-}$. For $[Fe^{III}(bpy)(CN)_4]^-$, $dipic^{2-}$ does not completely inhibit copper catalysis, but EDTA (pH ≤ 10.0) and cyclam (pH > 10.0) successfully suppress copper catalysis. The direct oxidation of *L*-cysteine by $[Fe^{III}(bpy)(CN)_4]^-$ was studied with the addition of 5.0 mM EDTA (pH ≤

9.00), 10.0 mM EDTA (9.00 < pH ≤ 10.0) and 1.0 mM cyclam (pH > 10.0). The rates of the above two reactions are pH dependent, and they increase with an increase in pH.

The copper catalyzed auto oxidation of *L*-cysteine at pH 13 was carefully studied by Cavallini et al.[123] Their UV-vis, EPR spectra and kinetic results indicate that the cysteine-Cu(II) complex represents the real intermediate catalyst. The cysteine-Cu(II) is slowly reduced to cysteine-Cu(I) when oxygen is removed. Recently, the oxidation of *L*-cysteine by ferricytochrome, nitro blue tetrazolium and oxygen was investigated by Pecci et al. at pH 7.4.[124] Their UV-vis and EPR results show that the cuprous bis-cysteine complex ($RS\text{-}Cu^{I}\text{-}SR$) is the catalytic species involved in the oxidation of cysteine. The two totally different results may be ascribed to their inconsistent pH environment. In our case, the kinetics was studied from pH 6.95 to 12.0 under anaerobic condition. So bis-cysteine complex ($RS\text{-}Cu^{I}\text{-}SR$) may be the catalytic species for the oxidation of *L*-cysteine by $[Fe^{III}(bpy)(CN)_4]^-$. Due to its complexity, understanding the mechanism of the copper catalytic oxidation of *L*-cysteine by $[Fe^{III}(bpy)(CN)_4]^-$ could be an area for future studies.

Generally, cuprous cation, soft acid, is coordinated to fairly soft base S^- and NH_2 to form five-member-ring cuprous cysteinate (RSCu(I)) and cuprous dicysteinate (RSCu(I)SR).[96,124-126] There are only a few reports about the stability constant of cuprous cysteinate (RSCu(I)) in the literature. Firstly, Kolthoff et al. [126] determined the stability constant of cuprous cysteinate (K_1) by polarographic titration in ammonia buffer (pH = 9.25), with a value of 1.5×10^{19} M^{-1}. Then Knoblock et al. [127] mistakenly reported the overall stability constant (β) of cupric dicysteinate (RSCu(II)SR) at pH 7.40 and ionic strength of 1.0 M, which should correspond to the overall stability constant of cuprous dicysteinate (RSCu(I)SR), with a value of 1.0×10^{16} M^{-1}. The above reported stability

constants show that it decreases with a decrease in pH, consistent with the theoretical estimation from the coordination chemistry of cysteine with cuprous cation. To break the strong binding of Cu(I) to the cysteine, strong chelating reagent EDTA or cyclam was added in the oxidation of *L*-cysteine by $[Fe^{III}(bpy)(CN)_4]^-$. Its copper-catalysis was inhibited with the addition of 5.0 mM EDTA (pH ≤ 9.00), 10.0 mM EDTA (9.00 < pH ≤ 10.0) and 1.0 mM cyclam (pH > 10.0).

Our ^{1}H-NMR and UV-vis spectra results indicate that the products of the reaction are *L*-cystine and the corresponding Fe(II) complexes; while in the oxidation of *L*-cysteine with octacyanomolybdate(V), *L*-cysteine-sulfinate was formed as well as $[Mo(CN)_8]^{4-}$ and *L*-cysteine.[52] This is attributed to the lower oxidative capability of $[Fe^{III}(bpy)_2(CN)_2]^+$ and $[Fe^{III}(bpy)(CN)_4]^-$ ($E_{1/2}$, $[Fe(bpy)_2(CN)_2]^{+/0}$ = 0.759 V; $E_{1/2}$, $[Fe(bpy)(CN)_4]^{-/2-}$ = 0.537 V; $E_{1/2}$, $[Mo(CN)_8]^{3-/4-}$ = 0.771 V [52]). The same phenomena were observed in the oxidation of TGA: dithiodiglycolic acid (RSSR) and sulfoacetate (RSO_3^-) were formed when hexachloroiridate(IV) was used as the oxidant; while only dithiodiglycolic acid (RSSR) was produced if octacyanomolybdate(V) was used as an oxidant ($E_{1/2}$, $[IrCl_6^-]^{2-/3-}$ = 0.892 V, $E_{1/2}$, $[Mo(CN)_8]^{3-/4-}$ = 0.771 V).[103,102] The results from ^{1}H-NMR spectra and spectrophotometric analysis demonstrate that the stoichiometric ratio of Δ[*L*-cysteine]/Δ[Fe(III)] is around 1:1. Based on the products' and stoichiometric ratio results, it is presumed that Fe(III) first reacts with *L*-cysteine to form *L*-cysteine thiyl radical, then cysteine combines with cysteine thiyl radical to form cystine radical, and finally cystine radical is oxidized by Fe(III) to produce Fe(II) and *L*-cystine (see mechanism, page 101 and 106).

The observance of non-pseudo-first-order kinetics in the presence of $Fe^{II}(bpy)_2(CN)_2$ at lower pH for the oxidation of *L*-cysteine by $[Fe^{III}(bpy)_2(CN)_2]^+$ is ascribed to the forward rate constant pH-dependence in Equation 2-10. Recently, Mezyk [128] measured the rate constants of radical disulfide anion formation for cysteine at different pH values: at pH 7.00, the rate constant (k_{10}) is $(3.77 \pm 0.33) \times 10^8$ M^{-1} s^{-1}, and the rate constant increases by a factor of nearly 2 at pH 8.00. Although the measurements were not performed in acidic media, the rate constants are assumed to decrease at pH values less than 7.00. So the slower forward rate constant of Equation 2-10 in acidic media may shift Equation 2-12 to backward direction, therefore the kinetic inhibition by $Fe^{II}(bpy)_2(CN)_2$ at lower pH was observed.

Perfect pseudo-first-order kinetics was obtained with the addition of 0.20 mM PBN to the reactants: at lower pH values, the rate constant increases by 15%; at higher pH values, the rate constant decreases by 6.7%. Earlier EPR results showed that PBN scavenges *L*-cysteine radical efficiently. [121] Although no rate constant for the reaction between PBN and *L*-cysteine was reported, the rate constant for formation of the adduct of cysteine thiyl radical to DMPO was determined by Davies et al., with a value of 2.10×10^8 M^{-1} s^{-1}.[129] It is also known that PBN is less reactive than DMPO, so the rate constant k_{11} in Equation 2-11 may be smaller than 2.10×10^8 M^{-1} s^{-1}. The addition of PBN induces the competition between Reaction 2-10 and 2-11. At lower pH values, the forward rate constant (k_{11}) in Equation 2-11 is higher than that (k_{10}) in Equation 2-10, which enables PBN to scavenge cysteine thiyl radical efficiently. So the reaction in Equation 2-12 shifts to the right, increasing the forward rate constant, k_{12}. At higher pH values, k_{11} is very close to or smaller than k_{10}, so the addition of PBN will not change k_{12}. Unfortunately, the

decrease of k_{obs} with the addition of PBN at pH 7.61 remains a puzzle. With the addition of PBN, the ^{1}H-NMR spectra show that the products of the reaction are $Fe^{II}(bpy)_2(CN)_2$, *L*-cystine and some unidentified compound with singlets. Since the adduct of PBN/cysteine thiyl radical is reportedly very unstable,[121] the singlets are possibly due to the decomposition of the adduct. The stoichiometric ratio of Δ[*L*-cysteine]/Δ[Fe(III)] is still 1:1 in the presence of PBN. Furthermore, according to our results, PBN reacts with $[Fe^{III}(bpy)_2(CN)_2]^+$ very slowly at pH 7.56, and no reaction takes place between PBN and *L*-cysteine. Thus, it is safe to add PBN to the reactants to scavenge the cyteine thiyl radicals that were formed in the oxidation of *L*-cysteine by $[Fe^{III}(bpy)_2(CN)_2]^+$.

$$RS^{\bullet} + RSH \rightleftharpoons RSSR^{\bullet -} + H^+ \qquad k_{10}, k_{-10}, K_{rad} \qquad (2\text{-}10)$$

$$RS^{\bullet} + PBN \rightleftharpoons PBN/RS^{\bullet} \qquad k_{11}, k_{-11} \qquad (2\text{-}11)$$

$$RS^- + [Fe(bpy)_2(CN)_2]^+ \rightleftharpoons RS^{\bullet} + Fe(bpy)_2(CN)_2 \qquad k_{12}, k_{-12} \qquad (2\text{-}12)$$

The mechanism of oxidation of *L*-cysteine by $[Fe^{III}(bpy)_2(CN)_2]^+$ is proposed as:

$$HSCH_2CH(NH_3^+)CO_2H \rightleftharpoons HSCH_2CH(NH_3^+)CO_2^- + H^+ \qquad pK_{a1} = 1.90 \qquad (2\text{-}3)$$

$$HSCH_2CH(NH_3^+)CO_2^- \rightleftharpoons {}^-SCH_2CH(NH_3^+)CO_2^- + H^+ \qquad pK_{a2} = 8.18 \qquad (2\text{-}4)$$

$$HSCH_2CH(NH_3^+)CO_2^- \rightleftharpoons {}^-SCH_2CH(NH_3^+)CO_2H \qquad pK_i = 5.5 \qquad (2\text{-}13)$$

$${}^-SCH_2CH(NH_3^+)CO_2H + [Fe(bpy)_2(CN)_2]^+ \rightleftharpoons Fe(bpy)_2(CN)_2 + {}^{\bullet}SCH_2CH(NH_3^+)CO_2H \qquad k_a, k_{-a} \qquad (2\text{-}14)$$

$$^{-}SCH_2CH(NH_3^{+})CO_2^{-} + [Fe(bpy)_2(CN)_2]^{+} \rightleftharpoons Fe(bpy)_2(CN)_2 + {}^{\bullet}SCH_2CH(NH_3^{+})CO_2^{-} \qquad k_b, k_{-b} \qquad (2\text{-}15)$$

$$RS^{\bullet} + RSH \rightleftharpoons RSSR^{\bullet -} + H^{+} \qquad k_{10}\, k_{-10}\, K_{rad}, \qquad (2\text{-}10)$$

$$RS^{\bullet} + PBN \rightleftharpoons PBN/RS^{\bullet} \qquad k_{11}, k_{-11} \qquad (2\text{-}11)$$

$$RSSR^{\bullet -} + [Fe(bpy)_2(CN)_2]^{+} \longrightarrow RSSR + Fe(bpy)_2(CN)_2 \qquad k_d \qquad (2\text{-}16)$$

The distinct kinetic inhibition by $Fe^{II}(bpy)_2(CN)_2$ at pH 3.20, in the absence of PBN, was well simulated by using Specfit/32 software package, as shown in Table 2-15. The mathematical model and one of the simulated results are listed in Table 2-16. The inhibition by $Fe^{II}(bpy)_2(CN)_2$ is insignificant if the rate constant of k_{-3a} (see Table 2-16) is set at lower than 5.0×10^8 M^{-1} s^{-1}. The above simulations assist us to understand the contribution of PBN to the lower pH's kinetic behavior. At lower pH, efficient scavenging of the cysteine radial by PBN slows down the backward reaction of Equation 2-14 dramatically. At higher pH, the cysteine radical is scavenged by cysteine efficiently. So it is reasonable to consider Equations 2-14 and 2-15 as irreversible in derivation of the rate law.

Applying steady-state for $RS^{\bullet}$ and $RSSR^{\bullet -}$, the rate law of the reaction is derived:

$$\frac{-\mathrm{d[Fe(III)]}}{\mathrm{dt}} = 2\left\{\frac{k_a K_{a1} K_i [H^+]^2 + k_b K_{a1} K_{a2} [H^+]}{[H^+]^3 + K_{a1}[H^+]^2 + K_{a1}K_{a2}[H^+] + K_{a1}K_{a2}K_{a3}}\right\}[RSH]_{tot}[Fe(III)] \qquad (2\text{-}17\text{-}a)$$

where k_{obs} is:

Table 2-15. Simulation results for the kinetic inhibition by $Fe^{II}(bpy)_2(CN)_2$ in the oxidation of *L*-cysteine by $[Fe^{III}(bpy)_2(CN)_2]^+$ at pH 3.20. In the presence of 1.0 mM dipic/dipic^{2-}(1:1), at μ = 0.10 M and 25.0 ^{o}C, using Specfit/32 software package.

$[Fe^{II}(bpy)_2(CN)_2]_0$, μM	$t_{1/2}$, s	
	Experimental[b]	Theory[c]
0	36.8	37.7
25	52.2	52.6
100	90.0	90.0

[a] $[L\text{-cysteine}]_0 = 1.25 \times 10^{-3}$ M, $[Fe^{III}(bpy)_2(CN)_2^+]_0 = 2.5 \times 10^{-5}$ M, [b] Calculated from k_{obs}.[c] Obtained from simulation

Table 2-16. Mathematical models for the simulation of the oxidation of 1.25×10^{-3} M *L*-cysteine by 2.5×10^{-5} M $[Fe^{III}(bpy)_2(CN)_2]^+$ at pH 3.20. In the presence of 1.0 mM dipic/dipic^{2-}(1:1) and 2.5×10^{-5} M $Fe^{II}(bpy)_2(CN)_2$, at μ = 0.10 M and 25.0 ^{o}C, using Specfit/32 software package.

Model Reaction Equation	Name	Rate constants	Initial Concentration, M		Half-life, s
$A \rightarrow B + C$	k_{1a}	10.0	A	1.25×10^{-3}	
$B + C \rightarrow A$	k_{-1a}	79.4	B	0.0	
$B \rightarrow D$	k_{2a}	1.0	C	6.31×10^{-4}	
$D \rightarrow B$	k_{-2a}	3.1×10^{5}	D	0.0	
$D + E \rightarrow F + G$	k_{3a}	2.80×10^{6}	E	2.5×10^{-5}	52.6
$F + G \rightarrow D + E$	k_{-3a}	4.00×10^{9}	F	0.0	
$B + F \rightarrow C + H$	k_{4a}	2.20×10^{8}	G	2.5×10^{-5}	
$C + H \rightarrow B + F$	k_{-4a}	1.38×10^{7}	H	0.0	
$E + H \rightarrow G + I$	k_{5a}	2.4×10^{9}	I	0.0	

A: $HSCH_2CH(NH_3^+)CO_2H$; B: $HSCH_2CH(NH_3^+)CO_2^-$; C: H^+; D: $^-SCH_2CH(NH_3^+)CO_2H$; E: $[Fe^{III}(bpy)_2(CN)_2]^+$; F: $^{\bullet}SCH_2CH(NH_3^+)CO_2H$; G: $Fe^{II}(bpy)_2(CN)_2$; H: $RSSR^{\bullet-}$; I: RSSR

$$k_{\text{obs}} = 2\left\{\frac{k_a K_{a1} K_i [\text{H}^+]^2 + k_b K_{a1} K_{a2} [\text{H}^+]}{[\text{H}^+]^3 + K_{a1}[\text{H}^+]^2 + K_{a1}K_{a2}[\text{H}^+] + K_{a1}K_{a2}K_{a3}}\right\}[\text{RSH}]_{\text{tot}} \qquad \text{(2-18-a)}$$

Comparing Equation 2-18-a with Equation 2-8, $2k_aK_i = k_2 = (2.93 \pm 0.23)$ and $2k_b = k_3 = (1.22 \pm 0.02) \times 10^6$ for the oxidation of *L*-cysteine by $[Fe^{III}(bpy)_2(CN)_4]^+$.

Very recently, a substantial kinetic isotope effect was observed in the oxidation of hydroxylamine by hexachloroiridate(IV) by Stanbury and his coworkers.[130] They ascribed the kinetic isotope effect to concerted proton-coupled electron transfer (PCET) from the neutral form of hydroxylamine to hexachloroiridate(IV). Therefore, PCET from the neutral form of *L*-cysteine to $[Fe^{III}(bpy)_2(CN)_2]^+$ (Equation 2-19) needs to be considered. If Equation 2-19 is the correct mechanism, then its rate constant, k_c, would correspond to half of k_2 in Equation 2-8, with (1.46 ± 0.12) M^{-1} s^{-1} for k_c. The standard potential of $RS^{\bullet}/RSH$ was calculated by using the standard potential of $RS^{\bullet}/RS^-$ ($E_{1/2}$ = 0.88 V vs NHE, refer to page 111) and the dissocation constant of neutral cysteine (pK_{a2} = 8.18), with $E_{1/2}$, $RS^{\bullet}/RSH$ = 1.36 V vs NHE. Based on the half-wave potential of $[Fe(bpy)_2(CN)_2]^{+/0}$, and that of $RS^{\bullet}/RSH$, ΔG^o for Equation 2-19 is 58 kJ mol^{-1}. Although this PCET mechanism can't be ruled out, the high ΔG^o value of Equation 2-19 implies that this process is unfavorable. The resonable self-exchange rate constants of $^{\bullet}SCH_2CH(NH_3^+)CO_2^-/^-SCH_2CH(NH_3^+)CO_2^-$ and $^{\bullet}SCH_2CH(NH_2)CO_2^-/$ $^-SCH_2CH(NH_2)CO_2^-$ that were calculated from Marcus equations also imply that this process occurs through electron transfer, not PCET. In contrast to electron transfer being favored for cysteine oxidation, PCET may be the favored pathway in oxidation of H_2NOH because ΔG^o is not unfavorable.

$$HSCH_2CH(NH_3^+)CO_2^- + [Fe(bpy)_2(CN)_2]^+ \rightleftharpoons$$

$$^{\bullet}SCH_2CH(NH_3^+)CO_2^- + Fe(bpy)_2(CN)_2 + H^+ \quad k_c \quad (2\text{-}19)$$

The oxidation of *L*-cysteine by $[Fe^{III}(bpy)(CN)_4]^-$ shows rather different behavior. For the oxidation of 2.60×10^{-3} M *L*-cysteine by 5.0×10^{-5} M $[Fe^{III}(bpy)(CN)_4]^-$ at pH 5.98 (0.093 M $NaClO_4$, 10.0 mM cacodylate, and 5.0 mM EDTA), non-first-order kinetics were obtained; when the concentration of *L*-cysteine increases by 10 times, first-order kinetics were successfully achieved. At pH values higher than 8.0, even when only 5.0×10^{-4} M *L*-cysteine were added, perfect first-order kinetics was obtained. Most importantly, the rate of the reaction does not change with the addition of PBN.

The above kinetic behavior is ascribed to the pH-dependence on the equilibrium of Equation 2-10. The equilibrium constant of Equation 2-10 was measured by Mezyk[131] using two techniques: integrated yields and measurements of kinetics. Both methods gave consistent results: at pH 6.0, the equilibrium constant (K_{10}) is 24.6 ± 5.4; at pH 7.0, K_{10} is 228 ± 4.3; at pH 8.5, it reaches a maximum, with a value of 1451 ± 16; then it decreases slowly with the increase of pH, it is 394.6 ± 8.6 at pH 13.0.[131] At lower pH and lower concentration of *L*-cysteine, less cysteine thiyl radical that was formed in the oxidation of *L*-cysteine by $[Fe^{III}(bpy)(CN)_4]^-$ combines with *L*-cysteine to form radical disulfide anion; with an increase of concentration of *L*-cysteine, more cysteine thiyl radical is consumed to form radical disulfide anion, favoring the achievement of first-order kinetics. With the increase of pH, the equilibrium constant of Equation 2-10 increases dramatically, so

Equation 2-10 shifts to the forward direction even at very low concentrations of *L*-cysteine. Therefore, first-order kinetics were observed in the oxidation of *L*-cysteine by $[Fe^{III}(bpy)(CN)_4]^-$ complex at higher pH.

Based on above information, the mechanism for the oxidation of *L*-cysteine by $[Fe^{III}(bpy)(CN)_4]^-$ is proposed:

$$^-SCH_2CH(NH_3^+)CO_2^- + [Fe(bpy)(CN)_4]^- \rightleftharpoons [Fe(bpy)(CN)_4]^{2-} + {}^\bullet SCH_2CH(NH_3^+)CO_2^- \qquad k_{b'}, k_{-b'} \quad (2\text{-}20)$$

$$^-SCH_2CH(NH_2)CO_2^- + [Fe(bpy)(CN)_4]^- \rightleftharpoons [Fe(bpy)(CN)_4]^{2-} + {}^\bullet SCH_2CH(NH_2)CO_2^- \qquad k_{c'}, \ k_{-c'} \quad (2\text{-}21)$$

$$RS^\bullet + RSH \rightleftharpoons RSSR^{\bullet -} + H^+ \qquad k_{10}, k_{-10}, K_{rad}, \quad (2\text{-}10)$$

$$RSSR^{\bullet -} + [Fe(bpy)(CN)_4]^- \longrightarrow RSSR + [Fe(bpy)(CN)_4]^{2-} \qquad k_{d'} \quad (2\text{-}22)$$

Furthermore, the mild kinetic inhibition by $[Fe^{II}(bpy)(CN)_4]^{2-}$ at pH 5.98 was well simulated by using Specfit/32 software package,[132] as shown in Table 2-17. The mathematical model and one of the simulated results are listed in Table 2-18. The simulations indicate that the forward rate constant of Equation 2-10 is one of the rate limiting steps, not the typical forward rate constant of Equation 2-22. Since the inhibition is insignificant for the reaction without the addition of $[Fe^{II}(bpy)(CN)_4]^{2-}$, the reactions from 2-20 to 2-21 are safely considered irreversible in the following derivation of rate law.

Table 2-17. Simulation results for the kinetic inhibition by $[Fe^{II}(bpy)(CN)_4]^{2-}$ in the oxidation of 2.6×10^{-3} M *L*-cysteine by 5.0×10^{-5} M $[Fe^{III}(bpy)(CN)_4]^-$ at pH 5.98. In the presence of 5.0 mM EDTA, at μ = 0.10 M and 25.0 ^oC, using Specfit/32 software.

$[[Fe^{II}(bpy)(CN)_4]^-]_0$, μM	$t_{1/2}$, s	
	Experimental[a]	Theory[b]
0	20.2	21.0
50	25.4	24.6
100	28.0	28.2

[a] Calculated from k_{obs}. [b] Obtained from simulation

Table 2-18. Mathematical models for the simulation of the oxidation of 2.6×10^{-3} M *L*-cysteine by 5.0×10^{-5} M $[Fe^{III}(bpy)(CN)_4]^-$ at pH 5.98. In the presence of 5.0 mM EDTA and 5.0×10^{-5} M $[Fe^{II}(bpy)(CN)_4]^{2-}$, at μ = 0.10 M and 25.0 ^oC, using Specfit/32 software.

Model Reaction Equation	Name	Rate constants	Initial Concentration, M		Half-life, s
$A \rightarrow B + C$	k_{1b}	10.0	A	2.6×10^{-3}	
$B + C \rightarrow A$	k_{-1b}	1.50×10^9	B	0.0	
$B \rightarrow C + D$	k_{2b}	1.0	C	1.06×10^{-6}	
$C + D \rightarrow B$	k_{-2b}	2.0×10^{10}	D	0.0	
$B + E \rightarrow F + G$	k_{3b}	1.05×10^3	E	5.0×10^{-5}	24.6
$F+G \rightarrow B + E$	k_{-3b}	1.75×10^9	F	0.0	
$A + F \rightarrow C + H$	k_{4b}	2.20×10^8	G	5.0×10^{-5}	
$C + H \rightarrow A + F$	k_{-4b}	1.38×10^7	H	0.0	
$E + H \rightarrow G + I$	k_{5b}	2.4×10^8	I	0.0	

A: $HSCH_2CH(NH_3^+)CO_2^-$; B: $^-SCH_2CH(NH_3^+)CO_2^-$; C: H^+; D: $^-SCH_2CH(NH_2)CO_2^-$; E: $[Fe^{III}(bpy)(CN)_4]^-$; F: $^\bullet SCH_2CH(NH_3^+)CO_2^-$; G: $[Fe^{II}(bpy)(CN)_4]^{2-}$; H: $RSSR^{\bullet-}$; I: RSSR

Applying steady-state for $RS^{\bullet}$ and $RSSR^{\bullet-}$, the rate law of the reaction is derived:

$$\frac{-\mathrm{d[Fe(III)]}}{\mathrm{dt}} = 2\left\{\frac{k_{b'}K_{a1}K_{a2}[\mathrm{H^+}] + k_{c'}K_{a1}K_{a2}K_{a3}}{[\mathrm{H^+}]^3 + K_{a1}[\mathrm{H^+}]^2 + K_{a1}K_{a2}[\mathrm{H^+}] + K_{a1}K_{a2}K_{a3}}\right\}[\mathrm{RSH}]_{\mathrm{tot}}[\mathrm{Fe(III)}] \quad (2\text{-}17\text{-b})$$

where k_{obs} is:

$$k_{\mathrm{obs}} = 2\left\{\frac{k_{b'}K_{a1}K_{a2}[\mathrm{H^+}] + k_{c'}K_{a1}K_{a2}K_{a3}}{[\mathrm{H^+}]^3 + K_{a1}[\mathrm{H^+}]^2 + K_{a1}K_{a2}[\mathrm{H^+}] + K_{a1}K_{a2}K_{a3}}\right\}[\mathrm{RSH}]_{\mathrm{tot}} \quad (2\text{-}18\text{-b})$$

The rate law has the same form as the empirical rate law (Equation 2-9). Comparing Equation 2-18-b with Equation 2-9, $2k_{b'} = k_{3'} = (2.04 \pm 0.16) \times 10^3\ M^{-1}\ s^{-1}$, $2k_{c'} = k_{4'}' = (1.07 \pm 0.25) \times 10^4\ M^{-1}\ s^{-1}$ for the oxidation of *L*-cysteine by $[Fe^{III}(bpy)(CN)_4]^-$.

In the above mechanism, the rate-limiting steps correspond to Equations 2-14 and 2-15 for the reduction of $[Fe^{III}(bpy)_2(CN)_2]^+$, and Equations 2-20 and 2-21 for the reduction of $[Fe^{III}(bpy)(CN)_4]^-$. They involve one-electron transfer from the thiolate forms of cysteine to the corresponding Fe(III) complex. The cysteine thiyl radicals generated in the above reactions react with cysteine rapidly to form disulfide radical anion, as shown in Equation 2-10.[133,134] Then the disulfide radical anion is oxidized to form *L*-cystine, as shown in Equation 2-16 and 2-22.

$$HSCH_2CH(NH_3^+)CO_2^- \rightleftharpoons HSCH_2CH(NH_2)CO_2H \qquad K_{23} \qquad (2\text{-}23)$$

Cysteine can exist as different tautomers in its neutral and monoanionic forms.[135,136] $HSCH_2CH(NH_3^+)CO_2^-$, the zwitterion, predominates in the neutral form, as well as a

small amount of $^{-}SCH_2CH(NH_3^+)CO_2H$ and $HSCH_2CHNH_2CO_2H$ ($pK_i = 5.5$, $pK_{23} = 4.88$).[136] $^{-}SCH_2CH(NH_3^+)CO_2^-$ is the main form in monoanionic cysteine, and the minor tautomers are $HSCH_2CHNH_2CO_2^-$ and $^{-}SCH_2CHNH_2CO_2H$. The equilibrium constant for the tautomerization of the monoanion to the thiol form is 0.40, while the equilibrium constant to the carboxylic form is quite small ($K = 6.02 \times 10^{-6}$).[136] Since the thiolate is the reactive form in the oxidation of *L*-cysteine by Fe(III), and the concentration of $^{-}SCH_2CHNH_2CO_2H$ is rather low, only $^{-}SCH_2CH(NH_3^+)CO_2^-$ needs to be included. Combining the estimated K_i with the measured value for $2k_aK_i = k_2 = (2.93 \pm 0.23)$ M^{-1} s^{-1} gives k_a value of $(4.63 \pm 0.36) \times 10^5$ M^{-1} s^{-1} and $2k_b = k_3 = (1.22 \pm 0.02) \times 10^6$ gives k_b $(6.10 \pm 0.01) \times 10^5$ M^{-1} s^{-1} for the oxidation of *L*-cysteine by $[Fe^{III}(bpy)_2(CN)_2]^+$; $2k_{b'} = k_{3'} = (2.04 \pm 0.16) \times 10^3$ M^{-1} s^{-1} gives $k_{b'}$ $(1.02 \pm 0.08) \times 10^3$ M^{-1} s^{-1} and $2k_{c'} = k_{4'} = (1.07 \pm 0.25) \times 10^4$ M^{-1} s^{-1} gives $k_{c'}$ $(5.35 \pm 1.20) \times 10^3$ M^{-1} s^{-1} for the oxidation of *L*-cysteine by $[Fe^{III}(bpy)(CN)_4]^-$.

$$RS^{\bullet -} + RS^{2-} \rightleftharpoons RSSR^{\bullet 3-} \qquad k_{24}, k_{-24} \qquad (2\text{-}24)$$

$$RSSR^{\bullet 3-} + e^- \rightleftharpoons 2\,RS^{2-} \qquad E_{25}^{o} \qquad (2\text{-}25)$$

$$RS^{\bullet -} + e^- \rightleftharpoons RS^{2-} \qquad E_{26}^{o} \qquad (2\text{-}26)$$

$$RS^{2-} + Fe(III) \rightleftharpoons RS^{\bullet -} + Fe(II) \qquad k_{27}, k_{-27} \qquad (2\text{-}27)$$

$$RS^{-} + Fe(III) \rightleftharpoons RS^{\bullet} + Fe(II) \qquad k_{28}, k_{-28} \qquad (2\text{-}28)$$

Here $RS^{\bullet}$, RS^-, $RS^{\bullet -}$, RS^{2-} and $RSSR^{\bullet 3-}$ refer to $^{\bullet}SCH_2CH(NH_3^+)CO_2^-$,

$^{-}SCH_2CH(NH_3^{+})CO_2^{-}$, $^{\bullet}SCH_2CH(NH_2)CO_2^{-}$, $^{-}SCH_2CH(NH_2)CO_2^{-}$ and

$^{-}O_2C(NH_2)CCHCH_2S\therefore SCH_2CH(NH_2)CO_2^{-}$.

The driving force for the one-electron transfer reaction can be evaluated if the standard potentials of $[Fe(bpy)_2(CN)_2]^{+/0}$, $[Fe(bpy)(CN)_4]^{-/2-}$ and $Cys^{\bullet-}/Cys^{2-}$ are known. The first reported standard potential of $Cys^{\bullet-}/Cys^{2-}$ was (0.73 ± 0.05) V, which was obtained by measurement of the electron-transfer equilibrium constants between the cystine radical anion and tyrosine at pH 13.0, with a value of 0.73 ± 0.05 V.[137] Recently, Mezyk[131] and Zhao et al.[133] determined the equilibrium constant for the formation of the cysteine radical disulfide anion (K_{24}), and both of them gave very close results. The equilibrium constant determined by Mezyk is 514 ± 13 M^{-1}, 466 ± 20 $M^{-1}$and 414.5 ± 6.2 M^{-1} at pH 10.0, 11.0 and 12.0, respectively; while that from Zhao is 706 M^{-1} at pH 10.5. Then Mezyk and Armstrong theoretically calculated the standard potential of $RSSR^{\bullet 3-}/2RS^{2-}$, with $E_{1/2,}$ $(RSSR^{\bullet 3-}/2RS^{2-})$ = 0.60 V vs NHE.[134] At pH 12.0, nearly all of *L*-cysteine exists in dianion form. Based upon the standard potential (E_{25}^{o} = 0.60 V vs NHE) of Equation 2-25 and the equilibrium constant of Equation 2-24 at pH 12.0 (K_{24} = 414.5 ± 6.2 M^{-1}), the standard potential of $RS^{\bullet-}/RS^{2-}$ was calculated, with $E_{1/2}$, $RS^{\bullet-}/RS^{2-}$ = 0.755 V vs NHE. The standard potential of $Cys^{\bullet-}/Cys^{2-}$ was also calculated by Hung et al.[52], with $E_{1/2}$, $(Cys^{\bullet-}/Cys^{2-})$ = (0.76 ± 0.02) V at pH 13, consistent with our results. The standard potential of $Cys^{\bullet}/Cys^{-}$ was calculated by using the standard potential of $Cys^{\bullet-}/Cys^{2-}$($E_{1/2}$ = 0.76 V), microscopic dissociation constant of cysteine radical ($^{\bullet}SCH_2CH(NH_3^{+})CO_2^{-}$, $pK_{S'}$ = 8.26 ± 0.04 [134]) and the macroscopic dissociation constant

of cysteine monanion ($^{-}SCH_2CH(NH_3^{+})CO_2^{-}$, p$K_{SNN}$ = 10.36 [134]), with $E_{1/2}$, $Cys^{\bullet}/Cys^{-}$ = 0.88 V vs NHE.

Then ΔG^{o}, (21.5 ± 1.9 kJ mol^{-1}), is derived from the corrected standard potential of $Cys^{\bullet-}/Cys^{2-}$ and $[Fe(bpy)(CN)_4]^{-/2-}$ ($E_{1/2}$, $[Fe(bpy)(CN)_4]^{-/2-}$ = 0.537 V, $E_{1/2}$, $Cys^{\bullet-}/Cys^{2-}$ = 0.76 V), corresponding to the equilibrium constant of 1.70×10^{-4} for Equation 2-27. The ΔG^{o} of Equation 2-28 is derived from the corrected standard potentials of $Cys^{\bullet}/Cys^{-}$, $[Fe(bpy)_2(CN)_2]^{+/0}$ and $[Fe(bpy)(CN)_4]^{-/2-}$ ($E_{1/2}$, $Cys^{\bullet}/Cys^{-}$ = 0.88 V, $E_{1/2}$, $[Fe(bpy)(CN)_4]^{-/2-}$ = 0.537 V, $E_{1/2}$, $[Fe(bpy)_2(CN)_2]^{+/0}$ = 0.759 V), which are 33.1 kJ mol^{-1}, 11.7 kJ mol^{-1} for the reduction of $[Fe(bpy)_2(CN)_2]^{+}$ and $[Fe(bpy)(CN)_4]^{-}$, corresponding to the equilibrium constants of 9.0×10^{-3} and 1.59×10^{-6}.

The cross-relationship of Marcus theory is applicable to the self-exchange rate constant of the $^{\bullet}SCH_2CH(NH_2)CO_2^{-}/^{-}SCH_2CH(NH_2)CO_2^{-}$ couple provided reaction 2-27 follows an outer-sphere mechanism. The following equations from Marcus theory were used to calculate the self-exchange rate constant of the $^{\bullet}SCH_2CH(NH_2)CO_2^{-}/^{-}SCH_2CH(NH_2)CO_2^{-}$ couple:[92]

$$k_{12} = (k_{11}k_{22}K_{12}f_{12})^{1/2}W_{12} \tag{2-29}$$

$$\ln f_{12} = \frac{[\ln K_{12} + (w_{12} - w_{21})/\mathrm{RT}]^2}{4[\ln(k_{11}k_{22}/Z^2) + (w_{11} + w_{22})/\mathrm{RT})]} \tag{2-30}$$

$$W_{12} = \exp(-w_{12} - w_{21} + w_{11} + w_{22})/2\mathrm{RT} \tag{2-31}$$

$$w_{ij} = 4.23 Z_i Z_j / [r(1 + 0.328 r\sqrt{\mu})] \quad (2\text{-}32)$$

In these equations, k_{12} is the observed cross electron-transfer rate constant, $(5.20 \pm 0.11) \times 10^3$ M^{-1} s^{-1}, and k_{11} and k_{22} are the self-exchange rate constants of the $\bullet SCH_2CH(NH_2)CO_2^-/^-SCH_2CH(NH_2)CO_2^-$ and $[Fe(bpy)(CN)_4]^{-/2-}$ redox couples. The self-exchange rate constant (k_{22}) of $[Fe(bpy)(CN)_4]^{-/2-}$ redox couple was reported by Stasiw and Wilkins in the study of the oxidation of $[Fe(bpy)(CN)_4]^{2-}$ by $[Fe(CN)_6]^{3-}$, with the value of 4×10^7 M^{-1} s^{-1}.[138] However, the charge effect was not included in the calculation, and the self-exchange rate constant of $[Fe(CN)_6]^{3-/4-}$($k_{11} = 5 \times 10^3$ M^{-1} s^{-1}) is not accurate. It is known that the electron-transfer reaction between $[M(CN)_6]^{3-}$ and $[M(CN)_6]^{4-}$(M = Fe, Os) in homogeneous solution is catalyzed by alkali metal ion.[139,140] The uncatalyzed self exchange rate constant of $[Fe(CN)_6]^{3-/4-}$ was determined by NMR line broadening method using either crypt-2,2,2 or 18-crown-6 to inactivate the potassium counterion catalysis, with k_0 of 2.4×10^2 M^{-1} s^{-1}, much smaller than Stasiw and Wilkins' report.[140] To avoid the high charge effect of $[Fe(CN)_6]^{3-/4-}$, the self-exchange rate constant (k_{22}) of $[Fe(phen)(CN)_4]^{-/2-}$ redox couple was recalculated by us using Marcus' equations from the oxidation *L*-ascorbic acid by $[Fe(phen)(CN)_4]^-$.[92,111,141,142] K_{33} is the electron-transfer equilibrium constant of Equation 2-33, with a value of 0.02. Z is the collision frequency that the value of 1×10^{11} M^{-1} s^{-1} is used in our calculation. Z_i and Z_j are ionic charges on the reactants, R is the ideal gas constant (1.987×10^{-3} kcal mol^{-1}), and r is the center-to-center distance between reactants while in contact. The radii of $[Fe(phen)(CN)_4]^-$ and HA^- are 5.33 [111] and 3.00 Å[141], respectively. Using the above

known parameters, the self-exchange rate constant of $[Fe(phen)(CN)_4]^{-/2-}$ was recalculated with 8.39×10^5 M^{-1} s^{-1}.

$$[Fe(phen)(CN)_4]^- + HA^- \rightleftharpoons [Fe(phen)(CN)_4]^{2-} + HA^{\bullet} \qquad K_{33} \qquad (2\text{-}33)$$

Since $[Fe(bpy)(CN)_4]^-$ has similar size as that of $[Fe(phen)(CN)_4]^-$, the self-exchange rate constant (k_{22}) of $[Fe(bpy)(CN)_4]^{-/2-}$ redox couple is assumed as 8.39×10^5 M^{-1} s^{-1}, and it is applied for the following calculation. K_{12} is the electron-transfer equilibrium constant of Equation 2-27, with a value of 1.70×10^{-4}. Z is the collision frequency that the value of 1×10^{11} M^{-1} s^{-1} is used in our calculation. Z_i and Z_j are ionic charges on the reactants, R is the ideal gas constant (1.987×10^{-3} kcal mol^{-1}), and r is the center-to-center distance between reactants while in contact. The radii of $[Fe(bpy)(CN)_4]^-$ and $^-SCH_2CH(NH_2)CO_2^-$ are 5.33 Å[111] and 3.00 Å[52], respectively. Using the above known parameters, the self-exchange rate constant of $^{\bullet}SCH_2CH(NH_2)CO_2^{-}/^{-}SCH_2CH(NH_2)CO_2^-$, k_{11}, is calculated as 3.66×10^5 M^{-1} s^{-1}, which is higher than that derived from the reaction of $[Mo(CN)_8]^{3-}$ with *L*-cysteine ($k_{11} = 5.4\times 10^3$ M^{-1} s^{-1}).[52] The smaller self-exchange rate constant of $\bullet SCH_2CH(NH_2)CO_2^{-}/^{-}SCH_2CH(NH_2)CO_2^-$ that was derived from the oxidation of *L*-cysteine by $[Mo(CN)_8]^{3-}$ is ascribed to the high negative charge of Mo(V). Although alkaline metal cation catalysis exists for the oxidation of *L*-cysteine by $[Mo(CN)_8]^{3-}$,[52] the lower self-exchange rate constant implies that repulsion between Mo(V) and RS^{2-} is dominant at higher pH values. However, less negative charge in $[Fe(bpy)(CN)_4]^-$ endows its weaker repulsion with *L*-cysteine dianion

(RS^{2-}), and no alkaline metal cation effect was observed in the oxidation *L*-cysteine by $[Fe(bpy)(CN)_4]^-$ at pH 11.0. Therefore, the higher k_{11} value of $^{\bullet}SCH_2CH(NH_2)CO_2^-$/ $^-SCH_2CH(NH_2)CO_2^-$ that was derived from the oxidation of *L*-cysteine by $[Fe(bpy)(CN)_4]^-$ is reasonable. Using Marcus' Equations (2-29 to 2-32) and the known parameters, the self-exchange rate constant of $^{\bullet}SCH_2CH(NH_3^+)CO_2^-$/ $^-SCH_2CH(NH_3^+)CO_2^-$, k_{11}, is calculated as 2.62×10^6 M^{-1} s^{-1}.

Marcus' theory is also applicable for the oxidation of *L*-cysteine by $[Fe^{III}(bpy)_2(CN)_2]^+$. There is no report about the self-exchange rate constant (k_{22}) of the $[Fe(bpy)_2(CN)_2]^{+/0}$ redox couple. It was calculated using Marcus' equations from the oxidation *L*-ascorbic acid by $[Fe(bpy)_2(CN)_2]^+$, [92,111,141,142] with the value of 1.30×10^7 M^{-1} s^{-1}. The radii of $[Fe(bpy)_2(CN)_2]^+$ and $^-SCH_2CH(NH_3^+)CO_2^-$ estimated from CPK models are 6.77 Å [111] and 3.00 Å [52], respectively. Using the above known parameters, the self-exchange rate constant of $\bullet SCH_2CH(NH_3^+)CO_2^-/^-SCH_2CH(NH_3^+)CO_2^-$, k_{11}, is calculated as 2.50×10^6 M^{-1} s^{-1}, very close to that obtained from the oxidation of *L*-cysteine by $[Fe(bpy)(CN)_4]^-$ (k_{11}= 2.62×10^6 M^{-1} s^{-1}). Comparing the self-exchange rate constant of $^{\bullet}SCH_2CH(NH_2)CO_2^-/^-SCH_2CH(NH_2)CO_2^-$ with $\bullet SCH_2CH(NH_3^+)CO_2^-/^-$ $SCH_2CH(NH_3^+)CO_2^-$, the smaller self-exchange rate constant of $^{\bullet}SCH_2CH(NH_2)CO_2^-/^-$ $SCH_2CH(NH_2)CO_2^-$ is ascribed to their negative-negative charge repulsion. The rapid self-exchange rate constants of $^{\bullet}SCH_2CH(NH_2)CO_2^-/^-SCH_2CH(NH_2)CO_2^-$ and $^{\bullet}SCH_2CH(NH_3^+)CO_2^-/^-SCH_2CH(NH_3^+)CO_2^-$) are consistent with the small internal reorganizational energy for the formation of cysteine radical.[143] This implies that the

oxidation of *L*-cysteine by $[Fe(bpy)(CN)_4]^-$ may occur through one-electron outer-sphere transfer reactions.

Conclusion

Copper catalysis was observed in the oxidation of *L*-cysteine by $[Fe(bpy)_2(CN)_2]^+$ and $[Fe(bpy)(CN)_4]^-$ in anaerobic aqueous solution. With the addition of 1.0 mM $dipic^{2-}$, 5.0 mM EDTA/1.0 mM cyclam, the copper-catalysis was effectively inhibited, and the direct oxidation of *L*-cysteine by outer-sphere oxidants ($[Fe(bpy)_2(CN)_2]^+$ and $[Fe(bpy)(CN)_4]^-$) was first reported by us. The rate-limiting step is electron transfer to form a cysteine radical and the corresponding Fe(II) complex. Only the thiolate forms of cysteine are reactive. The products of the reaction are *L*-cystine and the corresponding Fe(II) complex. The rate constants increase with increasing pH. For the oxidation of *L*-cysteine by $[Fe(bpy)(CN)_4]^-$, the self-exchange rate constants of $^{\bullet}SCH_2CH(NH_3^+)CO_2^-/^-SCH_2CH(NH_3^+)CO_2^-$ and $\bullet SCH_2CH(NH_2)CO_2^-/^-SCH_2CH(NH_2)CO_2^-$, k_{11}, were obtained by applying Marcus theory with 2.62×10^6 M^{-1} $s^{-1}$and 3.66×10^5 M^{-1} s^{-1}, respectively. The self-exchange rate constants of $^{\bullet}SCH_2CH(NH_3^+)CO_2^-/^-SCH_2CH(NH_3^+)CO_2^-$ was also obtained from the reaction between *L*-cysteine and $[Fe(bpy)_2(CN)_2]^+$ by applying Marcus theory, with 2.50×10^6 M^{-1} s^{-1}. No observance of a long lived intermediate state in the reaction and the rapid self-exchange rate constants of cysteine/cysteine radical imply that the oxidation of *L*-cysteine by the Fe(III) complexes may occur through a one-electron outer-sphere transfer reaction.

CHAPTER THREE

OXIDATION OF IODIDE BY A SERIES OF Fe(III) COMPLEXES IN ACETONITRILE

Introduction

The general features of the kinetics and mechanisms of oxidation of excess iodide by typical outer-sphere oxidants in aqueous solution are well understood. Currently, there are insufficient experimental data about the kinetics of oxidation of iodide in nonaqueous solvent. All of the relevant studies are carried out in aqueous-nonaqueous cosolvent systems, and are limited to three oxidants: $[Fe^{III}(phen)_3]^{3+}$, $[Ir^{IV}Cl_6]^{2-}$ and $[Co^{III}W_{12}O_{40}]^{5-}$.[144-146] The reaction of $[Fe^{III}(phen)_3]^{3+}$ was studied in water/methanol with up to 20% alcohol.[144] In the case of $[Ir^{IV}Cl_6]^{2-}$, a variety of aqueous solvent mixtures were used, but the aqueous fraction was never < 20%.[145] With $[Co^{III}W_{12}O_{40}]^{5-}$, aqueous solvent mixtures again were used in this case, with up to 40% methanol, 40% acetonitrile, and 60% dimethyl sulfoxide (DMSO).[146] Hence, little is revealed about the oxidation of iodide in genuine nonaqueous media. Moreover, the association constant of I^- with I_2 in acetonitrile is much higher than that in aqueous solution,[147] which introduces a strong driving force for the oxidation of iodide in acetonitrile. Therefore, this redox reaction in acetonitrile may have some new kinetic features.

The development of dye-sensitized solar cell (DSSC) prompts us to understand the oxidation of iodide in acetonitrile. In 1990s, Grätzel and his coworkers initially invented nanoncrystalline dye-sensitized solar cell (DSSC) with a solar-to-electric energy conversion efficiency of 11%.[57,64] They are typically fabricated with the two electrodes immersed in a nonaqueous solvent with an I^-/I_3^- electrolyte that mediates the redox reaction. One of the electrodes is composed of TiO_2 with a surface-adsorbed dye, (Ru(4,4'-dicarboxylic acid-2,2'-bipyridine)$_2$(NCS)$_2$.[64,148] It is generally believed that one function of the iodide is to reduce the photochemically oxidized dye back to its resting state.[60,72] A variety of $[Ru^{II}(bpy)_2(SCN)_2]$ derivatives have been used in the Grätzel photoelectrochemical cell over the last decade. Unfortunately, the poor stability of $[Ru^{III}(bpy)_2(SCN)_2]^+$ derivatives in acetonitrile impedes studies of its reduction by iodide.

Recently, it was observed that electron transfer from the excited states of the adsorbed sensitizers to the conduction band of TiO_2 occurs within hundreds of femtoseconds.[78,79,149] With its near unity quantum efficiency, it implies that this electron transfer occurs from initially populated, nonrelaxed excited states, not from the lowest excited states.[150] This new theory makes it possible to introduce iron(II) polypyridyls to replace current $[Ru^{II}(bpy)_2(SCN)_2]$ derivatives. More recently, Ferrere and Gregg demonstrated that [Fe(4,4'-dicarboxylic acid-2,2'-bipyridine)$_2$(CN)$_2$], an iron(II) polypyridyl, can sensitize nanocrystalline TiO_2 in acetonitrile/3-methyl-2-oxazolidinone (9/1).[151] So iron(II) polypyridyls can be potentially effective and inexpensive dyes in DSSCs. Therefore, four different substitution-inert Fe(III) complexes were selected, including $[Fe^{III}(5\text{-Cl-phen})_2(CN)_2]^+$, $[Fe^{III}(bpy)_2(CN)_2]^+$, $[Fe^{III}(dmbpy)_2(CN)_2]^+$ and $[Fe^{III}(CH_3Cp)_2]^+$.

Herein, the kinetics and mechanism of the oxidation of excess iodide by a series of substitution-inert Fe(III) complexes in acetonitrile are studied. The copper catalysis was effectively inhibited with the addition of 5.0 mM 2,2'-bipyridine (bpy). The rate of the copper-catalysis inhibited reaction is closely related to the half-wave potentials of the Fe(III) complexes: the higher of the half-wave potential, the faster of the reaction it is. The rate law of the direct oxidation of iodide has the same form as that in aqueous media. The standard potential of $I^{\bullet}/I^{-}$ is derived from the kinetic inhibition by $Fe^{II}(bpy)_2(CN)_2$.

Experimental Section

Reagents and Solutions. 2, 2'-bipyridyl (Aldrich), 4, 4'-dimethyl-2, 2'-bipyridyl (Aldrich), 5-chloro-phenanthroline (GFS Chemicals), ferrous ammonium sulfate hexahydrate (Fisher), potassium cyanide (Fisher), sodium hexafluorophosphate (Aldrich), ferric nitrate (Fisher), decamethylferrocene (Aldrich), cupric nitrate trihydrate (Fisher), iodine (J. T. Baker), silver nitrate (Fisher), nitric acid (Fisher), sulfuric acid (Fisher), acetonitrile (Fisher), acetonitrile-d_3 (Aldrich), acetone (Fisher), n-hexane (Fisher), methanol (Fisher), ethanol (Fisher), acetic acid (Fisher), diethyl ether (Fisher), and Sephadex LH-20-100 resin (Sigma) were used without further purification. 1,1'-dimethylferrocene (Aldrich) was recrystallized from ethanol. Et_4NBF_4 (Aldrich) was recrystallized three times from a mixture of methanol and n-hexane (4:1) and dried under vacuum at 96 ^{o}C for 12 hours. Et_4NI (Aldrich) was recrystallized from water and dried under vacuum at 100 ^{o}C for 12 hours. The concentration of Et_4NI in acetonitrile was standardized by titration with standard aqueous $AgNO_3$, using Eosin as indicator.[152]

Distilled deionized water was obtained from a Barnstead NANO pure infinity ultrapure water system. Solutions of Fe(III) complexes and iodide in acetonitrile were prepared just prior to use, and kept in the dark to prevent any photochemical change. For reaction between $[Fe^{III}(CH_3Cp)_2]^+$ and iodide conducted in the stopped-flow spectrophotometer, both Et_4NI and $[Fe^{III}(CH_3Cp)_2]^+$ were prepared maintaining the appropriate concentrations of the other reagents, purged with argon gas, and transferred via gastight glass syringe. For the oxidation of iodide by the other three Fe(III) complexes, the reactants are not sensitive to O_2. However, all solutions were purged with Ar or N_2 before reaction to prevent potential complications caused by O_2.

Preparation of $[Fe^{II}(bpy)_2(CN)_2]\cdot 3H_2O$ and $[Fe^{III}(bpy)_2(CN)_2]NO_3\cdot 2H_2O$. $[Fe^{II}(bpy)_2(CN)_2]\cdot 3H_2O$ and $[Fe^{III}(bpy)_2(CN)_2]NO_3\cdot 2H_2O$ were prepared by following Schlit's method.[107] The detailed procedures for the synthesis of these two iron complexes are described in Chapter Two. ^{1}H-NMR (400 MHz/CD_3CN) of $[Fe^{II}(bpy)_2(CN)_2]\cdot 3H_2O$: 8.94 (s, 2H); 8.34 (d, J = 8.1, 2H), 8.19 (d, J = 8.0, 2H), 7.96 (t, J = 11.6, 2H), 7.70 (d, J = 5.8, 2H), 7.31 (s, 2H), 7.15 (s, 2H), 6.50 (s, 2H).

Preparation of $[Fe^{II}$(4,4'-dimethyl-bipyridine)$_2(CN)_2]\cdot 3H_2O$. $[Fe^{II}$(4,4'-dimethyl-bipyridine)$_2(CN)_2]\cdot 3H_2O$ ($[Fe^{II}(dmbpy)_2(CN)_2]\cdot 3H_2O$) was prepared as described in the literature.[153] 0.378 g (0.96 mmol) $(NH_4)_2Fe(SO_4)_2\cdot 6H_2O$, 0.535 g (2.90 mmol) 4,4'-dimethyl-2,2'-bipyridyl (dmbpy), and 30.0 mL deionized water were mixed together. 5.0 mL acetone was added to promote dissolution and reaction. Then the solution was heated to remove acetone. A solution of 0.995 g KCN in 4 mL water was added all at once. The solution was heated to near boiling for 30 minutes, and allowed to cool overnight. The precipitate was collected by vacuum filtration, rinsed with water and

diethyl ether. Pure $[Fe^{II}(dmbpy)_2(CN)_2]\bullet 3H_2O$ was obtained by passing a saturated ethanol solution through a column of Sephadex LH-20-100 resin, eluting with ethanol, and removing ethanol by rotary evaporation. Anal. Calcd for $C_{26}FeH_{30}N_6O_3$: C, 58.88; H, 5.70; N, 15.84. Found: C, 58.86; H, 5.58; N, 15.47. ^{1}H-NMR (400 MHz/CD_3CN): 9.52 (d, J = 5.8, 2H); 8.14 (s, 2H), 8.11 (s, 2H), 7.36 (d, J = 5.8, 2H), 7.12 (d, J = 5.8, 2H), 7.00 (d, J = 5.8, 2H), 2.55 (s, 6H), 2.39 (s, 6H).

Preparation of $[Fe^{III}(dmbpy)_2(CN)_2]NO_3\bullet 2H_2O$. The synthesis of this Fe(III) compound was similar to that of $[Fe^{III}(bpy)_2(CN)_2]NO_3\bullet 2H_2O$. $Fe^{II}(dmbpy)_2(CN)_2$ was oxidized by concentrated HNO_3 to form $[Fe^{III}(dmbpy)_2(CN)_2]NO_3$. Then it was purified by recrystallization from hot distilled deionized water. Yield of $[Fe^{III}(dmbpy)_2(CN)_2]NO_3\bullet 2H_2O$: 73%. Anal. Calcd for $C_{26}FeH_{28}N_7O_5$: C, 54.37; H, 4.91; N, 17.07. Found: C, 54.39; H, 4.79; N, 17.24. ^{1}H-NMR (400 MHz/CD_3CN): 8.94 (s, 2H); 8.34 (d, J = 8.1, 2H), 8.18 (d, J = 7.9, 2H), 7.95 (t, 2H), 7.69 (d, 2H), 7.31 (s, 2H), 7.15 (s, 6H), 6.50 (s, 2H).

Preparation of $[Fe^{III}(CH_3Cp)_2]PF_6$. $[Fe^{III}(CH_3Cp)_2]PF_6$ was prepared by following Pladziewicz's procedure.[154] 0.604 g (2.73 mmol) 1,1'-dimethylferrocene was dissolved in 5.0 mL ether. 2.27 g (5.62 mmol) ferric nitrate was added to 5.0 mL of 0.04 N HCl. The two solutions were mixed together with the appearance of blue color immediately. Then 0.724 g (4.31 mmol) sodium hexafluorophosphate was added to the above blue solution. The precipitate was collected by vacuum filtration, rinsed with cold dilute acid, water, diethyl ether, and dried in a vacuum desiccator. Yield of $[Fe^{III}(CH_3Cp)_2]PF_6$: 61%. For UV-vis spectra and kinetic study, $[Fe^{III}(CH_3Cp)_2]PF_6$ was

recrystallized from hot water, and dried under vacuum for 12 hours. Anal. Calcd for $C_{12}FeH_{14}PF_6$: C, 40.14; H, 3.93; F, 31.75. Found: C, 39.89; H, 3.80; F, 31.47.

Preparation of $[Fe^{II}(5\text{-Cl-phen})_2(CN)_2]\cdot 2H_2O$. $[Fe^{II}(5\text{-Cl-phen})_2(CN)_2]\cdot 2H_2O$ was prepared according to Schilt's method.[155] 0.744 g (3.0 mmol) 5-chloro-1,10-phenanthroline and 0.399 g (1.0 mmol) ammonium ferrous sulfate hexahydrate were added to 250 mL water. The red mixture was stirred and heated at nearing boiling point for 30 minutes. A solution of 1.0 g KCN in 4.0 mL H_2O was added, and it was continued heating for 5 more minutes. Then the solution was cooled to room temperature. 3 hours later, the solvent was removed by vacuum suction. The residue was rinsed with 15.0 mL 0.5 N ammonia and 20.0 mL cool water, and dried in vacuum for 4 hours. ^{1}H-NMR (400 MHz/MeOD): 10.04 (dd, 1H); 9.55 (dd, 1H), 8.94 (dd, 1H), 8.70 (dd, 1H), 8.66 (d, 1H), 8.43 (dd, 2H), 8.36 (s, 1H), 8.14 (dd, 1H), 8.04 (dd, 1H), 7.66 (dd, 1H), 7.62 (dd, 1H), 7.57 (dd, 1H), 7.51 (dd, 1H).

Preparation of $[Fe^{III}(5\text{-Cl-phen})_2(CN)_2]NO_3\cdot 2H_2O$. $[Fe^{III}(5\text{-Cl-phen})_2(CN)_2]NO_3\cdot 2H_2O$ was prepared by oxidizing the crude $[Fe^{II}(5\text{-Cl-phen})_2(CN)_2]\cdot 2H_2O$ with 70% nitric acid. The Fe(III) complex was precipitated out with the addition of some amount of water. It was collected by vacuum suction, rinsed with water to remove acid, and dried in vacuum. Yield of $[Fe^{III}(5\text{-Cl-phen})_2(CN)_2]NO_3\cdot 2H_2O$: 51%. Anal. Calcd for $C_{26}FeH_{18}N_7Cl_2O_5$: C, 49.16; H, 2.86; N, 15.43. Found: C, 49.37; H, 2.66; N, 15.47.

Methods. All single UV-vis spectra were recorded on a HP-8453 diode-array spectrophotometer with 1.0 cm rectangular quartz cells, equipped with Brinkman Lauda

RM6 thermostated water bath to maintain the temperature at 25.0 ± 0.1 ^{o}C. Cyclic voltammograms (CV) and Osteryoung Square Wave Voltammograms (OSWV) were recorded at room temperature on a BAS 100 B electrochemical analyzer with scan rate of 100 mV/s, equipped with BAS cell stand C3 with purging and stirring system, using a glassy carbon working electrode, Ag/AgCl (saturated aqueous KCl) reference electrode, and a Pt wire auxiliary electrode. In acetonitrile, the standard potential of $[Fe(Cp)_2]^{+/0}$ is close to that of $[Fe(dmbpy)_2(CN)_2]^{+/0}$, so decamethylferrocene was used as internal reference in all CV and OSWV experiments. Since the standard potential of $[Fe(Cp)_2]^{+/0}$ versus $[Fe(Cp^*)_2]^{+/0}$ is known,[156,157] it is of no difficulty to present the standard potentials of the four Fe(III) complexes with reference to $[Fe(Cp)_2]^{+/0}$. ^{1}H NMR spectra were recorded on a Bruker AV 400 spectrometer.

For fast reactions, kinetic studies were performed by mixing equal volumes of the two reactants on a Hi-Tech Scientific model SF-51 stopped-flow apparatus that is equipped with a SU-40 spectrophotometer unit and a C-400 circulatory water bath. For slow reaction, equal volumes of the two reactants were mixed in cuvette, then kinetic studies were immediately performed on HP-8453 diode-array spectrophotometer that is equipped with a RMS Lauda circulatory water bath, from which the rate constants (k_{obs}) were obtained by fitting the experimental data with the software that was provided by HP. Temperature was maintained at 25.0 ± 0.1 ^{o}C. On Hi-Tech Scientific model SF-51 stopped-flow apparatus, an Olis 4300S system was used for data acquisition and analysis. Reactions were monitored at fixed wavelength, and the rate constants were obtained by fitting the data with OLIS-supplied first-order functions. All apparent rate constants were the average of at least five runs with ± 5% error or less. A nonlinear-least squares

computer program with relative weighting (weighting by $1/Y^2$) was used to fit the overall rate law to the values of k_{obs}. The products were identified by ^1H NMR spectra and UV-visible spectra.

Results

1. UV-visible spectra. Figure 3-1 shows the UV-visible spectra of 0.10 mM $Fe^{II}(bpy)_2(CN)_2$ and 0.10 mM $[Fe^{III}(bpy)_2(CN)_2]NO_3$ in acetonitrile. For $Fe^{II}(bpy)_2(CN)_2$, there are two characteristic absorbance peaks at 388 and 605 nm, for which the extinction coefficients (ε) are 6988 and 7360 M^{-1} cm^{-1}; for $[Fe^{III}(bpy)_2(CN)_2]NO_3$, the absorbance at 605 nm is nearly zero. Iodide does not absorb in the visible range, and triiodide (I_3^-), one of products of the reaction that was confirmed by our experimental results, has characteristic absorbance at 365 nm (ε_{365} = 26,250 M^{-1} cm^{-1}; $\varepsilon_{605} \approx 10$ M^{-1} cm^{-1}). Thus, for the oxidation of iodide by $[Fe^{III}(bpy)_2(CN)_2]^+$, the stopped-flow experiments were monitored at the wavelength of 605 nm. The UV-visible absorbance characteristics of all iron complexes in acetonitrile are shown in Table 3-1, in which the extinction coefficients are very close to previous reports.[153,158-160] The wavelength for the oxidization of iodide by $[Fe^{III}(dmbpy)_2(CN)_2]^+$, $[Fe^{III}(CH_3Cp)_2]^+$ and $[Fe^{III}(5\text{-Cl-phen})_2(CN)_2]^+$ are monitored at 608, 650, and 609 nm, respectively.

2. Electrochemistry and NMR spectra. The CV and OSWV of 0.50 mM ferrocene in 0.10 M $Et_4NBF_{4(AN)}$, with 0.40 mM decamethylferrocene as internal reference, were recorded. The OSWV graph (Figure 3-2) shows that the half-wave potential, $E_{1/2}$, of $[Fe(Cp)_2]^{+/0}$ is 504 mV higher than that of $[Fe(Cp^*)_2]^{+/0}$, the same as previous reports.[156,157]

Table 3-1. UV-visible absorbance characteristics of the iron complexes in acetonitrile

Compounds	Band	λ_{max}, nm	ε, M^{-1} cm^{-1}
$[Fe^{II}(bpy)_2(CN)_2]$	I	388	6988
	II	605	7360
$[Fe^{III}(bpy)_2(CN)_2]NO_3$	I	301	25037
	II	503	226
$[Fe^{II}(dmbpy)_2(CN)_2]$	I	383	7370
	II	608	6930
$[Fe^{III}(dmbpy)_2(CN)_2]NO_3$	I	356	3884
$[Fe^{II}(CH_3Cp)_2]$	I	324	76
	II	438	110
$[Fe^{III}(CH_3Cp)_2]PF_6$	I	650	354
$[Fe^{II}(5\text{-Cl-phen})_2(CN)_2]$	I	609	10700
$[Fe^{III}(5\text{-Cl-phen})_2(CN)_2]NO_3$	I	362	3740

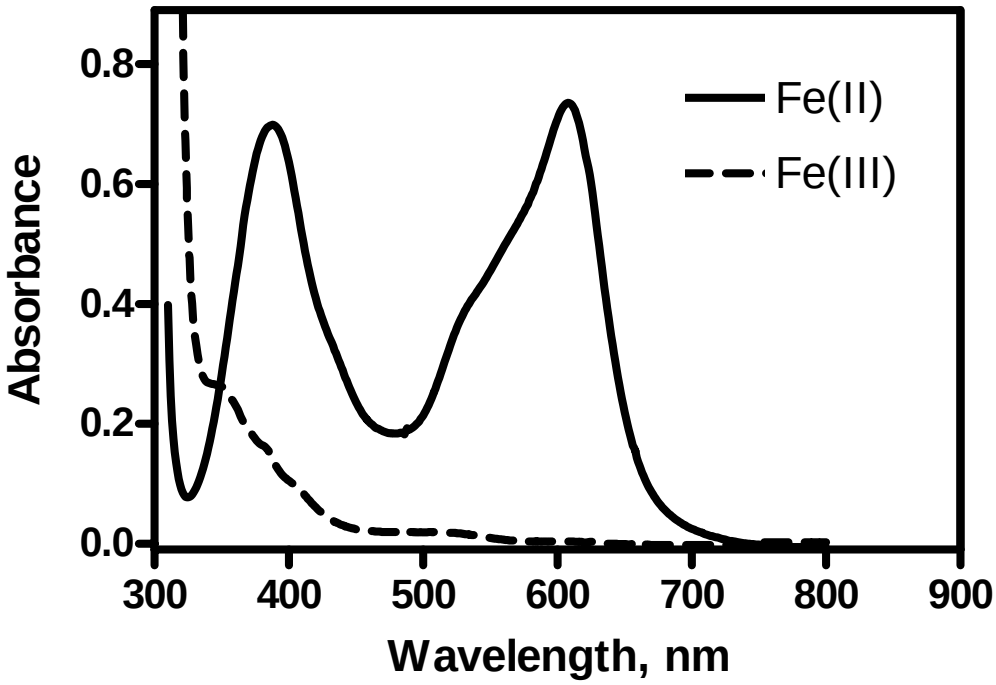

Figure 3-1. UV-visible spectra of 0.10 mM $Fe^{II}(bpy)_2(CN)_2$ (—) and 0.10 mM $[Fe^{III}(bpy)_2(CN)_2]NO_3$ (---) in acetonitrile

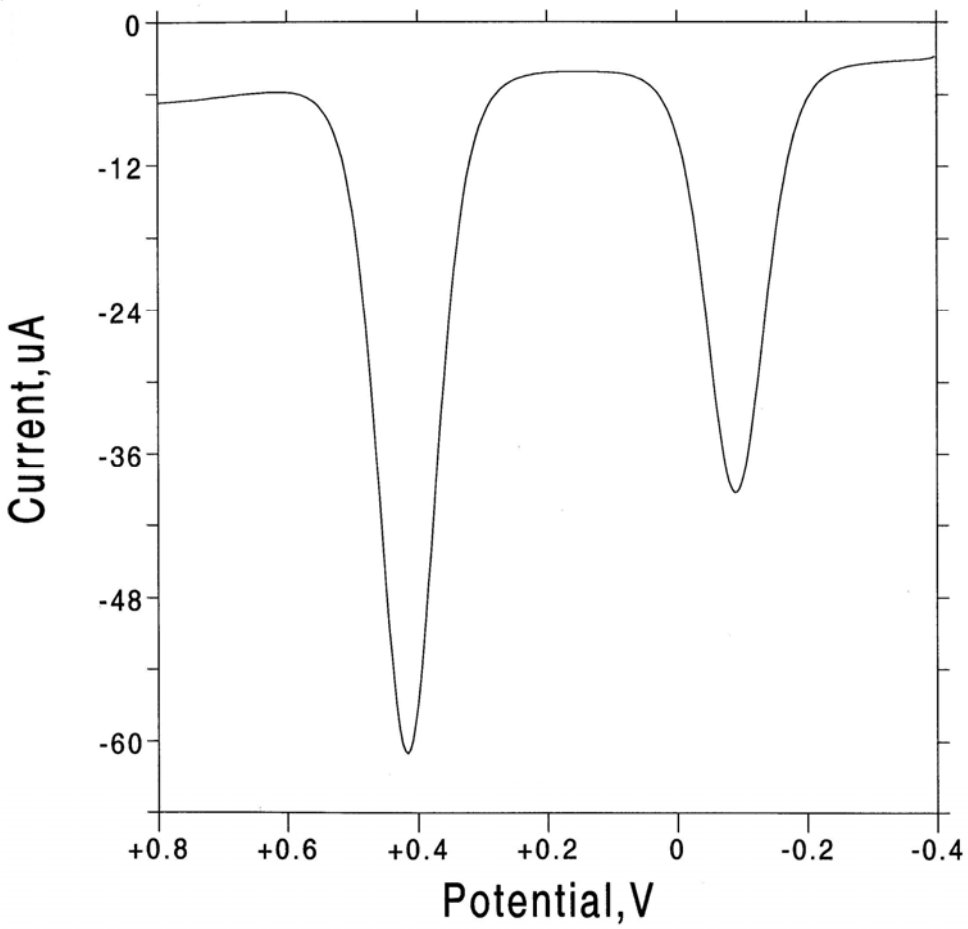

Figure 3-2. The OSWV of 0.50 mM $Fe^{II}(Cp)_2$ and 0.40 mM $Fe(Cp^*)_2$ in 0.10 M Et_4NBF_4. With a glassy carbon disc as working electrode, an $Ag/AgCl_{(s)}$ electrode as reference, and a Pt wire as a counter electrode.

$Fe^{II}(bpy)_2(CN)_2$. The CV (Figure 3-3) of 1.0 mM $Fe^{II}(bpy)_2(CN)_2$ in 0.10 M $Et_4NBF_{4(AN)}$, with 1.0 mM decamethylferrocene as internal reference, is quasi-reversible, with $\Delta E_{p/p}$ = 72 mV, $E_{1/2}$ = 71 mV vs. $[Fe(Cp)_2]^{+/0}$. The OSWV (Figure 3-4) of 1.0 mM $Fe^{II}(bpy)_2(CN)_2$ in 0.10 M $Et_4NBF_{4(AN)}$, with 1.0 mM decamethylferrocene as internal reference, has the half-potential, $E_{1/2}$, of 70 mV, nearly the same as the result from CV.

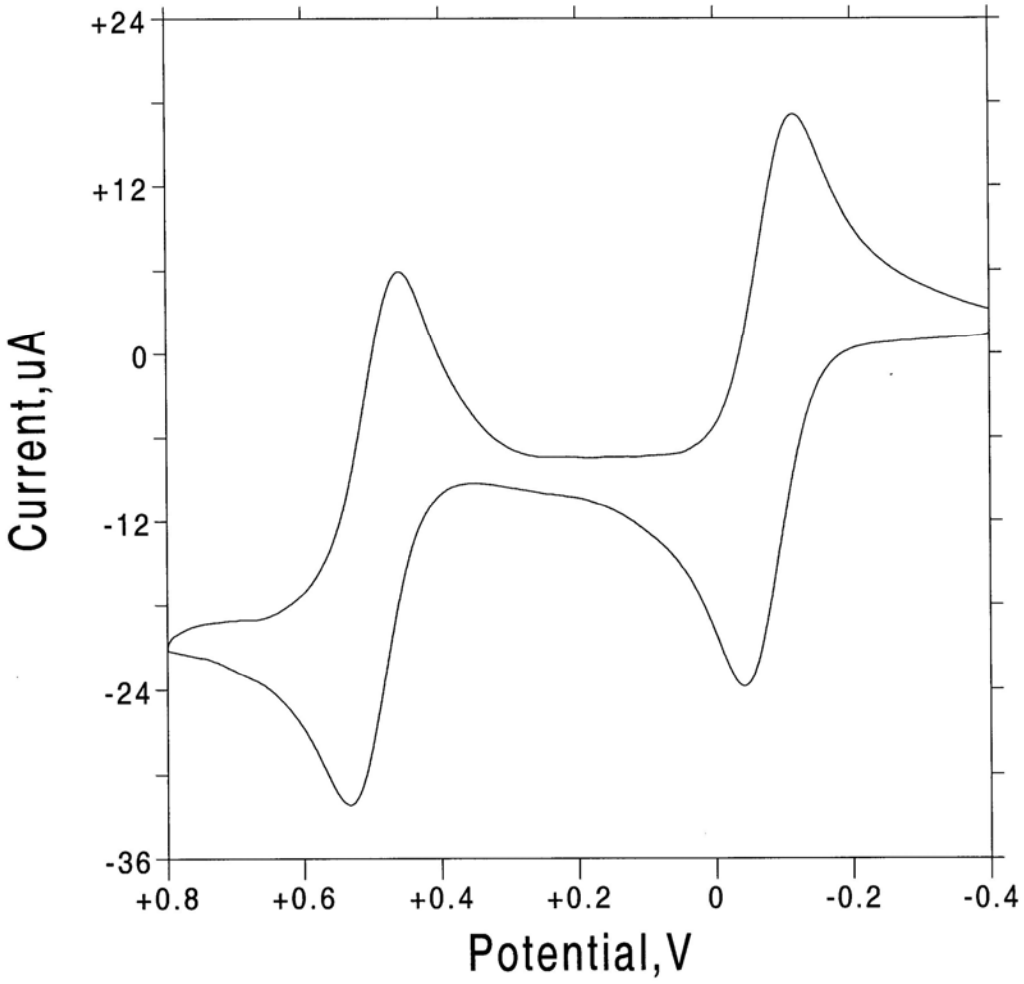

Figure 3-3. The CV of 1.0 mM $Fe^{II}(bpy)_2(CN)_2$ and 1.0 mM $Fe(Cp^*)_2$ in 0.10 M Et_4NBF_4. With a glassy carbon disc as working electrode, an $Ag/AgCl_{(s)}$ electrode as reference, and a Pt wire as a counter electrode.

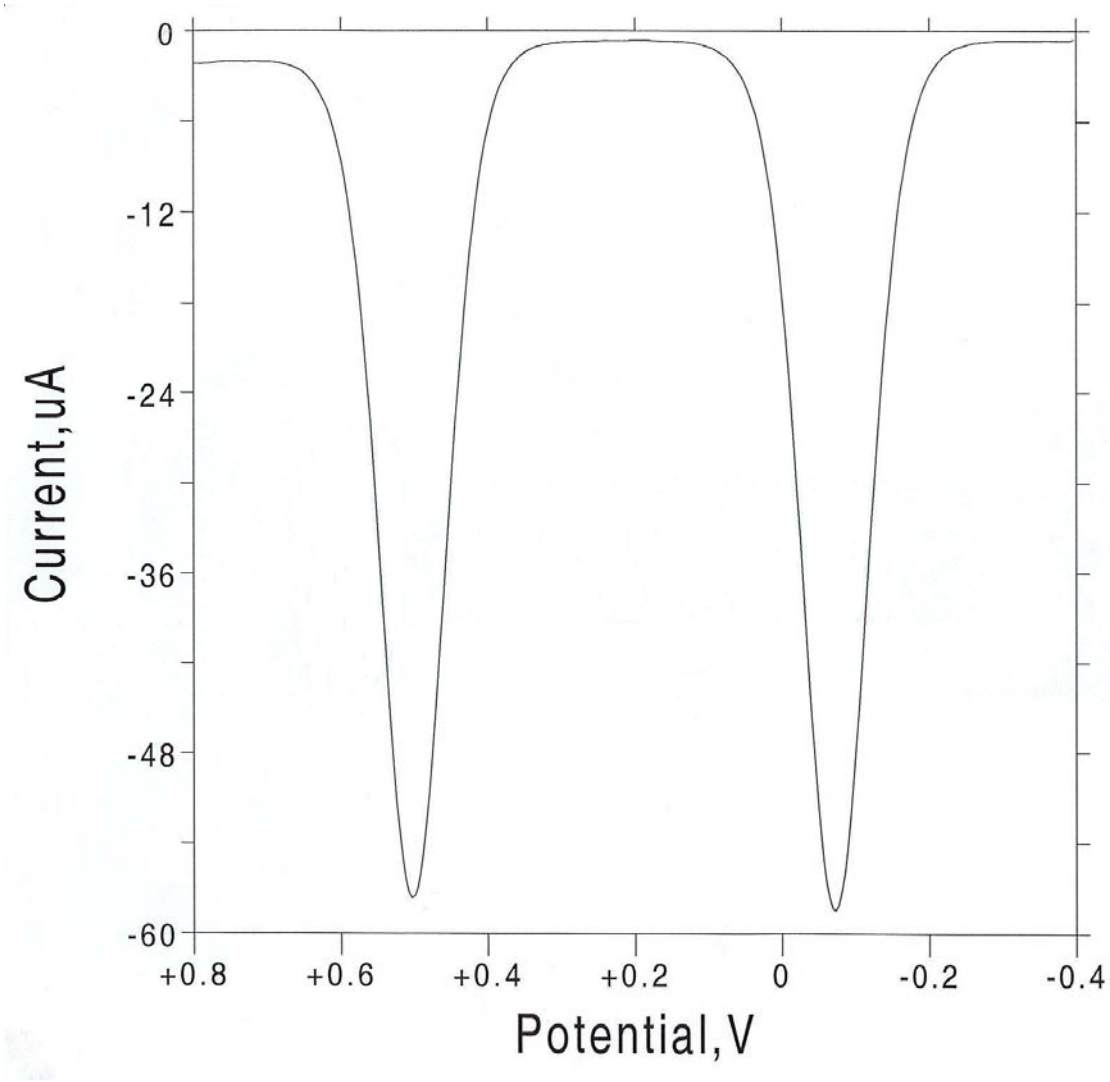

Figure 3-4. The OSWV of 1.0 mM $Fe^{II}(bpy)_2(CN)_2$ and 1.0 mM $Fe(Cp^*)_2$ in 0.10 M Et_4NBF_4. With a glassy carbon disc as working electrode, an $Ag/AgCl_{(s)}$ electrode as reference, and a Pt wire as a counter electrode.

$Fe^{II}(dmbpy)_2(CN)_2$. The CV (Figure 3-5) of 1.0 mM $Fe^{II}(dmbpy)_2(CN)_2$ in 0.10 M $Et_4NBF_{4(AN)}$, with 1.0 mM decamethylferrocene as internal reference, is quasi-reversible, with $\Delta E_{p/p}$ = 62 mV, $E_{1/2}$ = -35 mV. The OSWV (Figure 3-6) of 1.0 mM $Fe^{II}(dmbpy)_2(CN)_2$ in 0.10 M $Et_4NBF_{4(AN)}$, with 1.0 mM decamethylferrocene as internal reference, has the half-potential of -36 mV, nearly the same as that obtained from CV.

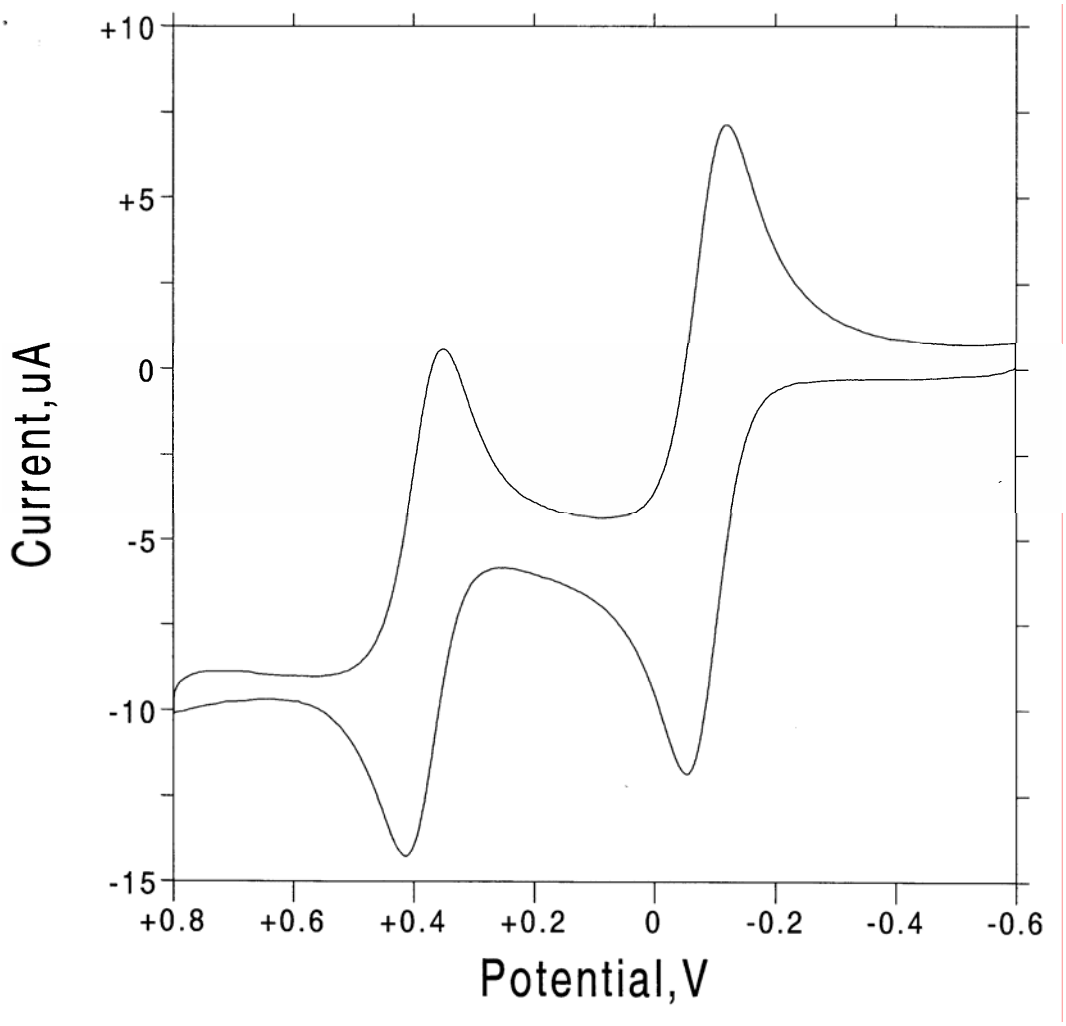

Figure 3-5. The CV of 1.0 mM $Fe^{II}(dmbpy)_2(CN)_2$ and 1.0 mM $Fe(Cp^*)_2$ in 0.10 M Et_4NBF_4. With a glassy carbon disc as working electrode, an $Ag/AgCl_{(s)}$ electrode as reference, and a Pt wire as a counter electrode.

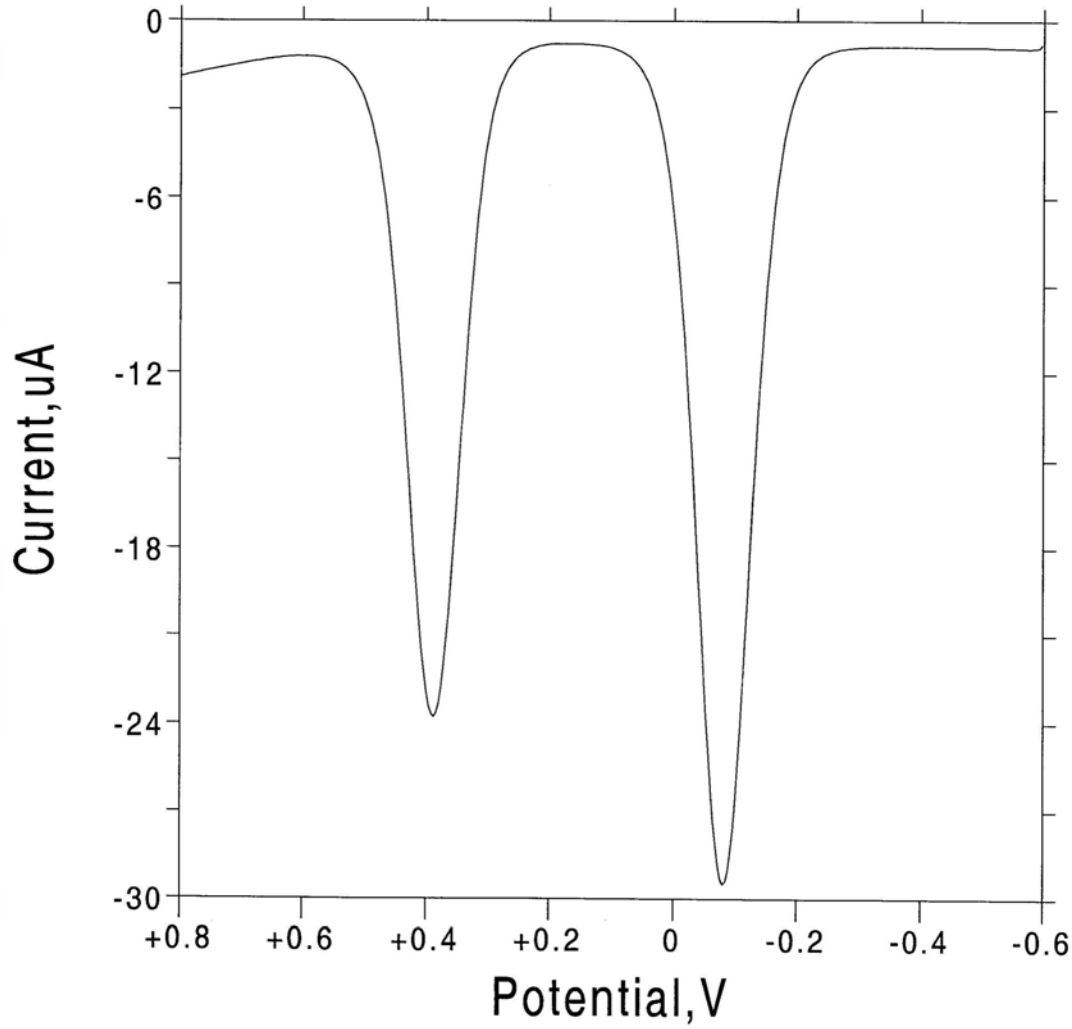

Figure 3-6. The OSWV of 1.0 mM $Fe^{II}(dmbpy)_2(CN)_2$ and 1.0 mM $Fe(Cp^*)_2$ in 0.10 M Et_4NBF_4. With a glassy carbon disc as working electrode, an $Ag/AgCl_{(s)}$ electrode as reference, and a Pt wire as a counter electrode.

$Fe^{II}(CH_3Cp)_2$. The CV (Figure 3-7) of 1.0 mM $Fe^{II}(CH_3Cp)_2$ in 0.10 M $Et_4NBF_{4(AN)}$, with 1.0 mM decamethylferrocene as internal reference, is quasi-reversible, with $\Delta E_{p/p}$ = 82 mV, $E_{1/2}$ = -110 mV. The OSWV (Figure 3-8) of 1.0 mM $Fe^{II}(CH_3Cp)_2$ in 0.10 M $Et_4NBF_{4(AN)}$, with 1.0 mM decamethylferrocene as internal reference, has the half-wave potential of -108 mV. The half-wave potential from OSWV is 2 mV higher than that from CV.

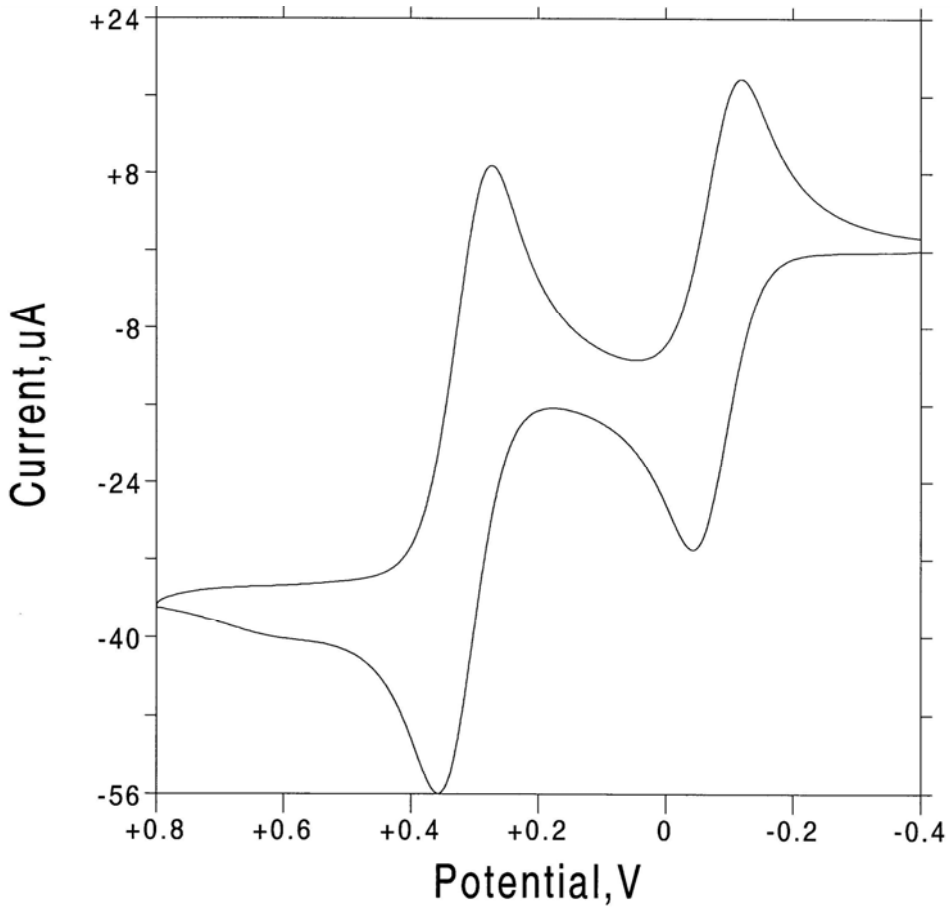

Figure 3-7. The CV of 1.0 mM $Fe^{II}(CH_3Cp)_2$ and 1.0 mM $Fe(Cp^*)_2$ in 0.10 M Et_4NBF_4. With a glassy carbon disc as working electrode, an $Ag/AgCl_{(s)}$ electrode as reference, and a Pt wire as a counter electrode.

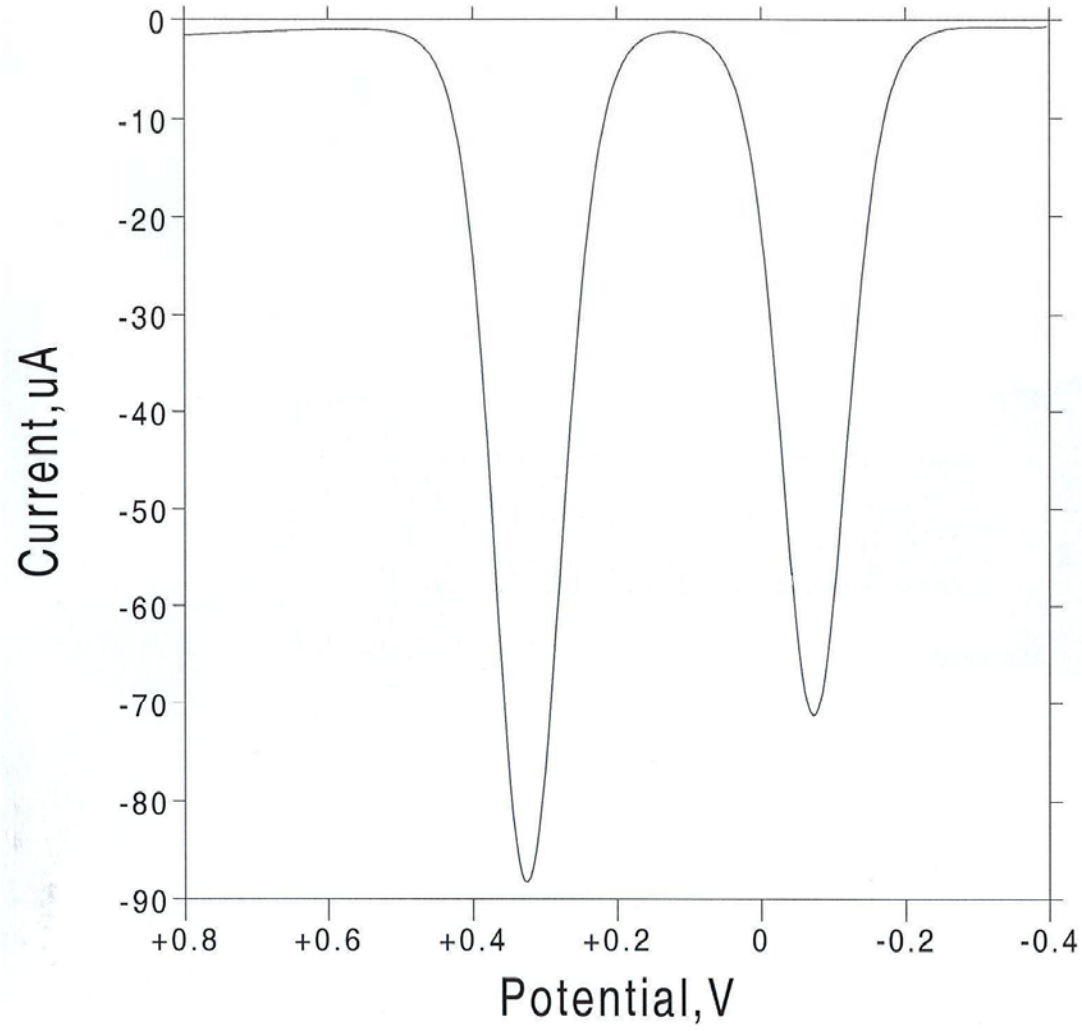

Figure 3-8. The OSWV of 1.0 mM $Fe^{II}(CH_3Cp)_2$ and 1.0 mM $Fe^{II}(Cp^*)_2$ in 0.10 M Et_4NBF_4. With a glassy carbon disc as working electrode, an $Ag/AgCl_{(s)}$ electrode as reference, and a Pt wire as a counter electrode.

$[Fe^{III}(5\text{-Cl-phen})_2(CN)_2]NO_3$ and $Fe^{II}(5\text{-Cl-phen})_2(CN)_2$. No decamethylferrocene was added in the CV of $[Fe^{III}(5\text{-Cl-phen})_2(CN)_2]NO_3$ due to the redox reaction between $[Fe^{III}(5\text{-Cl-phen})_2(CN)_2]NO_3$ and decamethylferrocene. The CV (Figure 3-9) of 0.50 mM $[Fe^{III}(5\text{-Cl-phen})_2(CN)_2]NO_3$ in 0.10 M $Et_4NBF_{4(AN)}$ is quasi-reversible, with $\Delta E_{p/p} = 91$ mV, $E_{1/2} = 610$ mV (vs. $Ag/AgCl_{(s)}$), i.e. 176 mV vs $[Fe(Cp)]^{+/0}$.[161-163] The OSWV (Figure 3-10) of 0.20 mM $Fe^{II}(5\text{-Cl-phen})_2(CN)_2$ in 0.10 M $Et_4NBF_{4(AN)}$, with 1.0 mM decamethylferrocene as internal reference, has the half-wave potential of 168 mV.

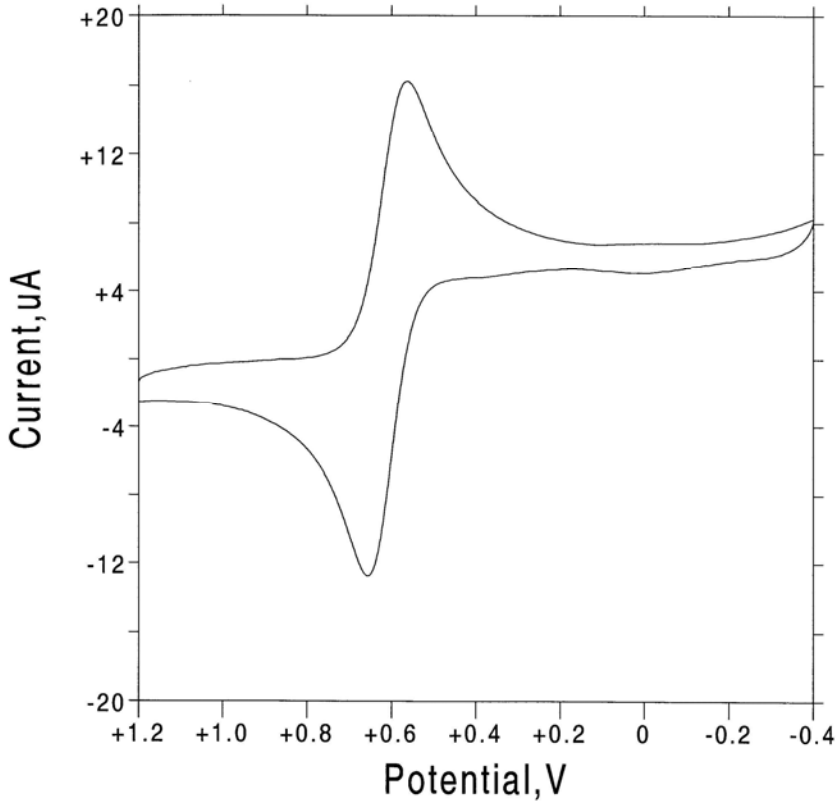

Figure 3-9. The CV of 0.50 mM $[Fe^{III}(5\text{-Cl-phen})_2(CN)_2]NO_3$ in 0.10 M Et_4NBF_4. With a glassy carbon disc as working electrode, an $Ag/AgCl_{(s)}$ electrode as reference, and a Pt wire as a counter electrode.

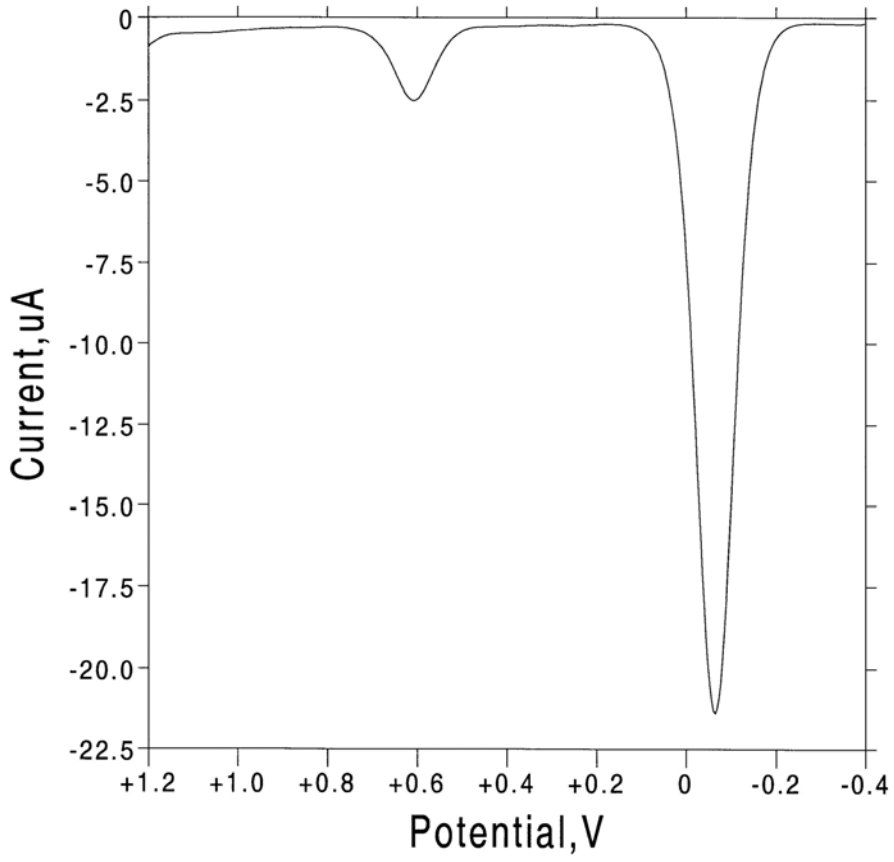

Figure 3-10. The OSWV of 0.20 mM $Fe^{II}(5\text{-Cl-phen})_2(CN)_2$ and 1.0 mM $Fe(Cp^*)_2$ in 0.10 M Et_4NBF_4. With a glassy carbon disc as working electrode, an $Ag/AgCl_{(s)}$ electrode as reference, and a Pt wire as a counter electrode.

The half-wave potentials of the four iron complexes versus $[Fe(Cp)_2]^{+/0}$ are shown in Table 3-2. In the case of $Fe^{II}(CH_3Cp)_2$, it has the same half-wave potential as previous report;[157] while half-wave potential of $[Fe(dmbpy)_2(CN)_2]^{+/0}$ is 58 mV higher than the literature.[153] However, nobody reported the half-wave potentials of $[Fe(bpy)_2(CN)_2]^{+/0}$ and $[Fe(5\text{-Cl-phen})_2(CN)_2]^{+/0}$ in acetonitrile. The half-wave potentials in Table 3-2 demonstrate that $[Fe^{III}(CH_3Cp)_2]^+$ is the weakest oxidant, and $[Fe^{III}(5\text{-Cl-phen})_2(CN)_2]^+$ is the strongest oxidant, with a difference of 276 mV between them; $[Fe^{III}(bpy)_2(CN)_2]^+$, one mild oxidant, has 108 mV higher than $[Fe^{III}(dmbpy)_2(CN)_2]^+$. The rate constants of the oxidation of the iodide are closely related to the half-wave potential of the iron complexes. This will be discussed in kinetics section.

Table 3-2. The half- wave potentials of the iron complexes in acetonitrile

Compounds	$E_{1/2}$, mV [a]
$[Fe(CH_3Cp)_2]^{+/0}$	-108 ± 2
$[Fe(dmbpy)_2(CN)_2]^{+/0}$	- 36 ± 2
$[Fe(bpy)_2(CN)_2]^{+/0}$	+ 70 ± 2
$[Fe(5\text{-Cl-phen})_2(CN)_2]^{+/0}$	168 ± 2

[a] $E_{1/2}$ vs $[Fe(Cp)_2]^{+/0}$, at 22.0 °C and μ = 0.10 M. $E_{1/2} = E_f$

^{1}H-NMR spectra. The ^{1}H-NMR spectra of $Fe^{II}(bpy)_2(CN)_2$ and $Fe^{II}(dmbpy)_2(CN)_2$ show that both of them have cis geometries without any impure component. The ^{1}H-NMR spectrum (Figure 3-11) of recrystallized $Fe(CH_3Cp)_2$ has two characteristic chemical shift at 3.94 and 1.95 ppm (overlap with CD_3CN), with the intensity of 4:3. For *cis*-$Fe^{II}(5\text{-Cl-phen})_2(CN)_2$, it has three isomers, as shown in Scheme 3-1. The ^{1}H-NMR

spectrum of 1.0 mM $Fe^{II}(5\text{-Cl-phen})_2(CN)_2$ in MeOD has 14 peaks with the same intensity, confirming that only isomer (C) exists in the compound. So the ^{1}H-NMR spectra of the four Fe(II) complexes are consistent with their structure.

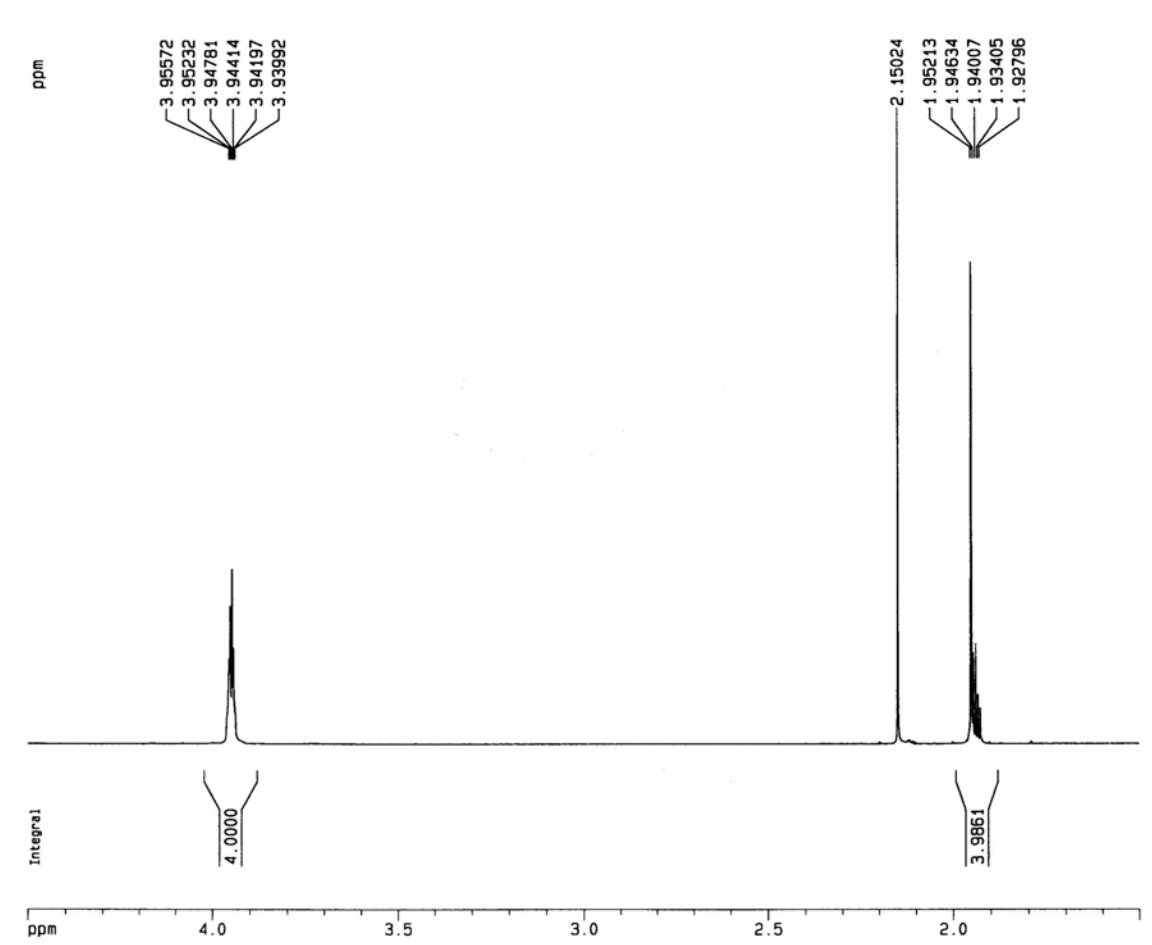

Figure 3-11.^{1}H-NMR spectrum of recrystallized $Fe(CH_3Cp)_2$ in CD_3CN

Scheme 3-1. The structure of *cis*-$Fe^{II}(5\text{-Cl-phen})_2(CN)_2$ with three different isomers. ClN represents the Cl-substituted part of the 5-Cl-phen ligand.

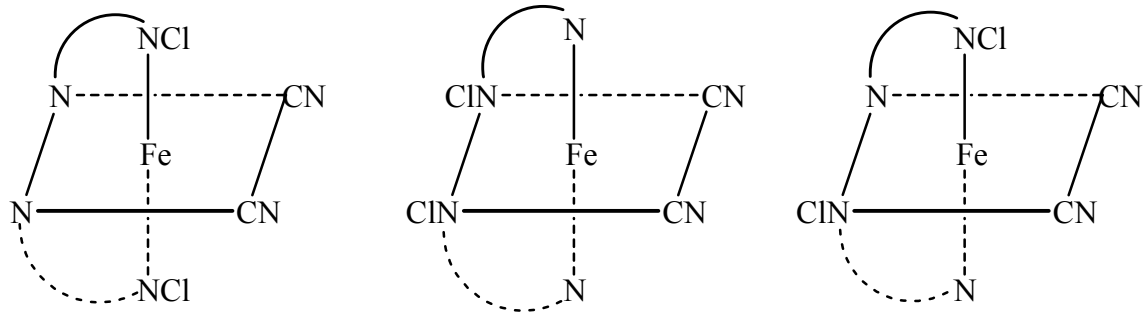

3. Metal-ion catalysis and scavenger effect. We initially studied the kinetics of the oxidation of iodide by $[Fe^{III}(bpy)_2(CN)_2]^+$ in acetonitrile due to its mild oxidative capability. Our preliminary kinetic studies were plagued by its irreproducibility. For a typical reaction of 2.0×10^{-3} M NaI with 5.0×10^{-5} M $[Fe^{III}(bpy)_2(CN)_2]^+$ in 0.10 M Et_4NBF_4, the half-life ranges from 0.31 to 0.81 s. Then 5.0 μM Ni^{2+}, Fe^{3+} and Cu^{2+} were deliberately added to the reactant of iodide. After the addition of 5.0 μM Cu^{2+}, the rates of reaction are much faster, with the half-life of 3 ms; while there is no distinct change for Ni^{2+} and Fe^{3+}, as shown in Table 3-3. Therefore, trace of Cu ions are good catalyst for the redox reaction between $[Fe^{III}(bpy)_2(CN)_2]^+$ and iodide in acetonitrile.[164] Due to the copper-catalysis effect, the reaction of $[Fe^{III}(bpy)_2(CN)_2]^+$ with excess iodide in acetonitrile does not follow first-order behavior, so the rate of the reaction is represented by half-life, rather than by k_{obs}. The copper-catalysis effect was also observed for the other three Fe(III) complexes, although it is not distinct for $[Fe^{III}(5\text{-Cl-phen})_2(CN)_2]^+$ and $[Fe^{III}(CH_3Cp)_2]^+$. For the oxidation of 2.0×10^{-3} M NaI by 5.0×10^{-5} M

$[Fe^{III}(dmbpy)_2(CN)_2]^+$ in 0.10 M Et_4NBF_4 at 25.0 °C, the half-life for the formation of $Fe^{II}(dmbpy)_2(CN)_2$ decreases by 33 times after the addition of 1.0 μM $Cu(NO_3)_2$. For the oxidation of 8.0×10^{-2} M NaI by 2.5×10^{-4} M $[Fe^{III}(CH_3Cp)_2]^+$ in 0.02 M Et_4NBF_4 at 25.0 °C, the half-life for the formation of $Fe^{II}(CH_3Cp)_2$ decreases by 7 times when 1.0 μM $Cu(NO_3)_2$ was deliberately added. For the oxidation of 0.20 mM I^- by 10.0 μM $[Fe^{III}(5\text{-Cl-phen})_2(CN)_2]^+$ in 0.10 M Et_4NBF_4 at 25.0 °C, the half-life for the formation of $Fe^{II}(5\text{-Cl-phen})_2(CN)_2$ decreases by a factor of four due to the addition of 1.0 μM $Cu(NO_3)_2$. All of the results are shown in Table 3-4.

Table 3-3. Effect of metal ions on the oxidation of Et_4NI by $[Fe^{III}(bpy)_2(CN)_2]^+$ in acetonitrile. At μ = 0.10 M (Et_4NBF_4), and 25.0 °C.

Molarity of cation, μM	$t_{1/2}$, s
0	0.60
$[Cu^{2+}]$ = 5.0 μM	0.003
$[Ni^{2+}]$ = 5.0 μM	0.11
$[Fe^{2+}]$ = 5.0 μM	0.20

[a] $[Et_4NI]_0$ = 2.0 mM, $[Fe^{III}(bpy)_2(CN)_2^+]_0$ = 50 μM.

To inhibit its copper-catalysis effect, some chelating reagents should be added to the reactants. In our group, Saha and Hung[103,52] have found that 2,2'-bipyridine (bpy), 2,6-pyridinedicarboxylic acid (dipic), and 1,10-phenanthroline (phen) can effectively mask the copper-catalysis effect in the reduction of octacyanomolybdate(V) by thioglycolic acid and cysteine in aqueous media.

Table 3-4. The effect of Cu^{2+} and bpy on the oxidation of Et_4NI by 50 μM Fe(III) complexes in acetonitrile. At μ = 0.10 M (Et_4NBF_4), and 25.0 °C.

Compounds	$[I^-]_0$, mM	$[Et_4NBF_4]$, M	$[Cu^{2+}]$, μM	[bpy], mM	$t_{1/2}$, s
	80.0	0.02	0.0	0.0	0.375
$[Fe^{III}(CH_3Cp)_2]^+$ [a]	80.0	0.02	5.0	0.0	0.044
	80.0	0.02	5.0	5.0	1.16
	2.0	0.10	0.0	0.0	15.50
$[Fe^{III}(dmbpy)_2(CN)_2]^+$	2.0	0.10	1.0	0.0	0.46
	2.0	0.10	1.0	5.0	86.48
	2.0	0.10	0.0	0.0	0.60
$[Fe^{III}(bpy)_2(CN)_2]^+$	2.0	0.10	1.0	0.0	0.015
	2.0	0.10	1.0	5.0	4.20
	0.2	0.10	0.0	0.0	0.037
$[Fe^{III}(5\text{-Cl-phen})_2(CN)_2]^+$ [b]	0.2	0.10	1.0	0.0	0.011
	0.2	0.10	1.0	5.0	0.969

[a] $[[Fe^{III}(CH_3Cp)_2]^+]_0$ = 0.25 mM; [b] $[[Fe^{III}(5\text{-Cl-phen})_2(CN)_2]^+]_0$ = 10 μM

Firstly, the effect of bpy on the oxidation of NaI by $[Fe^{III}(bpy)_2(CN)_2]^+$ was tested. 1.0 mM and 5.0 mM bpy was added to the reactants (2.0 mM NaI, 50.0 μM $[Fe^{III}(bpy)_2(CN)_2]^+$, 0.098 M Et_4NBF_4), respectively. It was found that both reactions have the same half-life, 4.20 s. Ethylenediamine (en) also was tested. 1.0 mM ethylenediamine (en) was added to the same concentration of the above reactants, the half-life is 4.52 s. It indicates that en has the same function as bpy in the inhibition of the Cu^{2+} ion catalysis. It was also found that the half-life for the reaction between 5.0×10^{-5} M $[Fe^{III}(bpy)_2(CN)_2]^+$ and 1.0×10^{-3} M en in acetonitrile is about 700 s, while there is no

reaction between $[Fe^{III}(bpy)_2(CN)_2]^+$ and bpy. To avoid the complication caused by the reaction of en with $[Fe^{III}(bpy)_2(CN)_2]^+$, bpy, rather than en, was selected to inhibit the copper catalysis. Direct oxidation of iodide by the four outer-sphere Fe(III) complexes was achieved by the addition of 5.0 mM bpy to the reactants. Figure 3-12 shows a kinetic trace of reaction between 2.0×10^{-3} M I^- and 5.0×10^{-5} M $[Fe^{III}(bpy)_2(CN)_2]^+$. The inset in Figure 3-12 shows that, with the addition of 5.0 mM bpy, the rate of the reaction is much slower and it follows pseudo-first-order kinetic behavior; however, it does not follow pseudo-first-order kinetics in the absence of bpy. The same kinetic features were observed for the reduction of $[Fe^{III}(CH_3Cp)_2]^+$, $[Fe^{III}(dmbpy)_2(CN)_2]^+$ and $[Fe^{III}(5\text{-Cl-phen})_2(CN)_2]^+$.

4. Effect of small amount of water on the kinetics study. Our preliminary kinetic results demonstrate that the non-catalyzed oxidation of iodide by $[Fe^{III}(bpy)_2(CN)_2]^+$ is much slower in water than in acetonitrile. For the oxidation of 2.0×10^{-3} M NaI by 5.0×10^{-5} M $[Fe^{III}(bpy)_2(CN)_2]^+$, at $\mu = 0.10$ M and 25.0 ^oC, the half-lives of the reaction are 0.60 s in acetonitrile and 58.7 s in water, respectively. Therefore, the trace amount of water in acetonitrile and reactants may affect the rate of the reaction. The water-content effect on the rate of the oxidation of iodide was studied by selecting $[Fe^{III}(bpy)_2(CN)_2]^+$ as oxidant.

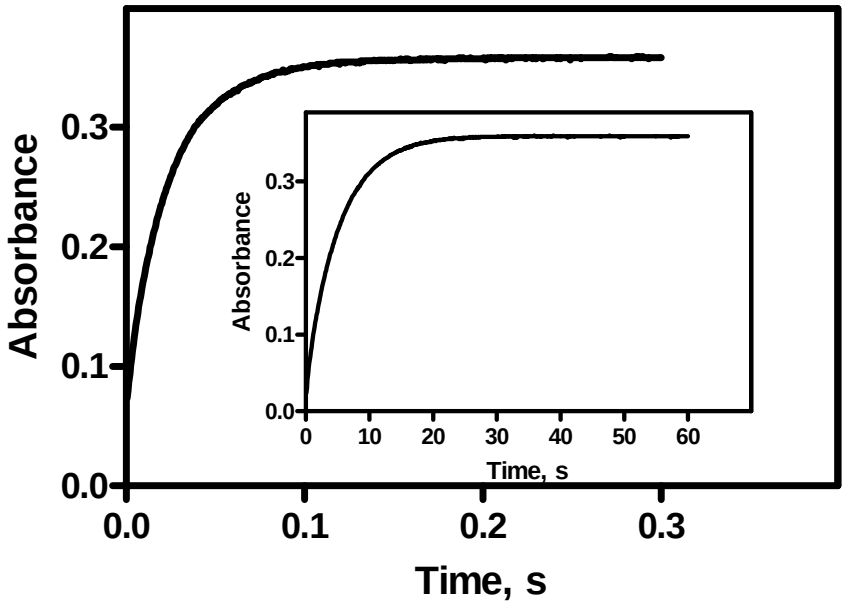

Figure 3-12. Kinetic traces for the oxidation of 2.0×10^{-3} M NaI by 5.0×10^{-5} M $[Fe^{III}(bpy)_2(CN)_2]^+$ in acetonitrile. At $\mu = 0.10$ M (Et_4NBF_4), and 25.0 ^oC. Data was recorded at 605 nm. Main trace with 1.0 μM $Cu(NO_3)_2 \bullet 3H_2O$. Inset shows data with 1.0 mM bpy but no added Cu^{2+}. Note the vastly differing time scales for the two traces.

Firstly, the concentration of water for the nominally anhydrous stopped-flow experiment was determined by ^{1}H-NMR spectra. 2.0 mM NaI and 0.20 mM $[Fe^{III}(bpy)_2(CN)_2]^+$ in acetonitrile, in the presence of 0.10 M Et_4NBF_4, was mixed with equal volume in the syringes of SF-51 instrument. Analysis of the integrate intensities of Et_4NBF_4 and H_2O in the ^{1}H-NMR spectrum (Figure 3-13) demonstrates that it contains 0.20% (v/v) water in the product solution. Then 1% water was deliberately added to the

reactants that contained 1.0 mM bpy, the rate constants decrease from 0.57 to 0.53 s^{-1}. In the absence of bpy but with 1.0 μM $Cu(NO_3)_2$, the addition of 1% water to the reactants does not change the rate of the reaction, either. Therefore, the effect of small amount of water (0.2 %) in nominally anhydrous conditions on the rate of the reaction is negligible.

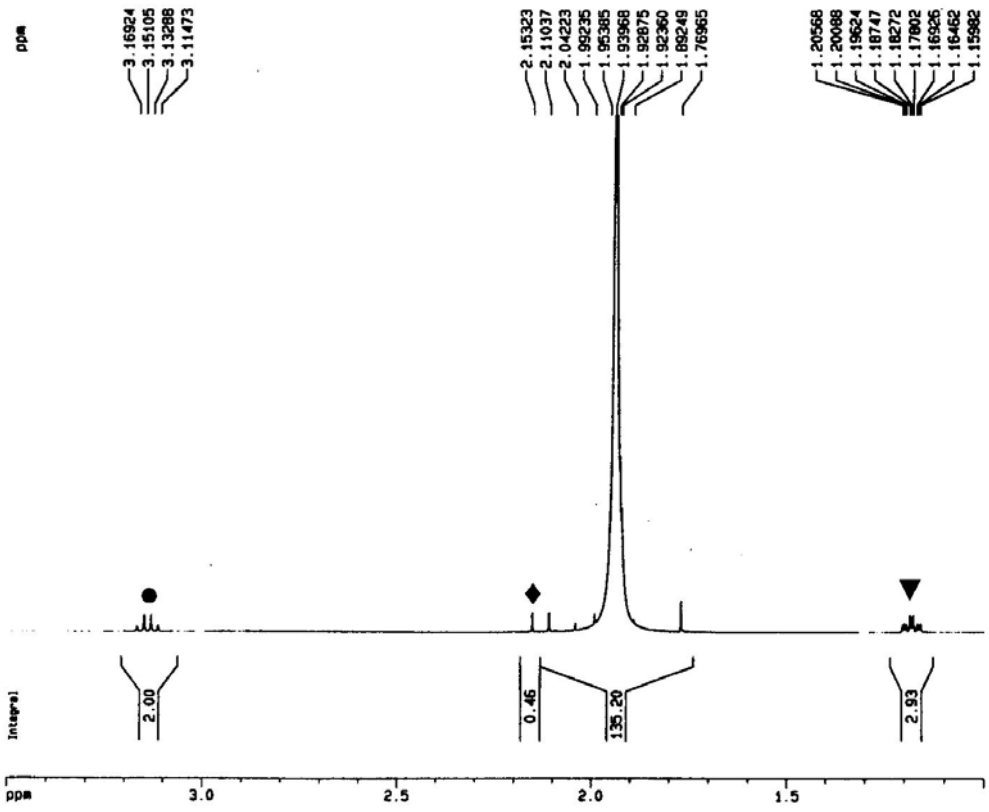

Figure 3-13. ^{1}H-NMR spectrum of product for the reaction of 1.0 mM NaI with 0.10 mM $[Fe^{III}(bpy)_2(CN)_2]^+$ in acetonitrile. In the presence of 0.10 M Et_4NBF_4.

●: $-CH_2$ in Et_4NBF_4; ♦: H_2O; ▼: $-CH_3$ in Et_4NBF_4

Since the structure of $[Fe^{III}(CH_3Cp)_2]^+$ is quite different from that of the other three Fe(III) complexes, it is of high importance to test the water effect on the oxidation of

iodide by $[Fe^{III}(CH_3Cp)_2]^+$ in acetonitrile. Figure 3-14 shows that k_{obs} decreases linearly as the water content increases from 0.2 to 1.0%. When 0.20 % of water was deliberately added to the reaction system (80.0 mM NaI, 0.25 mM $[Fe^{III}(CH_3Cp)_2]^+$, 10.0 mM bpy and 20.0 mM Et_4NBF_4, at 25.0 ^oC), the rate constant decreases from 0.28 to 0.26 s^{-1}. For all kinetic experiments, acetonitrile was used directly, without any further drying process. Furthermore, a series of kinetic experiments was performed with the same concentrations of NaI and Et_4NI. At lower concentration of iodide, the rate constant is nearly the same; at higher concentration of iodide, the rate of the reaction is much slower for NaI, as shown in Table 3-5. This can be ascribed to the more hygroscopic character of NaI. With the increase of NaI, significant great amount of water can be introduced to the reaction system. Accordingly, non-hygroscopic Et_4NI was used, rather than NaI, in all later kinetic studies.

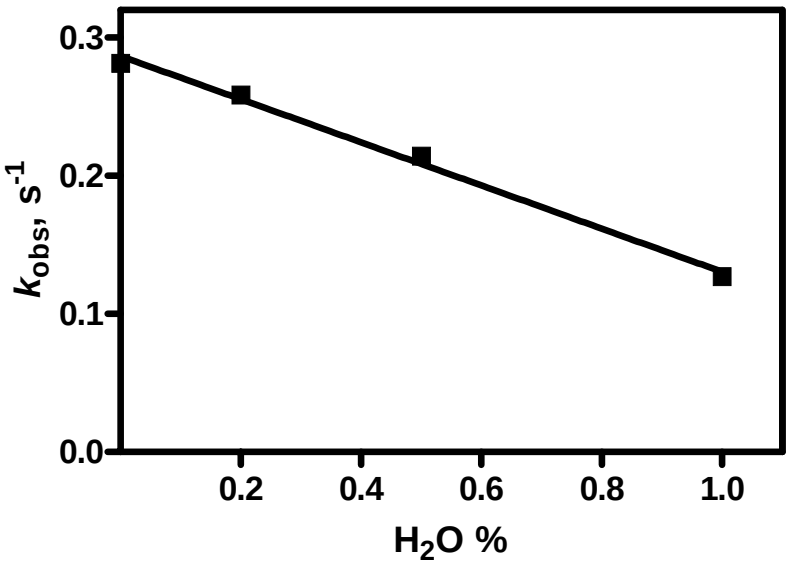

Figure 3-14. Water effect on the rate constants for the oxidation of 80.0 mM NaI by 0.25 mM $[Fe^{III}(CH_3Cp)_2]^+$. In the presence of 10.0 mM bpy and 20.0 mM Et_4NBF_4, at 25.0 ^oC.

Table 3-5. Kinetic comparison of NaI and Et_4NI in the reduction by $[Fe^{III}(CH_3Cp)_2]^+$. In the presence of 5.0 mM bpy, at μ = 0.10 M and 25.0 ^oC.

Iodide	$[I^-]$, mM	k_{obs}, s^{-1}
NaI	5.0	0.0018
	10.0	0.0058
	20.0	0.0211
	40.0	0.0822
Et_4NI	5.0	0.0022
	10.0	0.0066
	20.0	0.0247
	40.0	0.0895

5. Product identification and stoichiometry. The products of the four copper-catalysis inhibited reactions were identified by ^{1}H-NMR and UV-visible spectra. The stoichiometry of the reactions was determined by ^{1}H-NMR and spectrophotometric analysis.

Oxidation of iodide by $[Fe^{III}(bpy)_2(CN)_2]^+$. The products of the non-copper catalyzed reaction for the oxidation of Et_4NI by $[Fe^{III}(bpy)_2(CN)_2]^+$ were identified by spectrophotometric analysis. The UV-vis spectrum (Figure 3-15) of the product solution of 30.0 mM Et_4NI and 50 μM $[Fe^{III}(bpy)_2(CN)_2]^+$ in acetonitrile, with 0.10 M Et_4NBF_4 and 5.0 mM bpy, and at 25.0 ^oC, shows that there are two maxima peaks at 369 and 605 nm. Compared with the UV-vis spectra of pure $Fe^{II}(bpy)_2(CN)_2$ in acetonitrile, it is confirmed that $Fe^{II}(bpy)_2(CN)_2$ is one of the products. To assign other product of the reaction, UV-vis spectra of triiodide (I_3^-) were recorded, and it was observed that the I_3^- has characteristic absorbance at 363 nm with the extinction coefficient of 26,250 M^{-1} cm^{-1}, which is very close to Isci and Mason's result.[165] So the absorbance peak at 369 nm for the product solution is ascribed to the overlap of absorbance of I_3^- and $Fe^{II}(bpy)_2(CN)_2$. Thus, the products of the copper-catalysis inhibited reaction are I_3^- and $Fe^{II}(bpy)_2(CN)_2$. Quantitative dual-wavelength analysis at 605 and 369 nm (ε_{605} = 7360; ε_{369} = 5713 M^{-1} cm^{-1} for $Fe^{II}(bpy)_2(CN)_2$) demonstrates that the yield of $Fe^{II}(bpy)_2(CN)_2$ is 99.0%, and that the product ratio of $\Delta[I_3^-]/\Delta[Fe(II)]$ equals to 0.48 ± 0.03. The above results imply that the overall reaction is:

$$2\ Fe(III) + 3\ I^- \rightleftharpoons 2\ Fe(II) + I_3^- \qquad K_{tot} \qquad (3\text{-}1)$$

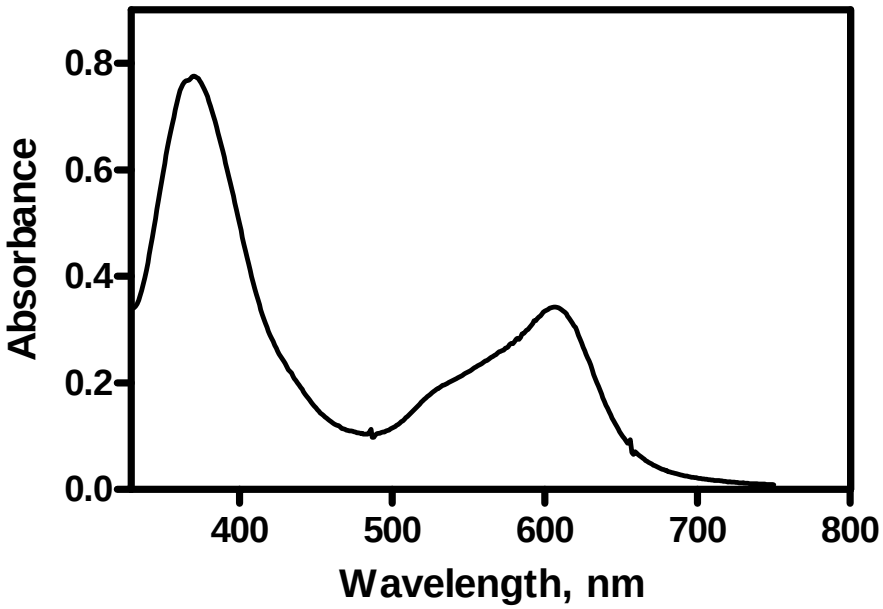

Figure 3-15. UV-vis spectrum of product for the oxidation of 30.0 mM Et_4NI by 50 μM $[Fe^{III}(bpy)_2(CN)_2]^+$ in acetonitrile, with 5.0 mM bpy.

Oxidation of iodide by $[Fe^{III}(dmbpy)_2(CN)_2]^+$. The products of the direct oxidation of iodide by $[Fe^{III}(dmbpy)_2(CN)_2]^+$ were also identified by spectrophotometric analysis. The UV-vis spectrum (Figure 3-16) of the product solution of 5.0 mM Et_4NI and 47 μM $[Fe^{III}(bpy)_2(CN)_2]^+$ in acetonitrile, in the presence of 5.0 mM bpy, at $\mu = 0.10$ M and at 25.0 ^oC, shows that there are two maxima peaks at 368 and 605 nm. The spectrophotometric analysis of the spectrum indicates that the products of the reaction are I_3^- and $Fe^{II}(dmbpy)_2(CN)_2$, and that the product ratio of $\Delta[I_3^-]/\Delta[Fe(II)]$ is 0.43 ± 0.03, consistent with Equation 3-1.

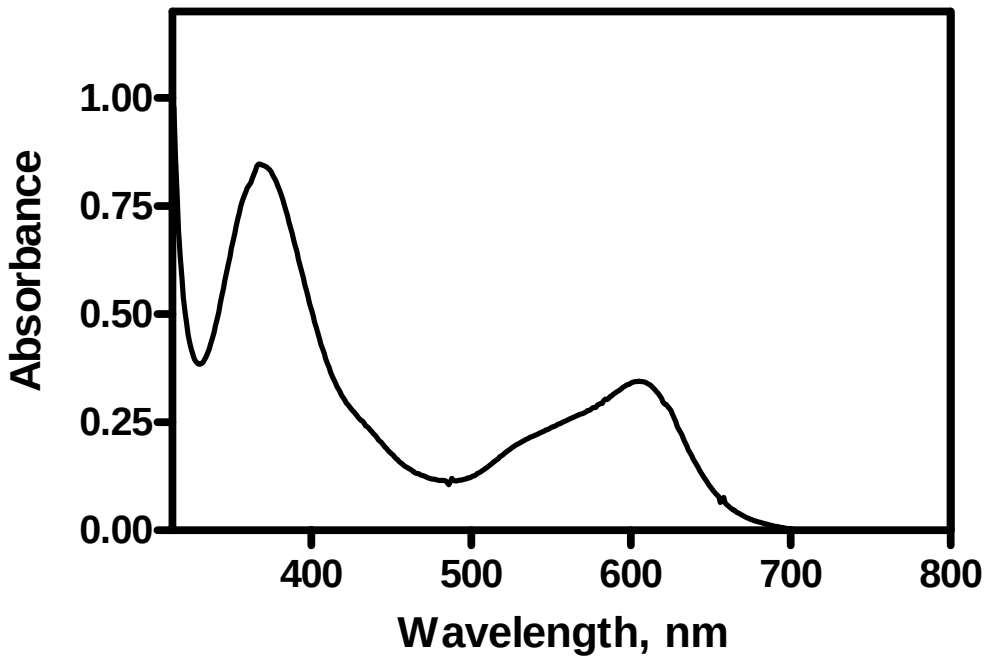

Figure 3-16. UV-vis spectrum of product of the reaction between 47 μM $[Fe^{III}(dmbpy)_2(CN)_2]^+$ and 5.0 mM Et_4NI in acetonitrile. In the presence of 5.0 mM bpy and 0.095 M Et_4NBF_4, at 25.0 ^oC.

Oxidation of iodide by $[Fe^{III}(CH_3Cp)_2]^+$. The products of the direct oxidation of iodide by $[Fe^{III}(CH_3Cp)_2]^+$ were identified by ^{1}H-NMR spectra and spectrophotometric analysis. The ^{1}H-NMR spectrum of product solution of the oxidation of 80.0 mM NaI by 2.5 mM $[Fe^{III}(CH_3Cp)_2]^+$ in acetonitrile, in the presence of 10.0 mM bpy and 20.0 mM Et_4NBF_4, is shown in Figure 3-17, demonstrates that $Fe^{II}(CH_3Cp)_2$ is one of the products,[166,167] and the yield of $Fe(CH_3Cp)_2$ is (99 ± 1)%. To identify other product of the reaction, UV-vis spectra of the product solution were recorded. Figure 3-18 is the UV-vis spectra for the oxidation of 5.0 mM NaI by 0.10 mM $[Fe^{III}(CH_3Cp)_2]^+$ in acetonitrile, in

the presence of 10.0 mM bpy, at μ = 0.10 M (Et_4NBF_4) and 25.0 ^oC. The product solution has strong absorbance at 363 nm that is assigned to that of I_3^- ($\varepsilon_{363} \approx 8\ M^{-1}\ cm^{-1}$ for $Fe^{II}(CH_3Cp)_2$; $\varepsilon_{363} = 26{,}250\ M^{-1}\ cm^{-1}$ for I_3^-). Thus, the products of the reaction are $Fe^{II}(CH_3Cp)_2$ and I_3^-.

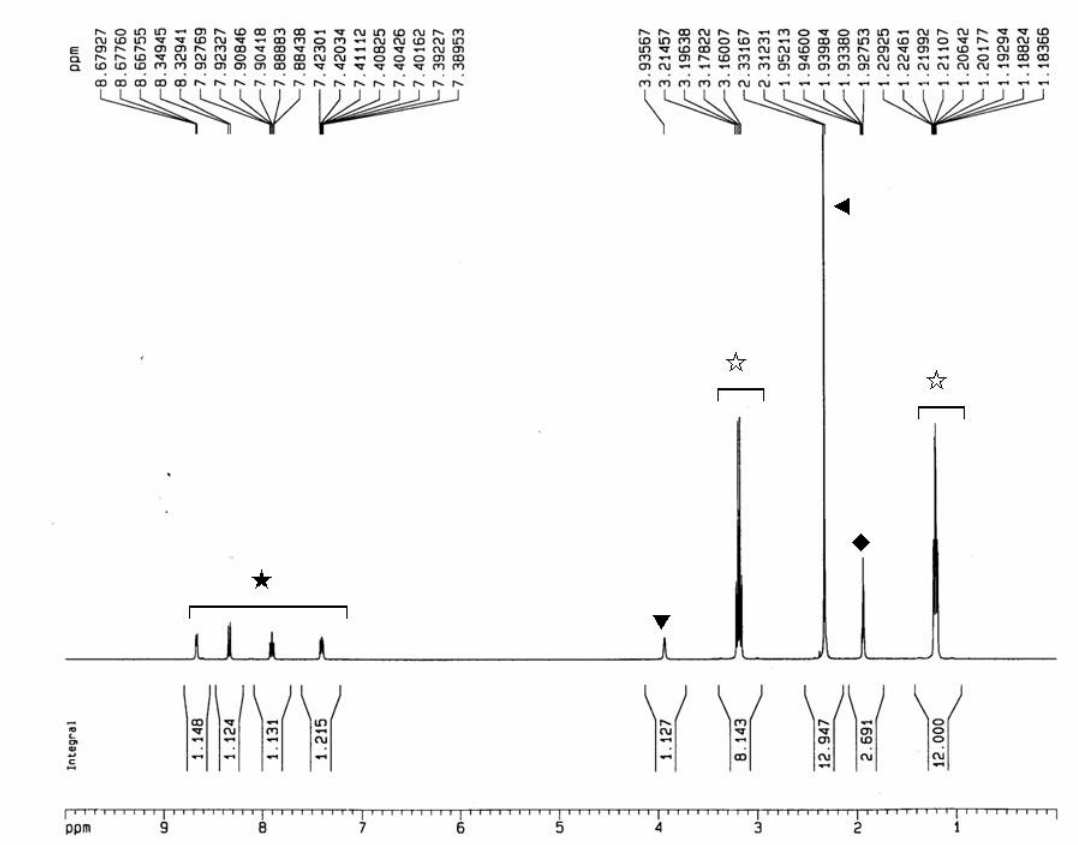

Figure 3-17. ^{1}H-NMR spectrum of product for the oxidation of 80.0 mM NaI by 2.5 mM $[Fe^{III}(CH_3Cp)_2]^+$ in CD_3CN. In the presence of 10.0 mM bpy and 20.0 mM Et_4NBF_4. ★: bpy; ☆: Et_4NBF_4; ▼: $Fe(CH_3Cp)_2$; ◄: H_2O; ♦: overlap of CD_3CN and $-CH_3$ in $Fe(CH_3Cp)_2$.

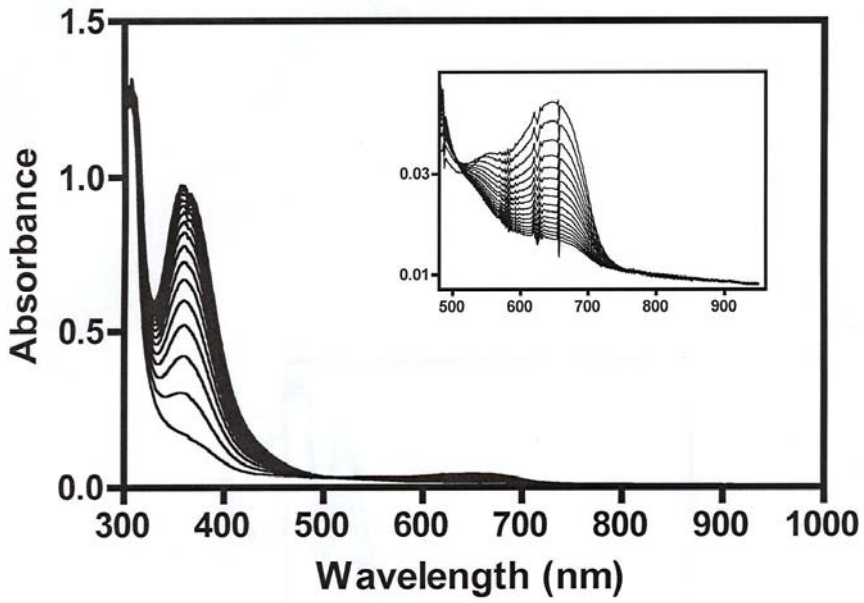

Figure 3-18. The UV-vis spectra for the oxidation of 5.0 mM NaI by 0.10 mM $[Fe^{III}(CH_3Cp)_2]^+$ in acetonitrile. In the presence of 10.0 mM bpy, at μ = 0.10 M (Et_4NBF_4) and 25.0 ^oC, 60 seconds interval between two spectra.
(Inset shows the enlarged spectra from 480 to 950 nm).

The stoichiometric ratio of the reaction was determined from UV-vis spectra. The product ratio of $\Delta[I_3^-]/\Delta[Fe^{II}(CH_3Cp)_2]$ is 0.45 (yield of $Fe(CH_3Cp)_2$ is 99%; $\varepsilon_{363} \approx 8$ M^{-1} cm^{-1} for $Fe^{II}(CH_3Cp)_2$; $\varepsilon_{363} = 26{,}250$ M^{-1} cm^{-1} for I_3^-). Therefore, the stoichiometric ratio of above reaction is consistent with Equation 3-1.

Oxidation of iodide by $[Fe^{III}(5\text{-Cl-phen})_2(CN)_2]^+$. The products of the direct oxidation of iodide by $[Fe^{III}(5\text{-Cl-phen})_2(CN)_2]^+$ were identified by ^{1}H-NMR spectra. The ^{1}H-NMR spectrum (Figure 3-19) of the product of the reaction between 0.50 mM [Fe^{III}(5-

Cl-phen)$_2$(CN)$_2$]$^+$ and 3.0 mM Et_4NI in CD_3CN has 14 peaks with the same intensity, which implies that only one isomer of Fe^{II}(5-Cl-phen)$_2$(CN)$_2$ was formed. The UV-vis spectrum of the product for the oxidation of 10.0 mM Et_4NI by 50 μM [Fe^{III}(5-Cl-phen)$_2$(CN)$_2$]$^+$ in acetonitrile, with 5.0 mM bpy, at μ = 0.10 M and 25.0 ^oC, is shown in Figure 3-20. The spectrophotometric analysis indicates that the product ratio of $\Delta[I_3^-]/\Delta[Fe^{II}(5\text{-Cl-phen})_2(CN)_2]$ is 0.51 ± 0.02. Thus, the stoichiometric ratio of the reaction complies with Equation 3-1 as well.

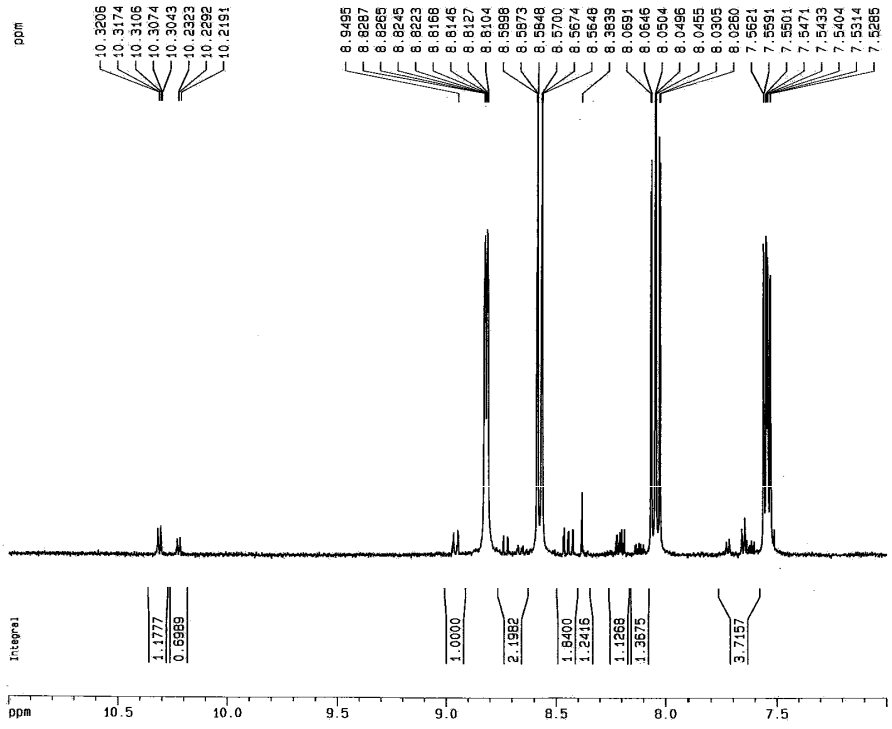

Figure 3-19. ^{1}H-NMR spectrum of the product of the reaction between 0.50 mM [Fe^{III}(5-Cl-phen)$_2$(CN)$_2$]$^+$ and 3.0 mM Et_4NI in CD_3CN, with 2.0 mM bpy.

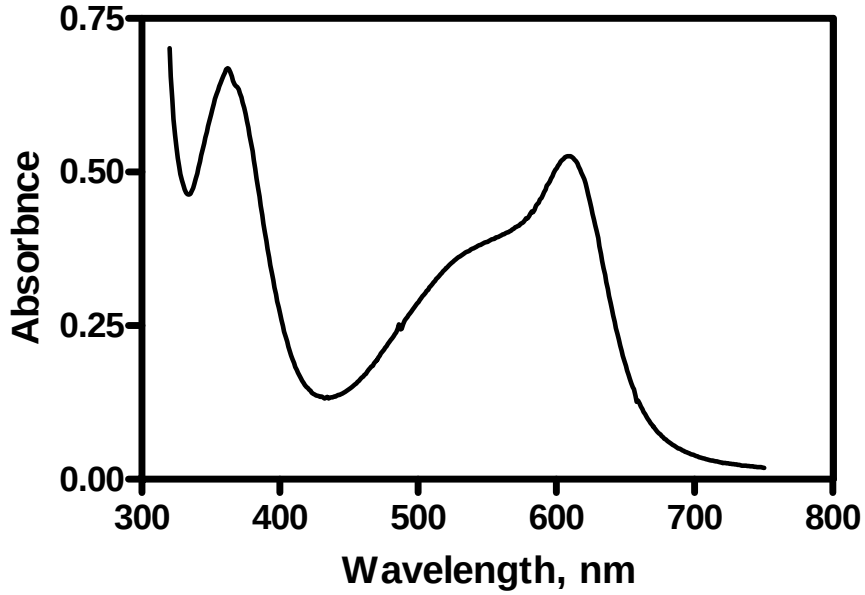

Figure 3-20.UV-vis spectra of product of the reaction of 10.0 mM Et_4NI with 50 μM $[Fe^{III}(5\text{-Cl-phen})_2(CN)_2]^+$ in acetonitrile. In the presence of 5.0 mM bpy, at μ = 0.10 M (Et_4NBF_4) and 25.0 ^oC.

6. Reaction of iodine with bpy. For the oxidation of iodide by Fe(III) complexes in acetonitrile, I_2 was firstly formed in the reaction. Spectroscopic studies have shown that iodine reacts with π-donors to form DI^+ and I_3^-.[168,169] Bpy, one good π-donor, is known to react with iodine very fast to form bpy_2I^+ and I_3^-, as shown in reaction 3-2. Thus, I_2 may combine with bpy to form bpy_2I^+ and I_3^- in present reaction system. The UV-vis spectra of 0.60 mM I_2 in air-saturated acetonitrile show that it is stable more than 60 minutes. Then a solution containing 0.20 mM I_2 and 5.0 mM bpy was prepared in anaerobic acetonitrile, and UV-vis spectra were recorded. These spectra show the slow formation of 0.027 mM I_3^- with a half-life of about 580 s. It implies that the equilibrium constant for

reaction 3-2 is unfavorable under such dilute conditions. The large associate constant (pK_{eq} = -7.18[147]) of triiodide from iodine and iodide in acetonitrile ensures that reaction 3-2 will shift to backward direction, excluding the possibility of the formation of bpy_2I^+ in the direct oxidation of iodide by Fe(III) complexes. Furthermore, the evidence that the Fe(III)/I^- rate constants independent of the concentration of bpy supports the insignificant role of I_2/bpy in the current study.

$$2bpy + 2I_2 \rightleftharpoons bpy_2I^+ + I_3^- \qquad (3\text{-}2)$$

7. Kinetics.

Oxidation of iodide by $[Fe^{III}(bpy)_2(CN)_2]^+$. According to above results, the products of the reaction are $Fe^{II}(bpy)_2(CN)_2$ and I_3^-. It is of importance to know the effect of products on the rate of the reaction. For the reaction between 7.5×10^{-6} M $[Fe^{III}(bpy)_2(CN)_2]^+$ and 7.5×10^{-5} M Et_4NI, in the presence of 0.10 M Et_4NBF_4 and 5.0 mM bpy, various concentrations of $Fe^{II}(bpy)_2(CN)_2$ were added to the above reaction system. The rate constant decreases with the addition of $Fe^{II}(bpy)_2(CN)_2$. Plot of $1/k_{obs}$ vs $[Fe^{II}(bpy)_2(CN)_2]$ is linear with the slope of $(3.07 \pm 0.30) \times 10^6$ s/M and intercept of 200 ± 8.7 s, as shown in Figure 3-21.

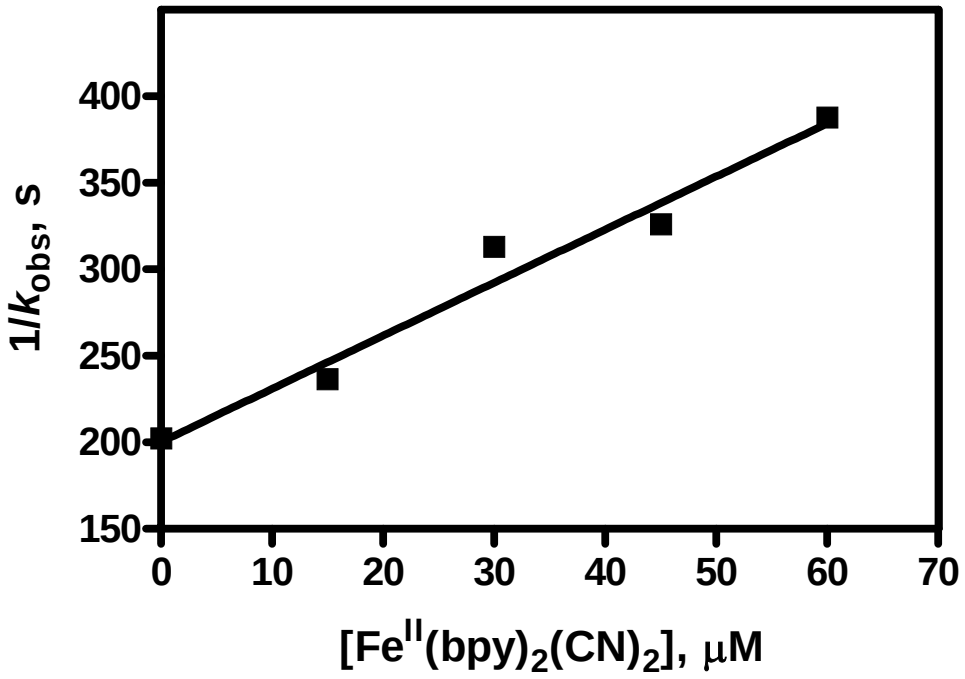

Figure 3-21. Plot of $1/k_{obs}$ vs $[Fe^{II}(bpy)_2(CN)_2]$ for the reaction between 7.5×10^{-6} M $[Fe^{III}(bpy)_2(CN)_2]^+$ and 7.5×10^{-5} M Et_4NI in acetonitrile. In the presence of 0.10 M Et_4NBF_4 and 5.0 mM bpy, at 25.0 ^oC.

Then the reduction of $[Fe^{III}(bpy)_2(CN)_2]^+$ by various concentrations of Et_4NI in acetonitrile, in the presence of 5.0 mM bpy, was investigated under 25.0 ^oC and constant ionic strength (μ = 0.10 M, Et_4NBF_4). A pseudo-first-order dependence of the rate constant was established by fitting the experimental curves with one exponential equation. The pseudo-first-order rate constants, k_{obs}, were obtained from the fits, and replicate runs agree to better than 5%. Figure 3-22 is the reaction trace of oxidation of 2.0×10^{-4} M Et_4NI by 5×10^{-5} M $[Fe^{III}(bpy)_2(CN)_2]^+$ in acetonitrile, with 5.0 mM bpy and μ = 0.10 M, at 25.0 ^oC. It indicates that the rate of the reaction follows pseudo-first-order kinetic

behavior. The rate constants for various concentrations of I^- are shown in Table 3-6. Plots of $k_{obs}/[I^-]$ vs $[I^-]$ (Figure 3-23) are linear, in which the intercept is 58.4 M^{-1} s^{-1}, and slope is 7760 M^{-2} s^{-1}. Based on the above results, the rate law of the reaction can be expressed by Equation 3-3, with k_1 and k_2 being $(2.9 \pm 0.1) \times 10^1$ M^{-1} s^{-1} and $(3.88 \pm 0.14) \times 10^3$ M^{-2} s^{-1}, respectively.

$$\text{Rate} = - d[\text{Fe(III)}]/dt = 2 (k_1[I^-] + k_2[I^-]^2) [\text{Fe(III)}] \qquad (3\text{-}3)$$

Table 3-6. $[I^-]$ dependence for the oxidation of Et_4NI by 5.0×10^{-5} M $[Fe^{III}(bpy)_2(CN)_2]^+$. In the presence of 5.0 mM bpy, at μ = 0.10 M and 25.0 ^oC.

$[Et_4NI]$, mM	k_{obs}, s^{-1}
0.5	0.028
1.0	0.0672
2.0	0.151
5.0	0.50
10.0	1.51
20.0	4.18
25.0	6.46
30.0	8.73
40.0	13.6

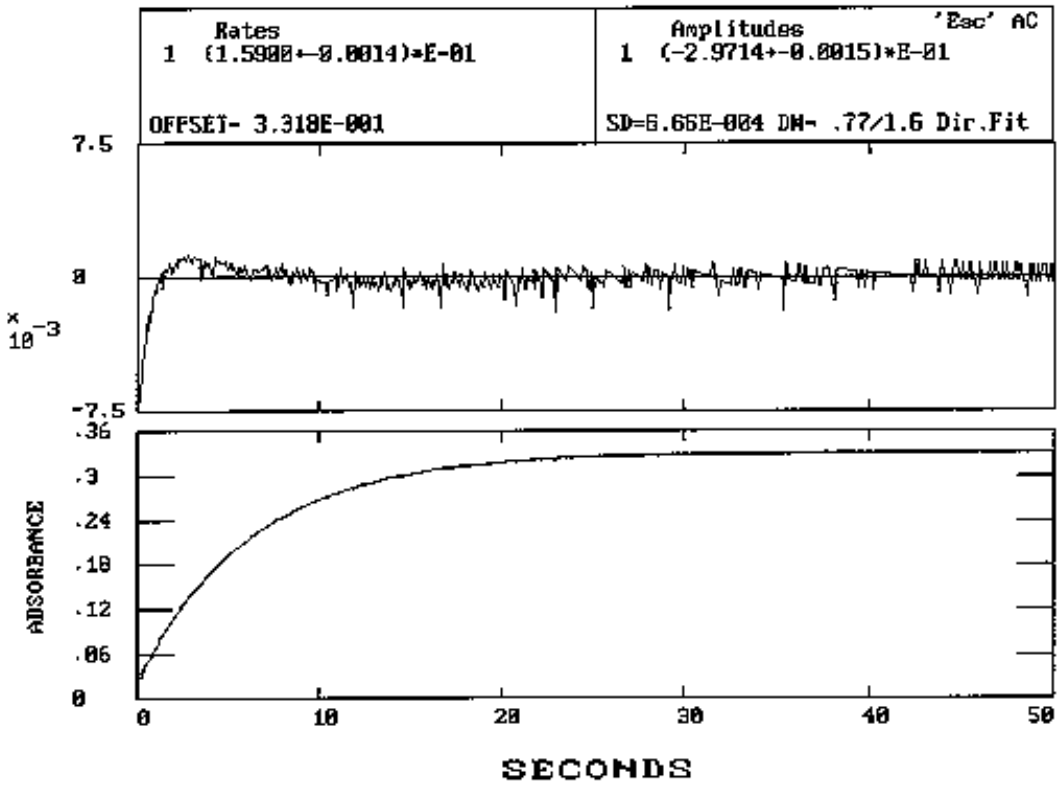

Figure 3-22. Reaction trace for the oxidation of 2.0×10^{-3} M Et_4NI by 5.0×10^{-5} M $[Fe^{III}(bpy)_2(CN)_2]^+$. In the presence of 5.0 mM bpy, at μ = 0.10 M (Et_4NBF_4) and 25.0 ^oC.

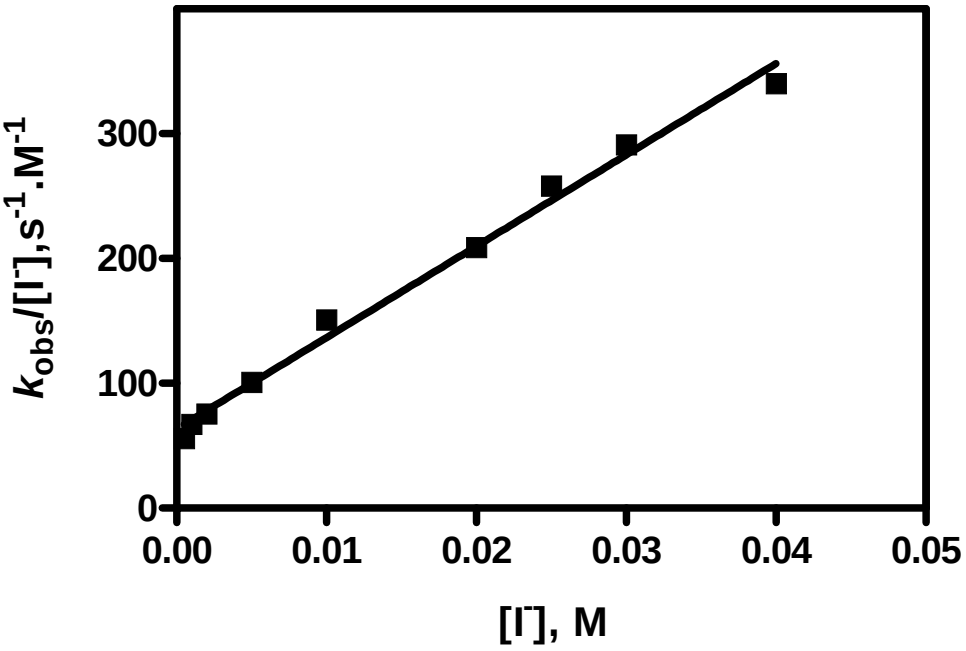

Figure 3-23. $k_{obs}/[I^-]$ vs $[I^-]$ for the reaction of $[Fe^{III}(bpy)_2(CN)_2]^+$ with Et_4NI. In the presence of 5.0 mM bpy, at μ = 0.10 M and 25.0 ^oC, $[Fe^{III}(bpy)_2(CN)_2^+]_0 = 5.0 \times 10^{-5}$ M.

Oxidation of iodide by $[Fe^{III}(dmbpy)_2(CN)_2]^+$. The rate of reduction of $[Fe^{III}(dmbpy)_2(CN)_2]^+$ by various concentrations of Et_4NI in acetonitrile, in the presence of 5.0 mM bpy, was investigated under 25.0 ^oC and constant ionic strength (μ = 0.10 M, Et_4NBF_4). The rate constants follow pseudo-first-order kinetics, as shown in Figure 3-24. The iodide-dependent rate constants are shown in Table 3-7. Plots of $k_{obs}/[I^-]$ vs $[I^-]$ (Figure 3-25) are linear with intercept of 1.30 M^{-1} s^{-1} and slope of 692 M^{-2} s^{-1}. The rate law conforms to Equation 3-3, with k_1 of (0.65 ± 0.05) M^{-1} s^{-1} and k_2 of (3.46 ± 0.16) × 10^2 M^{-2} s^{-1}.

Table 3-7. [I^-] dependence for the oxidation of Et_4NI by 5.0×10^{-5} M $[Fe^{III}(dmbpy)_2(CN)_2]^+$. In the presence of 5.0 mM bpy, at $\mu = 0.10$ M and 25.0 °C.

$[Et_4NI]$, mM	k_{obs}, s^{-1}
0.5	7.81×10^{-4}
1.0	1.94×10^{-3}
2.0	5.80×10^{-3}
5.0	2.39×10^{-2}
10.0	1.07×10^{-1}
20.0	3.16×10^{-1}
30.1	6.08×10^{-1}
40.1	1.10
50.2	1.64

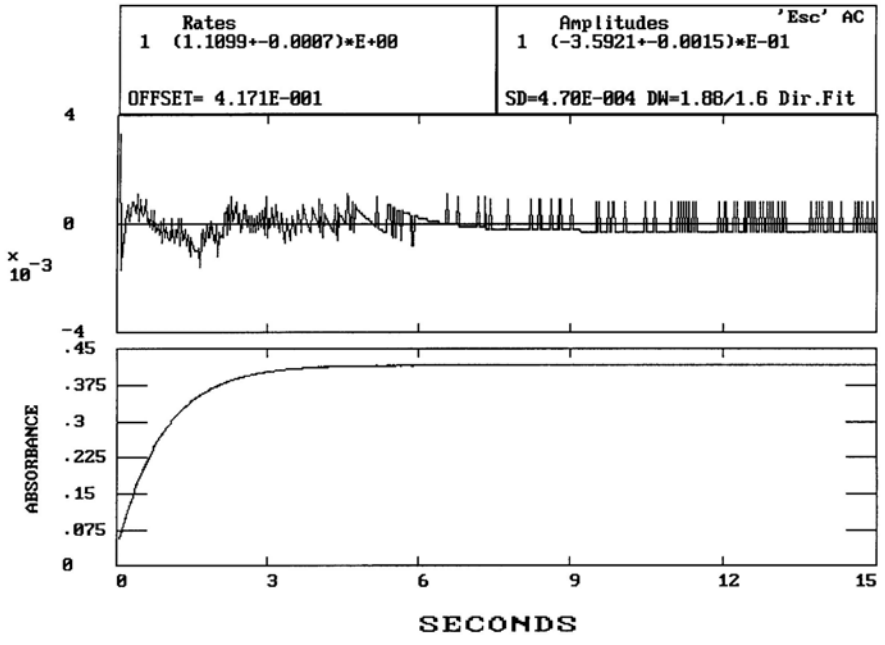

Figure 3-24. Reaction trace for the oxidation of 4.01×10^{-2} M Et_4NI by 5.0×10^{-5} M $[Fe^{III}(dmbpy)_2(CN)_2]^+$. In the presence of 5.0 mM bpy, at $\mu = 0.10$ M (Et_4NBF_4) and 25.0 °C.

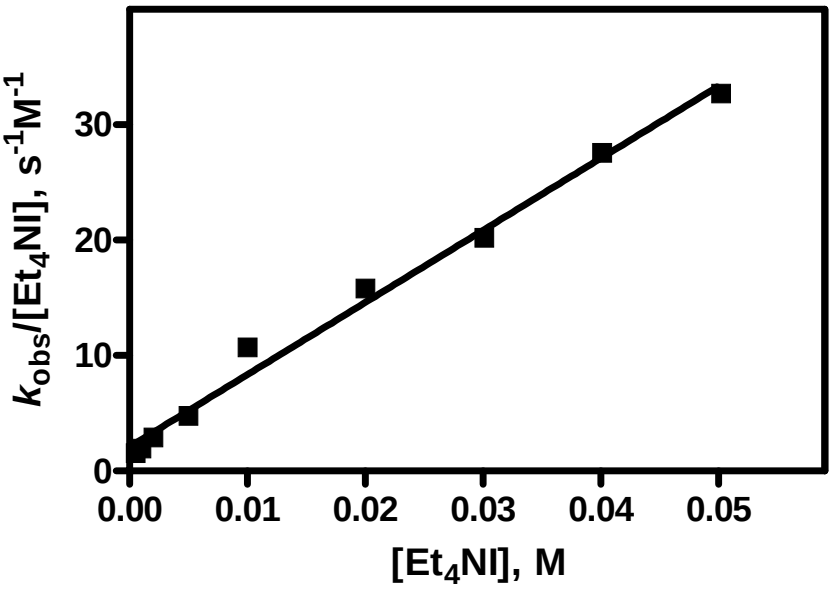

Figure 3-25. Plot of $k_{obs}/[I^-]$ vs $[I^-]$ for the oxidation of Et_4NI by 5.0×10^{-5} M $[Fe^{III}(dmbpy)_2(CN)_2]^+$. In the presence of 5.0 mM bpy, at μ = 0.10 M (Et_4NBF_4) and 25.0 ^oC.

Oxidation of iodide by $[Fe^{III}(CH_3Cp)_2]^+$. $[Fe^{III}(CH_3Cp)_2]PF_6$ is very air sensitive in acetonitrile. The half-life for the decomposition of 1.0 mM $[Fe^{III}(CH_3Cp)_2]PF_6$ in air-saturated acetonitrile is comparable to that of the reduction by lower concentration of iodide. To prevent its decomposition, all of solutions were purged with argon or N_2 for all of kinetic studies.

The kinetic experiments for the reduction of $[Fe^{III}(CH_3Cp)_2]^+$ by various concentrations of Et_4NI in acetonitrile, in the presence of 5.0 mM bpy, was investigated using both SF-51 and HP 8453 diode-array spectrophotometer, under 25.0 ^oC and

constant ionic strength (μ = 0.10 M, Et_4NBF_4). Figure 3-26 shows that the rate constants follow pseudo-first-order kinetic behavior. The rate constants for various concentrations of I^- are shown in Table 3-8. Plot of $k_{obs}/[I^-]$ vs $[I^-]$ (Figure 3-27) are linear with intercept of 0.10 M^{-1} s^{-1} and slope of 54.2 M^{-2} s^{-1}. The rate law is consistent with Equation 3-3, in which k_1 and k_2 are (0.05 ± 0.01) M^{-1} s^{-1} and (27.1 ± 1.0) M^{-2} s^{-1}, respectively.

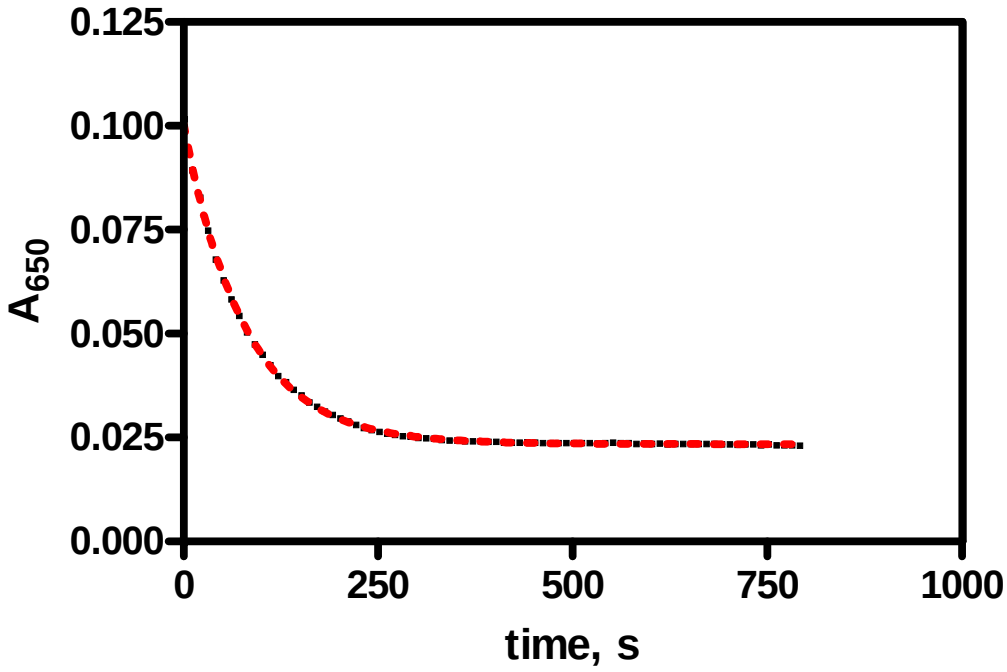

Figure 3-26. Reaction traces for the oxidation of 1.50 × 10^{-2} M Et_4NI by 2.50 × 10^{-4} M $[Fe^{III}(CH_3Cp)_2]^+$. In the presence of 5.0 mM bpy, at μ = 0.10M and 25.0 °C, using first-order fitting (k_{obs} = 0.0125 s^{-1}). (Red dash line: pseudo-first-order fitting)

Table 3-8. $[I^-]$ dependence for the oxidation of Et_4NI by 2.50×10^{-4} M $[Fe^{III}(CH_3Cp)_2]^+$. In the presence of 5.0 mM bpy, at $\mu = 0.10$ M (Et_4NBF_4) and 25.0 °C.

$[Et_4NI]$, mM	k_{obs}, s^{-1}
0.0050	0.00208
0.0073	0.00370
0.010	0.00611
0.0142	0.0125
0.020	0.0247
0.030	0.055
0.040	0.0895
0.050	0.143

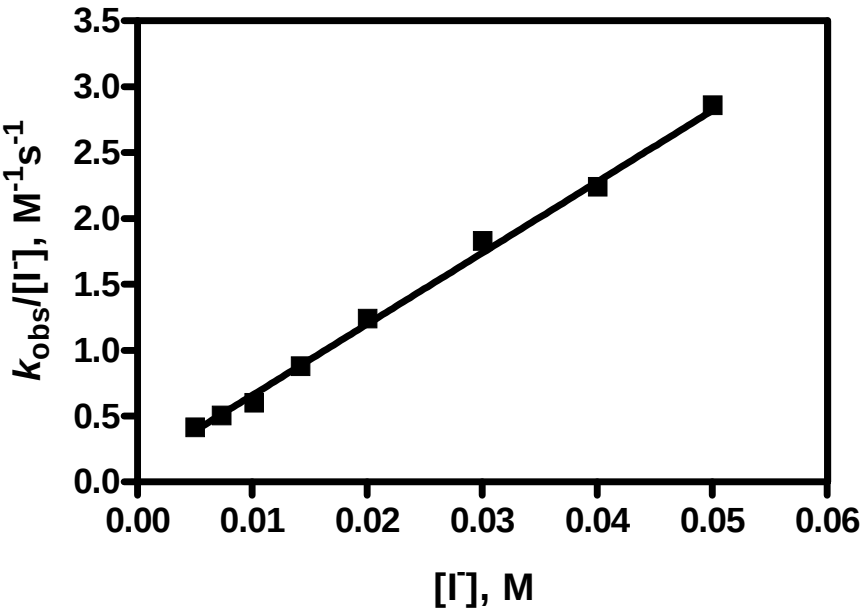

Figure 3-27. Plot of $k_{obs}/[I^-]$ vs $[I^-]$ for the oxidation of Et_4NI by $[Fe^{III}(CH_3Cp)_2]^+$. In the presence of 5.0 mM bpy, at $\mu = 0.10$ M and 25.0 °C. $[Fe^{III}(CH_3Cp)_2^+]_0 = 2.50 \times 10^{-4}$ M

Oxidation of iodide by $[Fe^{III}(5\text{-Cl-phen})_2(CN)_2]^+$. The reaction of $[Fe^{III}(5\text{-Cl-phen})_2(CN)_2]^+$ with excess iodide in acetonitrile, in the presence of 5.0 mM bpy, at μ = 0.10 M and 25.0 ^oC, follows pseudo-first-order kinetics. The rate constants for various concentrations of I^- are shown in Table 3-9. Plots of $k_{obs}/[I^-]$ vs $[I^-]$ are shown in Figure 3-28, with the intercept of 2900 M^{-1} s^{-1} and slope of 3.36×10^5 M^{-2} s^{-1}. The experimental data are not exactly linear in Figure 3-28, which implies that k_1 is dominant in the above reaction, especially at the concentration of iodide higher than 5.0 mM. The rate law is consistent with Equation 3-3, in which k_1 and k_2 are $(1.45 \pm 0.03) \times 10^3$ M^{-1} s^{-1} and $(1.68 \pm 0.11) \times 10^5$ M^{-2} s^{-1}, respectively.

Table 3-9. $[I^-]$ dependence for the oxidation of Et_4NI by 10^{-5} M $[Fe^{III}(5\text{-Cl-phen})_2(CN)_2]^+$. In the presence of 5.0 mM bpy, at μ = 0.10 M and 25.0 ^oC.

$[Et_4NI]$, mM	k_{obs}, s^{-1}
0.20	0.57
0.50	1.61
1.00	3.28
2.60	9.36
4.00	17.8
5.00	23.1
6.00	29.2
7.00	36.7
8.00	40.0
9.00	45.4
10.0	52.2

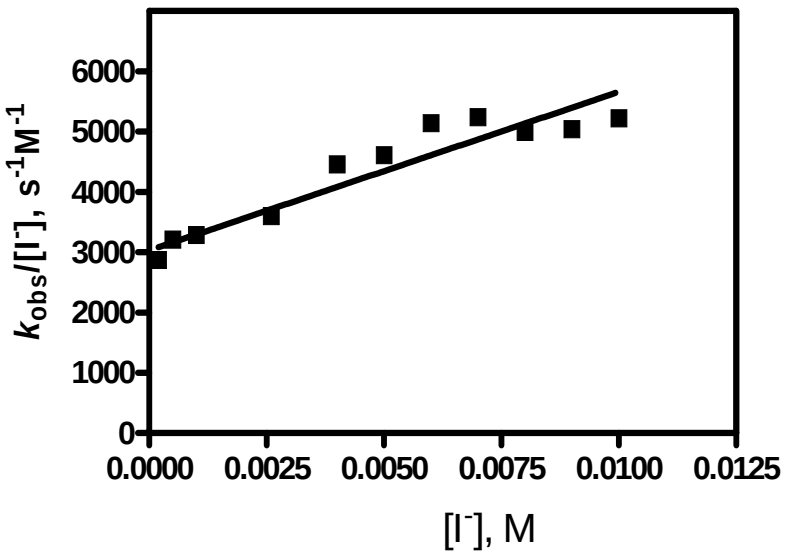

Figure 3-28. Plot of $k_{obs}/[I^-]$ vs $[I^-]$ for the oxidation of Et_4NI by $[Fe^{III}(5\text{-Cl-phen})_2(CN)_2]^+$. In the presence of 5.0 mM bpy, at μ = 0.10 M and 25.0 ^oC. $[Fe^{III}(5\text{-Cl-phen})_2(CN)_2^+]_0 = 10^{-5}$ M

Table 3-10. The rate constants for the oxidation of iodide by Fe(III) complexes in acetonitrile. In the presence of 5.0 mM bpy, at μ = 0.10 M (Et_4NBF_4) and 25.0 ^oC.

Oxidants	$E_{1/2}$, mV [a]	k_1, M^{-1} s^{-1}	k_2, M^{-2} s^{-1}
$[Fe^{III}(CH_3Cp)_2]^+$	-108 ± 2	0.05 ± 0.01	27.1 ± 1.0
$[Fe^{III}(dmbpy)_2(CN)_2]^+$	- 36 ± 2	0.65 ± 0.05	(3.46 ± 0.16) × 10^2
$[Fe^{III}(bpy)_2(CN)_2]^+$	+ 70 ± 2	29.2 ± 0.82	(3.88 ± 0.14) × 10^3
$[Fe^{III}(5\text{-Cl-phen})_2(CN)_2]^+$	168 ± 2	(1.45 ± 0.03) × 10^3	(1.68 ± 0.11) × 10^5

[a] The $E_{1/2}$ vs $[Fe(Cp)_2]^{+/0}$

The rate constants for the above reactions are summarized in Table 3-10. For the reduction of $[Fe^{III}(5\text{-Cl-phen})_2(CN)_2]^+$, it has the highest rate constants; while in the case

of $[Fe^{III}(CH_3Cp)_2]^+$, it has the smallest values. The kinetic experimental results indicate that the rate constants of the above reactions is proportional to the oxidative capability of the four Fe(III) complexes.

Discussion

The half-wave potentials of Fe(III) complexes are obtained from CV and OSWV, as shown in Table 3-10. The equilibrium constants (K_{tot}, Equation 3-1) for the oxidation of iodide by Fe(III) complexes in acetonitrile can be calculated provided that the standard potential of I_3^-/I^- is known.

The standard potential of I_3^-/I^- was reported by several groups in their voltammetric studies.[163,170-172] However, the employment of various reference electrodes in their determination yields seemingly incomparable values. The above impedance was overcome by converting them relative to the same reference, ie. $[Fe(Cp)_2]^{+/0}$. The results from our calculation (see appendix A) indicate that their determination gave similar standard-potential value of I_3^-/I^-: from Popov and Geske, $E^o(I_3^-/I^-)$ = -0.36 V[163] vs $[Fe(Cp)_2]^{+/0}$; from Desbarres et al., $E^o(I_3^-/I^-)$ = -0.337 V[170] vs $[Fe(Cp)_2]^{+/0}$; from Benoit et al., $E^o(I_3^-/I^-)$ = -0.315 V [171] vs $[Fe(Cp)_2]^{+/0}$; from Nelson et al., $E^o(I_3^-/I^-)$ = -0.329 V [172] vs $[Fe(Cp)_2]^{+/0}$; from Datta et al., $E^o(I_3^-/I^-)$ = -0.372 V [172] vs $[Fe(Cp)_2]^{+/0}$. The average value, $E^o(I_3^-/I^-)$ = - (0.35 ± 0.02) V vs $[Fe(Cp)_2]^{+/0}$, was used in the calculation of equilibrium constants in Equation 3-1. Furthermore, the known equilibrium constant for the association of I^- with I_2 to form I_3^- in acetonitrile ensures us to calculate the equilibrium constants in Equation 3-5. All of the equilibrium constants for the reaction of I^- with the

four Fe(III) complexes are shown in Table 3-11. Even for the oxidation of I^- by the weakest oxidant, $[Fe^{III}(CH_3Cp)_2]^+$, it is still favorable for the forward direction due to the higher equilibrium constants of K_{I2} and K_{tot}. Theoretically, the yield of Fe(II) for these four redox reactions can reach 100%. Our results in product identification and stoichiometry section support this thermodynamic calculation.

$$I_2 + I^- \rightleftharpoons I_3^- \qquad K_{eq} = 10^{7.18} \qquad (3\text{-}4)$$

$$2\ Fe(III) + 2\ I^- \rightleftharpoons 2\ Fe(II) + I_2 \qquad K_{I2} \qquad (3\text{-}5)$$

Table 3-11. The equilibrium constants (K_{tot} and K_{I2}) for the oxidation of iodide by Fe(III) complexes in acetonitrile.

Compounds	K_{tot}, M^{-2}	K_{I2}, M^{-1}
$[Fe^{III}(CH_3Cp)_2]^+$	7.0×10^7	4.6
$[Fe^{III}(dmbpy)_2(CN)_2]^+$	1.9×10^{10}	1.2×10^3
$[Fe^{III}(bpy)_2(CN)_2]^+$	7.3×10^{13}	4.8×10^6
$[Fe^{III}(5\text{-Cl-phen})_2(CN)_2]^+$	1.5×10^{17}	1.0×10^{10}

The results from CV and OSWV show that $[Fe(5\text{-Cl-phen})_2(CN)_2]^{+/0}$ has the highest standard potential (E^o), and that $[Fe(CH_3Cp)_2]^{+/0}$ has the lowest value. The kinetic results for the oxidation of I^- by four Fe(III) complexes are closely related to their standard potential values: the rate constant is the fastest for the reaction of $[Fe^{III}(5\text{-Cl-phen})_2(CN)_2]^+$, while it has the slowest rate constant for the reaction of $[Fe^{III}(CH_3Cp)_2]^+$.

Plots of log k versus E_f (LFER curves) in Figure 3-29 are linear with the slope of 16.1 (log k_1) and 13.3 (log k_2), respectively. The higher slope of log k_1 than log k_2 implies that the rate constant k_1 will be dominant when the half-wave potential of substitution-inert transition metal complex reaches to some value. Moreover, Linear Free-Energy Relationship (LFER) curves imply that the reaction may follow one-electron outer-sphere mechanism.

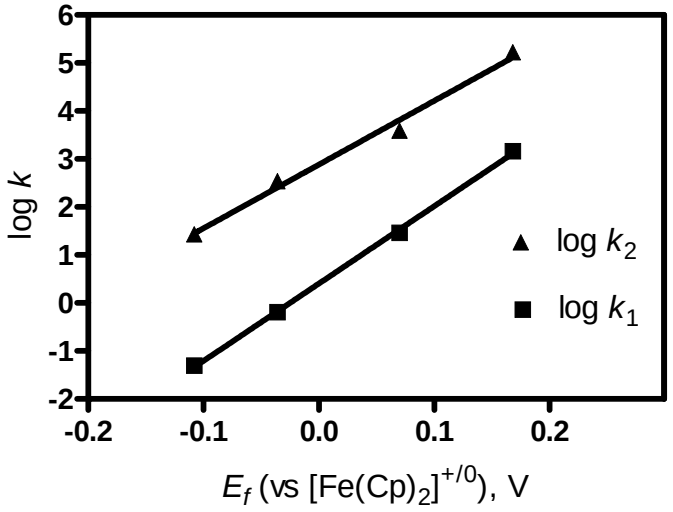

Figure 3-29. Plot of log k vs E_f for the oxidation of I^- by $[Fe^{III}(5\text{-Cl-phen})_2(CN)_2]^+$, $[Fe^{III}(bpy)_2(CN)_2]^+$, $[Fe^{III}(dmbpy)_2(CN)_2]^+$ and $[Fe^{III}(CH_3Cp)_2]^+$ in acetonitrile.

The oxidation of iodide by substation-inert transition metal complexes in aqueous solution has been well studied.[83,85] It shows that no copper-catalysis effect is present in the reaction. For the copper-catalysis inhibited oxidation of I^- by the Fe(III) complexes in acetonitrile, it is possible that the reaction follows the similar mechanism. Here, the

mechanism of the copper-catalysis inhibited oxidation of I^- by Fe(III) complexes in acetonitrile is proposed as:

$$Fe(III) + I^- \rightleftharpoons Fe(II) + I^\bullet \qquad k_1,\ k_{-1} \qquad (3\text{-}6)$$

$$Fe(III) + 2I^- \rightleftharpoons Fe(II) + I_2^{\bullet -} \qquad k_2,\ k_{-2} \qquad (3\text{-}7)$$

$$I^\bullet + I^- \rightleftharpoons I_2^{\bullet -} \qquad K_{rad} = k_3 / k_{-3} \qquad (3\text{-}8)$$

$$Fe(III) + I_2^{\bullet -} \longrightarrow Fe(II) + I_2 \qquad k_4 \qquad (3\text{-}9)$$

$$I^- + I_2 \rightleftharpoons I_3^- \qquad K_{eq} \qquad (3\text{-}10)$$

Applying steady-state approximation for $I^\bullet$ and $I_2^{\bullet -}$, the rate law of the reaction is represented by Equation 3-11:

$$\text{rate} = \frac{2\{k_1k_3k_4 + k_2k_4k_{-1}[Fe^{II}] + k_2k_3k_4[I^-]\}[Fe^{III}]^2[I^-]^2}{k_{-1}k_{-2}[Fe^{II}]^2 + k_4k_{-1}[Fe^{II}][Fe^{III}] + k_{-2}k_3[I^-][Fe^{II}] + k_3k_4[Fe^{III}][I^-] + k_{-1}k_{-3}[Fe^{II}]} \qquad (3\text{-}11)$$

In the above equation, the rate constants k_1, k_{-1}, k_2, k_{-2}, k_3 and k_{-3} are not independent of each other. They are correlated with the following equation:

$$\left(\frac{k_1}{k_{-1}}\right)\left(\frac{k_3}{k_{-3}}\right) = \frac{k_2}{k_{-2}} \qquad (3\text{-}12)$$

In the copper-catalysis inhibited oxidation of excess iodide by $[Fe^{III}(bpy)_2(CN)_2]^+$ in acetonitrile, it was observed that the rate of the reaction decreases with the addition of $Fe^{II}(bpy)_2(CN)_2$. Supposes that k_4[Fe(III)] is much higher than k_{-2}[Fe(II)], and k_4[Fe(III)] is much higher than k_{-3}, Equation 3-11 is simplified into such form:

$$\text{rate} = \left(\frac{2k_1k_3}{k_{-1}[Fe^{II}] + k_3[I^-]} + 2k_2 \right)[Fe^{III}][I^-]^2 \tag{3-13}$$

Where k_{obs} is:

$$k_{obs} = \left(\frac{2k_1k_3}{k_{-1}[Fe^{II}] + k_3[I^-]} + 2k_2 \right)[I^-]^2 \tag{3-14}$$

Furthermore, Equation 3-14 can be converted into another form:

$$\frac{1}{k_{obs} - 2k_2[I^-]^2} = \frac{k_{-1}}{2k_1k_3[I^-]^2}[Fe^{II}] + \frac{1}{2k_1[I^-]} \tag{3-15}$$

k_{obs} will be much higher than 2 k_2 $[I^-]^2$ provided that the concentration of I^- is about 10 times as that of Fe(III) complexes. Under such experimental condition, Equation 3-15 can be simplified into the following form:

$$\frac{1}{k_{obs}} = \frac{k_{-1}}{2k_1k_3[I^-]^2}[Fe^{II}] + \frac{1}{2k_1[I^-]} \tag{3-16}$$

The theoretical linearity of $1/k_{obs}$ relative to [Fe(II)] is confirmed by our $Fe^{II}(bpy)_2(CN)_2$ kinetic inhibition results in the direct oxidation of 75 μM Et_4NI by 7.5μM $[Fe^{III}(bpy)_2(CN)_2]^+$. Combing the slope value in Figure 3-21 with the slope term in Equation 3-16, k_{-1}/k_3 was obtained with the value of 1.06. The rate constant (k_3, see the mechanism) of the reaction between iodide and iodine radical in acetonitrile was reported as 2.3×10^{10} M^{-1} s^{-1}.[173] Then k_{-1} was derived, with the value of 2.4×10^{10} M^{-1} s^{-1}. The derived k_{-1} value implies that the reverse reaction of Equation 3-6 is diffusion-control.[174,175]

The validity of the approximations in the derivation of Equation 3-16 is confirmed by simulating the complete proposed mechanism (Equation 3-6 to 3-10) using the Specfit/32 software package.[132] Note that in such simulation the rate constants are constrained by Equation 3-12. Using the value of k_1 and k_2 in Table 3-10, k_{-1} and k_3 given above, and working with the above constraint, an excellent simulation of the observed kinetic inhibition by $Fe^{II}(bpy)_2(CN)_2$ was achieved, as shown in Table 3-12. A full description of the simulation model is shown in Table 3-13.

Applying the diffusion-control reverse rate constants (k_{-1}), the experimental forward rate constant ($k_1 = 29.2 \pm 0.82$ M^{-1} s^{-1}), and the standard potential of $[Fe(bpy)_2(CN)_2]^{+/0}$ ($E_{1/2} = 0.070$ V vs $[Fe(Cp)_2]^{+/0}$), the half-wave potential of $I^{\bullet}/I^-$ was calculated by us with the employment of the following equations:

$$\Delta E_{rxn} = (RT \text{ Ln } K_1)/nF \qquad (3\text{-}17)$$

Table 3-12. Simulation results for the inhibition by $[Fe^{II}(bpy)_2(CN)_2]$ in the oxidation of I^- by $[Fe^{III}(bpy)_2(CN)_2]^+$. In the presence of 5.0 mM bpy, at μ = 0.10 M (Et_4NBF_4) and 25.0 ^oC, using Specfit/32 software package.

$[Fe^{II}(bpy)_2(CN)_2]_0$, μM	$k_{obs} \times 10^3$, s^{-1}	$t_{1/2}$, s	
		Experimental	Theory[b]
0	4.94	140	142
15	4.23	164	171
30	3.19	217	204
45	3.06	226	237
60	2.58	269	270

[a] $[Et_4NI]_0$ = 75.0 μM, $[Fe^{III}(bpy)_2(CN)_2^+]_0$ = 7.5 μM; [b] Obtained from simulation

Table 3-13. Mathematical models for the simulation of the oxidation of I^- by $[Fe^{III}(bpy)_2(CN)_2]^+$. In the presence of 5.0 mM bpy, at μ = 0.10 M (Et_4NBF_4) and 25.0 ^oC, using Specfit/32 software package. $[Et_4NI]_0$ = 75.0 μM, $[Fe^{III}(bpy)_2(CN)_2^+]_0$ = 7.5 μM, $[Fe^{II}(bpy)_2(CN)_2]_0$ = 60.0 μM.

Model Reaction Equation	Name	Rate constants	Initial Concentration, M		Half-life, s
$A + B \rightarrow C + D$	k_{1c}	35.2	A	7.5×10^{-6}	
$C + D \rightarrow A + B$	k_{-1c}	2.4×10^{10}	B	7.5×10^{-5}	
$A + 2*B \rightarrow C + E$	k_{2c}	3.88×10^3	C	6.0×10^{-5}	
$C + E \rightarrow A + 2*B$	k_{-2c}	8.0×10^7	D	0.0	270
$B + D \rightarrow E$	k_{3c}	2.4×10^{10}	E	0.0	
$E \rightarrow B + D$	k_{-3c}	1.0×10^4	F	0.0	
$A + E \rightarrow C + F$	k_{4c}	2.4×10^{10}			

A: $[Fe^{III}(bpy)_2(CN)_2]^+$; B: I^-; C: $Fe^{II}(bpy)_2(CN)_2$; D: $I^\bullet$; E: $I_2^{\bullet-}$; F: I_2.

$$\Delta E_{rxn} = E_f(Fe^{III}/Fe^{II}) - E_f(I^{\bullet}/I^-) \quad (3\text{-}18)$$

Where K_1, equilibrium constant for reaction 3-6, equals to k_1/k_{-1}; T: the temperature of reaction; R: gas law constant, 8.314 m^2 kg s^{-2} K^{-1} mol^{-1}; n, number of electron transfer in reaction 3-6; F, Faraday constant, 96,485 C/mol. The half-wave potential of $I^{\bullet}/I^-$ is obtained, with 0.597 ± 0.002 V vs $[Fe(Cp)_2]^{+/0}$. Then the reverse rate constants (k_{-1}) for the oxidation of I^- by the other three Fe(III) complexes were calculated using the standard potential of $I^{\bullet}/I^-$ (0.597 ± 0.002 V vs $[Fe(Cp)_2]^{+/0}$), of $Fe^{III/II}$, and the experimental forward rate constants k_1. All of the calculated reverse rate constants (k_{-1}) shown in Table 3-14 are close to diffusion-control, which further supports that the validity of our derivation of the half-wave potential of $I^{\bullet}/I^-$.

The half-wave potential of $I^{\bullet}/I^-$ was also estimated by using thermodynamic cycle. Non-close values were obtained with the employment of different assumptions. Firstly, it is assumed that iodine radical has the same free transfer energy from water to acetonitrile as Xe, the half-wave potential of $I^{\bullet}/I^-$ was obtained, with $E_{1/2}$ = (0.54 ± 0.04) V vs $([Fe(Cp)_2]^{+/0}$; secondly, suppose that iodine radical has the same free transfer energy from gas phase to acetonitrile as Xe, $E_{1/2}$ was obtained, with a value of (0.61± 0.04) V vs $([Fe(Cp)_2]^{+/0}$. The detail calculation was described in Appendix B. Actually, the calculated half-wave potential of $I^{\bullet}/I^-$ from the second assumption is more close to that obtained from our experimental results. It implies that Xe is a better model for iodine radical in acetonitrile than in water.

Table 3-14. The calculated rate constants (k_{-1}) for the oxidation of I^- by Fe(III) complexes in acetonitrile.[a]

Oxidants	$E_{1/2}$, mV [b]	k_1, M^{-1} s^{-1}	K_1 [c]	$k_{-1} \times 10^{-10}$, [c] M^{-1} s^{-1}
$[Fe(CH_3Cp)_2]^+$	-108 ± 2	0.05 ± 0.01	1.2×10^{-12}	4.2 ± 0.8
$[Fe(dmbpy)_2(CN)_2]^+$	- 36 ± 2	0.65 ± 0.05	2.0×10^{-11}	3.3 ± 0.3
$[Fe(bpy)_2(CN)_2]^+$	+ 70 ± 2	29.2 ± 0.82	1.2×10^{-9}	2.4 ± 0.1
$[Fe(5\text{-Cl-phen})_2(CN)_2]^+$	168 ± 2	1454 ± 30	5.6×10^{-8}	2.6 ± 0.1

[a] [bpy] = 5.0 mM, μ = 0.10 M (Et_4NBF_4), T = 25.0 °C; [b] $E_{1/2}$ vs $[Fe(Cp)_2]^{+/0}$, [c] Calculated with $E_{1/2}(I^\bullet/I^-) = 0.597$ V

For a typical outer-sphere reaction, it is generally believed that the oxidative and reducing reagents combine to form ion pair (precursor); then electron transfer occurs within the ion pairs to form successor; finally, the successor dissociates to obtain the products, as shown in Scheme 3-2.[85,176] The theoretical rate constant, k_1, can be represented by:[85]

$$k_1 = K_{1ip}k_{1et}k_{1d}/(k_{-1et} + k_{1d}) \quad (3\text{-}19)$$

If the rate-limiting step is diffusion-control, not electron transfer, Equation 3-19 can be simplified into such form:

$$k_1 = K_{1ip}k_{1et}k_{1d}/k_{-1et} = K_{1eq}k_{-1d} \quad (3\text{-}20)$$

Then the theoretical slope for a plot of logk_1 versus E_f, where k_{-1} is diffusion-control, was obtained from Equation 3-20, with the value of 16.9, close to the experimental data (with slope of 16.1 in Figure 3-29). Therefore, Marcus theory is not applicable to calculate the exchange rate constant of $I^{\bullet}/I^-$.

Scheme 3-2

$$Ox + X^- \rightleftharpoons Ox,X^- \qquad K_{1ip}$$

$$Ox,X^- \rightleftharpoons Red, X^{\bullet} \qquad k_{1et}, k_{-1et}$$

$$Red, X^{\bullet} \rightleftharpoons Red + X^{\bullet} \qquad k_{1d}, k_{-1d}$$

The exchange rate constant of $I_2^{\bullet-}/I^-$ could be estimated if the reverse reaction of 3-7 is not diffusion-control and the half-wave potential of $I_2^{\bullet-}/I^-$ is known. The equilibrium constant, K_{rad}, for Equation 3-8 is reported with a value higher than 10^5 M^{-1}.[173] Combining the equilibrium constant ($K_{rad} \geq 10^5$ M^{-1}) with the half-wave potential of $I^{\bullet}/I^-$ (0.597 V vs $[Fe(Cp)_2]^{+/0}$), the half-wave potential of $I_2^{\bullet-}/I^-$ was calculated, with upper limit of 0.301 V (E_f, $I_2^{\bullet-}/I^-$) vs $[Fe(Cp)_2]^{+/0}$. Then the rate constant, k_{-2}, was obtained with upper limit of 2.2×10^8 M^{-1} s^{-1}, much smaller than the diffusion control rate constant in acetonitrile.[174,175] Furthermore, the non-diffusion-control of k_{-2} is further confirmed from the smaller slope value of log k_2 in Figure 3-29. Unfortunately, the unavailability of standard potential of $I_2^{\bullet-}/I^-$ impedes us to obtain its exchange rate constants.

Conclusion

Trace copper-ion catalysis appears to be a general phenomenon in the oxidation of iodide by substitution-inert transition metal complex in acetonitrile. The direct oxidation of iodide has the same stoichiometry and two-term rate law as in aqueous solution. Analysis of the slopes in LFERs implies that the reverse rate constants for the two paths are diffusion-controlled and activation controlled, respectively. The intermediate state of $I^{\bullet}$ and $I_2^{\bullet-}$ is inferred, and the standard potential of $I^{\bullet}/I^{-}$ is derived from the kinetic inhibition by $Fe^{II}(bpy)_2(CN)_2$.

REFERENCES

(1) Moriarty-Craige, S. E.; Jones, D. P. *Annu. Rev. Nutr.* **2004**, *24*, 481-509.

(2) Jacob, C.; Giles, G. I.; Giles, N. M.; Sies, H. *Angew. Chem. Int. Ed.* **2003**, *42*, 4742-4758.

(3) Hand, C. E.; Honek, J. F. *J. Nat. Prod.* **2005**, *68*, 293-308.

(4) Tsuchiya, K.; Kirima, K.; Yoshizumi, M.; Houchi, H.; Tamaki, T.; Mason, R. P. *Biochem. J.* **2002**, *367*, 771-779.

(5) Jacob, C.; Knight, I.; Winyard, P. G. *Biol. Chem.* **2006**, *387*, 1385-1397.

(6) Jocelyn, P. C. *Biochemistry of the SH group*; Academic Press: London, **1972**, pp 190-226.

(7) Jocelyn, P. C. *Biochemistry of the SH group*; Academic Press: London, **1972**, pp 94-115.

(8) Darkwa, J.; Olojo, R.; Chikwana, E.; Simoyi, R. H. *J. Phys. Chem. A* **2004**, *108*, 5576-5587.

(9) Giles, N. M.; Giles, G. I.; Jacob, C. *Biochem. Biophys. Res. Commun.* **2003**, *300*, 1-4.

(10) Arrigo, A. P. *Free Radic. Biol. Med.* **1999**, *27*, 936-944.

(11) Schafer, F. Q.; Buettner, G. R. *Free Radic. Biol. Med.* **2001**, *30*, 1191-1212.

(12) Jones, D. P.; Go, Y.; Anderson, C. L.; Ziegler, T. R.; Kinkade, J. M.; Kirlin, W. G. *FASEB J.* **2004**, *18*, 1246-1248.

(13) Meister, A.; Anderson, M. E. *Annu. Rev. Biochem.* **1983**, *52*, 711-760.

(14) Stipanuk, M. H.; Dominy, J. E.; Lee, J. J.; Coloso, R. M. *J. Nutr.* **2006**, *136*, 1652S-1659S.

(15) Pai, E. F.; Schulz, G. E. *J. Biol. Chem.* **1983**, *258*, 1752-1757.

(16) Dai, S.; Schwendtmayer, C.; Schurmann, P.; Ramaswamy, S.; Eklund, H. *Science* **2000**, *287*, 655-658.

(17) Frey, P. A. *Annu. Rev. Biochem.* **2001**, *70*, 121-148.

(18) Wagner, A. F. V.; Frey, M.; Neugebauer, F. A.; Schafer, W.; Knappe, J. *Proc. Natl. Acad. Sci. USA* **1992**, *89*, 996-1000.

(19) Biteau, B.; Labarre, J.; Toledano, M. B. *Nature* **2003**, *425*, 980-984.

(20) van Montfort, R. L. M.; Congreve, M.; Tisi, D.; Carr, R.; Jhoti, H. *Nature* **2003**, *423*, 773-777.

(21) Salmeen, A.; Andersen, J. N.; Myers, M. P.; Meng, T.; Hinks, J. A.; Tonks, N. K.; Barford, D. *Nature* **2003**, *423*, 769-773.

(22) Sono, M.; Roach, M. P.; Coulter, E. D.; Dawson, J. H. *Chem. Rev.* **1996**, *96*, 2841-2887.

(23) Auclair, K.; Moenne-Loccoz, P.; Ortiz de Montellano, P. R. *J. Am. Chem. Soc.* **2001**, *123*, 4877-4885.

(24) Hirota, S.; Azuma, K.; Fukuba, M.; Kuroiwa, S.; Funasaki, N. *Biochemistry* **2005**, *44*, 10322-10327.

(25) Gross, E.; Sevier, C. S.; Vala, A.; Kaiser, C. A.; Fass, D. *Nat. Struct. Biol.* **2002**, *9*, 61-67.

(26) Pecht, I.; Farver, O. *Adv. Chem. Ser.* **1998**, *254*, 65-80.

(27) Farver, O.; Bonander, N.; Skov, L. K.; Pecht, I. *Inorg. Chim. Acta* **1996**, *243*, 127-133.

(28) Pirie, N. W. *Biochem. J.* **1931**, *25*, 1565-1579.

(29) Hanaki, A.; Kamide, H. *Chem. Pharm. Bull.* **1973**, *21*, 1421-1425.

(30) Hill, J. W.; Coy, R. B.; Lewandowski, P. E. *J. Chem. Edu.* **1990**, *67*, 172.

(31) Pirie, N. W. *Biochem. J.* **1933**, *27*, 1181-1188.

(32) Barton, J. P.; Packer, J. E.; Sims, R. J. *J. Chem. Soc., Perkin Trans. 2* **1973**, 1547-1549.

(33) Winterbourn, C. C.; Metodiewa, D. *Free Radic. Biol. Med.* **1999**, *27*, 322-328.

(34) Lynch, E.; Sheerin, A.; Claxson, A. W.; Atherton, M. D.; Rhodes, C. J.; Silwood, C. J.; Naughton, D. P.; Grootveld, M. *Free Radic. Res.* **1997**, *26*, 209-234.

(35) Ison, A.; Odeh, I. N.; Margerum, D. W. *Inorg. Chem.* **2006**, *45*, 8768-8775.

(36) Yassi, A.; Nieboer, E. *Chromium in the natural and human environments*; Wiley and Sons: New York, **1988**; Vol. 20, pp 443-495.

(37) Shi, X.; Sun, X.; Dalal, N. S. *FEBS* **1990**, *271*, 185-188.

(38) McCann, J. P.; McAuley, A. *J. Chem. Soc., Dalton Trans.* **1975**, 783-790.

(39) Kwong, D. W. J.; Pennington, D. E. *Inorg. Chem.* **1984**, *23*, 2528-2532.

(40) Payasi, A. P.; Sharma, K.; Sharma, V. K. *J. Indian Chem. Soc.* **1987**, *64*, 186-187.

(41) Grases, F.; Palou, J.; Amat, E. *Transition Met. Chem.* **1986**, *11*, 253-255.

(42) Jameson, R. F.; Linert, W.; Tschinkowitz, A.; Gutmann, V. *J. Chem. Soc., Dalton Trans.* **1988**, 943-946.

(43) Jameson, R. F.; Linert, W.; Tschinkowitz, A. *J. Chem. Soc., Dalton Trans.* **1988**, *2109-2112*.

(44) Sisley, M. J.; Jordan, R. B. *Inorg. Chem.* **1995**, *34*, 6015-6023.

(45) Salamon, C. W.; Jameson, R. F.; Linert, W. *Inorg. Chim. Acta* **2004**, *357*, 41-50.

(46) Wolf, W.; Kertesz, J. C.; Landgraf, W. C. *J. Magn. Reson.* **1969**, *1*, 618-632.

(47) Lawal, H. M.; Iyun, J. F. *Indian J. Chem.* **1998**, *37 A*, 155-157.

(48) Kottapalli, K. K.; Adari, K. K.; Vani, P.; Govindan, S. K. *Transition Met. Chem.* **2005**, *30*, 773-777.

(49) Ayoko, G. A.; Olatunji, M. A. *Polyhedron* **1983**, *2*, 577-582.

(50) Bridgart, G. J.; Fuller, M. W.; Wilson, I. R. *J. Chem. Soc., Dalton Trans.* **1973**, 1274-1280.

(51) Bridgart, G. J.; Wilson, I. R. *J. Chem. Soc., Dalton Trans.* **1973**, 1281-1284.

(52) Hung, M.; Stanbury, D. M. *Inorg. Chem.* **2005**, *44*, 3541-3550.

(53) Ghosh, S. K.; Saha, S. K.; Ghosh, M. C.; Bose, R. N.; Reed, J. W.; Gould, E. S. *Inorg. Chem.* **1992**, *31*, 3358-3362.

(54) Iyun, J. F.; Musa, K. Y.; Ayoko, G. A. *Indian J. Chem.* **1996**, *35 A*, 210-213.

(55) Lewis, N. S. *Energy and Transportation*; The National Academies Press: Washington, DC, **2003**, pp 33-39.

(56) Nault, R. M. "Basic Research Needs for solar Energy Utilization," Argonne National Laboratory, 2005.

(57) O'Regan, B.; Gratzel, M. *Nature* **1991**, *353*, 737-740.

(58) Gratzel, M. *Inorg. Chem.* **2005**, *44*, 6841-6851.

(59) Gratzel, M. *J. Photochem. Photobiol., A: Chem.* **2004**, *164*, 3-14.

(60) Nasr, C.; Hotchandani, S.; Kamat, P. V. *J. Phys. Chem. B* **1998**, *102*, 4944-4951.

(61) Durrant, J. R.; Haque, S. A.; Palomares, E. *Chem. Commun.* **2006**, 3279-3289.

(62) Robertson, N. *Angew. Chem. Int. Ed.* **2006**, *45*, 2338-2345.

(63) Meyer, G. J. *Inorg. Chem.* **2005**, *44*, 6852-6864.

(64) Nazeeruddin, M. K.; Kay, A.; Rodicio, I.; Humphry-Baker, R.; Mueller, E.; Liska, P.; Vlachopoulos, N.; Gratzel, M. *J. Am. Chem. Soc.* **1993**, *115*, 6382-6390.

(65) Hattori, S.; Wada, Y.; Yanagida, S.; Fukuzumi, S. *J. Am. Chem. Soc.* **2005**, *127*, 9648-9654.

(66) Kang, M.; Kim, Y. J.; Won, J.; Kang, Y. S. *Chem. Commun.* **2005**, 2686-2688.

(67) Wang, P.; Zakeeruddin, S. M.; Moser, J. E.; Nazeeruddin, M. K.; Sekiguchi, T.; Gratzel, M. *Nat. Mater.* **2003**, *2*, 402-407.

(68) Wang, P.; Dai, Q.; Zakeeruddin, S. M.; Forsyth, M.; Macfarlane, D. R.; Gratzel, M. *J. Am. Chem. Soc.* **2004**, *126*, 13590-13591.

(69) Wang, P.; Zakeeruddin, S. M.; Moser, J.-E.; Humphry-Baker, R.; Gratzel, M. *J. Am. Chem. Soc.* **2004**, *126*, 7164-7165.

(70) Meng, Q.; Takahashi, K.; Zhang, X.; Sutanto, I.; Rao, T. N.; Sato, O.; Fujishima, A.; Watanabe, H.; Nakamori, T.; Uragami, M. *langmuir* **2003**, *19*, 3572-3574.

(71) Wang, Z.; Sayama, K.; Sugihara, H. *J. Phys. Chem. B* **2005**, *109*, 22449-22455.

(72) Kuciauskas, D.; Freund, M. S.; Gray, H. B.; Winkler, J. R.; Lewis, N. S. *J. Phys. Chem. B* **2001**, *105*, 392-403.

(73) Geary, E. A. M.; Yellowlees, L. J.; Jack, L. A.; Oswald, I. D. H.; Parsons, S.; Hirata, N.; Durrant, J. R.; Robertson, N. *Inorg. Chem.* **2005**, *44*, 242-250.

(74) Hasselmann, G. M.; Meyer, G. J. *Z. Phys. Chem.* **1999**, *212*, 39-44.

(75) Alonso-Vante, N.; Nierengarten, J.-F.; Sauvage, J.-P. *J. Chem. Soc. Dalton Trans.* **1994**, 1649-1654.

(76) Jayaweera, P. M.; Palayangoda, S. S.; Tennakone, K. *J. Photochem. Photobiol., A: Chem.* **2001**, *140*, 173-177.

(77) Tachibana, Y.; Haque, S. A.; Mercer, I. P.; Durrant, J. R.; Klug, D. R. *J. Phys. Chem. B* **2000**, *104*, 1198-1205.

(78) Ellingson, R. J.; Asbury, J. B.; Ferrere, S.; Ghosh, H. N.; Sprague, J. R.; Lian, T.; Nozik, A. J. *J. Phys. Chem. B* **1998**, *102*, 6455-6458.

(79) Hannappel, T.; Burfeindt, B.; Storck, W.; Willig, F. *J. Phys. Chem. B* **1997**, *101*, 6799-6802.

(80) Haque, S. A.; Tachibana, Y.; Willis, R. L.; Moser, J. E.; Gratzel, M.; Klug, D. R.; Durrant, J. R. *J. Phys. Chem. B* **2000**, *104*, 538-547.

(81) Alebbi, M.; Bignozzi, C. A.; Heimer, T. A.; Hasselmann, G. M.; Meyer, G. J. *J. Phys. Chem. B* **1998**, *102*, 7577-7581.

(82) Nord, G.; Pedersen, B.; Farver, O. *Inorg. Chem.* **1978**, *17*, 2233-2238.

(83) Nord, G. *Comments Inorg. Chem.* **1992**, *13*, 221-239.

(84) Adedinsewo, C. O.; Adegite, A. *Inorg. Chem.* **1979**, *18*, 3597-3601.

(85) Stanbury, D. M.; Wilmarth, W. K.; Khalaf, S.; Po, H. N.; Byrd, J. E. *Inorg. Chem.* **1980**, *19*, 2715-2722.

(86) Stanbury, D. M. *Adv. Inorg. Chem.* **1989**, *33*, 69-138.

(87) Kimura, M.; Shiota, Y.; Kishi, S.; Tsukahara, K. *Bull. Chem. Soc. JPN.* **1999**, *72*, 1293-1299.

(88) Espenson, J. H. *Chemical Kinectic and Reaction Mechanism*; 1st ed.; McGraw-Hill, Inc., **1981**, pp 12-41.

(89) Taube, H.; Myers, H.; Rich, R. L. *J. Am. Chem. Soc.* **1953**, *75*, 4118-4119.

(90) Taube, H.; Myers, H. *J. Am. Chem. Soc.* **1954**, *76*, 2103-2111.

(91) Jordan, R. B. *Reaction Mechanisms of Inorganic and Organometallic Systems*; 2nd ed.; Oxford University: New York, Oxford, **1998**, pp 188-220.

(92) Zuckerman, J. J. *Inorganic Reactions and Methods*; VCH: Deerfield Beach, FL, **1986**, pp 16-49.

(93) Jordan, R. B. *Reaction Mechanisms of Inorganic and Organometallic Systems*; 2nd ed.; Oxford University: New York, Oxford, **1998**, pp 291-326

(94) Sun, J. In *Chemistry and Biochemistry*; Auburn Unversity: Auburn, 2000, pp 1-26.

(95) Halliwell, B.; Gutteridge, J. M. *Lancet* **1984**, *323*, 1396-1397.

(96) Munday, R.; Munday, C. M.; Winterbourn, C. C. *Free Radic. Biol. Med.* **2004**, *36*, 757-764.

(97) Nekrassova, O.; Kershaw, J.; Wadhawan, J. D.; Lawrence, N. S.; Compton, R. G. *Phys. Chem. Chem. Phys.* **2004**, *6*, 1316-1320.

(98) White, P. C.; Lawrence, N. S.; Davis, J.; Compton, R. G. *Electroanalysis* **2002**, *14*, 89-98.

(99) Shi, T.; Berglund, J.; Elding, L. I. *Inorg. Chem.* **1996**, *35*, 3498-3503.

(100) Stevens, G. D.; Holwerda, R. A. *Inorg. Chem.* **1984**, *23*, 2777-2780.

(101) Olatunji, M. A.; Okechukwu, R. C. *Inorg. Chim. Acta* **1987**, *131*, 89-94.

(102) Sun, J.; Stanbury, D. M. *J. Chem. Soc., Dalton Trans.* **2002**, 785-791.

(103) Saha, B.; Hung, M.; Stanbury, D. M. *Inorg. Chem.* **2002**, *41*, 5538-5543.

(104) Hung, M.; Stanbury, D. M. *Inorg. Chem.* **2005**, *44*, 9952-9960.

(105) Garman, A. J. *Non-radioactive labeling: A Practical Introduction*; Academic Press: London, **1997**, p 119.

(106) Riddles, P. W.; Blakeley, R. L.; Zerner, B. *Anal. Biochem.* **1979**, *94*, 75-81.

(107) Schilt, A. A. *J. Am. Chem. Soc.* **1960**, *82*, 3000-3005.

(108) Lescouezec, R.; Lloret, F.; Julve, M.; Vaissermann, J.; Verdaguer, M. *Inorg. Chem.* **2002**, *41*, 818-826.

(109) Papula, L.; Horvath, O.; Papp, S. *J. Photochem. Photobiol., A: Chem.* **1990**, *54*, 205-212.

(110) Sawyer, D. T.; Sobkowiak, A.; Roberts, J. L. *Electrochemistry for Chemists*; 2nd ed.; John Wiley & Sons: New York, **1995**, p 192.

(111) Terrettaz, S.; Becka, A. M.; Traub, M. J.; Fettinger, J. C.; Miller, C. J. *J. Phys. Chem.* **1995**, *99*, 11216-11224.

(112) George, P.; Hanania, G. I. H.; Irvine, D. H. *J. Chem. Soc.* **1959**, 2548-2554.

(113) Agarwala, B. V.; Ramanathan, K. V.; Khetrapal, C. L. *J. Coord. Chem.* **1985**, *14*, 133-137.

(114) Mandal, S.; Bose, R. N.; Reed, J. W.; Gould, E. S. *Inorg. Chem.* **1996**, *35*, 3159-3162.

(115) Bridgart, G. J.; Waters, W. A.; Wilson, I. R. *J. Chem. Soc., Dalton Trans.* **1973**, 1582-1584.

(116) Kodama, M.; Kimura, E. *J. Chem. Soc., Dalton Trans.* **1977**, 1473-1478.

(117) Martell, A. E.; Smith, R. M.; Motekaitis, R. J. *NIST Critically Selected Stability Constants of Metal Complexes Database*; 7.0 ed. Gaithersburg, **2003**.

(118) Kodama, M.; Kimura, E. *J. Chem. Soc., Dalton Trans.* **1977**, 2269-2276.

(119) Josceanu, A. M.; Moore, P.; Rawle, S. C.; Sheldon, P.; Smith, S. M. *Inorg. Chim. Acta* **1995**, *240*, 159-168.

(120) Sano, K. *Biochem. Z.* **1926**, *168*, 14-33.

(121) Graceffa, P. *Biochim. Biophys. Acta* **1988**, *954*, 227-230.

(122) Potapenko, D. I.; Bagryanskaya, E. G.; Tsentalovich, Y. P.; Reznikov, V. A.; Clanton, T. L.; Khramtsov, V. V. *J. Phys. Chem. B* **2004**, *108*, 9315-9324.

(123) Cavallini, D.; Marco, C. D.; Dupre, S.; Rotilio, G. *Arch. Biochem. Biophys.* **1969**, *130*, 354-361.

(124) Pecci, L.; Montefoschi, G.; Musci, G.; Cavallini, D. *Amino Acids* **1997**, *13*, 355-367.

(125) Vortisch, V.; Kroneck, P.; Hemmerich, P. *J. Am. Chem. Soc.* **1976**, *98*, 2821-2826.

(126) Stricks, W.; Kolthoff, I. M. *J. Am. Chem. Soc.* **1951**, *73*, 1723-1727.

(127) Knoblock, E. C.; Purdy, W. C. *J. Electroanal. Chem.* **1961**, *2*, 493-496.

(128) Mezyk, S. P. *Chem. Phys. Lett.* **1995**, *235*, 89-93.

(129) Davies, M. J.; Forni, L. G.; Shuter, S. L. *Chem. Biol. Interactions* **1987**, *61*, 177-188.

(130) Makarycheva-Mikhailova, A. V.; Stanbury, D. M.; McKee, M. L. *J. Phys. Chem. B* **2007**, In press.

(131) Mezyk, S. P. *Radiat. Res.* **1996**, *145*, 102-106.

(132) Binstead, R. A.; Jung, B.; Zuberbuhler, A. D. *Specfit/32 Global Analysis System*; 3.0 ed.; Spectrum Software Associate: Marlborough, **2000**.

(133) Zhao, R.; Lind, J.; Merenyi, G.; Eriksen, T. E. *J. Am. Chem. Soc.* **1994**, *116*, 12010-12015.

(134) Mezyk, S. P.; Armstrong, D. A. *J. Chem. Soc., Perkin Trans. 2* **1999**, 1411-1419.

(135) Friedman, M. *The Chemistry and Biochemistry of the Sulfhydryl Group in Amino Acids, Peptides and Proteins*; Pergamon Press: New York, **1973**, p 4.

(136) Kallen, R. G. *J. Am. Chem. Soc.* **1971**, *93*, 6227-6235.

(137) Prutz, W. A.; Butler, J.; Land, E. J.; Swallow, A. J. *Free Rad. Res. Comms.* **1986**, *2*, 69-75.

(138) Stasiw, R.; Wilkins, R. G. *Inorg. Chem.* **1969**, *8*, 156-157.

(139) Macartney, D. H. *Inorg. Chem.* **1991**, *30*, 3337-3342.

(140) Zahl, A.; van Eldik, R.; Swaddle, T. W. *Inorg. Chem.* **2002**, *41*, 757-764.

(141) Pelizzetti, E.; Mentasti, E.; Pramauro, E. *Inorg. Chem.* **1978**, *17*, 1181-1186.

(142) Macartney, D. H.; Sutin, N. *Inorg. Chim. Acta* **1983**, *74*, 221-228.

(143) van Gastel, M.; Lubitz, W.; Lassmann, G.; Neese, F. *J. Am. Chem. Soc.* **2004**, *126*, 2237-2246.

(144) Kimura, M.; Wada, G. *Inorg. Chem.* **1978**, *17*, 2239-2242.

(145) Blandamer, M. J.; Burgess, J.; Duce, P. P.; Haines, R. I.; McAuley, A. *Transition Met. Chem.* **1982**, *7*, 10-13.

(146) Blandamer, M. J.; Burgess, J.; Hamshere, S. J.; White, A.; Haines, R. I.; McAuley, A. *Can. J. Chem.* **1983**, *61*, 1361-1370.

(147) Baucke, F. G. K.; Betram, R.; Cruse, K. *J. Electroanal. Chem.* **1971**, *32*, 247-256.

(148) Hagfeldt, A.; Gratzel, M. *Acc. Chem. Res.* **2000**, *33*, 269-277.

(149) Tachibana, Y.; Moser, J. E.; Gratzel, M.; Klug, D. R.; Durrant, J. R. *J. Phys. Chem.* **1996**, *100*, 20056-20062.

(150) Ferrere, S. *Chem. Mater.* **2000**, *12*, 1083-1089.

(151) Ferrere, S.; Gregg, B. A. *J. Am. Chem. Soc.* **1998**, *120*, 843-844.

(152) Kolthoff, I. M.; Sandell, E. B.; Meehan, E. J.; Bruckenstein, S. *Quantitative Chemical Analysis*; 4th ed.; Macmillan: New York, **1969**, pp 849-852

(153) Ferrere, S. *Inorg. Chim. Acta* **2002**, *329*, 79-92.

(154) Carney, M. J.; Lesniak, J. S.; Likar, M. D.; Pladziewicz, J. R. *J. Am. Chem. Soc.* **1984**, *106*, 2565-2569.

(155) Schilt, A. A.; Leman, T. W. *J. Am. Chem. Soc.* **1967**, *89*, 2012-2014.

(156) Noviandri, I.; Brown, K. N.; Fleming, D. S.; Gulyas, P. T.; Lay, P. A.; Masters, A. F.; Phillips, L. *J. Phys. Chem. B* **1999**, *103*, 6713-6722.

(157) Nelsen, S. F.; Wang, Y.; Ramm, M. T.; Accola, M. A.; Pladziewicz, J. R. *J. Phys. Chem.* **1992**, *96*, 10654-10658.

(158) Pladziewicz, J. R.; Brenner, M. S.; Rodeberg, D. A.; Likar, M. A. *Inorg. Chem.* **1985**, *24*, 1450-1453.

(159) Burgess, J. *Spectrochim. Acta* **1970**, *26A*, 1369-1374.

(160) Barr, T. H.; Watts, W. E. *J. Organomet. Chem.* **1968**, *15*, 177-185.

(161) Sawyer, D. T.; Sobkowiak, A.; Roberts, J. L. *Electrochemistry for Chemists*; 2nd ed.; John Wiley & Sons, INC: New York, **1995**, pp 190-194

(162) Gritzner, G. *Pure & Appl. Chem.* **1990**, *62*, 1839-1858.

(163) Popov, A. I.; Geske, D. H. *J. Am. Chem. Soc.* **1958**, *80*, 1340-1352.

(164) Wang, X.; Stanbury, D. M. *J. Phys. Chem. A* **2004**, *108*, 7637-7638.

(165) Isci, H.; Mason, W. R. *Inorg. Chem.* **1985**, *24*, 271-274.

(166) Kamezawa, N. *J. Magn. Reson.* **1973**, *11*, 88-99.

(167) Materikova, R. B.; Babin, V. N.; Lyatifov, I. R.; Kurbanov, T. K.; Fedin, E. I.; Petrovskii, P. V.; Lutsenko, A. I. *J. Organomet. Chem.* **1977**, *142*, 81-87.

(168) Kebede, Z.; Lindquist, S. E. *Sol. Energy Mater. Sol. Cells* **1999**, *57*, 259-275.

(169) Rao, N. S.; Rao, G. B.; Ziessow, D. *Spectrochim. Acta* **1990**, *46A*, 1107-1124.

(170) Desbarres, J. *Bull. Soc. Chim. France* **1961**, 502-506.

(171) Benoit, R. L. *Inorg. Nucl. Chem. Lett.* **1968**, *4*, 723-729.

(172) Nelson, I. V.; Iwamoto, R. T. *J. Electroanal. Chem.* **1964**, *7*, 218-222.

(173) Treinin, A.; Hayon, E. *Int. J. Radiat. Phys. Chem.* **1975**, *7*, 387-393.

(174) Won, T. J.; Espenson, J. H. *Organometallics* **1995**, *14*, 4275-4280.

(175) Flors, C.; Nonell, S. *J. Photochem. Photobiol. A: Chem.* **2004**, *163*, 9-12.

(176) Lappin, A. G. *Redox Mechanisms in Inorganic Chemistry*; Ellis Horwood: Chichester, **1994**, pp 75-76.

(177) Izutsu, K. *Electrochemistry in nonaqueous solutions*; Wiley-vch, **2002**, p 172.

(178) Larson, R. C.; Iwamoto, R. T.; Adams, R. N. *Anal. Chim. Acta* **1961**, *25*, 371-374.

(179) Datta, J.; Bhattacharya, A.; Kundu, K. K. *Bull. Chem. Soc. JPN.* **1988**, *61*, 1735-1742.

(180) Bahnemann, D.; Asmus, K. D.; Willson, R. L. *J. Chem. Soc. Perkin Trans. 2* **1983**, 1669-1673.

(181) Lingane, J. J.; Larson, W. D. *J. Am. Chem. Soc.* **1936**, *58*, 2647-2648.

(182) Marcus, Y. *Pure & Appl. Chem.* **1983**, *55*, 977-1021.

(183) Bruckel, F.; Kim, J. I. *Zeitschrift Physikalische Chemie Neue Folge, Bd,* **1981**, *126*, 133-150.

(184) Clever, L. H. *Solubility Data Series*; Pergamaon Press: Oxford, **1979**; Vol. 2, pp 134-145.

(185) Wagman, D. D.; Evans, W. H.; Parker, V. B.; Schumm, R. H.; Halow, I.; Bailey, S. M.; Churney, K. L.; Nuttall, R. L. *J. Phys. Chem. Ref. Data* **1982**, *11 (Suppl. 2)*.

(186) Endo, A.; Kajitani, M.; Mukaida, M.; Shimizu, K.; Sato, G. P. *Inorg. Chim. Acta* **1988**, *150*, 25-34.

(187) Baird, I. R.; Rettig, S. J.; James, B. R.; Skov, K. A. *Can. J. Chem.* **1999**, *77*, 1821-1833.

(188) Yang, E. S.; Chan, M.; Wahl, A. C. *J. Phys. Chem.* **1975**, *79*, 2049-2052.

(189) Cox, B. G.; Jedral, W.; Palou, J. *J. Chem. Soc. Dalton Trans.* **1988**, 733-740.

(190) Ahrland, S.; Nilsson, K.; Tagesson, B. *Acta Chem. Scand. A* **1983**, *A37*, 193-201.

(191) Wang, X.; Stanbury, D. M. *Inorg. Chem.* **2006**, *45*, 3415-3423.

(192) Kubas, G. J. *Inorg. Synth.* **1990**, *28*, 68-70.

(193) Kauffman, G. B.; Teter, L. A. *Inorg. Synth.* **1963**, *7*, 9-12.

(194) Doine, H.; Yano, Y.; Swaddle, T. W. *Inorg. Chem.* **1989**, *28*, 2319-2322.

(195) Xie, B.; Wilson, L. J.; Stanbury, D. M. *Inorg. Chem.* **2001**, *40*, 3606-3614.

(196) Ahrland, S. *Pure & Appl. Chem.* **1990**, *62*, 2077-2082.

APPENDIX A

CALCULATION OF THE EQUILIBIUM CONSTANTS FOR THE OXIDATION OF I^- BY $[Fe^{III}(bpy)_2(CN)_2]^+$ IN ACETONITRILE

$$2\ Fe(III) + 3\ I^- \rightleftharpoons 2\ Fe(II) + I_3^- \qquad K_{eq1} \qquad (A\text{-}1)$$

$$2\ Fe(III) + 2\ I^- \rightleftharpoons 2\ Fe(II) + I_2 \qquad K_{eq2} \qquad (A\text{-}2)$$

$$I^- + I_2 \rightleftharpoons I_3^- \qquad pK_0 \qquad (A\text{-}3)$$

$E_{1/2}$, $[Fe^{III}(bpy)_2(CN)_2]^{+/0}$ = 0.072 V vs $[Fe(Cp)_2]^{+/0}$

1. $E_{1/2}$, I_2/I_3^- = 0.39 V[163] vs $Ag/AgNO_3$ (0.01M, AN)

$E_{1/2}$, I_3^-/I^- = -0.27 V[163] vs $Ag/AgNO_3$ (0.01M, AN)

$E_{1/2}$, $[(Fe(Cp)_2]^{+/0}$ = 0.089 V[177] vs $Ag/AgNO_3$ (0.01M)

Thus, $E_{1/2}$, I_2/I_3^- = 0.30 V vs $[Fe(Cp)_2]^{+/0}$, $E_{1/2}$, I_3^-/I^- = -0.36 V vs $[Fe(Cp)_2]^{+/0}$

$E_{1/2}$, I_2/I^- = -0.14 V vs $[Fe(Cp)_2]^{+/0}$

For reaction (A-1),

$\ln K_{eq1} = (nF\Delta E_{rxn})/(RT) = 2 \times 96485 \times (0.072-(-0.36))/(8.314 \times 298) = 33.65$

$K_{eq1} = 4.1 \times 10^{14}\ M^{-2}$

For reaction (A-2),

$\ln K_{eq2} = (nF\Delta E_{rxn})/(RT) = 2 \times 96485 \times (0.072-(-0.14)/(8.314 \times 298) = 16.51$

$K_{eq2} = 1.5 \times 10^{7}\ M^{-1}$

(A-1) - (A-2):

$I^- + I_2 \rightleftharpoons I_3^-$ (A-3)

$K_0 = K_{eq1}/K_{eq2} = 4.1 \times 10^{14}\ M^{-2}/1.5 \times 10^7\ M^{-1} = 2.73 \times 10^7\ M^{-1}$

$pK_0 = -7.44$

2. $E_{1/2}$, I_2/I_3^- = 0.396 V[170] vs $Ag/AgNO_3$ (AN), $E_{1/2}$, I_3^-/I^- = -0.248 V[170] vs $Ag/AgNO_3$ (AN)

$E_{1/2}$, $[Fe(Cp)_2]^{+/0}$ = 0.089 V[177] vs $Ag/AgNO_3$ (AN)

Thus, $E_{1/2}$, I_2/I_3^- = 0.309 V vs $[Fe(Cp)_2]^{+/0}$, $E_{1/2}$, I_3^-/I^- = -0.337 V $[Fe(Cp)_2]^{+/0}$

$E_{1/2}$, I_2/I^- = -0.122 V vs $[Fe(Cp)_2]^{+/0}$

For reaction (A-1),

$\ln K_{eq1} = (nF\Delta E_{rxn})/(RT) = 2 \times 96485 \times (0.072-(-0.337))/(8.314 \times 298) = 31.85$

$K_{eq1} = 6.84 \times 10^{13}\ M^{-2}$

For reaction (A-2),

$\ln K_{eq2} = (nF\Delta E_{rxn})/(RT) = 2 \times 96485 \times (0.072-(-0.122))/(8.314 \times 298) = 15.11$

$K_{eq2} = 3.6 \times 10^6\ M^{-1}$

(A-1) - (A-2):

$I^- + I_2 \rightleftharpoons I_3^-$ (A-3)

$K_0 = K_{eq1}/K_{eq2} = 6.84 \times 10^{13}\ M^{-2}/3.6 \times 10^6\ M^{-1} = 1.9 \times 10^7\ M^{-1}$

$pK_0 = -7.27$

3 $E_{1/2}$, I_2/I_3^- = 0.65 V[172] vs S.C.E, $E_{1/2}$, I_3^-/I^- = 0.06 V[172,178] vs S.C.E

$E_{1/2}$, $Ag/AgNO_3$ (AN) = 0.30 V[163] vs S.C.E (aq)

$E_{1/2}$, $[Fe(Cp)_2]^{+/0}$ = 0.089 V[177] vs $Ag/AgNO_3$ (AN)

Thus, $E_{1/2}$, I_2/I_3^- = 0.261 V vs $[Fe(Cp)_2]^{+/0}$, $E_{1/2}$, I_3^-/I^- = -0.329 V vs $[Fe(Cp)_2]^{+/0}$

$E_{1/2}$, I_2/I^- = -0.132 V vs $[Fe(Cp)_2]^{+/0}$

For reaction (A-1),

$\ln K_{eq1} = (nF\Delta E_{rxn})/(RT) = 2 \times 96485 \times (0.072-(-0.329))/(8.314 \times 298) = 31.23$

$K_{eq1} = 3.7 \times 10^{13}\ M^{-2}$

For reaction (A-2),

$\ln K_{eq2} = (nF\Delta E_{rxn})/(RT) = 2 \times 96485 \times (0.072-(-0.132))/(8.314 \times 298) = 15.9$

$K_{eq2} = 8.0 \times 10^{6}\ M^{-1}$

(A-1) - (A-2):

$I^- + I_2 \rightleftharpoons I_3^-$ (A-3)

$K_0 = K_{eq1}/K_{eq2} = 3.7 \times 10^{13}\ M^{-2}/8.0 \times 10^{6}\ M^{-1} = 4.6 \times 10^{6}\ M^{-1}$

$pK_0 = -6.66$

4. $E_{1/2}$, I_2/I_3^- = 0.33 V[171] vs $[Fe(Cp)_2]^{+/0}$, $E_{1/2}$, I_3^-/I^- = -0.315 V[171] vs $[Fe(Cp)_2]^{+/0}$

$\therefore E_{1/2}$, I_2/I^- = -0.10 V vs $[Fe(Cp)_2]^{+/0}$

For reaction (A-1),

$\ln K_{eq1} = (nF\Delta E_{rxn})/(RT) = 2 \times 96485 \times (0.072-(-0.315))/(8.314 \times 298) = 30.14$

$K_{eq1} = 1.2 \times 10^{13}\ M^{-2}$

For reaction (A-2),

$\ln K_{eq2} = (nF\Delta E_{rxn})/(RT) = 2 \times 96485 \times (0.072-(-0.10))/(8.314 \times 298) = 13.4$

$K_{eq2} = 6.6 \times 10^{5}\ M^{-1}$

(A-1) - (A-2):

$I^- + I_2 \rightleftharpoons I_3^-$ (A-3)

$K_0 = K_{eq1}/K_{eq2} = 1.2 \times 10^{13}\ M^{-2}/6.6\times 10^5\ M^{-1} = 1.8 \times 10^7\ M^{-1}$

$pK_0 = -7.26$

5. $E_{1/2}$, I_2/I_3^- = 0.617 V[179] vs S.C.E, $E_{1/2}$, I_3^-/I^- = 0.017 V[179] vs S.C.E

$E_{1/2}$, $Ag/AgNO_3$ (AN) = 0.30 V[163] vs S.C.E (aq)

$E_{1/2}$, $[Fe(Cp)_2]^{+/0}$ = 0.089 V[177] vs $Ag/AgNO_3$ (AN)

Thus, $E_{1/2}$, I_2/I_3^- = 0.228 V vs $[Fe(Cp)_2]^{+/0}$, $E_{1/2}$, I_3^-/I^- = -0.372 V vs $[Fe(Cp)_2]^{+/0}$

$E_{1/2}$, I_2/I^- = -0.172 V vs $[Fe(Cp)_2]^{+/0}$

For reaction (A-1),

$\ln K_{eq1} = (nF\Delta E_{rxn})/(RT) = 2 \times 96485 \times (0.072-(-0.372))/(8.314 \times 298) = 34.58$

$K_{eq1} = 1.0 \times 10^{15}\ M^{-2}$

For reaction (A-2),

$\ln K_{eq2} = (nF\Delta E_{rxn})/(RT) = 2 \times 96485 \times (0.072-(-0.172))/(8.314 \times 298) = 19.0$

$K_{eq2} = 1.8 \times 10^8\ M^{-1}$

(A-1) - (A-2):

$I^- + I_2 \rightleftharpoons I_3^-$ (A-3)

$K_0 = K_{eq1}/K_{eq2} = 1.0 \times 10^{15}\ M^{-2}/1.8 \times 10^8\ M^{-1} = 5.6 \times 10^6\ M^{-1} \Rightarrow pK_0 = -6.74$

Reported pK_0 from literature:

$pK_0 = -7.18$[147]

Thus, the standard potentials from Popov et al.[163], Desbarres et al.[170] and Benoit et al. [171] reports look more accurate.

APPENDIX B

CALCULATION OF E^0 ($I^\bullet/I^-$) IN ACETONITRILE

1. METHOD ONE

$I^\bullet$ (aq) + ½ H_2 (g) ⇌ I^- (aq) + H^+ (aq), E^o = (1.33 ± 0.02) V[83,85,180] vs NHE (B-1)

Ag^+ (aq) + ½ H_2 (g) ⇌ Ag (s) + H^+ (aq), E^o = (0.7996 ± 0.001) V[181] vs NHE (B-2)

Ag^+ (aq) + I^- (aq) ⇌ Ag^+ (AN) + I^- (AN), (B-3)

$I^\bullet$ (aq) ⇌ $I^\bullet$ (AN) (B-4)

$[Fe(Cp)_2]^+$ (AN) + Ag (s) ⇌ $Fe(Cp)_2$ (AN) + Ag^+ (AN) (B-5)

(B-1) - (B-2) ⇒

$I^\bullet$ (aq) + Ag (s) ⇌ I^- (aq) + Ag^+ (aq) (B-6)

$\Delta G^\circ_6 = \Delta G^\circ_1 - \Delta G^\circ_2 \Rightarrow \Delta E^\circ_6$ = (1.33 ± 0.02) V - (0.7996 ± 0.001) V = (0.53 ± 0.02) V

ΔG°_6 = -n*F*ΔE°_6 = -1* (96485 C)* ((0.53 ± 0.02) V) = - (51.14 ± 2.00) kJ mol^{-1}

(B-6) + (B-3):

$I^\bullet$ (aq) + Ag (s) ⇌ I^- (AN) + Ag^+ (AN) (B-7)

$\Delta G^\circ_7 = \Delta G^\circ_6 + \Delta G^\circ_3$, $\Delta G^\circ_3 = \Delta G^\circ_{tr}$ (I^-) + ΔG°_{tr} (Ag^+),

ΔG°_{tr} (I^-) = - (23.2 ± 2.00) kJ mol^{-1},[182] ΔG°_{tr} (Ag^+) = (16.8 ± 2.00) kJ mol^{-1},[182]

ΔG°_7 = (-51.14 ± 2.00) + (-23.2 ± 2.00) + (16.8 ± 2.00) = - (57.5 ± 3.5) kJ mol^{-1}

$I^{\bullet}$ (aq) ⇌ $I^{\bullet}$ (AN), ΔG°_{tr} ($I^{\bullet}$)

Suppose ΔG°_{tr} ($I^{\bullet}$) = ΔG°_{tr} (Xe),

ln K_H (AN) = (- 4.98 ± 0.01) [183], ln K_H (H_2O) = (- 9.46 ± 0.03) [183,184]

$$V_{AN} = \frac{n_{Xe} \times M_{Xe} + n_{AN} \times M_{AN}}{d_{AN}} = \frac{(e^{(-4.98)} \times 131.29 + 1 \times 41.05)(g)}{0.777(g/ml)} = 52.8ml$$

$$[Xe]_{AN} = \frac{n_{Xe}}{V_{AN}} = \frac{e^{(-4.98)}(mol)}{52.8(ml)} = 0.0189 \times e^{(-4.98)}M$$

$$V_{H_2O} = \frac{n_{Xe} \times M_{Xe} + n_{H_2O} \times M_{H_2O}}{d_{H_2O}} = \frac{(e^{(-9.46)} \times 131.29 + 1 \times 18)(g)}{0.998(g/ml)} = 18.0ml$$

$$[Xe]_{H_2O} = \frac{n_{Xe}}{V_{H_2O}} = \frac{e^{(-9.46)}(mol)}{18.0(ml)} = 0.0554 \times e^{(-9.96)}M$$

For Xe (aq) ⇌ Xe (AN),

K_{eq} = [Xe (AN)] / [Xe (H_2O)]

= (0.0189 × $e^{(-4.98)}$ M)/(0.0554 × $e^{(-9.96)}$ M)

= 30.0 ± 0.04

ΔG°_4 = - RT ln K_{eq}

= - (8.314 J mol^{-1} K^{-1})* (298 K)* (3.40 ± 0.04)

= - (8.43 ± 0.10) kJ mol^{-1}

(B-7) - (B-4):

$I^{\bullet}$ (AN) + Ag (s) ⇌ I^- (AN) + Ag^+ (AN) (B-8)

$\Delta G^{\circ}_8 = \Delta G^{\circ}_7 - \Delta G^{\circ}_4$ = - (57.5 ± 3.5) – (- (8.43 ± 0.10)) = - (49.07 ± 3.60) kJ mol^{-1}

ΔE^{o}_{8} = (-49.07 kJ mol^{-1}) / {(-1)* 96485 C)} = (0.508 ± 0.037) V

For reaction (B-5), E^{o} ($[Fe(Cp)_2]^{+/0}$) = 0.089 V[162] vs $Ag/AgNO_3$(0.01 N)(AN)

E^{o} ($[Fe(Cp)_2]^{+/0}$) vs $Ag/AgNO_3$ (0.01 N)) =

E^{o} ($[Fe(Cp)_2]^{+/0}$) vs $Ag/AgNO_3$ (1.0 N))-0.059 log (0.01)

Thus, E^{o} ($[Fe(Cp)_2]^{+/0}$) vs $Ag/AgNO_3$(1.0 N)) = -0.029 V

(B-8) – (B-5):

$Fe(Cp)_2$ (AN) + $I^{\bullet}$ (AN) → $[Fe(Cp)_2]^{+}$ (AN) + I^{-} (AN) (B-9)

$\Delta G^{\circ}_{9} = \Delta G^{\circ}_{8} - \Delta G^{\circ}_{5} \Rightarrow \Delta E^{o}_{9}$ = 0.508 + 0.029 = (0.537 ± 0.037) V

$\therefore E^{o}$ ($I^{\bullet}/I^{-}$) = (0.537 ± 0.037) V vs ($[Fe(Cp)_2]^{+/0}$

2. METHOD TWO

$I^{\bullet}$ (AN) + Ag (s) ⇌ I^{-} (AN) + Ag^{+} (AN) ΔG°_{8}, (B-8)

Ag^{+} (aq) ⇌ Ag^{+} (AN), ΔG°_{tr} (Ag^{+}) = (16.8 ± 2) kJ mol^{-1} (B-10)

$\Delta_f G^{\circ}_{Ag(+)}$(aq) = 77.11 kJ mol^{-1} [185]

ΔG°_{tr} (Ag^{+}) = $\Delta_f G^{\circ}_{Ag(+)}$(AN) - $\Delta_f G^{\circ}_{Ag(+)}$(aq) ⇒

$\Delta_f G^{\circ}_{Ag(+)}$(AN) = ΔG°_{tr} (Ag^{+}) + $\Delta_f G^{\circ}_{Ag(+)}$(aq)

= ((16.8 ± 2) + 77.11) kJ mol^{-1} = (93.91 ± 2) kJ mol^{-1}

I^{-} (aq) ⇌ I^{-} (AN) ΔG°_{tr} (I^{-}) = (-23.2 ± 2) kJ mol^{-1} (B-11)

$\Delta_f G^{\circ}_{I(-)}$(aq) = -51.57 kJ mol^{-1} [185]

ΔG°_{tr}(I^{-}) = $\Delta_f G^{\circ}_{I(-)}$(AN) - $\Delta_f G^{\circ}_{I(-)}$(aq) ⇒

$\Delta_f G^{\circ}_{I(-)}$(AN) = ΔG°_{tr}(I^{-}) + $\Delta_f G^{\circ}_{I(-)}$(aq)

= {(-23.2 ± 2) + (-51.57)} kJ mol^{-1}

$= (-74.77 \pm 2)$ kJ mol^{-1}

$I^{\bullet}$ (g) ⇌ $I^{\bullet}$ (AN) ΔG°_{12}, (B-12)

Xe (g) ⇌ Xe (AN) ΔG°_{13}, (B-13)

$$[Xe]_{AN} = \frac{n_{Xe}}{V_{AN}} = \frac{e^{(-4.98)}(mol)}{52.8(ml)} = 0.0189 \times e^{(-4.98)} M$$

ΔG°_{13} = -R*T*ln$[Xe]_{AN}$

= (-)* 8.314* 298.15*ln(0.0189*$e^{(-4.98)}$)

= (5.05 ± 0.03) kJ mol^{-1}

$\therefore \Delta G^{\circ}_{12} = \Delta G^{\circ}_{13} = (5.05 \pm 0.03)$ kJ mol^{-1}

$\Delta_f G^{\circ}_{I\bullet}$ (g) = 70.25 kJ mol^{-1} [185]

$\therefore \Delta_f G^{\circ}_{I\bullet}$ (AN) = ΔG°_{12} + $\Delta_f G^{\circ}_{I\bullet}$ (g)

$= (5.05 \pm 0.03) + 70.25 = (75.30 \pm 0.03)$ kJ mol^{-1}

From reaction B-8,

$\Delta G^{\circ}_{8} = \Delta_f G^{\circ}_{Ag(+)}$(AN) + $\Delta_f G^{\circ}_{I(-)}$(AN) -$\Delta_f G^{\circ}_{I\bullet}$ (AN)

$= (93.91 \pm 2) + (-74.77 \pm 2) - (75.30 \pm 0.03)$

$= -(56.4 \pm 2.8)$ kJ mol^{-1}

$\therefore E^{o}$ ($I^{\bullet}/I^{-}$) = (ΔG°_{8})/(-n*F) = (-(56.4 ± 2.8) kJ mol^{-1})/(-1*96485 C mol^{-1})

$= (0.58 \pm 0.04)$ vs $Ag/AgNO_3$(1.0 N)

Since E^{o} ($[Fe(Cp)_2]^{+/0}$) vs $Ag/AgNO_3$(1.0 N))= -0.029 V

$\therefore E^{o}$ ($I^{\bullet}/I^{-}$) = (0.58 ± 0.04) - (-0.029) = (0.61 ± 0.04) V vs $[Fe(Cp)_2]^{+/0}$

APPENDIX C

PRELIMINARY STUDY OF THE OXIDATION OF I^- BY VARIOUS OUTER-SPHERE OXIDANTS IN ACETONITRILE

I. Oxidation of iodide by $Ru^{III}(hfac)_3$

Preparation of $K[Ru^{II}(hfac)_3]$. $K[Ru^{II}(hfac)_3]$ was prepared by following standard procedure.[186] 2.40 mmol of ruthenium chloride was added to 50.0 mL of degassed $EtOH/H_2O$ (1:1). The solution was refluxed for 4 hours. Then 1.0 mmol of 1,1,1,5,5,5-hexafluoro-2,4-pentanedione (hfac) was added to the solution, and it was continued refluxing for 2 hours. 12.0 mmol of potassium bicarbonate was added to the solution after it was cooled to room temperature. It was heated a little bit and a lot of bubble was formed. Then it was refluxed for several hours until the solution turned into pink. Collect the precipitate by vacuum filtration. Rinse it with 10.0 mL of toluene. Then dissolve it in 25.0 mL of acetone, and purify it by passing through one column of silica gel (200-400 mesh, 60 Å). Remove the acetone in the eluant by rotary evaporation. Dry it in hood for 12 hours. Note: the solution was purged with nitrogen gas during the refluxing processes. Yield of $K[Ru^{II}(hfac)_3]$: 35%. ^{1}H-NMR (400 MHz/CD_3CN): 2.16 (s, 2H).

Preparation of $Ru^{III}(hfac)_3$. $Ru^{III}(hfac)_3$ was prepared according to Endo's report.[186] 0.13 mmol of $K[Ru^{II}(hfac)_3]$ was added to 6.0 mL of water, and suspension was

formed. 6.0 mL of toluene and 0.30 mL of 4.0 M HCl was added to the suspension, respectively. Then 0.75 mL of 30% H_2O_2 was added dropwise, and some bubble was formed. The $Ru^{III}(hfac)_3$ was extracted with 6.0 mL of toluene and 12.0 mL of n-hexane, respectively. Remove the n-hexane to obtain $Ru^{III}(hfac)_3$ by rotary evaporation. Dry it in hood for 30 minutes.

Characterization of $K[Ru^{II}(hfac)_3]$ and $Ru^{III}(hfac)_3$. The UV-visible absorbance characteristics of the ruthenium complexes are shown in Table C-1. The spectral properties of $K[Ru^{II}(hfac)_3]$ are close to that reported by Endo et al.[186]; while the extinction coefficient of $Ru^{III}(hfac)_3$ at 529 nm is about 10% higher than their report.[186]

Table C-1. UV-visible absorbance and electrochemical characteristics of the Ru and Fe complexes in acetonitrile

Compounds	Band	λ_{max}, nm	ε, M^{-1} cm^{-1}	$E_{1/2}$, mV [a]
$K[Ru^{II}(hfac)_3]$	I	289	21091	352
	II	529	16697	
$Ru^{III}(hfac)_3$	I	289	11977	355
	II	375	7760	
$[Fe^{III}(CH_3Cp)_2]^+$	I	618	418	0

[a] $E_{1/2}$ vs $[Fe(CH_3Cp)_2]^{+/0}$, at 22.0 °C and μ = 0.10 M. $E_{1/2} = E_f$

The CV (Figure C-1) of 1.0 mM $K[Ru^{II}(hfac)_3]$ in 0.10 M $Et_4NBF_{4(AN)}$, with 1.0 mM decamethylferrocene as internal reference, is quasi-reversible, with $\Delta E_{p/p}$ = 76 mV, $E_{1/2}$ = 352 mV vs $[Fe(Cp)_2]^{+/0}$. The OSWV (Figure C-2) of 1.0 mM $K[Ru^{II}(hfac)_3]$ in 0.10 M $Et_4NBF_{4(AN)}$, with 1.0 mM decamethylferrocene as internal reference, has the half-

potential, $E_{1/2}$, of 355 mV vs $[Fe(Cp)_2]^{+/0}$, 19 mV higher than that reported by Baird et al.[187].

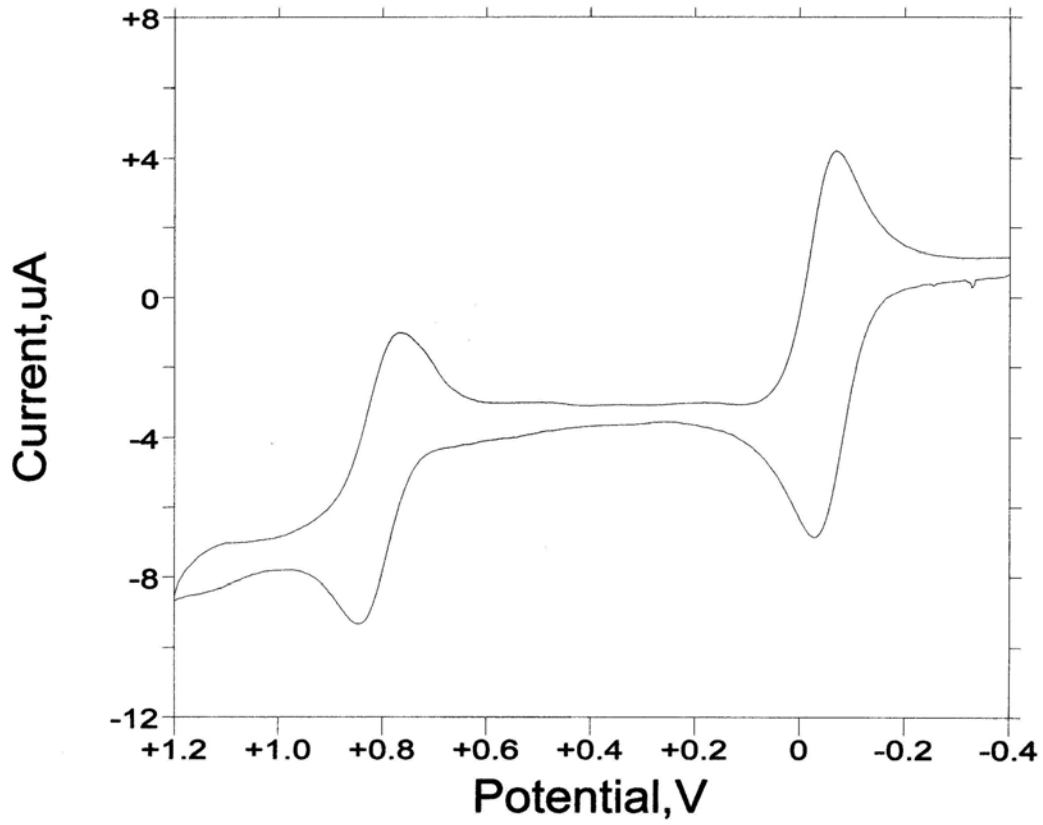

Figure C-1. The CV of 1.0 mM of $K[Ru^{II}(hfac)_3]$ and 1.0 mM $Fe(Cp^*)_2$ in 0.10 M Et_4NBF_4. With a platinum disc as working electrode, an $Ag/AgCl_{(s)}$ referebce electrode, and a Pt wire as a counter electrode.

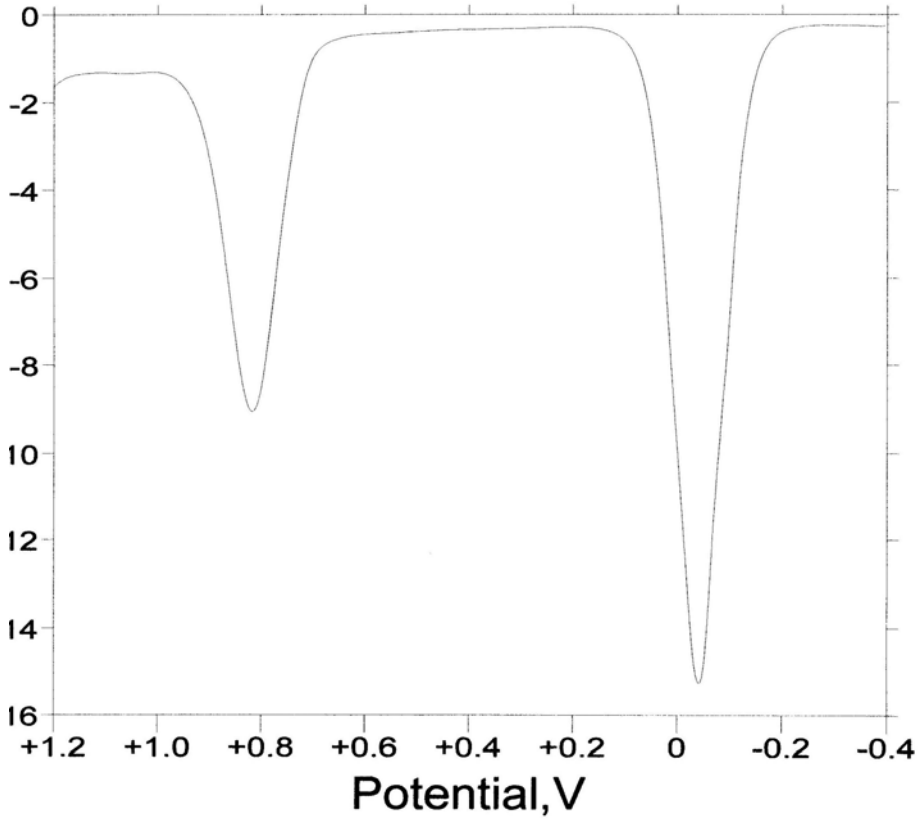

Figure C-2. The OSWV of 1.0 mM of $K[Ru^{II}(hfac)_3]$ and 1.0 mM $Fe(Cp^*)_2$ in 0.10 M Et_4NBF_4. With a platinum disc as working electrode, an $Ag/AgCl_{(s)}$ electrode as reference, and a Pt wire as a counter electrode.

Kinetics. The reaction trace of oxidation of 8.0×10^{-5} M Et_4NI by 1.2×10^{-5} M $Ru^{III}(hfac)_3$, in the presence of 2.0 mM bpy, at μ = 0.10 M (Et_4NBF_4) and 25.0 ^oC, is shown in Figure C-3, with the half-life of 3.7 ms. Generally, the dead time for stopped-flow instrument is 2 ms. If five times concentration of iodide (0.40 mM) were employed, the rate of the reaction would be out of limit of the stopped-flow instrument. So the oxidation of iodide by $Ru^{III}(hfac)_3$ in acetonitrile can not be performed on SF-51.

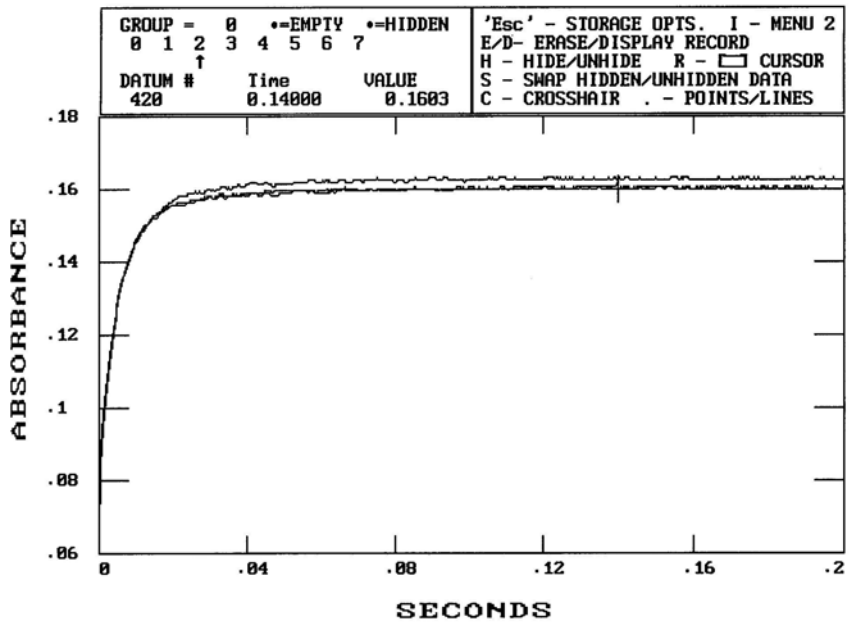

Figure C-3. Reaction trace for oxidation of 8.0×10^{-5} M Et_4NI by 1.2×10^{-5} M $Ru^{III}(hfac)_3$. In the presence of 2.0 mM bpy, at $\mu = 0.10$ M (Et_4NBF_4) and 25.0 °C.

II. Oxidation of iodide by $[Fe^{III}(Cp)_2]^+$.

Preparation of $[Fe^{III}(Cp)_2]PF_6$. The synthesis of $[Fe^{III}(Cp)_2]PF_6$ was referred to Yang et al.' s paper.[188] 2.70 mmol of $Fe^{II}(Cp)_2$ was added to 10.0 mL of concentrated H_2SO_4. The solution changed to blue color. Half an hour later, 150 mL of water was added to the blue solution. Then it was filtered by vacuum filtration, and 12.9 mmol of NH_4PF_6 was added to the filtrate. Some precipitate was formed. Filter and rinse it with water. Obtain the sample by drying the precipitate in vacuum disiccator for 6 hours.

Characterization of $[Fe^{III}(Cp)_2]PF_6$. The UV-visible absorbance characteristics of $[Fe^{III}(Cp)_2]PF_6$ is shown in Table C-1, from which it has the same extinction coefficient as previous report.[188]

Kinetics. Firstly, copper-catalysis effect was tested by us. For the oxidation of 1×10^{-2} M Et_4NI by 1.0×10^{-3} M $[Fe^{III}(Cp)_2]^+$ in acetonitrile, the following two experiments were performed on SF-51 instrument. Without the addition of Cu^{2+}, the half-life of the reaction is 11.0 s; with the addition of 5.0 μM Cu^{2+}, the half-life decreases by around 23 times, as shown in Table C-2. It indicates that copper cation is a good catalyst for the oxidation of iodide by $[Fe^{III}(Cp)_2]^+$ in acetonitrile. To inhibit its copper-catalysis effect, 5.0 mM bpy and 5.0 mM 2,9-dimethyl-1,10-phenanthroline (neocuproine) was added to the reactants, respectively (for neocuproine, 5×10^{-2} M, not 1×10^{-2} M, of iodide was added). Neither of them can suppress the copper catalysis effectively: the addition of bpy does not change the half-life of the reaction; while the rate of the reaction increases with the addition of neocuproine. All of the results are shown in Table C-2. These abnormal results are ascribed to the air sensitive property of $[Fe^{III}(Cp)_2]PF_6$ in acetonitrile. Therefore, $[Fe^{III}(Cp)_2]PF_6$ is not a good candidate for the oxidation of iodide in acetonitrile, either.

Table C-2. Effect of Cu^{2+}, bpy, and neocuproine on the oxidation of iodide by 1.0×10^{-3} M $[Fe^{III}(Cp)_2]^+$ in acetonitrile

$[I^-]_0$, mM	$[Cu^{2+}]$, μM	[bpy], mM	$t_{1/2}$, s
10	0.0	0.0	11.0
10	5.0	0.0	0.464
10	0.0	5.0	12.5
50	0.0	0.0	0.87
50	0.0	0.0[a]	0.25
50	5.0	0.0[a]	0.27

[a] 5.0 mM 2,9-dimethyl-1,10-phenanthroline (neocuproine)

APPENDIX D

COPPER-CATALYZED OXIDATION OF IODIDE BY $[Fe(CH_3Cp)_2]^+$ IN CH_3CN/H_2O (99/1, v/v) CO-SOLVENT

Introduction

The redox potentials of the copper(II)-copper(I) and copper(I)-copper(0) are very sensitive to solvent: the redox potentials of $Cu^{2+/+}$ and $Cu^{+/0}$ are 0.153 V and 0.521 V vs NHE in aqueous media, while that of $Cu^{2+/+}$ and $Cu^{+/0}$ are 1.181 V and -0.011 V vs NHE in acetonitrile.[189] This solvent-dependent electrochemical protery of cuprous cation necessitates that it has totally different thermodynamic characterics in these two media: it disproportionates completely to copper(II) and metallic copper in aqueous solution, while the stronger solvation of copper(I) makes it more favorable than copper(II) in acetonitrile.

Cu(I), as a d^{10} system, tends to adopt a tetrahedral geometry. In anhydrous acetonitrile, Cu(I) is believed to cooridinated to four molecules of acetonitrile. In the presence of excess iodide, acetonitrile ligand can be replaced by iodide to form $Cu(CH_3CN)_3(I)$ or $[Cu(CH_3CN)_2(I)_2]^-$. The stability constants of copper(I) iodide in acetonitrile was determined by Ahrland et al. using potentiometric and calorimetric measurements, with 1.3×10^5 M^{-1} for β_1 and 9.3×10^5 M^{-2} for β_2.[190]

Very recently, we found that copper cation is a good catalyst for the oxidation of iodide by a series of outer-sphere transition metal complexes in acetonitrile,[164,191] totally

different from the general kinetic feature of this redox reaction in aqueous media. The above copper catalytic behavior may arise from the unsual high redox potential of $Cu^{2+/+}$ and copper(I)-iodide chemistry in acetonitrile. In this research, the copper-catalysis of the oxidation of iodide by $[Fe^{III}(CH_3Cp)_2]^+$ is described.

Experimental section

Reagent and solution. Acetonitrile (Fisher, Certified A. C. S grade), n-hexane (Fisher), methanol (Fisher), diethyl ether (Fisher), hydrochloric acid (Fisher), ferric nitrate (Fisher), sodium hexafluorophosphate (Aldrich), 2,9-dimethyl-1,10-phenanthroline (Aldrich), silver nitrate (Fisher). Tetrakis(acetonitrile)copper(I) hexafluorophosphate (Strem Chemicals) was recrystallized from acetonitrile/diethyl ether.[192] Copper (I) iodide (Strem Chemicals) was purified according to Kauffman's method.[193] Due to their highly air-sensitive property, the dry and purified tetrakis(acetonitrile)copper(I) hexafluorophosphate and copper(I) iodide were then transferred to vacuum desiccator immediately. The concentrations of Cu(I) are standardized by UV-vis spectra of the mixture of the Cu(I) with the excess of 2,9-dimethyl-1,10-phenanthroline in acetonitrile.[194] 1,1'-dimethylferrocene (Aldrich) was recrystallized from ethanol. Et_4NI (Aldrich) was recrystallized from water and dried under vacuum at 100 ^oC for 12 hours. The concentration of Et_4NI in acetonitrile/H_2O (99/1, v/v) was standardized by titration with standard aqueous $AgNO_3$, using Eosin as indicator.[152] Et_4NBF_4 (Aldrich) was recrystallized three times from a mixture of methanol and n-hexane (4:1) and dried under vacuum at 96.0 ^oC.[195] Sample of $[Fe^{III}(CH_3Cp)_2]PF_6$ is from our previous experiments. (refer to Chapter 3)

Distilled deionized water was obtained from a Barnstead NANO pure infinity ultrapure water system. Solutions of $[Fe^{III}(CH_3Cp)_2]PF_6$ and iodide in CH_3CN/H_2O were prepared just prior to use, and kept in the dark to prevent any photochemical change. Both Fe(III) and Et_4NI were prepared maintaining the appropriate concentrations of the other reagents, purged with argon gas, and transferred via gastight glass syringe.

Methods. The instrumental conditions are referred to that described in Chapter 3. Reactions were monitored at fixed wavelengths (When the initial concentration of Fe(III) is at 0.25 mM, the reaction was monitored at 650 nm; when the initial concentration of Fe(III) is less than 50 μM, the reaction is monitored at 363 nm), and the rate constants were obtained by fitting the data with OLIS-supplied first-order functions. A nonlinear-least squares computer program was used to fit the overall rate law to the values of k_{obs}. The water content in the product's solution was determined by AF7 Coulometric Karl Fischer Titrator.

Results

Effect of small amount of water on the kinetics. The copper-catalyzed reaction was performed under nominally anhydrous condition. The experimental conditions are as follows: $[[Fe^{III}(CH_3Cp)_2]^+]_0$ = 0.25 mM, $[Et_4NI]_0$ = 8.0 mM, $[CuI]_0$ = 5.0 μM. It was observed that the rate of the reaction is irreproducible, with the half-life ranging from 0.44 to 0.50 s. This irreproducibility is ascribed to the water sensitivity of the standard potential of $Cu^{2+/+}$ in acetonitrile.[189] The standard potential of $Cu^{2+/+}$ in anhydrous acetonitrile is 1.181 V vs NHE; while in CH_3CN/H_2O (95/5, v/v) co-solvent, the standard potential of $Cu^{2+/+}$ decreases to 0.873 V vs NHE.[189] Therefore, the different

content of water in each shot contributes to the above irreproducible kinetic results. Then a series of experiments was performed with the addition of very small amounts of water to the above reaction system. Table D-1 shows that, even with the addition of 0.50% (by volume) of water, reproducible results were obtained, and the rate of the reaction is as fast as that under nominally anhydrous condition. With the addition of 1.0% water, the reaction runs slower, with the half-life increase by 20%. The half-life increases by a factor of 2 with the addition of 2.5% of water. Based on the above results, all of the following experiments are performed in CH_3CN/H_2O (99/1, v/v) co-solvent.

Table D-1. Water effect on the rate of the reaction between $[Fe^{III}(CH_3Cp)_2]^+$ and I^- in CH_3CN/H_2O co-solvent, in the presence of 5.0 μM CuI. $[Fe^{III}(CH_3Cp)_2^+]_0$ = 0.25 mM, $[Et_4NI]_0$ = 8.0 mM. (Reactions are monitored at 650 nm)

CH_3CN/H_2O,	$t_{1/2}$, s
100/0	0.44-0.50
99.5/0.5	0.42
99/1	0.50
97.5/2.5	0.80

The inhibition by $Fe^{II}(CH_3Cp)_2$ on the CuI-catalyzed oxidation of iodide. For the CuI-catalyzed oxidation of Et_4NI by $[Fe^{III}(CH_3Cp)_2]^+$ in CH_3CN/H_2O (99/1, v/v), a series of experiments was performed by adding various concentrations of $Fe^{II}(CH_3Cp)_2$ ($Fe^{II}(CH_3Cp)_2$, one of the products in the reaction, see product identification section) to the reactants. The initial concentrations of the reactants are as follows: $[Et_4NI]_0$ = 5.0 mM, $[[Fe^{III}(CH_3Cp)_2]^+]_0$ = 10.0 μM, $[CuI]_0$ = 10.0 μM, $[Fe^{II}(CH_3Cp)_2]_0$ = 0.10 to 2.40 mM, μ

= 0.10 M (Et_4NBF_4). The data shown in Table D-2 indicate that the rate of the reaction decreases with the increase of $Fe^{II}(CH_3Cp)_2$. It follows perfectly pseudo-first-order kinetics even though 0.20 mM of $Fe^{II}(CH_3Cp)$ was added, i.e., $[Fe(II)]_0/[Fe(III)]_0 = 20$.

Table D-2. Effect of $Fe^{II}(CH_3Cp)_2$ on the oxidation of I^- by $[Fe^{III}(CH_3Cp)_2]^+$ in CH_3CN/H_2O (99/1). In the presence of 10.0 μM CuI, at μ = 0.10 M and 25.0 °C. $[Fe^{III}(CH_3Cp)_2^+]_0 = 10$ μM, $[Et_4NI]_0 = 5.0$ mM.

$[Fe(II)]_0$, mM	k_{obs}, s^{-1}
2.40	0.0173
1.80	0.0197
1.20	0.0228
1.00	0.0250
0.80	0.0312
0.60	0.0355
0.40	0.0415
0.20	0.0600

Comparison CuI with $[Cu(NCCH_3)_4]PF_6$. Cu^+ is well known to combine with I^- to form CuI and CuI_2^- in acetonitrile.[190,196] To avoid the inevitable consumption of iodide by Cu^+, CuI, rather than $[Cu(NCCH_3)_4]PF_6$, is firstly selected as catalytic reagent in the reaction. For the oxidation of 5.0 mM Et_4NI by 10 μM $[Fe^{III}(CH_3Cp)_2]^+$ in CH_3CN/H_2O (99/1, v/v), with 0.60 mM Fe(II) and ionic strength of 0.10 M, 7.5, 10, and 100 μM of

crude CuI were added to the reactants, respectively. The experiments were repeated three times for each concentration of CuI. The data in Table D-3 demonstrate that the rate of the reaction has good reproducibility at 7.5 μM of CuI, while it is poorly reproducible at 100 μM of CuI. The irreproducible kinetic behavior is probably due to the poor stability of solid CuI in the air. Then 100 μM crude and purified CuI were separately added to the following reaction system: $[Et_4NI]_0$ = 5.0 mM, $[[Fe^{III}(CH_3Cp)_2]^+]_0$ = 10.0 μM, $[CuI]_0$ = 100.0 μM, $[Fe^{II}(CH_3Cp)_2]_0$ = 0.40 mM, μ = 0.10 M (Et_4NBF_4). With the use of purified CuI, the pseudo-first-order rate constant (0.0367 s^{-1}) is much smaller than that of crude CuI. Then the above kinetic experiments were repeated with the addition of another fresh, purified CuI solution. However, the rate constant increases by 25%, as shown in Table D-4. It implies the purified CuI solid sample decomposes quickly even though it is exposed to the air for a few minutes. Due to the poor stability of CuI in the air, then $[Cu(NCCH_3)_4]PF_6$ was selected in our kinetic studies. For the oxidation of 5.0 mM Et_4NI by 10 μM $[Fe^{III}(CH_3Cp)_2]^+$ in CH_3CN/H_2O (99/1, v/v), with 0.40 mM Fe(II) and ionic strength of 0.10 M, the rate constant is nearly the same for both crude and purified 100 μM $[Cu(NCCH_3)_4]PF_6$, i.e., 0.0350 s^{-1}, as shown in Table D-4. It indicates that the solid state of $[Cu(NCCH_3)_4]PF_6$ is more stable than that of CuI in the air. Therefore, purified $[Cu(NCCH_3)_4]PF_6$ will be used for all of later kinetic experiments.

Table D-3. Effect of CuI on the oxidation of I^- by $[Fe^{III}(CH_3Cp)_2]^+$ in CH_3CN/H_2O (99/1, v/v). In the presence of 0.60 mM $Fe^{II}(CH_3Cp)_2$, at μ = 0.10 M and 25.0 ^oC. $[Fe^{III}(CH_3Cp)_2^+]_0$ = 10 μM, $[Et_4NI]_0$ = 5.0 mM.

$[CuI]_0$, μM	k_{obs}, s^{-1}
7.5	0.0292
7.5	0.0272
7.5	0.0282
10.0	0.0355
10.0	0.0304
10.0	0.0371
100	0.0490
100	0.0361
100	0.0519

Table D-4. Comparison of CuI and $[Cu(acn)_4]PF_6$ for the oxidation of I^- by $[Fe^{III}(CH_3Cp)_2]^+$ in CH_3CN/H_2O(99/1). In the presence of 0.40 mM $Fe^{II}(CH_3Cp)_2$ and 100 μM Cu(I), at μ = 0.10 M and 25.0 ^oC. $[Fe^{III}(CH_3Cp)_2^+]_0$ = 10 μM, $[Et_4NI]_0$ = 5.0 mM.

$[CuI]_0$, μM	$[Cu(acn)_4^+]_0$, μM	k_{obs}, s^{-1}
100	0.0	0.0770[a]
100	0.0	0.0367[b]
100	0.0	0.0457[c]
0.0	100	0.0359[d]
0.0	100	0.0345[e]

[a] crude CuI; [b] firstly prepared fresh, purified CuI solution; [c] secondly fresh, purified CuI solution; [d] crude $[Cu(NC_3HC)_4]PF_6$; [e] purified $[Cu(NC_3HC)_4]PF_6$.

Reexamination of the effect of small amount of water on the kinetics.

Does $[Cu(NCCH_3)_4]PF_6$ play the same kinetic role as CuI in water/acetonitrile co-solvent?

For the oxidation of 8.0 mM of Et_4NI by 10 μM of $[Fe^{III}(CH_3Cp)_2]^+$ in CH_3CN, with 5.0 μM $[Cu(NCCH_3)_4]PF_6$ and ionic strength of 0.008 M, it was initially performed under nominally anhydrous condition. It shows that the reaction is perfectly reproducible, with the half-life of 0.44 s. Then 1.0 % and 2.5% (volume) of water was deliberately added to the above reactants, respectively. The half-lives shown in Table D-5 indicate that the rate of the reaction decreases by a factor of two even with the addition of 1% of water, totally different from that of CuI. In those water-effect experiments, the initial concentration of $[Fe^{III}(CH_3Cp)_2]^+$ is 0.25 mM, not 10 μM, and the non-purified CuI was employed. So these two experimental results are not comparable. To counteract the varying concentration of water in nominally anhydrous acetonitrile, 1.0 % of water, i.e., CH_3CN/H_2O (99/1, v/v), was added to acetonitrile in the kinetic studies.

Table D-5. Water effect on the copper-catalyzed oxidation of I^- by $[Fe^{III}(CH_3Cp)_2]^+$ in CH_3CN/H_2O co-solvent, in the presence of 5.0 μM $[Cu(acn)_4]PF_6$. At μ = 0.008 M and 25.0 ^oC, $[Fe^{III}(CH_3Cp)_2^+]_0$ = 10 μM, $[Et_4NI]_0$ = 8.0 mM.

CH_3CN/H_2O,	$t_{1/2}$, s
100/0	0.10
99/1	0.21
97.5/2.5	0.44

The inhibition by $Fe^{II}(CH_3Cp)_2$ on the $[Cu(NCCH_3)_4]^+$-catalyzed oxidation of iodide. For the oxidation of 5.0 mM Et_4NI by10 μM $[Fe^{III}(CH_3Cp)_2]^+$ in CH_3CN/H_2O (99/1, v/v), with 10.0 μM $[Cu(NCCH_3)_4]PF_6$ and ionic strength of 0.10 M, various concentrations of $Fe^{II}(CH_3Cp)_2$ ($Fe^{II}(CH_3Cp)_2$, one of the products in the reaction, see product identification section) were added to the reaction system. It follows perfectly pseudo-first-order kinetic behavior even though 0.10 mM Fe(II) was added, i.e. [Fe(II)]/[Fe(III)] = 10. All of the data corresponding to Fe(II) effect are shown in Table D-6. Plot of k_{obs} vs [Fe(II)] shown in Figure D-1 indicates that the rate constant decreases with the increase of Fe(II).

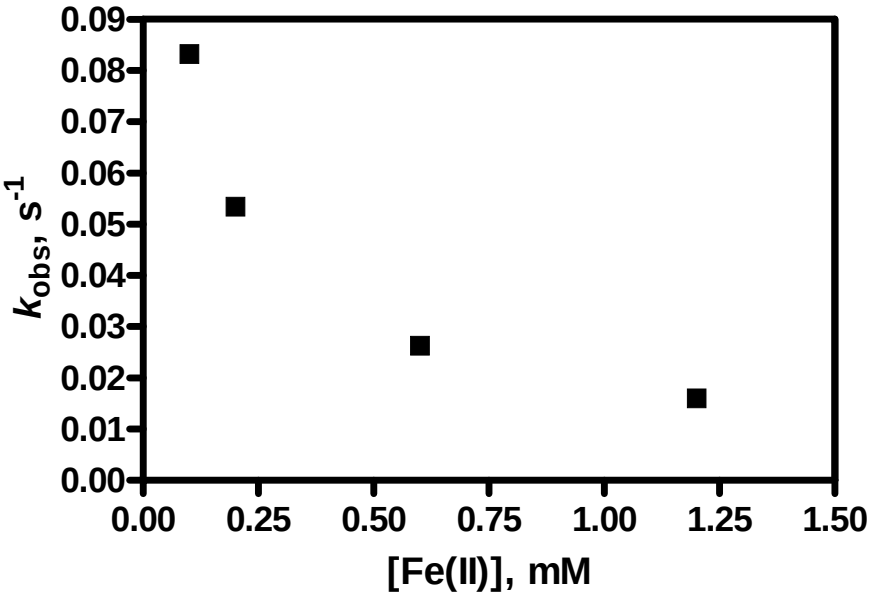

Figure D-1. Plot of k_{obs} vs [Fe(II)] for the oxidation of Et_4NI by $[Fe^{III}(CH_3Cp)_2]^+$ in CH_3CN/H_2O (99/1, v/v). with 10.0 μM $[Cu(acn)_4]PF_6$, at μ = 0.10 M and 25.0 °C. $[Et_4NI]_0$ = 5.0 mM, $[Fe^{III}(CH_3Cp)_2^+]_0$ = 10 μM

Table D-6. Effect of $[Fe^{II}(CH_3Cp)_2]$ on the oxidation of 5.0 mM Et_4NI by 10 μM $[Fe^{III}(CH_3Cp)_2]^+$ in CH_3CN/H_2O (99/1). In the presence of 10.0 μM $[Cu(NCCH_3)_4]PF_6$, at μ = 0.10 M and 25.0 °C.

[Fe(II)], mM	k_{obs}, s^{-1}
1.20	0.0160
0.60	0.0263
0.20	0.0534
0.10	0.0832

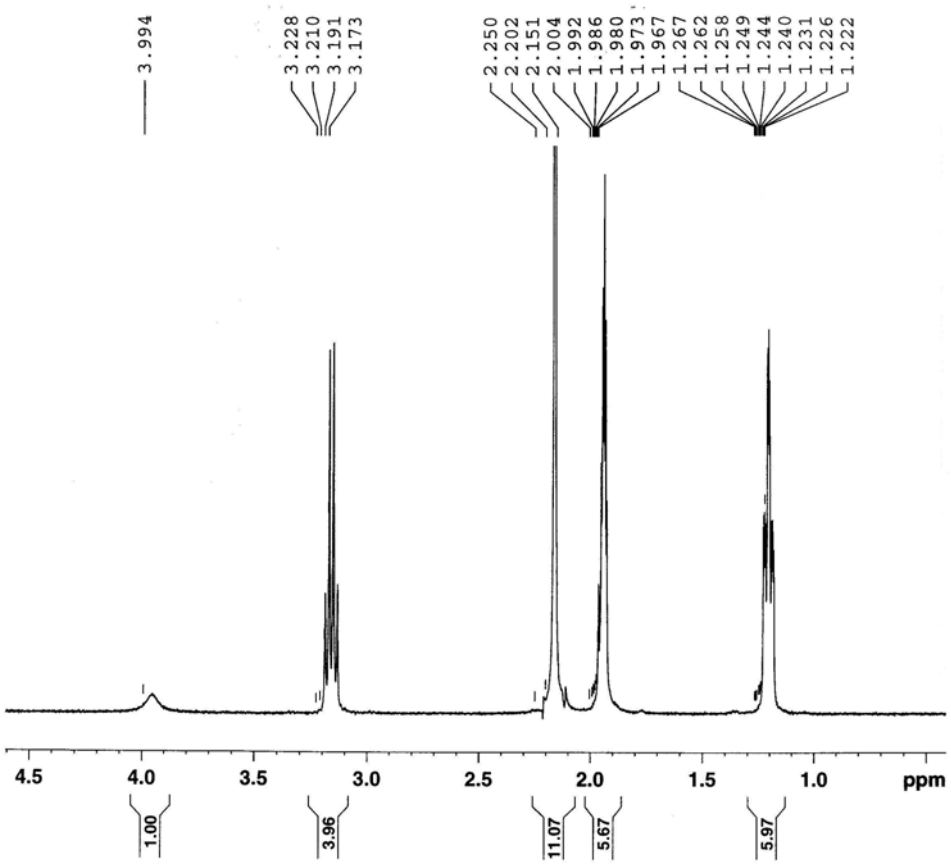

Figure D-2. ^{1}H-NMR spectrum of product for the oxidation of 8.0 mM Et_4NI by 2.0 mM $[Fe^{III}(CH_3Cp)_2]^+$ in CD_3CN. In the presence of 10.0 μM CuI.

Water content in the products' solution. The concentration of water in the products' solution was determined by Karl Fischer Titration.All of the results are shown in Table D-7, which demonstrates that the concentration of water from Karl Fischer Titration is very close to theoretical value.

Table D-7. The water content in the products for the oxidation of 5.0 mM I^- by $[Fe^{III}(CH_3Cp)_2]^+$ in CH_3CN/H_2O (99/1, v/v). At μ = 0.10 M (Et_4NBF_4) and 25.0 ^oC.

$[Fe(III)]_0$, μM	$[Fe(II)]_0$, mM	$[Cu(acn)_4^+]_0$, μM	$[H_2O]$, M	
			theory	titration
10.0	0.60	2.50	0.556	0.570
10.0	0.60	5.00	0.556	0.545
10.0	0.60	10.0	0.556	0.536
40.0	0.60	10.0	0.556	0.550
40.0	0.60	40.0	0.556	0.536
40.0	0.60	60.0	0.556	0.518

Identification of product and yield of Fe(II). Under argon protection, 8.0 mM Et_4NI and 20 μM CuI was mixed with 4.0 mM $[Fe^{III}(CH_3Cp)_2]^+$ equally, then the mixture was kept purging with argon for 10 minutes. The ^{1}H-NMR spectrum of the product shown in Figure D-2 has one very broad peak at 3.99 ppm, indicates that one of products in the reaction is $Fe^{II}(CH_3Cp)_2$, and implies that some paramagnetic $[Fe^{III}(CH_3Cp)_2]PF_6$ still remains in the solution. The yield of $Fe^{II}(CH_3Cp)_2$ (around 90.2%) was calculated from the integrated peak intensity of the spectrum, which confirms the incomplete conversion of $[Fe^{III}(CH_3Cp)_2]PF_6$. In the later kinetic experiments, the absorbance at 363

nm increases with the time of the reaction, which implies that I_3^- is one of the products. Therefore, the products of the copper-catalyzed reaction are $Fe^{II}(CH_3Cp)_2$ and I_3^-, the same as the direct oxidation of iodide in acetonitrile.

Kinetics. Figure D-3 shows the kinetic trace of the oxidation of 5.0×10^{-3} M Et_4NI by 10 μM $[Fe^{III}(CH_3Cp)_2]^+$, in the presence of 5.0 μM Cu(I) and 0.60 mM Fe(II), at μ = 0.10 M and 25.0 ^oC. It follows perfectly pseudo-first-order kinetics. For the oxidation of 5.0 mM Et_4NI by 10 μM $[Fe^{III}(CH_3Cp)_2]^+$ in CH_3CN/H_2O (99/1, v/v), with various concentrations of $[Cu(NCCH_3)_4]PF_6$, at ionic strength of 0.10 M and 25.0 ^oC, 0.10, 0.20, 0.60 and 1.20 mM Fe(II) were added to the above reactants, respectively. The results shown in Figure D-5 demonstrate that the rate constants increase with the increase of the concentration of Cu(I). Then the rate constants are saturated when the concentration of Cu(I) is greater than 10 μM. At the same concentration of Cu(I), the rate constants decrease with the increase of [Fe(II)]. It is of importance to remember that the initial concentration of $[Fe^{III}(CH_3Cp)_2]^+$ in the above experiments is exactly at 10 μM. If the initial concentration of $[Fe^{III}(CH_3Cp)_2]^+$ changes, does the reaction still follow such copper-saturated feature? Firstly, 40 μM $[Fe^{III}(CH_3Cp)_2]^+$ was added to such reactants: $[Et_4NI]_0$ = 5.0 mM; $[Fe(II)]_0$ = 0.60 mM; $[Cu(I)]_0$ = 10 μM; μ = 0.10 M (Et_4NBF_4). The reaction does not follow first-order kinetics, and the half-life decreases by half as that of 10 μM $[Fe^{III}(CH_3Cp)_2]^+$, which demonstrates that the initialconcentrations of [Fe(III)] and [Fe(II)] play a key role in this copper-catalyzed reaction, and that the inhibition by $Fe^{II}(CH_3Cp)_2$ is obviously very important. Then, for the oxidation of 5.0×10^{-3} M Et_4NI by 40 μM $[Fe^{III}(CH_3Cp)_2]^+$ in CH_3CN/H_2O (99/1, v/v), in the presence of 2.40 mM

$Fe^{II}(CH_3Cp)_2$, i.e., $[Fe(II)]_0/[Fe(III)]_0 = 60$, at ionic strength of 0.10 M and 25.0 °C, various concentrations of Cu(I) were added. The rate constants in Table D-8 shows that the reaction keeps constant when the concentration of Cu(I) is over 40 μM. Therefore, the copper-saturation is a general feature in such copper-catalyzed reaction.

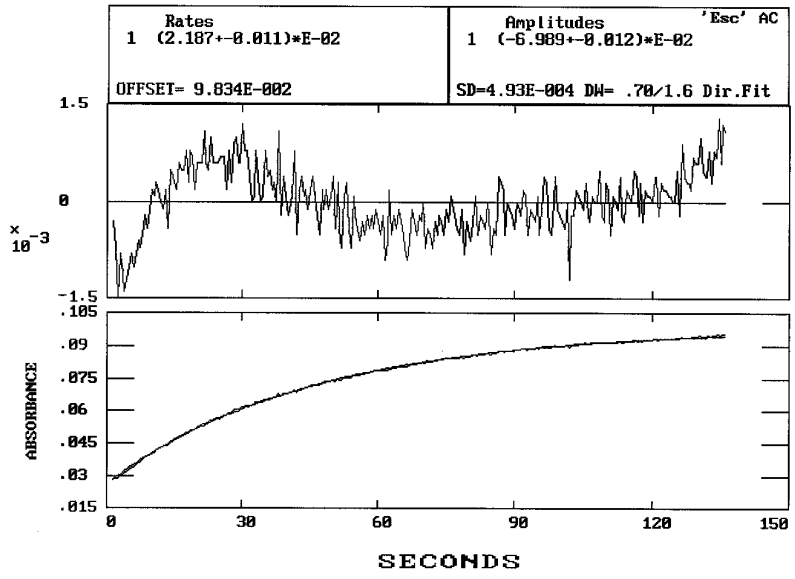

Figure D-3. Kinetic trace of the oxidation of 5.0 mM Et_4NI by $[Fe^{III}(CH_3Cp)_2]^+$. In the presence of 5.0 μM $[Cu(AN)_4]PF_6$ and 0.60 mM Fe(II), at μ = 0.10 M and 25.0 °C. $[Fe^{III}(CH_3Cp)_2^+]_0 = 10.0$ μM, CH_3CN/H_2O = 99/1, v/v. (wavelength: 363 nm)

Table D-8. The rate constants for the oxidation of 5.0 mM Et_4NI by $[Fe^{III}(CH_3Cp)_2]^+$ in CH_3CN/H_2O (99/1, v/v), in the presence of various concentrations of $[Cu(NCCH_3)_4]PF_6$ and $Fe^{II}(CH_3Cp)_2$. At μ = 0.10 M and 25.0 ^oC.

$[Fe(III)]_0$, μM	$[Fe(II)]_0$, mM	$[Fe(II)]_0/[Fe(III)]_0$	$[Cu(I)]_0$, μM	k_{obs}, s^{-1}
10	0.10	10	0.625	0.0428
10	0.10	10	1.25	0.0472
10	0.10	10	2.50	0.0633
10	0.10	10	5.00	0.0758
10	0.10	10	10.0	0.0836
10	0.10	10	20.0	0.0872
10	0.20	20	0.625	0.0244
10	0.20	20	1.25	0.0310
10	0.20	20	2.50	0.0419
10	0.20	20	5.00	0.0472
10	0.20	20	10.0	0.0534
10	0.20	20	20.0	0.0539
10	0.60	60	0.625	0.00916
10	0.60	60	1.25	0.0122
10	0.60	60	2.50	0.0181
10	0.60	60	5.00	0.0222
10	0.60	60	10.0	0.0263
10	0.60	60	20.0	0.0270
10	0.60	60	60.0	0.0278
10	0.60	60	100	0.0293
10	1.20	120	0.625	0.00910
10	1.20	120	1.25	0.0101
10	1.20	120	2.50	0.0117
10	1.20	120	5.00	0.0132
10	1.20	120	10.0	0.0160
10	1.20	120	20.0	0.0166
40	0.60	15	10	0.0590[a]
40	2.40	60	10	0.0238
40	2.40	60	20	0.0280
40	2.40	60	60	0.0304

[a] not perfect pseudo-first order

For the direct oxidation of 5.0×10^{-3} M iodide by 10 μM $[Fe^{III}(CH_3Cp)_2]^+$ in acetonitrile, at μ = 0.10 M and 25.0 °C, it was observed that the pseudo-first-order rate constant is 0.00208 s^{-1}.[191] When 1.0 mM Fe(II) was deliberately added to the above reactants, the rate constant decreases only by 9%. For the copper-catalyzed oxidation of 5.0×10^{-3} M Et_4NI by 10 μM $[Fe^{III}(CH_3Cp)_2]^+$ in CH_3CN/H_2O (99/1, v/v), in the presence of 0.10, 0.20, 0.60 and 1.20 mM Fe(II), at ionic strength of 0.10 M and 25.0 °C, the rate constants due to the non-copper-catalyzed contribution is assumed as 0.0019 s^{-1}. Plot of $(k_{obs}\text{-}0.0019)^{-1}$ vs $[Cu(I)]^{-1}$ is shown in Figure D-5. The intercept and slope in Figure D-5 increase with the increase of Fe(II), although it is not dramatic in the case of 1.20 mM Fe(II).

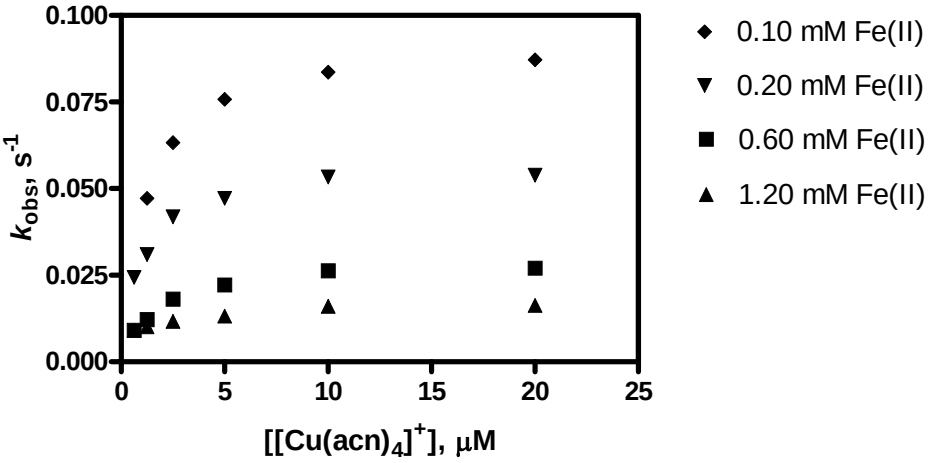

Figure D-4. Plot of k_{obs} vs $[Cu(acn)_4^+]$ for the oxidation of 5.0 mM Et_4NI by 10 μM $[Fe^{III}(CH_3Cp)_2]^+$ in CH_3CN/H_2O (99/1, v/v). With 0.10, 0.20, 0.60, and 1.20 mM $Fe^{II}(CH_3Cp)_2$, at μ = 0.10 M and 25.0 °C.

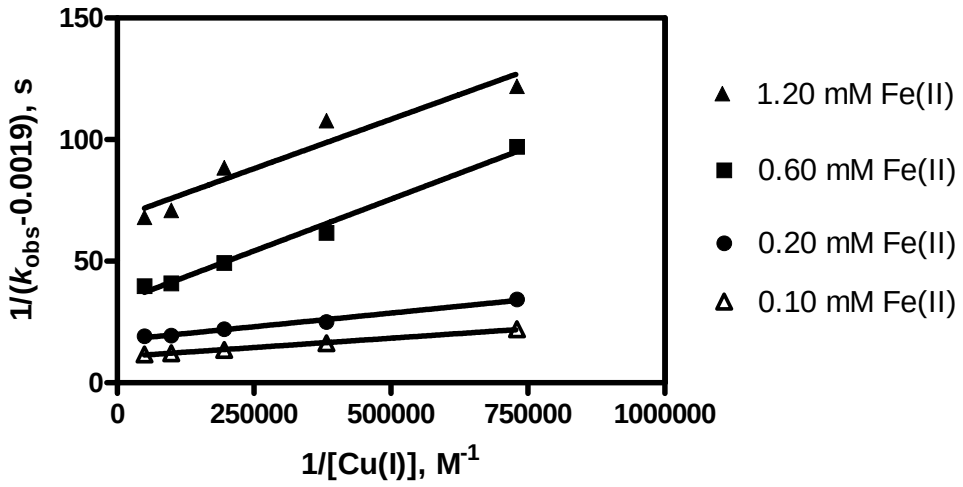

Figure D-5. Plot of $1/(k_{obs}\text{-}0.0019)$ vs 1/[Cu(I)] for the oxidation of 5.0 mM Et_4NI by 10 μM $[Fe^{III}(CH_3Cp)_2]^+$ in CH_3CN/H_2O (99/1). With 0.10, 0.20, 0.60, and 1.20 mM $Fe^{II}(CH_3Cp)_2$, at μ = 0.10 M and 25.0 °C.

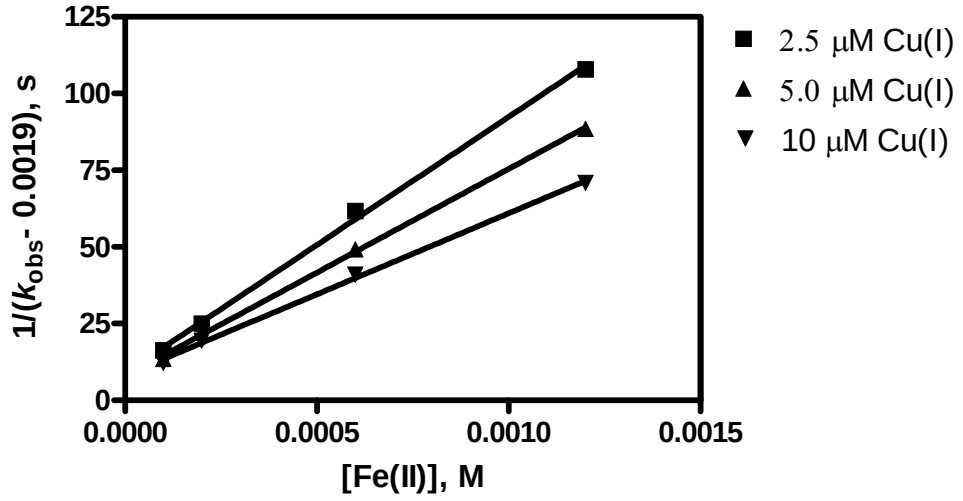

Figure D-6. Plot of $(k_{obs}\text{-}0.0019)^{-1}$ vs [Fe(II)] for the oxidation of 5.0 mM Et_4NI by 10.0 μM $[Fe^{III}(CH_3Cp)_2]^+$ in CH_3CN/H_2O (99/1, v/v). With 2.5, 5.0 and 10.0 μM $[Cu(acn)_4]PF_6$, at μ = 0.10 M and 25.0 °C.

For the oxidation of 5.0×10^{-3} M Et_4NI by 10 μM $[Fe^{III}(CH_3Cp)_2]^+$ in CH_3CN/H_2O (99/1, v/v), the inhibition by $Fe^{II}(CH_3Cp)_2$ was studied by adding various concentrations of $[Cu(NCCH_3)_4]PF_6$. A plot of $(k_{obs}\text{-}0.0019)^{-1}$ vs [Fe(II)] is shown in Figure D-6. The slope decreases with the increases of Cu(I), while the intercept is nearly the same, i.e., 8.20 s.

Based upon the above results, at constant concentration of iodide (5.0×10^{-3} M), the rate of the copper-catalyzed oxidation of I^- by $[Fe^{III}(CH_3Cp)_2]^+$ in CH_3CN/H_2O (99/1, v/v) is expressed as follows:

$$\text{Rate} = \frac{d[I_3^-]}{dt} = \frac{[\text{Fe(III)}][\text{Cu(I)}]}{([\text{Cu(I)}] + k_1)(k_2[\text{Fe(II)}] + k_3)} + \text{non} - \text{catalysis term} \qquad \text{(D-1)}$$

$$\text{where } k_{obs} = \frac{[\text{Cu(I)}]}{([\text{Cu(I)}] + k_1)(k_2[\text{Fe(II)}] + k_3)} + 0.0019 \qquad \text{(D-2)}$$

The copper content in the reactants was determined from Atomic Absorption Spectra. It was observed that most of copper comes from the recrystallized Et_4NI, and there is approximately 0.12 μM of Cu in 5.0 mM Et_4NI. So 0.12 μM of Cu was added in the following fitting.

$$k_{obs} = \frac{[\text{Cu(I)}]}{([\text{Cu(I)}] + a)(b[\text{Fe(II)}] + c)} + 0.0019 \qquad \text{(D-3)}$$

Then the rate constants in Table D-8 were fitted by Equation D-3, using DataFit 8.1 software package. The calculated rate constants are consistent with that of experimental data, except those of 0.625 μM of $[Cu(NCCH_3)_4]PF_6$. Due to the uncontrollably varying concentration of copper in Et_4NI, CH_3CN, water, *etc*, it is very diffcult to obtain reproducible kinetic results at the concentration of Cu(I) less than 1.0 μM. The values of k_1, k_2 and k_3 were obtained from the above fitting, with k_1 =a = $(1.46 \pm 0.34) \times 10^{-6}$ M, k_2 = b = $(5.35 \pm 0.64) \times 10^4$ M^{-1} s, and k_3 = c = (5.43 ± 1.39) s.

Unfortunately, we have difficulty in obtaining reproducible results in our kinetic experiments, especially at the concentration of Cu(I) no less than 20 μM, as shown in Table D-9. Currently, no reasonable mechanism could be proposed.

Table D-9. Irreproducible kinetic data for the oxidation of I^- by $[Fe^{III}(CH_3Cp)_2]^+$ in CH_3CN/H_2O (99/1). In the presence of 0.60 mM $Fe^{II}(CH_3Cp)_2$ and various concentrations of $[Cu(NC_3HC)_4]PF_6$, at μ = 0.10 M (Et_4NBF_4) and 25.0 °C. $[Fe^{III}(CH_3Cp)_2^+]_0$ = 10 μM, $[Et_4NI]_0$ = 5.0 mM.

$[[Cu(acn)_4]^+]_0$, μM	k_{obs}, s^{-1}	Date
5.0	0.0222	03/01/06
5.0	0.0252	05/21/06
5.0	0.0263	05/22/06
5.0	0.0245	05/31/06
5.0	0.0237	07/11/06
20.0	0.0270	03/01/06
20.0	0.0336	05/11/06
20.0	0.0342	05/26/06
20.0	0.0283	05/31/06
20.0	0.0302	07/11/06
40.0	0.0394	05/26/06
40.0	0.0408	05/29/06
40.0	0.0382	05/31/06
40.0	0.0349	07/11/06
60.0	0.0278	03/01/06
60.0	0.0460	05/11/06
60.0	0.0410	05/26/06
60.0	0.0372	05/29/06